

Copyright
by
William Gustavo Vizuite
2005

**The Dissertation Committee for William Gustavo Vizuite Certifies that this is the
approved version of the following dissertation:**

**Implementation of Process Analysis in a Three-Dimensional Air Quality
Model**

Committee:

David Allen, Supervisor

Roger Bonnecaze

Richard Corsi

Elena McDonald - Buller

Gary Rochelle

**Implementation of Process Analysis in a Three-Dimensional Air Quality
Model**

by

William Gustavo Vizuite, M.S., B.S.

Dissertation

Presented to the Faculty of the Graduate School of

The University of Texas at Austin

in Partial Fulfillment

of the Requirements

for the Degree of

Doctor of Philosophy

The University of Texas at Austin

May 2005

Dedication

This is dedicated to my wife, Natalie, and son, Guillermo, for their love, support, and smiles. I also would like to acknowledge my parents for their guidance, support, love, and enthusiasm.

Acknowledgements

From the initial stages of this thesis, to the final draft, I owe an immense debt of gratitude to my advisor, Dr. David Allen. His sound advice and careful guidance were invaluable. For his unselfish generosity, boundless energy, and valued assistance, a special thanks to Dr. Harvey Jeffries. I also would like to thank Dr. Yosuke Kimura for his technical assistance and dedication throughout the work that is published here. To each of the above, I extend my deepest appreciation.

April 13, 2005

Implementation of Process Analysis in a Three-Dimensional Air Quality Model

Publication No. _____

William Gustavo Vizuite, Ph.D.

The University of Texas at Austin, 2005

Supervisor: David T. Allen

Gridded, regional air quality models are used extensively in the development and evaluation of air quality regulations and in reconciling theoretical predictions of atmospheric behavior to observational data. Therefore, understanding the response of air quality models to changes in emissions or atmospheric conditions is important both for improving understanding of atmospheric processes and for designing effective air quality policies. Diagnosing model behavior is difficult because regional air quality models generally only output data on environmental state variables such as concentrations, and not on the rates of the processes that control the state variables. This thesis describes the development and application of Process Analysis Post Processing Tools (PAPPTs) for photochemical grid models; these tools provide dynamic information on environmental processes, such as horizontal and vertical pollutant fluxes crossing cell boundaries, chemical production and consumption rates, emission rates, and deposition rates, as well as initial and final concentrations. The PAPPTs were implemented in a regulatory photochemical grid model called the Comprehensive Air Quality Model with extensions

(CAMx). The use of the tools was demonstrated through the analysis of physical and chemical processes in regulatory models in central California and southeast Texas. The PAPPTs revealed the processes that contributed to model under-prediction of ozone generation in the Fresno area, and the processes that determined the impact of industrial emission events on ozone formation processes in the Houston-Galveston area. The PAPPTs also were used to develop a sub-domain model to evaluate stochastic emissions, to examine the impact of wild fire plumes on ozone formation processes, and to evaluate the isoprene emission inventory in southeast Texas. These case studies demonstrate the utility and versatility of the PAPPTs.

Table of Contents

List of Tables	x
List of Figures	xi
Chapter 1: Introduction	1
1.1 References	9
Chapter 2: Methodology development and application to central California	12
2.1 Introduction	12
2.2 Methodology	28
2.3 Results and Discussion	36
2.4 Conclusion	45
2.5 Acknowledgement	46
2.6 References	47
Chapter 3: Ozone Formation resulting from episodic emissions of highly reactive volatile organic carbons in Houston Texas	50
3.1 Introduction	50
3.2 Methodology	53
3.3 Results	67
3.3.1 August 25, 2000	67
3.3.2 August 30, 2000	85
3.4 Conclusion	95
3.5 Acknowledgements	96
3.6 References	97
Chapter 4: Development and Evaluation of the Sub-Domain Model	98
4.1 Introduction	98
4.2 Methodology	100
4.3 Results	109
4.4 Conclusion	116
4.5 References	117

Chapter 5: Wildfires in eastern Texas in August and September 2000: Emissions, aircraft measurements and impact on photochemistry.....	118
5.1 Introduction.....	118
5.2 Methodology.....	120
5.3 Results.....	122
5.4 Conclusion.....	134
5.5 References.....	135
Chapter 6: Comparisons of Modeled and Observed Isoprene Concentrations in Southeast Texas	136
6.1 Introduction.....	136
6.2 Methodology.....	138
6.3 Results.....	144
6.4 Discussion.....	152
6.5 Conclusion.....	160
6.6 Acknowledgements.....	161
6.7 References.....	162
Chapter 7: Summary of Findings.....	164
Chapter 8: Future Work	168
8.1 References.....	171
Appendices.....	172
Appendix A – Process Analysis Post Processing Tool Output for August 25, 2000.....	172
A.1 Introduction.....	172
Appendix B – Process Analysis Post Processing Tool Output for August 30, 2000.....	209
B.1 Introduction.....	209
Bibliography	234
Vita	240

List of Tables

Table 2-1. Vertical mixing parameters (m^2/s) for multiple vertical layers for five different horizontal grid cell locations in the CAMx air quality simulation for Fresno, CA. The data are for September 18, 2000 Hour 11.....	30
Table 3-1. Modeling scenarios that were tested with the CAMx model including emission rates, duration, date, and release time. The Carbon Bond IV reaction classification for each species is listed in parentheses.	66
Table 4-1. Processes modeled in the sub-domain model	107
Table 5-1: Burned area in km^2 (acres) during the study period; September 2–8 was characterized by the highest wildfire intensity.	122
Table 6-1. Statistical summary of the comparison of predicted isoprene concentrations and NOAA aircraft observations	146
Table 6-2. Statistical summary of the comparison of predicted isoprene concentrations and BNL G-1 aircraft observations	147
Table 6-3a. Statistical summary of the comparison of predicted isoprene concentrations and NOAA/NCAR aircraft PTR-MS observations, for Harris County	150
Table 6-3b. Statistical summary of the comparison of predicted isoprene concentrations and NOAA/NCAR aircraft PTR-MS observations, not in Harris County	150

List of Figures

Figure 1-1. Annual days exceeding federal one hour ozone standard for the years 1987 – 2001 (GHASP, 2005).....	2
Figure 2-1. Conceptual framework for a process-based photochemical model; the rates of individual chemical and physical processes are calculated to track changes in environmental state variables; process analysis tools track the rate processes, as well as the environmental state variables.	14
Figure 2-2. The 4 x 5 control volume of 4 km grid cells (16 km by 20 km) centered on the Fresno urban core chosen for the central California case study.	17
Figure 2-3. Control Volume height computed from Kv values in the CAMx modeling scenario for Fresno, CA September 18, 2000. The x-axis represents the hours of the simulation day and the modeling height is shown vertically. The red line is the mixing height and the light blue and yellow boxes show the layers that were entrained and detrained, respectively, during each hour.	18
Figure 2-4. Evolution of ozone concentrations and rates of change of ozone concentration over the course of a 24-hour period in Fresno, CA on September 18, 2000 for the base simulation. The aggregated concentrations and process magnitudes are created by post-processing data from the Integrated Process Rate (IPR) file created when CAMx was run.	19

Figure 2-5. Reaction cycles diagram, created by post processing data in the Integrated Reaction Rate (IRR) file. The diagram summarizes the cycling of oxides of nitrogen, the cycling of hydroxyl radical, and ozone formation processes.	20
Figure 2-6. Expanded NO and NO ₂ , cycles diagram produced by post-processing data in the Integrated Reaction Rate (IRR) file. Analysis was limited to the time period 08 – 18 hours. The diagram summarizes the physical and chemical processes for NO and NO ₂ and shows ozone formation process.....	27
Figure 2-7. A horizontal cross section from a 3-D grid model. The darkened grid cells are examples of (A) rectangular and (B) non-rectangular control volumes.	35
Figure 2-8. Time series for NO ₂ that shows the process rates and model concentrations for the Fresno California control volume on September 18, 2000 for the base simulation.	40
Figure 2-9. Time series of the VOC to NO _x ratios for the Fresno region control volume on September 18, 2000 for base simulation.	41
Figure 2-10. Example of a time series ozone plot that illustrates the process rates and model concentrations versus time for the Fresno California region on September 18, 2000. In this simulation all VOC emissions were tripled.	42
Figure 2-11. VOC to NO _x ratios for the Fresno region control volume for September 18, 2000 where all VOC emissions were tripled from the base simulation.....	43

Figure 2-12. Reaction cycles diagram summarizing the cycling of oxides of nitrogen, the cycling of hydroxyl radical, and ozone formation processes. This is for the Fresno region with tripled the VOC emissions of the base simulation.....	44
Figure 3-1. (a) Contour map of ozone concentrations from 10 a.m. until 5 p.m. on 10/23/2003. The figure shows the start of the ozone event at 11 a.m. when concentrations in excess of 200 ppb were recorded at the Clinton monitor. These high concentrations subsequently spread over a large region. (b) Ozone concentration data and VOC reactivity recorded at the Clinton monitor site. High hydrocarbon concentrations (represented in units of reactivity) were detected at the Clinton site at the start of the event (TCEQ, 2004).....	52
Figure 3-2. Modeling domain used in the study. The Regional, East Texas, Houston-Galveston-Beaumont-Port Arthur (HGBPA), Houston Galveston (HG), and Beaumont-Port Arthur (BPA) nested domains had 36, 12, 4 and 1 km resolution, respectively.	54
Figure 3-3. (a) Location of the three control volumes used for the PAPPT for the August 25, 2000 simulation day. (b) Location of the two control volumes used for the PAPPT for the August 30, 2000 simulation day. The red dot indicates the location where the simulated emission event was located.....	57
Figure 3-4. Control Volume Heights for the three control volumes on August 25, 2000 (a-c) and the two control volumes for August 30, 2000 (d-e). The x-axis represents the hours of the simulation day and the modeling height is shown vertically.	58

Figure 3-5a. Model predicted ground level ozone concentrations (ppb) for the Houston-Galveston (HG) domain (defined in Figure 3-2) on August 25, 2000.....	61
Figure 3-5b. Model predicted ground level ozone concentrations (ppb) for the Houston-Galveston (HG) domain (defined in Figure 3-2) on August 30, 2000.....	62
Figure 3-6a. Location of one of the elevated propylene and ethylene measurements made by a NOAA aircraft east of Houston during the August and September 2000 time period. The measurement was made on August 30, 2000. The site labeled “Emission Event Location” corresponds to the “release location” in the maps of Figure 3-3. The aircraft flight track is shown by red circles in the map; the wind direction (black arrow), industrial point sources (triangles), and the estimated release point (yellow triangle) also are shown.	63

Figure 3-6b. Summary of aircraft measurements on August 30, 2000 at the location of the high ethylene and propylene concentration measurements; time stamps along the horizontal axis can be matched to time stamps on the aircraft flight track in (a). Observations and model predictions (using an inventory with HRVOC emissions enhanced by approximately 150 t/d, but with no emission events) are shown. Note that the hydrocarbon concentrations dissipate rapidly around the maximum, lasting for only a few minutes of flight time. Since the aircraft flew at a speed of approximately 100 m/sec, the hydrocarbon plume width can be assumed to be less than 10 km wide. Note that at this stage, the hydrocarbons are just beginning to react; formaldehyde concentrations are less than 15 ppb (data abstracted from NOAA, 2004).....64

Figure 3-7a. Model output of ground level ozone concentrations (ppb) on August 25, 2000 from 10 a.m. – 3 p.m. The plots show the difference in ozone predictions between the propylene emission event case and the base case. The control volumes are outlined in black.....69

Figure 3-7b. Model output of ground level ozone concentrations (ppb) on August 30, 2000 from 10 a.m. – 3 p.m.. The plots show the difference in ozone predictions between the propylene emission event case and the base case. The control volumes are outlined in black.....70

Figure 3-8. (a),(b) Evolution of olefin concentrations and rates of change of ozone concentration over the course of a 24-hour period in the source control volume on August 25, 2000 for the base and propylene event emission simulation respectively. (c),(d) Olefin concentration for the base and propylene event emission simulation for the middle control volume. (e),(f) Olefin concentration for the base and propylene event emission simulation for the peak control volume.	72
Figure 3-9. (a),(b) Evolution of ozone concentrations and rates of change of ozone concentration over the course of a 24-hour period in the source control volume on August 25, 2000 for the base and propylene event emission simulation respectively. (c),(d) Ozone concentration for the base and propylene event emission simulation for the middle control volume. (e),(f) Ozone concentration for the base and propylene event emission simulation for the peak control volume.	74
Figure 3-10. Cycle diagrams for simulation day August 25, 2000 for the hours 10 a.m. – 1 p.m. in the source control volume for the (a) base case and (b) propylene event emission scenario.	77
Figure 3-11. Cycle diagrams for simulation day August 25, 2000 for the hours 1 p.m. – 4 p.m. in the peak control volume for the (a) base case and (b) propylene event emission scenario.	81
Figure 3-12. Key chemical parameters for the August 25, 2000 base case, propylene, ethylene, xylene, and n-pentane emission events for (a) the source control volume hours 10 a.m. – 1 p.m. and b) the middle control volume (c) the peak control volume hours 1 p.m. – 4 p.m.	83

Figure 3-13. Sources of new OH radicals for August 25, 2000 for the (a) source region, (b) middle region, and (c) peak region.	85
Figure 3-14. (a),(b) Evolution of olefin concentrations and rates of change of ozone concentration over the course of a 24-hour period in the source control volume on August 30, 2000 for the base and propylene event emission simulation respectively. (c),(d) Olefin concentration for the base and propylene event emission simulation for the peak control volume.	87
Figure 3-15. (a), (b) Evolution of ozone concentrations and rates of change of ozone concentration over the course of a 24-hour period in the source control volume on August 30, 2000 for the base and propylene event emission simulation respectively. (c),(d) Olefin concentration for the base and propylene event emission simulation for the peak control volume.	88
Figure 3-16. Cycle diagrams for simulation day August 30, 2000 for the hours 10 a.m. – 1 p.m. in the source control volume for the (a) base case and (b) propylene event emission scenario.	91
Figure 3-17. Cycle diagrams for simulation day August 30, 2000 for the hours 1 p.m. – 4 p.m. in the peak control volume for the (a) base case and (b) propylene event emission scenario.	92
Figure 3-18. Key chemical parameters for the August 30, 2000 base case, propylene, ethylene, xylene, and n-pentane emission events for (a) the source control volume hours 10 a.m. – 1 p.m. and (b) the peak control volume hours 1 p.m. – 4 p.m.	93
Figure 3-19. Sources of new OH radicals for August 30, 2000 for the (a) source control volume and (b) peak control volume.	94

Figure 4-1. Location of the PAPPT control volume used for August 25, 2000. The red dot indicates the location where the simulated emission event was located.....	102
Figure 4-2. Evolution of ozone concentrations and rates of change of ozone concentration over the course of a 24-hour period in the PAPPT control volume on August 25, 2000 for the (a) full grid and (b) sub-domain model respectively.	111
Figure 4-2. (c),(d) Evolution of ozone concentrations and rates of change of ozone concentration over the course of a 24-hour period in the control volume on August 25, 2000 for the (c) full grid and (d) sub-domain model respectively. Solid lines show the result with 11,638 lbs propylene added between 10:00 to 12:00. Thin lines were the results without addition.	112
Figure 4-3. Chemistry cycle diagram for a 4-hour period (10:00 to 14:00) in the control volume on August 25, 2000 for the (a) full grid, and (b) sub-domain models respectively.....	114
Figure 4-3. Chemistry cycle diagram for a 4-hour period (10:00 to 14:00) in the control volume on August 25, 2000 for the emission event simulation for the (c) full grid, and (d) sub-domain models respectively.	115
Figure 5-1. Horizontal and vertical structure of the modeling domain for the study. Fire emissions during the study period were estimated for the regional domain, with special attention paid to the Houston-Galveston, Beaumont Port Arthur (HGBPA) sub-domain. Emissions were assumed to enter a variety of vertical layers in an air quality model (Comprehensive Air Quality Model with extensions, CAMx).....	121

Figure 5-2. (a) Wildfires during the period from August 22–August 29, 2000. (b) Wildfires during the period from August 29–September 6, 2000. .	123
Figure 5-3: Emissions of CO, NMHCs, NO _x , and PM _{2.5} from wildfires in the HGBPA domain during August and September 2000. Emissions of CO and NMHC from wildfires exceeded emissions from Light Duty Gasoline Vehicles, LDGV (indicated by horizontal line) on some days.	124
Figure 5-4: Difference plots (concentrations predicted by the simulation including fire emissions – concentrations predicted by simulation without fire emissions) for CO (a) and ozone (b). The figure shows, for each grid cell, the maximum difference in CO and ozone concentrations throughout the period from August 22 nd to August 31 st	126
Figure 5-5. Difference plots (concentrations predicted by the simulation without fire emissions – concentrations predicted by simulation including fire emissions) for CO (a) and ozone (b). The figures are for September 6, 2000 hour 12; the time of the largest increase in ground level ozone concentrations due to fires.	128
Figure 5-6. Location of PAPPT control volumes on (a) August 30, 2000 and (b) September 6, 2000.	129
Figure 5-7. Time series of the VOC to NO _x ratios based on cell concentrations for the (a) August 30, 2000 and (b) September 6, 2000 control volumes. .	131
Figure 5-8. Origin of chemically produced ozone by each volatile organic carbon (VOC) for (a) August 30, 2000 hours 13-16, and (b) September 6, 2000 hours 10-13 control volumes.	132

Figure 5-9. Key parameters for the chemistry occurring in the control volumes for August 30, 2000 (hours 13-16), and September 6, 2000 (hours 10-13).	133
Figure 6-1. Modeling domain used in the study. The Regional, East Texas, Houston-Galveston-Beaumont-Port Arthur (HGBPA), Houston Galveston (HG), and Beaumont-Port Arthur (BPA) nested domains had 36, 12, 4 and 1 km resolution, respectively.	140
Figure 6-2. NOAA/NCAR PTR-MS data values for observed isoprene concentrations and the corresponding model predicted isoprene concentrations in the vertical layer and 1 km grid cell where the measurement was taken. (a) Flight path over the Houston urban core in Harris County at 2:00 pm on August 25, 2000, and (b) flight path in a rural region north of Houston at 12:00 pm on August 25, 2000.	149
Figure 6-3. Time series of modeled and observed isoprene concentrations in the grid cell containing the auto-GC at Clinton during the August 22-September 6, 2000 CAMx episode.	151
Figure 6-4. PAPPT time series of isoprene accumulation and loss processes in the (a) first vertical layer, (b) first three vertical layers, and (c) first nine vertical layers of the grid cell column containing the Clinton monitoring station on August 30, 2000. Only the period of the day when the mixing height is within layer 9 is shown in (c). In these diagrams, process rates are reported as ppb/hr of change in isoprene concentration and the isoprene concentration is reported as ppb. The sum of the process rates in each hour equals the hourly change in isoprene concentration.	155

Figure 6-5. PAPPT time series of isoprene accumulation and loss processes in the (a) first three vertical layers, and (b) first nine vertical layers of the grid cell column containing the site in the Sam Houston National Forest on August 25, 2000. In these diagrams, process rates are reported as ppb/hr of change in isoprene concentration and the isoprene concentration is reported as ppb. The sum of the process rates in each hour equals the hourly change in isoprene concentration.156

Figure 6-6. (a) Ground level isoprene concentrations in the Houston-Galveston domain (shown in red in Figure 6-1). (b) Vertical profile of isoprene concentrations along the gray horizontal line in Figure 6-6a. The vertical axis is reported as vertical layer number; the horizontal axis is reported as horizontal grid cell, numbered from west to east.158

Figure 6-7. (a) Difference in ground level isoprene concentrations in the Houston-Galveston domain (shown in red in Figure 6-1) between the case with K_v values increased by a factor of 5 minus the base case. (b) Difference in vertical profile of isoprene concentrations along the gray horizontal line in Figure 6-6a (case with K_v values increased by a factor of 5 - base case). The vertical axis is reported as vertical layer number; the horizontal axis is reported as horizontal grid cell, numbered from west to east.159

Chapter 1: Introduction

Air pollution is a major concern in Texas and throughout the world because of its harmful effects on health, crops, forests, and property. One of the dominant components of tropospheric air pollution is ozone. Ozone is a corrosive, toxic gas that can aggravate asthma and reduce lung function in children (Bates, 1995). Ozone is especially harmful to children 14 and younger due to their developing lungs and increased breathing rates relative to adults. This age group also spends a greater amount of time outdoors than adults, increasing their exposure to this harmful pollutant. Studies have suggested that long-term exposure to unhealthy levels of ozone may stunt lung function growth in children (Gauderman *et al.*, 2002; Horak *et al.*, 2002). A report by the California Air Resources Board and the Office of Environmental Health Hazard Assessment outlined several hundred community health studies that linked unhealthy levels of ozone to reduced lung function and increased rates of school absenteeism, emergency room visits, and hospital admissions (CARB, 2002; EPA, 1999; Künzli *et al.*, 1997). The American Lung Association's State of the Air 2004 Report concluded that nearly half the nation lives in areas where there is unhealthy amounts of ozone pollution (136 million Americans, ALA 2004).

The American Lung Association's State of the Air report 2004 also ranks the 25 most Ozone-Polluted Cities in the United States. According to the report Houston, Texas was the fifth most ozone polluted area in the country. Nearly half of Texas' population lives in four urban areas that do not meet the federal 1 hour standard for ozone: Houston-Galveston, Dallas-Fort Worth, Beaumont-Port Arthur, and El Paso. In 1999, the Houston area alone exceeded the federal standard for ozone concentrations averaged over one hour

(125 ppb) on 52 days. This was the first year that Houston had more days that exceeded the ozone air quality standard than the Los Angeles area, Figure 1-1 (GHASP, 2005). The following year, Houston was the only area in the United States to have three days with ozone levels over 200 ppb. The U.S. Environmental Protection Agency (EPA) has designated the Houston region as a “severe non-attainment area”. The state environmental agency, the Texas Commission on Environmental Quality (TCEQ), is responsible for developing control strategy policies that will bring the Houston-Galveston area and other areas in the state into compliance with federal National Ambient Air Quality Standards (NAAQS) for ozone. These control strategies are outlined in a plan known as the State Implementation Plan (SIP).

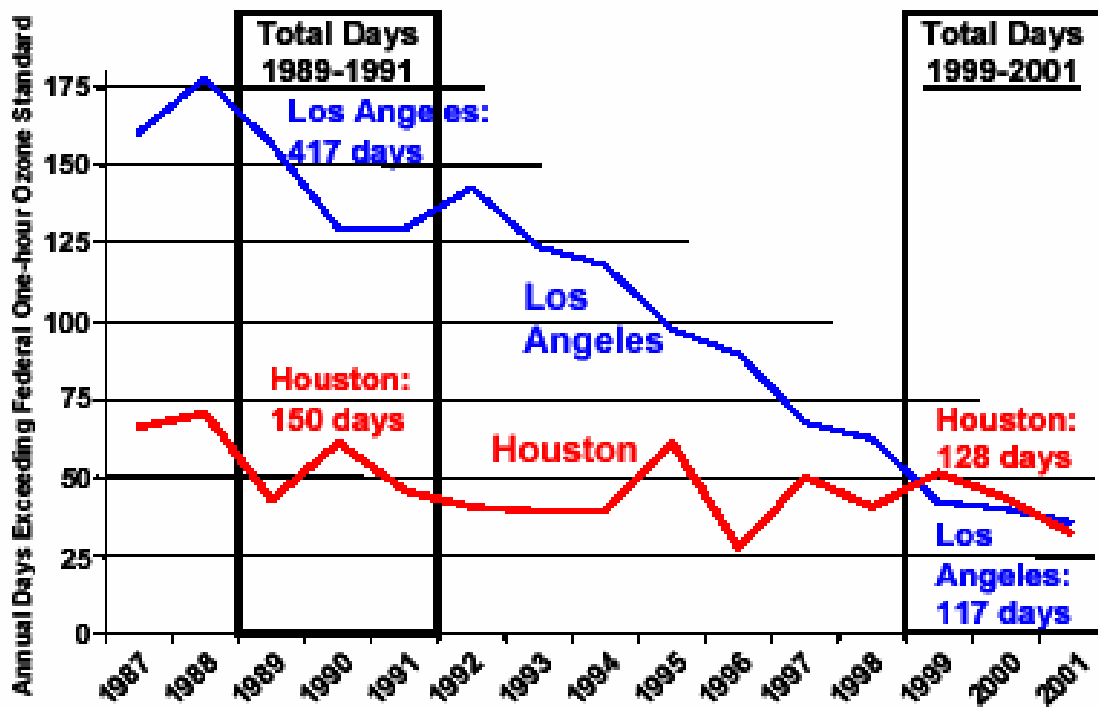


Figure 1-1. Annual days exceeding federal one hour ozone standard for the years 1987 – 2001 (GHASP, 2005).

Ozone is not directly emitted into the atmosphere but is the result of chemical and physical transformations that occur in the atmosphere. In general, ozone is formed in the atmosphere by photochemical reactions with nitrogen oxides (NO_x) and volatile organic compounds (VOC). Control strategies to reduce ozone typically involve reductions in emissions of NO_x and VOCs. Understanding the complex physical and chemical transformations leading to ozone formation is critical in addressing the reduction of this pollutant. Since ozone is a secondary pollutant, policy makers must use photochemical models to assess the effectiveness of the proposed emission reduction strategies. These photochemical air quality models input metrological and emissions data and couple them with descriptions of physical and chemical processes in the atmosphere (Allen and Durrenberger, 2001). The models then use mathematical algorithms to numerically process the information to predict air pollutant concentrations as a function of time and spatial location. The state of the science air quality model chosen by the TCEQ for development of the Houston SIP is the Comprehensive Air Quality Model with Extensions (CAMx). CAMx is an EPA approved photochemical grid model that simulates emission, chemical transformation, horizontal advection and diffusion, vertical transport and diffusion, dry deposition, and wet deposition of species in the atmosphere. In addition, the process analysis tools that are described in subsequent chapters of this work also are available in the official release of the CAMx source code.

The CAMx photochemical grid model used in the Houston-Galveston SIP must achieve two goals. The model must accurately predict the ozone concentration over an area as a function of time and space. A second important goal is that the model accurately predicts the sensitivity of ozone formation to changes in magnitude, location, and timing of emissions. The method to achieve these goals is first to use the model to simulate an

historical episode, or design day. The model's performance in predicting ozone conditions is evaluated with ambient monitoring stations. This process of comparing model predictions with ambient observations is referred to as a performance evaluation. Once a model meets the performance evaluation criteria, as defined by the EPA, it is then used to assess the sensitivity of ozone concentrations to changes in emissions data (EPA, 1991). The emissions used in the design day are then reduced to levels outlined in proposed regulations. The effectiveness of these VOC and NO_x control strategies are evaluated with the model. The modeled strategies that allow the region to comply with the Federal ozone standard are chosen and the State Implementation Plan is formed.

The CAMx photochemical air quality model is an eulerian (grid based) model. For each grid cell, the model calculates the rates of atmospheric processes that control air pollutant concentrations. In the CAMx model, these processes include chemical formation, chemical consumption, advection, diffusion, and deposition. These processes are coupled into a system of mass continuity equations used to predict the species concentrations in each grid cell. The CAMx model outputs only the spatial or temporal distribution of species concentrations discarding the information about the individual processes that lead to those changes. With only final concentration fields, it is difficult to infer why air pollutant concentrations change or understand the relationship among grid cells. To gain an increased understanding of the formation processes for pollutants a process analysis tool was linked to the CAMx photochemical air quality model to determine the roles of these individual processes that contribute to ozone formation. The tool allows for the analysis of all process information such as horizontal and vertical pollutant flux crossing cell boundaries, chemical production and consumption rates, emission rates, deposition rates, and initial and final concentrations.

The process analysis tool was originally developed by Jeffries and his co-workers (Jang *et al.*, 1995a; Jang *et al.*, 1995b ; Jeffries and Tonnesen, 1994; Jeffries, 1995; Tonnesen and Jeffries, 1994; Wang, 1997) and incorporated into an official release of CAMx. The process analysis tool generates a bewildering amount of data on model processes. Analysis of model phenomena proves difficult without a way to organize the data in a meaningful structure. Here we extend the basic tools developed by Jeffries and his co-workers to provide a post-simulation processing system and visualization output that helps explain CAMx predictions. The following chapters will describe the implementation of the process analysis post processing tools (PAPPTs) and their application to four separate case studies. The case studies will illustrate the insights that could be gained by careful analysis of the visualization output provided by the PAPPTs. In chapter 2 the development of the tools is described and the use of the tools is demonstrated through the analysis of ozone formation processes in a Central California Ozone Study. The processes that contributed to model under-prediction of ozone generation in the Fresno area were revealed. Subsequent chapters describe how the tools helped understand processes in the regulatory models used for the Houston SIP.

Chapters 3 and 4 outline how the tools were used to study the significant temporal variability found in industrial emissions of volatile organic compounds (VOCs) from non-Electrical Generating Units (NEGU) in the Houston-Galveston area. It has been reported that transient emission events from these facilities are a factor of 10 to 1,000 higher than the annual average emission rates for individual facilities (Murphy and Allen, 2005). In the Houston-Galveston area, reported events of this magnitude occur more than 1,000 times per year. The PAPPTs examined how these emission events impact ozone

formation and accumulation processes in the Houston-Galveston area. First, a sensitivity study of emission events of VOCs was performed with the full CAMx model. Emission event releases of ethylene, propylene, n-pentane, and xylene were modeled and compared in a NO_x rich and NO_x limited environments. The PAPPTs allowed for comparisons of the impact on ozone formation processes in each emission event. The computer costs related to running a full 3-D simulation restrains the total number of emission events that can be studied. A more robust analysis requires the simulation of the diverse range of emission event types and magnitudes found in southeast Texas. A more computationally efficient model was needed to study the wide range of conditions associated with industrial emission events. The sub-domain model developed for this purpose is described in Chapter 4 (Kimura *et al.*, 2005).

The sub-domain model attempts to approximate the same results provided by a full 3-dimensional regional air quality model, but with a small fraction of the computational effort. The sub-domain model imports model conditions from the full gridded model by using the PAPPTs. Data such as initial conditions, boundary conditions and other key conditions of the photochemistry from the full gridded model is incorporated into the sub-domain model. This allows the sub-domain model to more closely approximate the processes modeled by the full gridded model. Chapter 4 describes how the PAPPT output was used to compare atmospheric chemistry parameters between the full model and the sub-domain model. Once these differences between models were quantified the sub-domain model was used to provide a statistical characterization of the impacts of thousands of types of industrial emission events on ozone formation in southeast Texas.

In Chapter 5 the PAPPTs are used to quantify ozone formation rates resulting from wildfires, a different source of pollutant precursors. An emission inventory of wildfires in southeast Texas was developed for the 2000 regulatory CAMx simulation episode at the University of Texas – Austin (Junquera *et al.*, 2005). The PAPPT was used to characterize the photochemistry occurring in the wildfire plumes based on the recently developed inventory. Process analysis methods were applied on two simulation days. On one day an isolated rural wildfire northeast of Houston was studied to investigate ozone chemistry when the plume was advected over relatively limited number of NO_x sources. A second day was chosen when wildfires plumes were advected toward the Houston urban core encountering anthropogenic NO_x sources. These two days provide distinct environmental conditions where ozone formation processes differ. These processes were examined and compared with the PAPPTs.

Chapter 6 outlines how the PAPPT was applied to quantify processes leading to biogenic VOC concentrations in the atmosphere. Biogenic emissions are an important and significant source of VOCs in southeast Texas. Ambient measurements of isoprene, a component of biogenic emissions, were evaluated against predictions from the CAMx model. Ambient isoprene concentrations were recorded using ground and aircraft measurements at several locations in the Houston-Galveston area. Evaluations of the data found that the ground level isoprene concentrations predicted by the model were typically 2-3 times higher than observed concentrations, but mean predicted concentrations aloft generally were consistent with mean observations. An understanding of which model processes influenced the model predicted isoprene concentrations requires the use of the PAPPTs. The PAPPTs revealed large chemical destruction rates of isoprene in the first hundred meters above ground level. Overall, it was this balance between vertical

transport rates and chemical reaction rates in the model that had the largest influence on predicted isoprene concentrations.

After the description of PAPPT development (Chapter 2), and descriptions of its initial applications (Chapters 3-6), this thesis concludes with a summary of findings and suggestions for future work.

1.1 REFERENCES

- Bates D.V. 1995. "The effects of air pollution on children." *Environmental Health Perspective*, 103 (Suppl. 6): 49-53.
- Gauderman W.J., Gilliland G.F., Vora H., Avol E., Stram D., McConnell R., Thomas D., Lurmann F., Margolis H.G., Rappaport E.B., Berhane K., Peters J.M. 2002. "Association between air pollution and lung function growth in Southern California children." *American Journal of Respiratory and Critical Care Medicine*, 166 (1):76-84.
- Horak F. Jr., Studnicka M., Gartner C., Spengler J.D., Tauber E., Urbanek R., Veiter A., Frischer T. 2002. "Particulate matter and lung function growth in children: A 3-year Follow-up Study in Austrian Schoolchildren." [European Respiratory Journal](#), 19 (5):838-45.
- California Air Resources Board (CARB) and the Office of Environmental Health Hazard Assessment (2002). "Staff Report: Public Hearing to Consider Amendments to the Ambient Air Quality Standards for Particulate Matter and Sulfates" <ftp://ftp.arb.ca.gov/carbis/research/aaqs/std-rs/pm-final/ch1-6.pdf>
- U.S. Environmental Protection Agency (EPA). 1999. "Smog--Who Does It Hurt? What You Need to Know About Ozone and Your Health", EPA Publication No. EPA-452/K-99-001, Research Triangle Park, NC.
- Künzli N., Lurmann F., Segal M., Ngo L., Balmes J., Tager I.B. 1997. "Association Between Lifetime Ambient Ozone Exposure and Pulmonary Function in College Freshmen--Results of a Pilot Study." *Environmental Research*, 72 (1): 8-23.
- American Lung Association (ALA). 2004. "State of the Air Report: 2004." http://lungaction.org/reports/sota04_full.html

Galveston-Houston Association for Smog Prevention (GHASP). 2005. "Ozone Smog."
<http://www.ghasp.org/issues/smog.html>

Allen D.T., Durrenberger C. 2001. "Accelerated Science Evaluation of Ozone Formation in the Houston-Galveston Area: Photochemical Air Quality Modeling."
ftp://ftp.tnrcc.state.tx.us/pub/OEPAA/TAD/Modeling/HGAQSE/Reports_2002Feb/UT/AQModeling_20020204.pdf

U.S. Environmental Protection Agency (EPA) 1991. "Guidelines for Regulatory Application of the Urban Airshed Model." EPA Publication No. EPA-450/4-91-1013. Office of Air Quality Planning and Standards, Research Triangle Park, NC.

Jang J. C., Jeffries H. E., Byun D., Pleim J. E. 1995a. "Sensitivity of Ozone to Model Grid Resolution: Part I. Application of High Resolution Regional Acid Deposition Model." *Atmospheric Environment* 29(21): 3085-3100.

Jang J. C., Jeffries H. E., Tonnesen S. 1995b. "Sensitivity of Ozone to Model Grid Resolution: Part II. Detailed Process Analysis for Ozone Chemistry." *Atmospheric Environment* 29(21): 3101-3114.

Jeffries H. E., Tonnesen S. 1994. "A Comparison of Two Photochemical Reaction Mechanisms Using a Mass Balance Process Analysis." *Atmospheric Environment* 28(18): 2991-3003.

Jeffries H. E. 1995. "Photochemical Air Pollution. Chapter 9 in Composition, Chemistry, and Climate of the Atmosphere." Ed. H.B. Singh, Van Nostrand-Reinhold, New York, ISBN 0-442-01264-0

Tonnesen S., Jeffries H. E. 1994. "Inhibition of Odd Oxygen Production in Carbon Bond IV and Generic Reaction Set Mechanisms." *Atmospheric Environment* 28(7): 1339-1349.

Wang Z. 1997. "Comparison of Three Vertical Diffusion Schemes in The SARMAP Air Quality Model with Integrated Process Rate Analysis Method and Continuous Process Composition and Source Receptor Methodology." PhD Dissertation, University of North Carolina at Chapel Hill.
ftp://airsite.unc.edu/PDFS/ESE_UNC/Students/PhDThesis/Wang/

Murphy C., Allen D. T. 2005. "Hydrocarbon Emissions from Industrial Release Events in the Houston Galveston Area and their Impact on Ozone Formation." *Atmospheric Environment* In Press

Kimura Y., Vizuite W., Jeffries H. E., Allen D. T. 2005. "Implementation of Process Analysis in a 3-Dimensional Air Quality Model III: Development of sub-domain modeling tools to assess the impact of stochastic emission events on ozone formation in Houston Texas" submitted to *Atmospheric Environment*

Junquera V., Kimura Y., Vizuite W., Allen D. T., 2005. "Wildfires in Eastern Texas in August and September 2000: Emissions, Aircraft Measurements and Impact on Chemical and Physical Processes" submitted to *Atmospheric Environment*

Chapter 2: Methodology development and application to central California

2.1 INTRODUCTION

Gridded photochemical air quality models, commonly used in the development and evaluation of air quality regulations, calculate rates of atmospheric processes that control air pollutant concentrations in the framework of a 3-dimensional grid. These processes include chemical formation, chemical consumption, advection, diffusion, and deposition. In 3-D gridded photochemical models, these processes are coupled into a system of mass continuity equations used to predict the species concentrations in each grid cell (Russell and Dennis, 2000). Many models output only the spatial and temporal distribution of species concentrations, and rates of the individual processes that lead to these changes in species concentrations are not recorded. With only concentration fields, it is often difficult to infer why air pollutant concentrations change. A more detailed evaluation of all modeled processes can often lead to an increased understanding of the formation processes for pollutants.

“Process analysis” of gridded photochemical models refers to techniques developed and originally implemented by Jeffries and his co-workers (Jang *et al.*, 1995a; Jang *et al.*, 1995b ; Jeffries and Tonnesen, 1994; Jeffries, 1995; Tonnesen and Jeffries, 1994; Wang, 1997) to quantitatively track individual physical and chemical process that contribute to changing pollutant concentrations for a grid cell or collection of grid cells of photochemical models. The additional computations and output necessary to permit Process Analysis post processing (PAPP) have been integrated into several three-dimensional air quality models including the EPA’s Urban Airshed Model (SAI, 1999;

Wang *et al.*, 1995), California Air Resources Board SARMAP Air Quality Model (Wang, 1997; Wang and Jeffries, 1998), EPA's Community Multiscale Air Quality Model (Gibson, 1999), and ENVIRON's Comprehensive Air Quality Model with extensions, CAMx (ENVIRON, 2004). Process analysis model output provides dynamic information such as horizontal and vertical pollutant fluxes crossing cell boundaries, chemical production and consumption rates, emission rates, deposition rates, and initial and final concentrations. Figure 2-1 is an illustration of the conceptual basis of a "process-based" photochemical grid model. Concentrations of pollutants at every time step are modified due to chemical and physical processes. These processes are described by sets of differential equations that calculate the changes in species concentrations. These processes are allowed to operate simultaneously for a small amount of time, changes in species concentrations over a time step are predicted, concentrations are modified and the model proceeds to the next time step. This "marching in time" technique can be used to advance a given initial concentration to a future time by processing many incremental time steps. Process Analysis output provides not only initial concentrations, intermediate concentrations and final concentrations; it also provides the *separately integrated* rates of individual chemical and physical processes that lead to these concentrations. By assembling these individual integrated rates in different ways in post processing programs it becomes possible to explain exactly how the model achieved its predictions and to gain understanding of the dynamic interaction of the physical and chemical processes operating in the model. Wang implemented the additional integration and necessary outputs in CAMx (ENVIRON, 2004). In the CAMx system, however, few process analysis post processing tools (PAPPT) were provided for computing and displaying the output meaningfully. Here we extend the basic tools developed by Jeffries

and his co-workers to provide a post-simulation processing system and visualization output that helps explain CAMx predictions.

Conceptual Model

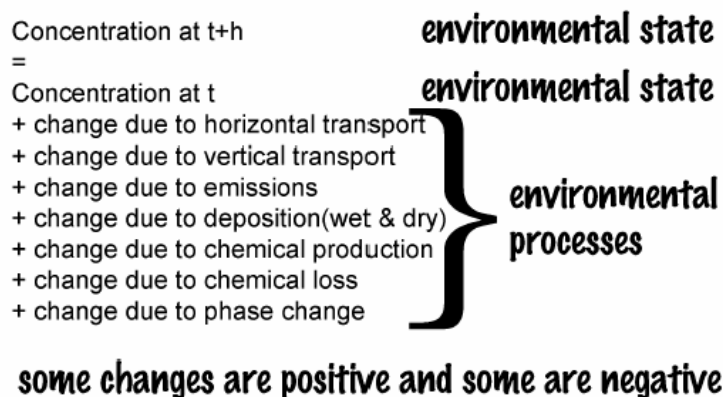


Figure 2-1. Conceptual framework for a process-based photochemical model; the rates of individual chemical and physical processes are calculated to track changes in environmental state variables; process analysis tools track the rate processes, as well as the environmental state variables.

When process analysis integration and outputs are added to a photochemical model, the photochemical model generates two additional files, an Integrated Process Rate (IPR) and Integrated Reaction Rate (IRR) file. The IPR file provides information about the rates of each physical process for each species in each grid cell, in each layer, at each time step. The IRR file provides integrated rates for each reaction in the chemical mechanism over each output time step and is used to determine how net changes in concentrations due to chemistry depend on individual reaction pathways or classes of pathways. Data from these files are extracted and merged in post processing operations and are then further processed into “time series” and “reaction cycles” diagrams. In

creating these diagrams, both a horizontal and vertical control volume must be selected. Figure 2-2 shows the horizontal dimensions of the control volume of an analysis to be described in detail below. The horizontal dimensions remain fixed over the course of the analysis. The vertical extent of the control volume varies with time and is depicted in Figure 2-3. All the mass is aggregated within the control volume, and exchanges between the control volume and cells adjacent to the control volume are summed to produce only exchanges at the faces of the aggregated control volume. The exact details of these operations will be described in the Methodology section below. The concentrations and magnitudes of process rates shown in the diagrams are therefore an average over the aggregated control volume.

Figure 2-4 shows an example of a time series plot for the species ozone (O_3) that has been generated by post-processing the IPR file; any species in the model can be analyzed in this manner. In the Figure, the modeled O_3 concentration is given for each hour and the hourly integrated concentration changes to O_3 , separately caused by emissions, net chemical production or consumption, net horizontal transport, net vertical transport, and deposition, are reported. The sum of the concentration changes due to processes at each hour equals the O_3 concentration change from the hour's starting concentration to the hour's ending concentration. The concentrations and integrated rates of change by process can be calculated for a single grid cell or a collection of grid cells. In the original Process Analysis post-processing implementation, the grid cells over which the process analysis was performed were kept fixed over the time period of the simulation. When the goal of the process analysis is to characterize the processes occurring in the mixed layer, and the mixing height changes over the course of a day, fixing the control volume over which the processes are tracked limits the value of the

Process Analysis. A control volume height that is lower than the mixing height results in large vertical transport of pollutants across the top boundary of the control volume. Conversely, a control volume height too far above the mixed layer may lead to an analysis that averages very different process rates (e.g., horizontal transport above the mixed layer and below the mixed layer). Control volume heights that are either larger or smaller than the mixing height are therefore undesirable, since they can mask the nature of chemical and physical processes that are occurring throughout the mixed layer. Therefore, as described in the Methodology section, a goal of the work reported here was to modify the post-processing tools to allow the control volume for the process analysis to follow mixing height evolution. This required that a small amount of additional data from the model simulation be included in the PA output files and the CAMx program was modified accordingly. ENVIRON has indicated that this change eventually will be incorporated into an official release version of the CAMx program (Yarwood, 2004). This approach also led to the need for an additional parameter in the time series charts, labeled in Figure 2-4 as cell volume change. The cell volume change accounts for the net effect of entrainment and dilution of material as the mixing height changes.

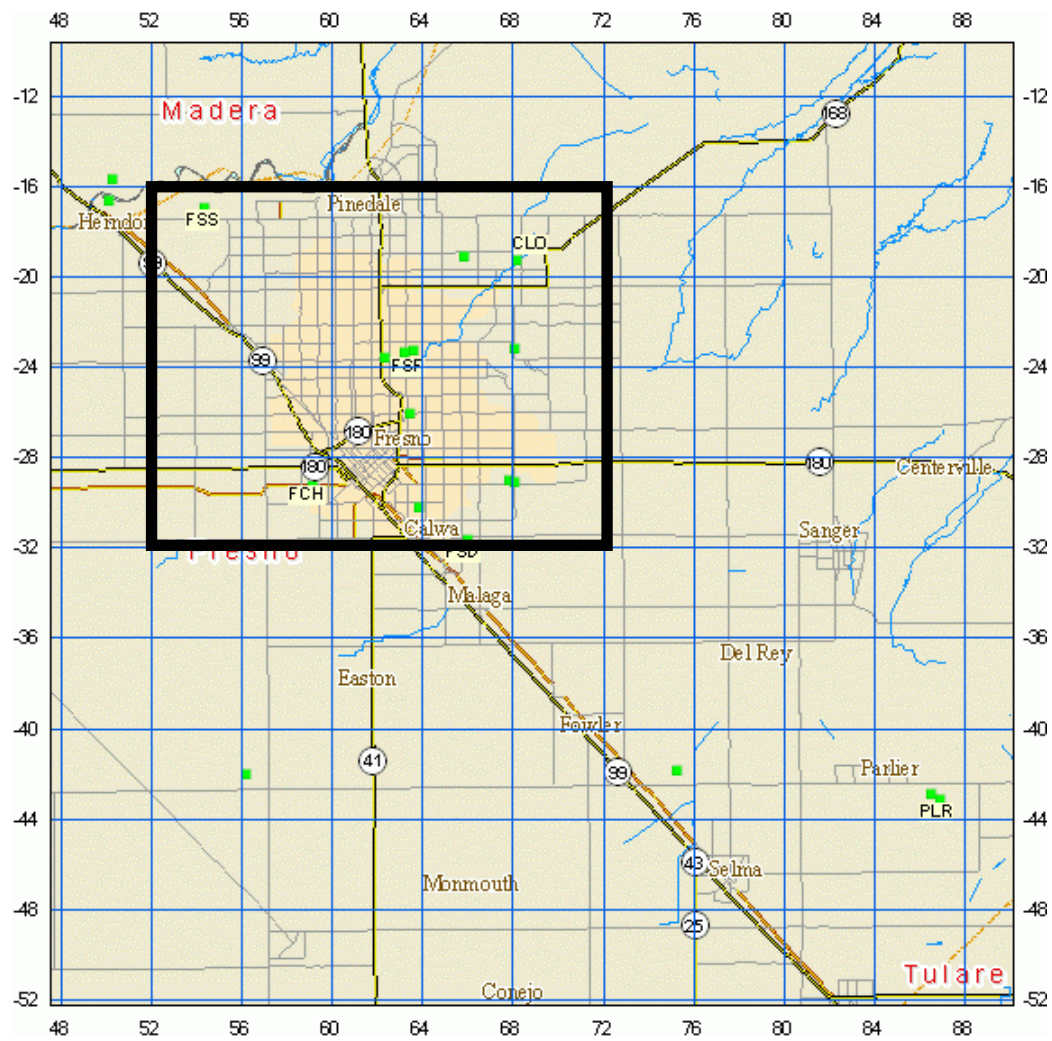


Figure 2-2. The 4 x 5 control volume of 4 km grid cells (16 km by 20 km) centered on the Fresno urban core chosen for the central California case study.

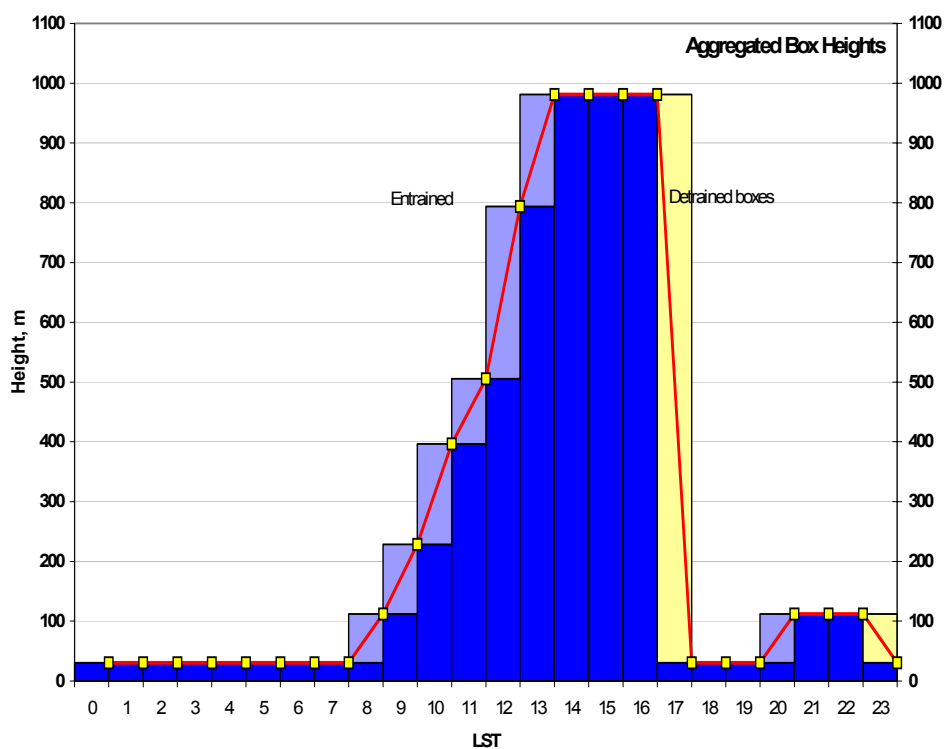


Figure 2-3. Control Volume height computed from K_v values in the CAMx modeling scenario for Fresno, CA September 18, 2000. The x-axis represents the hours of the simulation day and the modeling height is shown vertically. The red line is the mixing height and the light blue and yellow boxes show the layers that were entrained and detrained, respectively, during each hour.

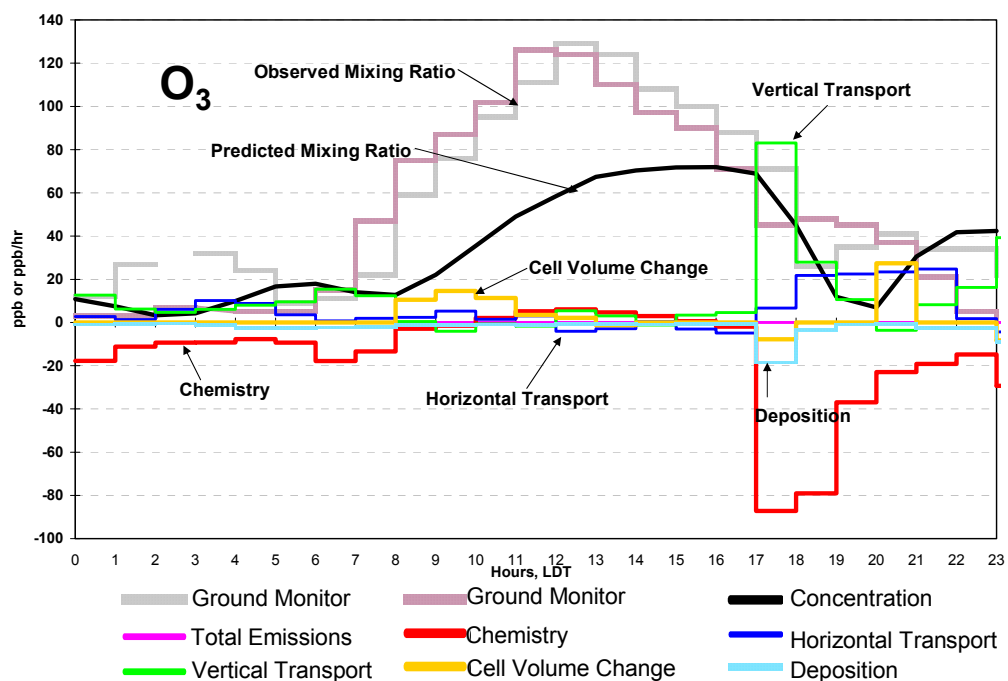


Figure 2-4. Evolution of ozone concentrations and rates of change of ozone concentration over the course of a 24-hour period in Fresno, CA on September 18, 2000 for the base simulation. The aggregated concentrations and process magnitudes are created by post-processing data from the Integrated Process Rate (IPR) file created when CAMx was run.

In the time series shown in Figure 2-4, the chemistry term is the net change due to multiple reaction pathways. Time series plots alone are not capable of explaining the contributions of specific reaction pathways to the net change. To characterize the chemistry, information from the IRR file is extracted and summarized in “reaction cycles” diagrams, of the type shown in Figure 2-5. The cycles diagram describes oxides of nitrogen (the sum of nitric oxide, NO, and nitrogen dioxide, NO₂, NO_x) and hydroxyl radical (OH) cycling over a specified time period, and introduces a number of parameters for characterizing the chemistry. The time period selected in the figure was hours 8 –18; this focused the analysis on the chemical processes occurring during daylight hours.

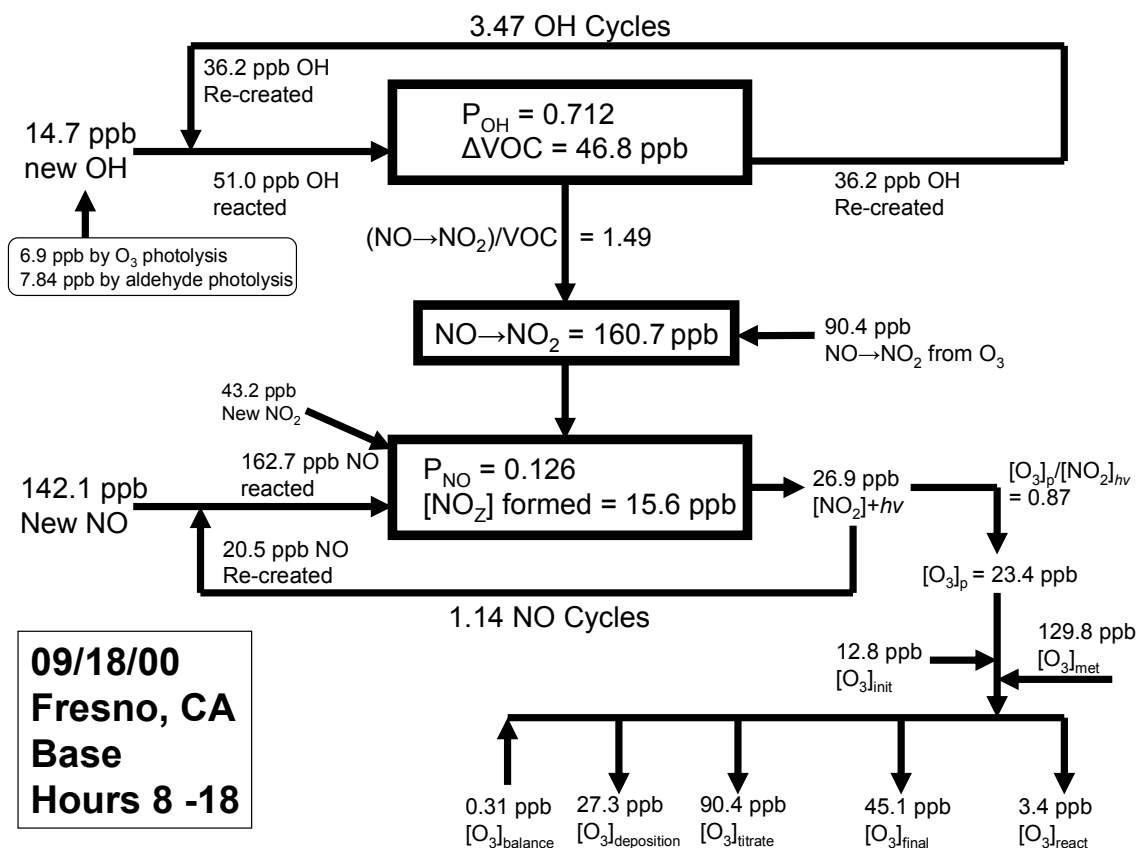


Figure 2-5. Reaction cycles diagram, created by post processing data in the Integrated Reaction Rate (IRR) file. The diagram summarizes the cycling of oxides of nitrogen, the cycling of hydroxyl radical, and ozone formation processes.

The figure displays radical initiation, propagation, and termination and NO emission, oxidation to NO₂, and photolysis to O₃ and NO as a linked, feed-back set of processes. It consists of four major clusters: the “OH-cycle” (top set of boxes and arrows), the total “NO to NO₂ conversion” (middle box and connecting arrows), the “NO cycle” (bottom set of boxes and connecting arrows), and the “ozone mass balances” (lower right boxes and arrows). The OH cycle cluster describes the origin and magnitude

of new OH radicals, the magnitude of OH reacted and the total VOC that reacted with OH molecules. New OH from ozone and aldehyde photolysis is represented in the rounded box on the left hand side of the OH cycle. In the example diagram, a total of 14.7 ppb of new OH is generated over the 10 hour period by these photolysis pathways; this new OH reacts and a fraction of the reaction pathways result in the reformation of OH which is available to react again. This OH reaction and reformation can occur multiple times until the OH eventually reacts through a pathway that does not regenerate OH. Each “new OH” that reacts with a VOC molecule has a probability of becoming a recreated OH, which can start another VOC oxidation chain. This probability is defined as the radical propagation factor, shown as P_{OH} in Figure 2-5. The number of recreated OH is given by multiplying P_{OH} with the total number of available OH radicals. The total number of OH cycles can be defined as follows:

$$Q = q + q \cdot P_{OH} + q \cdot P_{OH}^2 + q \cdot P_{OH}^3 + \dots + q \cdot P_{OH}^n \text{ (Equation 2-1)}$$

$$Q/q = 1/(1 - P_{OH}) = \text{number of OH cycles.}$$

where Q is the total number of OH radicals, q is the number of new OH radicals, and P_{OH} is the propagation factor. Therefore, Q/q is the number of OH cycles, and represents the average number of times each new OH cycles before being lost in termination reactions. If Q/q is high, P_{OH} is near 1, and termination reactions are slow relative to propagation reactions. In the example diagram, a typical OH radical goes through 3.47 reaction and regeneration cycles before being lost in a termination reaction. This means that, in this example, 36.2 ppb of OH is reformed over the course of the 10 hour period. Combined, the reformed OH and the new OH explains the 51.0 ppb of OH that reacts. The fraction of OH that reacts with hydrocarbons and reforms (P_{OH}), as opposed to reacting into

termination pathways, is a critical parameter in characterizing ozone formation. High values (>3.5) of the parameter $1/(1-P_{OH})$, the number of OH cycles, are representative of conditions when simple hydrocarbon reactivity (sum of $k_{OH}^i [VOC_i]$ over all VOC) is high relative to the OH termination reaction frequency (sum of $k_{OH}^i [NO_2]$ plus other radical + radical loss paths) and tend to be associated with conditions near the ozone ridge line on an ozone isopleth diagram.

The total NO to NO₂ conversion box (middle of diagram) records the amount of NO₂ that resulted from the reaction of NO with hydroperoxy and alkylperoxy radicals (VOC chemistry) and the magnitude of NO₂ resulting from NO reaction with entrained O₃. This type of O₃ is considered “old” or existing O₃ and is not to be explained by the chemistry in the control volume. In this example, a total of 46.8 ppb of VOC reacted with an average of 1.49 NO to NO₂ conversions per VOC. This leads to 70.3 ppb of NO₂. The remaining 90.4 ppb of NO₂ formation in this example, leading to a total of 160.7 ppb, is due to entrained ozone reacting with NO; this is an unusual situation characteristic of an NO_x-rich, VOC-poor control volume. The NO₂ generation, documented in the middle of the diagram, is input to the NO cycle box in the lower left portion of the diagram. The NO cycle box documents the origin and magnitude of new NO, the magnitude of total NO reacted, the magnitude of re-created NO by photolysis, the ozone formation efficiency from NO₂ photolysis processes ($[O_3]_p/[NO_2]_{hv}$), and the number of times each NO was cycled. The new NO is due to emissions and net transport (in-out) into the PAPPT control volume. In the example diagram, a total of 142.1 ppb of new NO enters the control volume; some of this new NO reacts with peroxy radicals to form NO₂ and a fraction of the reaction pathways form other nitrogen species (NO_z), which may be unreactive (e.g., HNO₃) or may be reactive (e.g., PAN). In this case, the majority of the

NO₂ that is formed in the control volume is transported vertically out of the control volume without photolyzing (this is documented in a time series diagram for NO₂, analogous to the time series diagram for ozone shown in Figure 2-4). Only 26.9 ppb of NO₂ is photolyzed, resulting in the formation of ozone and regenerating NO. The cycling of NO into NO₂, with subsequent photolysis, ozone formation and NO regeneration can occur multiple times until the NO eventually reacts through a pathway that does not regenerate NO or is transported away. In the example diagram, a typical NO molecule goes through 1.14 reaction and regeneration cycles before being lost to reaction. This means that, in this example, the 142.1 ppb of NO is used 1.14 times generating 162.7 ppb of NO that reacts over the course of the 10 hour period. Ultimately 15.6 ppb of NO_z is formed in termination reactions. The fraction of NO that reacts and is reformed (P_{NO}), as opposed to reacting to NO_z, is a critical parameter in characterizing ozone formation.

The ozone mass balances in the lower right of the diagram includes the magnitude of total O₃ produced by chemistry ($[O_3]_p$), the magnitude of initial O₃ existing in the cell ($[O_3]_{init}$), the magnitude of O₃ contributed from or lost by meteorological processes ($[O_3]_{met}$), the magnitude of O₃ loss by reacting with organics ($[O_3]_{react}$), O₃ loss by titration ($[O_3]_{titrate}$), O₃ source balance ($[O_3]_{balance}$) correction term, and the final O₃ concentration in the cell ($[O_3]_{final}$). The $[O_3]_{balance}$ correction term captures all ozone reaction pathways that are not included in this simplified diagram. If the balance term is significant, a further detailed investigation into other ozone reaction paths is warranted. The $[O_3]_p$ term is an important indicator of the extent of ozone productivity in the PAPPT control volume. This value, in addition to $[O_3]_{met}$, documents whether this pollutant was produced locally, or was a result of ozone production outside the boundaries of the control volume.

Figure 2-6 presents an expanded view of the pathways in the NO propagation cycle shown in Figure 2-5. As in Figure 2-5, the processes have been integrated from hours 08 to 18. This diagram is designed to trace the physical origins of the initial and emitted NO and NO₂, trace the chemical reactions and physical processes for these species and show how NO is re-created and oxidized again. In the process of re-creating the NO, the system creates ozone. Over the 10 hours, a total of 162.6 ppb of NO was oxidized in the system; this is shown at the top center of the diagram. The sources of this oxidized NO are two processes. The amount labeled “new NO” was the result of mass balance processes applied to the initial and emitted NO, and from NO resulting from once photolyzed initial and emitted NO₂ (see the middle right of the diagram).

The initial NO present in the control volume at 08 hours was 25.7 ppb. The emitted NO was 186.3 ppb. The initial NO₂ in the control volume at 08 hours was 26.1 ppb and the emitted NO₂ was 21.0 ppb. The term “new NO₂” describes NO₂ that had not been photolyzed. A total of 43.2 ppb of “new NO₂” was available and it was subject to chemical and physical processes along with the NO₂ created from chemically oxidizing NO. The subsequent physical and chemical processes resulted in a total of 6.4 ppb of NO that could be traced to the “new NO₂” as shown at the bottom right of the diagram. This is considered “new NO” that came from once photolyzed NO₂ and it is added to the other sources of new NO at the top right of the diagram. From the sources of NO in the top right, a significant amount, 79 ppb, was transported horizontally and vertically out of the control volume before it could be oxidized. A small amount of the emitted NO underwent dry deposition. This left a total of 142.1 ppb of “new NO” that is subject to chemical processes. The term “new NO” means NO that had not been oxidized by radicals to NO₂

at least once. NO that results from NO₂ photolysis in which the NO₂ was oxidized from NO (as opposed to being emitted as NO₂) is called ‘re-created NO’. In this case, a relatively small amount of re-created NO was produced, only 20.5 ppb in 10 hours. Of the 162.6 ppb of total NO oxidized, 42.3 ppb was oxidized by HO₂, 26.8 ppb by RO₂, and 91.4 ppb by “old O₃”. The term “old O₃” refers to ozone that was not created in the control volume by NO₂ photolysis, e.g., O₃ that was transported into the volume or that was entrained into the volume as the mixing height increased. In these chemical oxidation steps, some side reactions remove the NO as, for example, organic nitrates. Therefore only 160.7 ppb of NO₂ was produced by chemical processes and 1.9 ppb of nitrates was created. To this chemically oxidized amount is added the 43.2 ppb of “new NO₂” that was present initially or was emitted into the control volume. This resulted in a total of 203.9 ppb of available NO₂ in the control volume; it is subject to three processes: chemical reaction, physical processes, and accumulation in the control volume (i.e., remaining as final NO₂ concentration at hour 18).

The bulk of the 203.9 ppb of NO₂ was lost by physical processes (140.2 ppb transported and 2.1 ppb dry deposited) and 21.9 ppb remained in the control volume at hour 18. Thus, 39.7 ppb NO₂ underwent chemical reactions in which 13.5 ppb were lost to termination reactions and 26.9 ppb were photolyzed to produce NO to be reused again in the propagation cycle (called “re-created NO”). The diagram also shows the formation of 23.4 ppb ozone produced via chemical production (bottom center of diagram).

Figures 2-5 and 2-6 are the templates for interpreting the integrated reaction rate data. The numerical data in these figures are computed by the PAPPT software that will be described below. Other important parameters such as VOC to NO_x ratios, VOC

composition, and the amount of ozone produced by each VOC, are also calculated for the control volume. Examples will be given below.

The time series and reaction cycles diagram shown in Figures 2-4, 2-5, and 2-6 summarize the type of information that can be created by the PAPPTs; these analysis tools have been used within 3-D gridded photochemical models for a number of purposes. For example, process analysis has been used to study the inhibition of odd oxygen production in the Carbon Bond (CBIV) chemical mechanism (Tonnesen and Jeffries, 1994), to compare two photochemical reaction models, CBIV and SAPRC90, in a Lagrangian model (Jeffries and Tonnesen, 1994), and to assess the sensitivity of ozone to changes in model grid resolution (Jang *et al.*, 1995a,b). The goal of this work was to extend the process analysis post processing tools (PAPPT) so that control volumes are able to track changes in mixing height dynamically. This modified process analysis tools were integrated into the post processing of results from CAMx. The resulting PAPPTs were used in the analysis of air quality data from Central California.

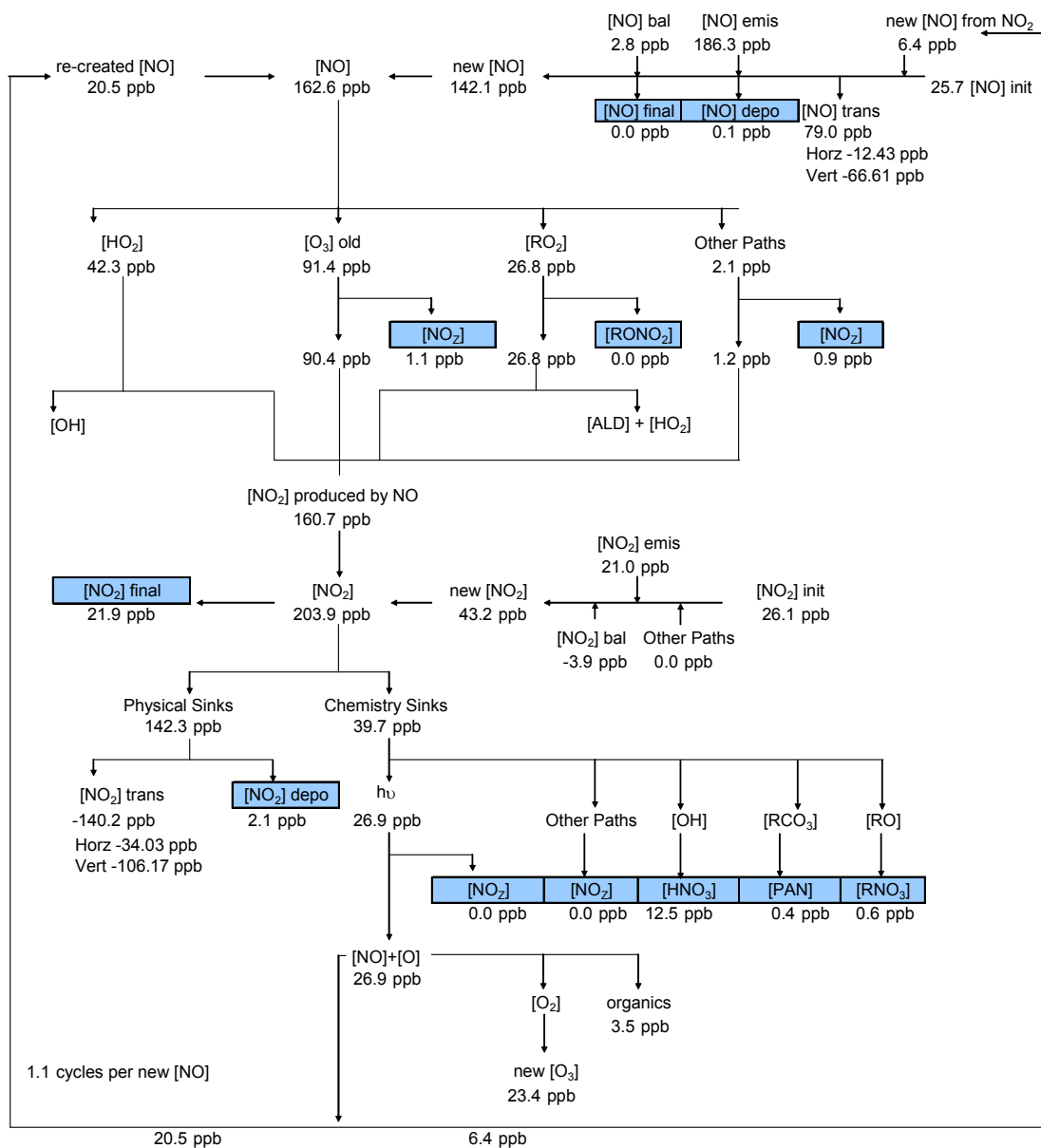


Figure 2-6. Expanded NO and NO₂ cycles diagram produced by post-processing data in the Integrated Reaction Rate (IRR) file. Analysis was limited to the time period 08 – 18 hours. The diagram summarizes the physical and chemical processes for NO and NO₂ and shows ozone formation process.

2.2 METHODOLOGY

All process analysis post-processing begins with the definition of a control volume; the post processing tools (PAPPTs) aggregate and merge concentrations and process rates within the requested control volume and write the files used to produce the time series, pie charts, bar charts, and cycle diagrams. In previous process analysis applications, the control volume was fixed over the time of the analysis. The CAMx version of the PAPPT developed in this work improves on the process analysis in previous applications by accounting for changes in concentrations and process rates within the control volume as it grows in vertical extent to account for the evolution of the mixing height within the model.

The mixing height is tracked by examining the vertical layer interface diffusivities or “ K_v ” values used by the photochemical model to compute layer to layer exchange. These values vary spatially and temporally due to the heterogeneity of terrain and meteorological conditions. A program was written to extract from the photochemical model input files the K_v parameter for each layer interface, for each hour, for each grid cell within the control volume.

Table 2-1 provides an example of the K_v parameter values at CAMx vertical layer heights for hour 11 in the Fresno region; each column represents a grid cell within the PAPPT control volume and each row a vertical layer in the model. In this example, there is a sharp decrease in the values of K_v , by two orders of magnitude, at vertical layers 8 and above. Therefore, the mixing height was determined to extend through layer 7. This analysis is conducted for each hour, resulting in an evolution of mixing heights, as shown

in Figure 2-3. The x-axis in the Figure represents the hours of the simulation day and the modeling height is shown vertically. The red line is the mixing height, the light blue and yellow boxes show the layers that were entrained or detrained, respectively, during each hour. For example, the mixing height increased from layer 5 in hour 9 to layer 7 in hour 10. To account for the changes in vertical height the control volume is separated into two volumes. These two volumes consist of a lower control volume at the height from the previous hour (e.g. layer 5 for the 10 a.m. hour in Figure 2-3) and an entrained control volume extending to the new height (e.g. layers 6 and 7 for the 10 a.m. hour in Figure 2-3). When the mixing height is falling, for example from hour 16 to hour 17, the lower control volume is at the new mixing height and represents the total control volume. In this case, the detrained volume is the volume denoted by the yellow box. The entrained/detrained control volume is calculated by:

$$V_u = |V_{T,t-1} - V_{T,t}| \text{ (Equation 2-2)}$$

where V_u is the volume that is entrained/detrained, $V_{T,t-1}$ represents the total volume in the previous hour, and $V_{T,t}$ the total volume in the current hour.

		Grid Cell (x,y)				
Layer	Top of Layer (m)	(108:068)	(109:068)	(110:068)	(111:068)	(112:068)
13	1561	0.1	0.1	0.1	0.1	0.1
12	127	0.1	0.1	0.1	0.1	0.1
11	981	0.1	0.1	0.1	0.1	0.1
10	794	0.1	0.1	0.1	0.1	0.1
9	638	0.1	0.1	0.1	0.1	0.1
8	506	0.1	0.1	0.1	0.1	0.1
7	397	9.73	8.14	5.24	1.44	2.58
6	306	24.34	22.61	19.11	12.28	14.99
5	229	34.52	33.26	30.61	25.02	27.33
4	160	37.4	36.67	35.14	31.78	33.18
3	112	33.57	33.25	32.59	31.11	31.73
2	68	24.54	24.46	24.31	23.96	24.11
1	30	12.16	12.16	12.16	12.15	12.15

Table 2-1. Vertical mixing parameters (m²/s) for multiple vertical layers for five different horizontal grid cell locations in the CAMx air quality simulation for Fresno, CA. The data are for September 18, 2000 Hour 11.

To track mixing height changes properly, PAPPT software creates separate data sets for each of the lower and entrained/detrained control volumes. These separate data sets contained all the critical pollutant concentration and process rates specific to each control volume. $C_{l,t}$, $C_{u,t}$ are the pollutant concentrations at the end of the hour for the lower and entrained/detrained (upper) control volumes. $V_{l,t}$, $V_{u,t}$ are the lower and entrained/detrained control volumes for the current hour. The concentrations in the lower and entrained/detrained volumes are calculated by adding the mass in each model layer (calculated from layer concentrations) contained in the control volume, and then dividing by the control volume. The concentration for the total control volume for the current hour can be calculated with the following equation:

$$C_{T,t} = C_{l,t} * (V_{l,t}/V_{T,t}) + C_{u,t} * (V_{u,t}/V_{T,t}) \text{ (Equation 2-3)}$$

When the mixing height is rising the lower and entrained control volumes contribute to the final concentration for the total control volume. For example, in hour 10, the mixing height had risen from 228 m to 396 m (layer 5 to layer 7). The lower control volume has a concentration of 42.6 ppb and the entrained control volume has a concentration of 57.1 ppb. The concentration for the total control volume can be calculated:

$$C_{T,t} = 42.6 \text{ ppb} * 0.58 + 57.1 \text{ ppb} * 0.42 = 48.7 \text{ ppb}$$

where $C_{T,t}$ is the concentration for the total control volume in the current hour. When the mixing height is falling there is no contribution to the concentration in the control volume from the detrained control volume. The detrained control volume is not included in the total volume so in these calculations $V_{l,t}$ is equal to $V_{T,t}$. In the Fresno case study, the mixing height fell from a height of 981 meters at hour 16 to 30 meters at hour 17. In this example, the lower control volume has a final ozone concentration, $C_{l,t}$ of 45.1 ppb at hour 17. Therefore, the final concentration for the total control volume is:

$$C_{T,t} = 45.1 \text{ ppb} * 1 + 0 = 45.1 \text{ ppb}$$

The process analysis post-processing tool also aggregates the various processes that are sinks and sources for pollutants at every hour. These processes include entrainment/detrainment ($\Delta C_{\text{entrain},t}$, $\Delta C_{\text{detrain},t}$), chemistry ($\Delta C_{\text{chemistry},t}$), vertical transport ($\Delta C_{\text{vertical},t}$), horizontal transport ($\Delta C_{\text{horizontal},t}$), and deposition ($\Delta C_{\text{deposition},t}$).

The PAPPT aggregates and reconciles changes to pollutant concentrations due to chemistry, $\Delta C_{chemistry,t}$. These changes are calculated by multiplying the chemical process rates from the IPR file by the time step (1 hour). These values are then multiplied by the layer volume and summed for all layers in the lower and entrained/detrained control volumes and then converted back into concentrations, by dividing by the total control volume. When the mixing height is rising, the total concentration change due to chemistry is the sum of the chemistry changes in the lower and entrained control volumes. For example, in the Fresno case, the mixing height rose from a height of 396 meters at hour 10 to 505 meters at hour 11. At hour 11 the lower control volume added 4.1 ppb ($\Delta C_{chemistry,l,t}$) of ozone through chemical processes and the entrained control volume added 8.97 ppb ($\Delta C_{chemistry,u,t}$). The contribution to ozone by chemical processes in the total control volume can be calculated as follows:

$$\Delta C_{chemistry,t} = \Delta C_{chemistry,l,t} * (V_{l,t} / V_{T,t}) + \Delta C_{chemistry,u,t} * (V_{u,t} / V_{T,t}) = 4.1 \text{ ppb} * 0.78 + 9.0 \text{ ppb} * 0.22 = 5.2 \text{ ppb} \text{ (Equation 2-4)}$$

where $\Delta C_{chemistry,l,t}$ is the chemical contribution from the lower control volume in the current hour, and $\Delta C_{chemistry,u,t}$ the chemical contribution from the entrained control volume in the current hour. For a falling mixing height there are no contributions from the detrained control volume, $\Delta C_{chemistry,u,t}$, and as described previously, $V_{l,t}$ is equal to $V_{T,t}$. In the Fresno case study, the mixing height fell from a height of 981 meters at hour 16 to 30 meters at hour 17. At hour 17 the lower control volume consumed 87.2 ppb ($\Delta C_{chemistry,l,t}$) of ozone through chemical processes. Therefore the contribution to ozone by chemical processes in the total control volume can be calculated as follows:

$$\Delta C_{chemistry,t} = -87.2 \text{ ppb} * 1 + 0 = -87.2 \text{ ppb}$$

When the mixing height rises, pollutants in the entrained control volume are added to the total control volume. The PAPPT tracks the amount of pollutants that are entrained and calculates their contribution to species concentrations in the total control volume. For example, from Figure 2-3, in hour 10, the mixing height had risen from 228 m to 396 m (layer 5 to layer 7). To calculate the change in concentration of ozone the concentration from the previous hour in the entrained volume is needed. In this example, the entrained control volume had an ozone concentration of, $C_{u,t}$, of 62.3 ppb. The concentration change due to entrainment, $\Delta C_{entrain,t}$, in the total control volume can be calculated:

$$\Delta C_{entrain,t} = C_{u,t} * (V_{u,t} / V_{T,t}) = 62.3 \text{ ppb} * 0.42 = 26.2 \text{ ppb} \text{ (Equation 2-5)}$$

In a similar way, when the mixing height is falling, the PAPPT tracks the amount of pollutants lost due to detrainment.

The deposition sink of pollutants is calculated for the total control volume using the following equation:

$$\Delta C_{deposition,t} = C_{deposition,l,t} * (V_{l,t} / V_{T,t}) \text{ (Equation 2-6)}$$

where $C_{deposition,l,t}$ is the deposition contribution in the lower control volume at the current hour. The deposition sink is always zero in the entrained/detrained control volume because these volumes are aloft. These concentration changes are calculated by using a deposition velocity, converted to a deposition flux using the CAMx grid cell

concentrations. In our example, the mixing height rose from a height of 396 meters at hour 10 to 505 meters at hour 11. $C_{deposition,l,t}$ for ozone at hour 11 was a loss of 1.3 ppb. The concentration change of ozone due to deposition, $\Delta C_{deposition,t}$, in the total control volume at hour 11 can be calculated:

$$\Delta C_{deposition,t} = -1.3 \text{ ppb} * 0.78 = -1.0 \text{ ppb}$$

The PAPPT also calculates vertical and horizontal transport rates. The code retrieves vertical transport rates ($\Delta C_{vertical,t}$) from the top horizontal face of the control volume. In the CAMx model the total vertical transport rates are the result of a combination of resolved vertical advection and mass exchange across layer interfaces (ENVIRON, 2004). When the mixing height is falling from one hour to the next the vertical transport rate is extracted from the lower control volume. However, when the mixing height is rising, the vertical transport rate of the entrained (upper) control volume is used.

The original version of the process analysis post-processing tools required that the horizontal domain of the control volume have a rectangular shape. The extraction program created for this study allowed the horizontal shape of the PAPPT domain to be non-rectangular. This is useful in excluding unwanted grid cells and minimizing the dilution of model phenomena in the control volume. To illustrate the types of calculations involved in non-rectangular control volumes, consider a horizontal cross section from a 3-D grid model, shown in Figure 2-7. To calculate horizontal advection ($\Delta C_{horizontal,t}$), the PAPPT retrieves data from each face of the grid cells on the outer perimeter of the control volume. These faces are identified by the dark arrows in Figure 2-7. The PAPPT

calculates net horizontal advection by multiplying the wind flow by the concentrations of species in the upwind grid cells. Advection out of the control volume is designated as a negative contribution. These fluxes are summed for all faces of the control volume to calculate the net concentration change due to horizontal transport. Once the vertical and horizontal dimensions of the PAPPT box were determined, the PAPPT generated the time series and cycle diagrams representing the physical and chemical processes occurring within the box.

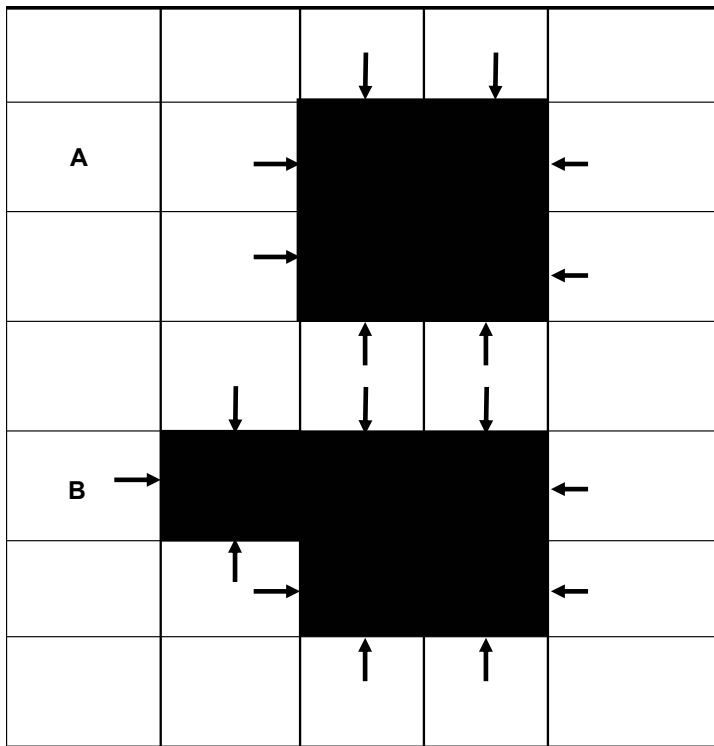


Figure 2-7. A horizontal cross section from a 3-D grid model. The darkened grid cells are examples of (A) rectangular and (B) non-rectangular control volumes.

2.3 RESULTS AND DISCUSSION

The Process Analysis Post-Processing Tools, modified in this work to track mixing height changes dynamically and to allow for horizontally irregular control volumes, were applied to 3-D photochemical modeling performed for central California. The modeling was performed with the Comprehensive Air Quality Model with extensions version 4.03 (ENVIRON, 2004). The modeling episode encompassed September 16-20, in 2000 and was part of the Central California Ozone Study (CCOS). The 2000 Central California Ozone Study (CCOS) was a multimillion-dollar field study designed to characterize emissions, meteorology, and atmospheric processes affecting the production and fate of ozone in central California (Tesche *et al.*, 2004). Anthropogenic emission input files for the model were estimated by the California Air Resources Board (ARB) using portions of the legacy EMS-95 regional modeling system (Wilkinson, 1994). For biogenic sources, the ARB used the Biogenic Emissions Inventory Geographic Information System (BEIGIS) (ARB, 2001). The Pennsylvania State University / National Center for Atmospheric Research Mesoscale Meteorological model (MM5) was used to develop the meteorological and air quality modeling data sets for the episode (NCAR, 2004). Detailed descriptions of model inputs used in the MM5 model are found in Tesche *et al.*, 2004. During this episode the CAMx model significantly underestimates daily maximum ozone across the CCOS domain for all modeling days. The model underestimates the daily maximum unpaired peak ozone by -17.1% to -42.7% in the entire CCOS domain (Tesche *et al.*, 2004). The accuracy of peak prediction over all monitors ranged daily from 14.9% to 24.3% with a mean for the episode of 21.2%. The mean normalized bias ranged from 0.6% to -10.7% across the entire CCOS domain. However, within the San Joaquin Valley, the normalized daily biases were larger, ranging

between -12.2% and -31.1%. The work presented below reports how the PAPPT can be used to diagnose the reasons for model underprediction.

A 4 x 5 control volume of 4 km grid cells (16 km by 20 km), Figure 2-2, centered on the Fresno urban core was chosen as the PAPPT control volume for the central California case study. This control volume was chosen so that the PAPPT could diagnose the model underprediction of ozone in that area. First, the extracted modeled K_V values were used to determine the mixing height of the control volume, as illustrated in Figure 2-3. It was assumed that the mixing height would include all layers with mixing parameter values greater than $0.1 \text{ m}^2/\text{s}$. From midnight until 8 a.m. the mixing height remained in the first layer (lowest 30 m). Starting at 9 a.m. the mixing height rises to a maximum height of 981 m (layer 11) at 2 p.m. The mixing height remained at 981 m until 4 p.m. There is a collapse of the mixing height at 5 p.m. to the first layer (30 m) and the mixing height remains there, with the exception of hours 21-22, for the rest of the simulated day.

Figure 2-4 shows an ozone time series plot for the Fresno simulation. The peak predicted ozone concentration was 72 ppb with net chemistry (production – consumption) only generating a maximum of 6 ppb ozone/hr. Significant amounts of ozone are lost to reactions with fresh NO molecules forming NO_2 . The data in Figure 2-6 provide details of the chemical pathways in the NO propagation cycle. The majority of the NO (186.3 ppb) is emitted into the control volume with a relatively small amount (20.5 ppb) resulting from propagation reactions. There are losses of 79 ppb of NO as it is transported out of the control volume. A total of 42.3 ppb of the NO was oxidized by HO_2 , 26.8 ppb by RO_2 , and 91.4 ppb by O_3 . This resulted in a total of 160.7 ppb of NO_2 produced by

chemical processes with an additional 43.2 ppb of NO₂ emitted and present initially in the control volume. It is clear from the extent of these reaction pathways that the oxidation of NO by O₃ dominates. The bulk of the 203.9 ppb of NO₂ are lost by transport (140.2 ppb) and deposition (2.1 ppb) processes. Of the remaining NO₂ molecules 13.5 ppb are lost to termination reactions and 26.9 ppb are photolyzed to produce NO to be reused again in the propagation cycle.

Losses due to chemistry are the most significant process sink for ozone with loss rates of up to 87 ppb/hr, as shown in Figure 2-4. As the ozone is titrated away in the lower layers, a vertical concentration gradient of ozone is formed. As a result, ozone diffuses into the control volume from above the mixed layer at rates nearly identical to the chemical consumption processes. This leaves ozone concentrations near background levels in the control volume.

Figure 2-5 is an ozone production diagram including radical and NO_x cycles for hours 8-18 for this region. The upper left corner shows the concentration of new OH radicals from the photolysis of aldehydes and O₃, 14.7 ppb, and the radical chain length was 3.47. In this example, this means that 36.2 ppb of OH is reformed over the course of the 10-hour period. Combined, the reformed OH and the new OH generate 51.0 ppb of OH that reacts. Of the 51.0 ppb total that reacts, 36.2 ppb (propagation rate 71.2%, $P_{OH} = 0.712$) reacts and is regenerated. Although the limited numbers of new OH radicals that are formed are used efficiently, there are insufficient VOCs to convert significant amounts of NO to NO₂, which in turn will generate O₃ and more new OH. The simulation reacted only 46.8 ppb of VOCs over 10 hours, resulting in 70 ppb of NO to NO₂ conversions. The majority of NO to NO₂ conversions, 90.2 ppb, came by reactions with

ozone. In the simulation, the NO chain length was 1.14, evidence of a radical limited environment where NO molecules are used only once. Only 27 ppb of NO₂ is photolyzed and O₃ is generated at a ratio of $([O_3]_p)/[NO_2]_{hv}$ of approximately 0.9.

With insufficient radicals to propagate the NO cycle, significant amounts of NO₂ are transported out of the control volume. Figure 2-8 shows a time series plot for NO₂. Over the course of the day, up to 78 ppb/hr and 28 ppb/hr of NO₂ are being transported vertically and horizontally, respectively, out of the process control volume. The large amounts of ozone reacting with NO and the amount of NO and NO₂ transported out of the control volume are evidence of radical limited conditions where insufficient radicals exist to compete with the titration processes.

Further evidence of radical limited conditions is provided by VOC to NO_x ratios. Figure 2-9 shows the VOC to NO_x ratios for the control volume. In Figure 2-9, one line shows the VOC to NO_x ratio based on cell concentrations, while a separate line gives ratios based on cell emissions. The modeled VOC/NO_x ratios are consistently higher than the inventory ratios because the average lifetimes of VOCs are longer than that of NO_x. This difference shows the importance of comparing observed VOC/NO_x ratios to modeled ratios, rather than inventory ratios. In addition, separate lines represent ratios with the total VOC (TVOC) and anthropogenic VOC (AVOC). The ratios based on cell emissions during daylight hours were in the range of 2.5 - 3; values indicative of a radical limited atmosphere, consistent with the data extracted from the “reaction cycle” diagram in Figure 2-5.

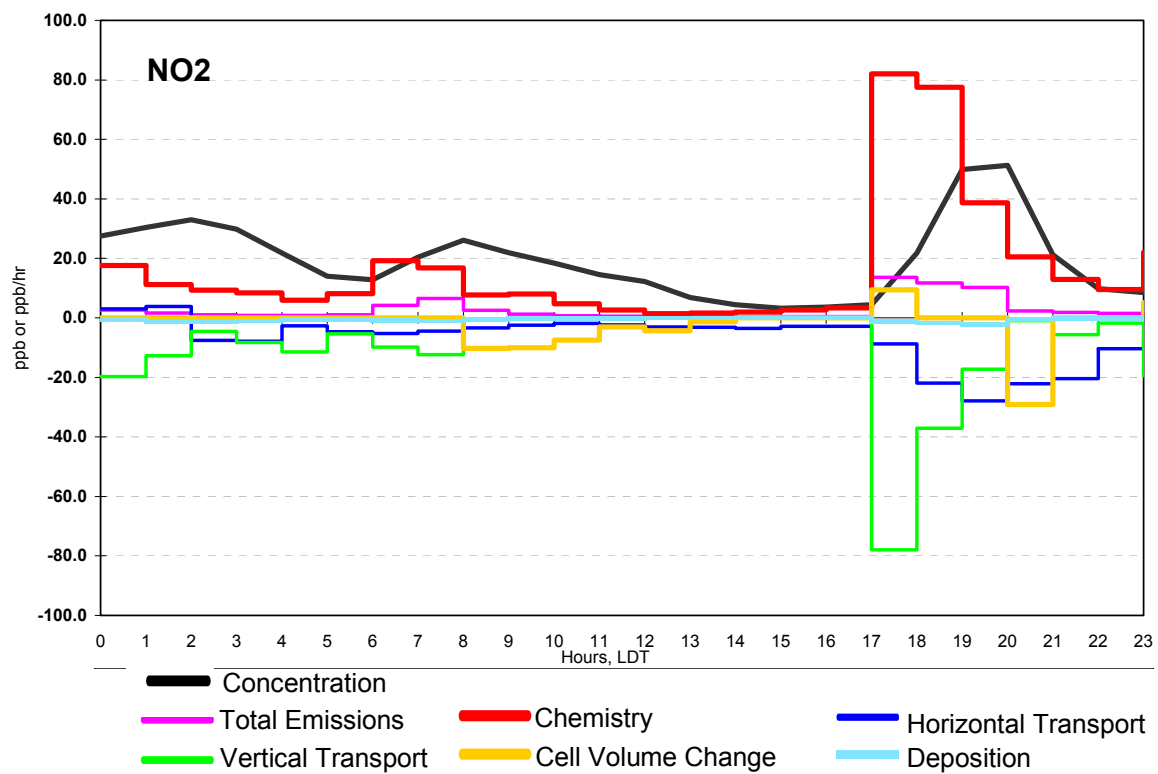


Figure 2-8. Time series for NO₂ that shows the process rates and model concentrations for the Fresno California control volume on September 18, 2000 for the base simulation.

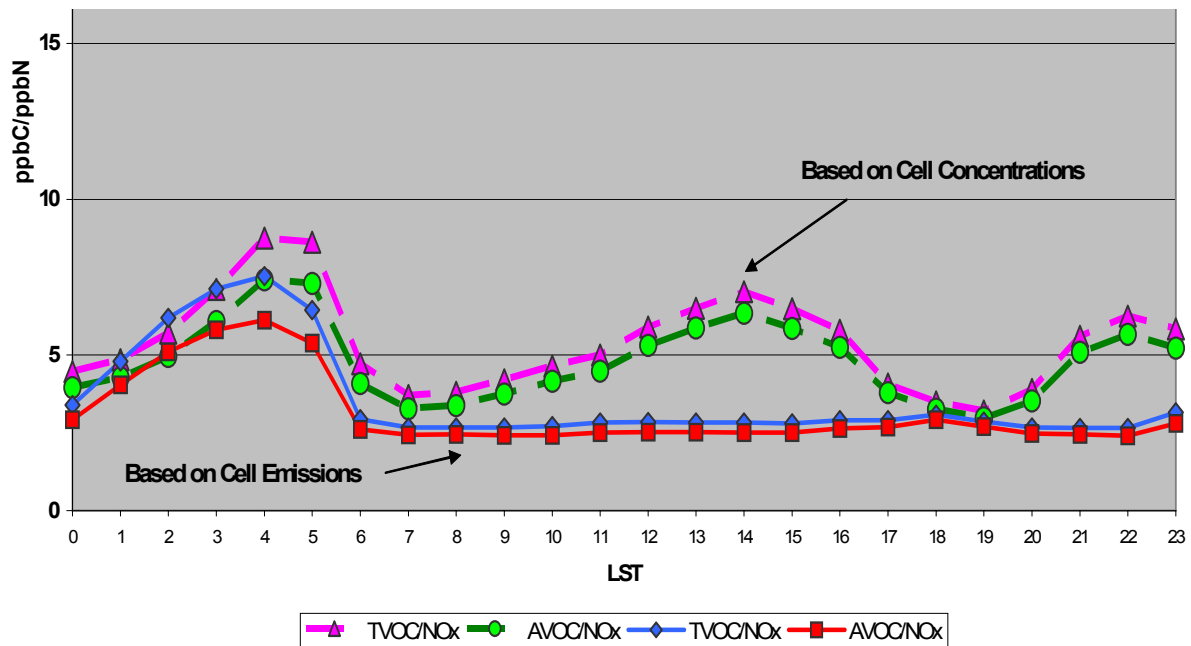


Figure 2-9. Time series of the VOC to NOx ratios for the Fresno region control volume on September 18, 2000 for base simulation.

Further analyses of the radical limited conditions in Fresno were performed by testing the sensitivity of ozone formation to VOC additions to the system. In the sensitivity analysis, all VOC emissions were tripled throughout the entire modeling domain (185 by 185 grid cells). Figure 2-10 shows an hourly ozone time series plot for the simulation with tripled VOC emissions. The peak ozone concentration increased to 98 ppb and peak chemical generation rates increased to 25 ppb/hr. Figure 2-11 shows the VOC to NOx ratios for the control volume. The ratios based on cell emissions during daylight hours increased to a range of 8 - 9; values indicative of NOx limited conditions. The “reaction cycle” diagram in Figure 2-12 presents further information on the changes to ozone chemistry when VOC emissions are increased. The clearest indication of

changes is in the OH cycle portion of the diagram. New OH radicals from the photolysis of aldehydes and O₃ have nearly doubled to 25.4 ppb. The radical chain length also increased to 4.41. The increased VOC simulation predicted nearly three times more reactions with VOCs than the base case, 119.3 ppb, resulting in 167 ppb of NO to NO₂ conversions. The majority of NO to NO₂ conversions now comes from VOC chemistry instead of reactions with ozone. The increased reactivity generates 110 ppb of NO₂ that are available to photolyze and generate ozone. These results in nearly a five fold increase in the amount of ozone produced chemically, to 104 ppb.

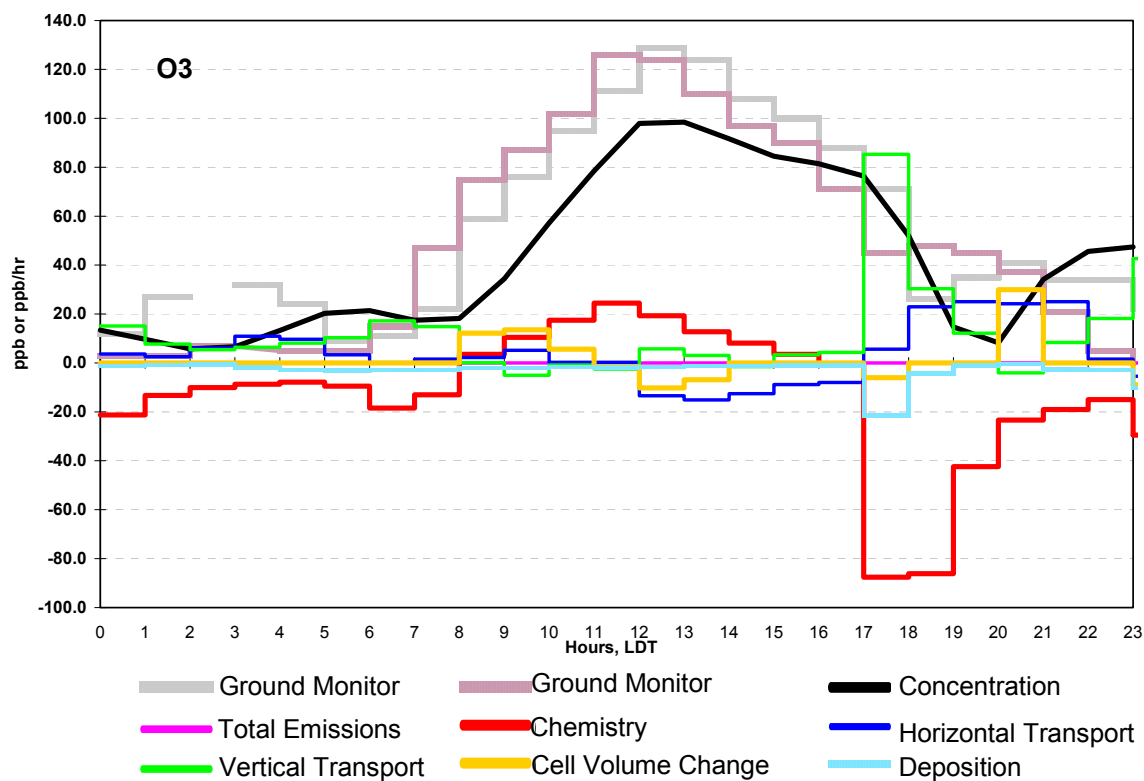


Figure 2-10. Example of a time series ozone plot that illustrates the process rates and model concentrations versus time for the Fresno California region on September 18, 2000. In this simulation all VOC emissions were tripled.

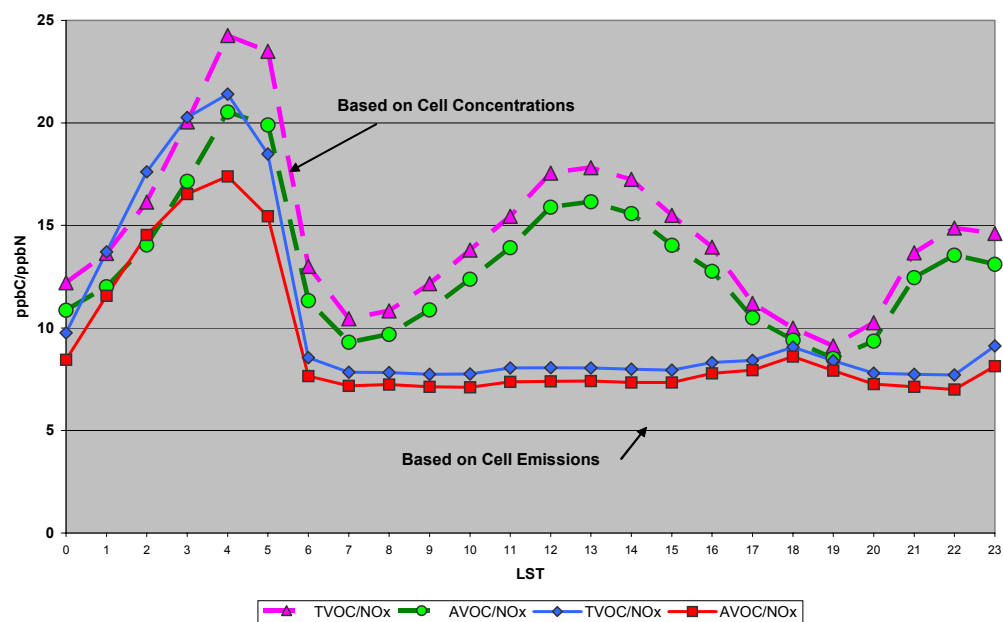


Figure 2-11. VOC to NOx ratios for the Fresno region control volume for September 18, 2000 where all VOC emissions were tripled from the base simulation.

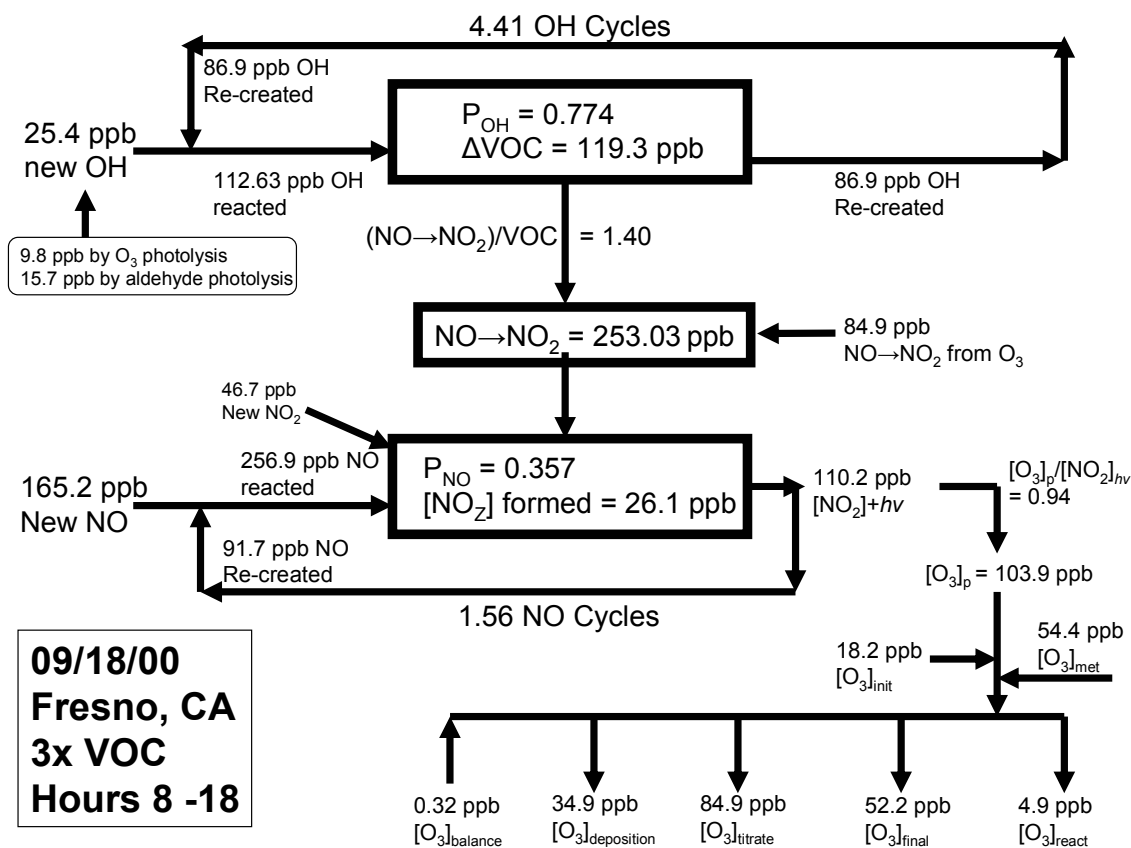


Figure 2-12. Reaction cycles diagram summarizing the cycling of oxides of nitrogen, the cycling of hydroxyl radical, and ozone formation processes. This is for the Fresno region with tripled the VOC emissions of the base simulation.

2.4 CONCLUSION

The PAPPT revealed the processes that contributed to model underprediction of ozone generation and accumulation in the Fresno area. In the Fresno model, the lack of ozone accumulation was linked to considerable ozone reaction with fresh NO molecules, forming NO₂, which subsequently advected out of the region. These losses due to chemical titration are the most significant process sink for ozone, with rates up to 87 ppb/hr. The large amounts of ozone reacting with NO and the amount of NO and NO₂ transported out of the control volume are evidence of radical limited conditions where insufficient radicals exist to compete with the titration processes. Further indications of radical limited environment are given by the VOC/NO_x ratios based on cell emissions during daylight hours, which were in the range of 2.5 - 3. Only 27 ppb of NO₂ is photolyzed and subsequently generates 23 ppb of O₃. When VOC emissions were tripled for this simulation, the peak ozone concentration increased from 72 ppb to 98 ppb, and peak chemical generation rates increased from 6 ppb/hr to 25 ppb/hr. The VOC/NO_x ratios based on cell emissions during daylight hours increased to a range of 8 - 9; values indicative of NO_x limited conditions. This case study of air quality modeling illustrates the value of the PAPPT in diagnosing model performance. Without the information generated by the PAPPT, it would be difficult to infer why the model is not generating observed levels of ozone.

2.5 ACKNOWLEDGEMENT

The authors thank Dennis McNally and Tom Tesche of Alpine Geophysics, LLC, who performed the CAMx simulations described here as part of a larger Central California Ozone Study. They also produced the CAMx Process Analysis output files that were subsequently post-processed and analyzed by the authors. The authors also thank ENVIRON International for support and cooperation in applying the process analysis tools to the CCOS. The authors also thank Byeong-Uk Kim, Ph.D candidate, University of North Carolina at Chapel Hill for his assistance in this project.

2.6 REFERENCES

- Russell A., Dennis R. 2000. "NARSTO critical review of photochemical models and modeling." *Atmospheric Environment* 34(12-14): 2283-2324.
- Jang J. C., Jeffries H. E., Byun D., Pleim J. E. 1995a. "Sensitivity of Ozone to Model Grid Resolution: Part I. Application of High Resolution Regional Acid Deposition Model." *Atmospheric Environment* 29(21): 3085-3100.
- Jang J. C., Jeffries H. E., Tonnesen S. 1995b. "Sensitivity of Ozone to Model Grid Resolution: Part II. Detailed Process Analysis for Ozone Chemistry." *Atmospheric Environment* 29(21): 3101-3114.
- Jeffries H. E., Tonnesen S. 1994. "A Comparison of Two Photochemical Reaction Mechanisms Using a Mass Balance Process Analysis." *Atmospheric Environment* 28(18): 2991-3003.
- Jeffries H. E. 1995. "Photochemical Air Pollution. Chapter 9 in Composition, Chemistry, and Climate of the Atmosphere." Ed. H.B. Singh, Van Nostand-Reinhold, New York, ISBN 0-442-01264-0
- Tonnesen S., Jeffries H. E. 1994. "Inhibition of Odd Oxygen Production in Carbon Bond IV and Generic Reaction Set Mechanisms." *Atmospheric Environment* 28(7): 1339-1349.
- Wang Z. 1997. "Comparison of Three Vertical Diffusion Schemes in The SARMAP Air Quality Model with Integrated Process Rate Analysis Method and Continuous Process Composition and Source Receptor Methodology." PhD Dissertation, University of North Carolina at Chapel Hill.
ftp://airsite.unc.edu/PDFS/ESE_UNC/Students/PhDThesis/Wang/

Systems Applications International (SAI). 1999. "User's Guide to the Variable Grid Urban Airshed Model (UAM-V)." <http://www.uamv.com/overview.htm>

Wang Z., Langstaff J. E., Jeffries H. E. 1995. "The Application of the Integrated Process Rate Analysis Method for Investigation of Urban Airshed Model (UAM) Sensitivity to Speciation in VOC Emissions Data." Air & Waste Management Association conference, San Antonio, TX.

Wang Z. 1997. "Comparison of Three Vertical Diffusion Schemes in The SARMAP Air Quality Model with Integrated Process Rate Analysis Method and Continuous Process Composition and Source Receptor Methodology." PhD Dissertation, University of North Carolina at Chapel Hill. ftp://airsite.unc.edu/PDFS/ESE_UNC/Students/PhDThesis/Wang/

Wang Z., Jeffries H. E. 1998. "SARMAP Air Quality Model (SAQM) Integrated Process Rate Analysis Method User's Guide." California Air Resources Board. <http://www.arb.ca.gov/ei/sarmap.htm>

Gibson G. L. 1999. "Science Algorithms of the EPA Models-3 Community Multiscale Air Quality (CMAQ) Modeling System. Chapter 16 Process Analysis." D. W. Byun, Ching, J.K.S. (Eds.). U. S. Environmental Protection Agency, <http://www.epa.gov/asmdnerl/CMAQ/ch16.pdf>

ENVIRON. 2004. CAMx Users Guide, v4.00. 2004. www.camx.com

Yarwood, G. 2004. Personal Correspondence with ENVIRON Holdings, Inc.

Tesche T. W., McNally D. E., Wilkinson J. G., Jeffries H. E., Kimura Y., Emery C., Yarwood G., Souten D. R. 2004. "Evaluation of the 16-20 September 2000 Ozone Episode for use in 1-HR SIP Development in the California Central Valley." Alpine Geophysics

Wilkinson J. G. 1994. "Technical Formulation Document: SARMAP/LMOS Emissions Modeling System (EMS-95)." Alpine Geophysics

Air Resources Board (ARB). 2001. "Protocol for Photochemical Air Quality Modeling for the San Joaquin Valley Severe-Area Ozone attainment Demonstration Plan." Sacramento, CA., California Air Resources Board
<http://www.arb.ca.gov/homepage.htm>

[National Center for Atmospheric Research](http://www.mmm.ucar.edu/) (NCAR). 2004. MM5 Community Model, Pennsylvania State University / National Center for Atmospheric Research.
<http://www.mmm.ucar.edu/>

Chapter 3: Ozone Formation resulting from episodic emissions of highly reactive volatile organic carbons in Houston Texas

3.1 INTRODUCTION

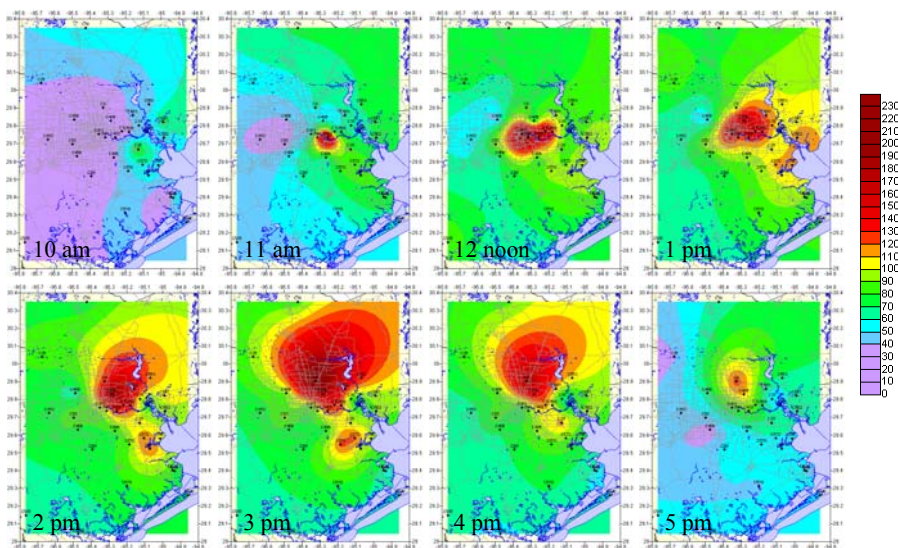
Recently compiled data in southeast Texas indicate that industrial emissions of volatile organic compounds (VOCs) from non-Electrical Generating Units (NEGU) can have significant temporal variability (Murphy and Allen, 2005). Specifically, short duration releases, lasting from hours to days, can increase annual average emission rates for individual facilities by a factor of 10-1000. At any single facility, events of this magnitude occur only a few times per year, but because of the large number of chemical manufacturing and petroleum refining facilities in the Houston-Galveston area, reported events of this magnitude occur more than 1000 times per year. These events are typically one to a few hours in duration and are comprised mainly of ethylene, propylene, butylenes or 1,3 butadiene. These chemicals have been classified by the State of Texas as highly reactive volatile organic compounds (HRVOC). Episodic emissions of other species, particularly alkanes and aromatics, also are reported.

Data documenting these short-term releases include an industry reported emission event database (Murphy and Allen, 2005), air pollutant measurements made by aircraft (Kleinman *et al.*, 2002), and air pollutant measurements made by ground monitors. Figure 3-1 shows a case study of one emission event detected by ground monitors. On October 23, 2003 at 11 a.m., a large increase in ozone concentration, exceeding 200 ppb, was observed at the Clinton ground monitoring site, located at the intersection of Interstate 10 and Interstate 610 east of Houston. Figure 3-1a shows a contour map of ozone concentrations from 10 a.m. until 5 p.m. The Figure shows the start of the ozone

event at 11a.m., when concentrations in excess of 200 ppb were isolated at the Clinton monitor. These high concentrations subsequently spread over a large region. Figure 3-1b shows the ozone concentration data and VOC concentrations weighted by hydroxyl radical reactivity, recorded at the Clinton site. Unusually high hydrocarbon concentrations (represented in units of reactivity) were detected at the Clinton site at the start of the event (Figure 3-1b).

While some short duration emission events, such as the case study illustrated in Figure 3-1, clearly cause very high ozone concentrations, other events lead to much less photochemical activity. The goals of this work are to use the process analysis post processing tools (PAPPTs) described in the previous chapter to examine how the characteristics of the emission events impact ozone formation and accumulation processes in the Houston-Galveston area. Specifically, the effects of the composition of the emissions and plume trajectories will be examined. Emission events involving ethylene, propylene, n-pentane and xylene will be modeled and plume processing over a NO_x rich environment will be contrasted with plume processing over water.

a.) Contour Maps Showing the Progression of High Ozone on 10-23-03



b.) Ozone Concentration (5 Min. Data) and VOC Reactivity V.s. Time at Clinton C403 for 10-23-03

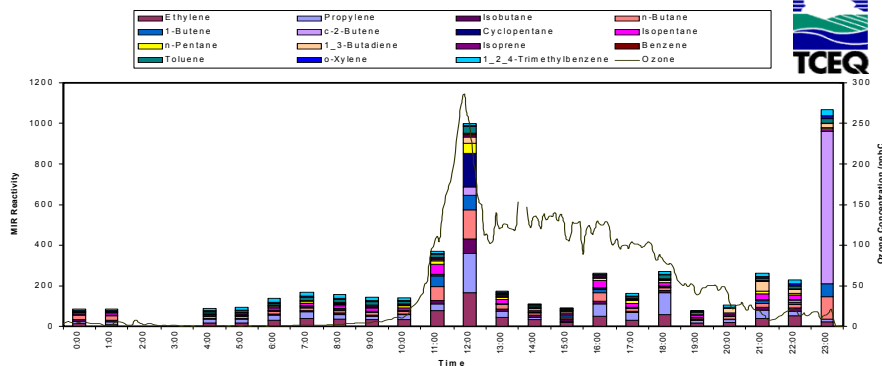


Figure 3-1. (a) Contour map of ozone concentrations from 10 a.m. until 5 p.m. on 10/23/2003. The figure shows the start of the ozone event at 11 a.m. when concentrations in excess of 200 ppb were recorded at the Clinton monitor. These high concentrations subsequently spread over a large region. (b) Ozone concentration data and VOC reactivity recorded at the Clinton monitor site. High hydrocarbon concentrations (represented in units of reactivity) were detected at the Clinton site at the start of the event (TCEQ, 2004).

3.2 METHODOLOGY

Model simulations were performed using the Comprehensive Air Quality Model, with extensions, version 4.03, referred to in this work as CAMx 4.03 (<http://www.camx.com>). CAMx is an EPA-approved eulerian photochemical grid model that simulates emission, chemical transformation, horizontal advection and diffusion, vertical transport and diffusion, dry deposition, and wet deposition of species in the atmosphere. CAMx was selected for this work because it is currently being used by the State of Texas for attainment demonstrations in areas that have violated the National Ambient Air Quality Standards for ozone and because of the availability of Process Analysis tools within CAMx; these tools are described in the previous chapter.

The State of Texas has developed an August 22 - September 6, 2000 photochemical modeling episode for evaluating its air quality management plans for southeast Texas. The modeling domain was a nested regional/urban scale 36-km/12-km/4-km/1km grid, shown in Figure 3-2.

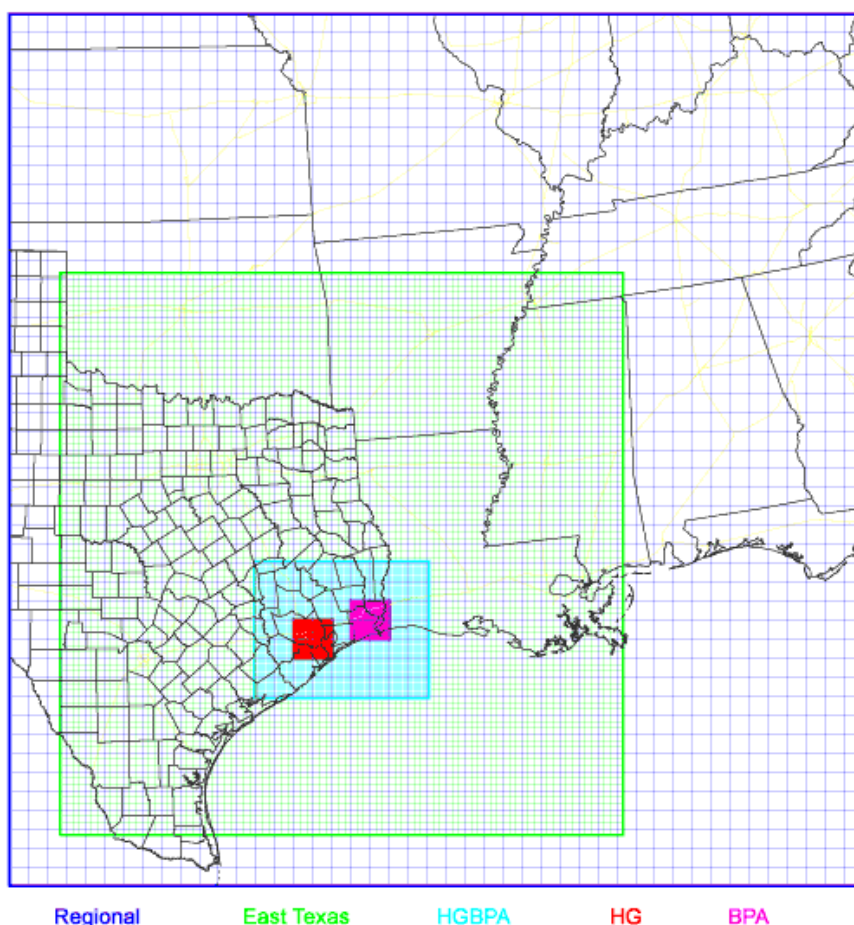


Figure 3-2. Modeling domain used in the study. The Regional, East Texas, Houston-Galveston-Beaumont-Port Arthur (HGBPA), Houston Galveston (HG), and Beaumont-Port Arthur (BPA) nested domains had 36, 12, 4 and 1 km resolution, respectively.

Meteorological inputs required by the model were based on results from the Mesoscale Meteorological Model, version 5, MM5. The volatile organic compound (VOC) and NO_x emission inventories used as input for the modeling episode were prepared by the Texas Commission on Environmental Quality (TCEQ) in accordance with EPA guidance. A MOBILE6-based inventory was developed for on-road mobile source emissions; emissions for non-road mobile and area sources were developed using

emission factors and the EPA's NONROAD model, using local activity data when available. Biogenic emission inventories were estimated using the GLOBEIS emission model with locally developed land cover data. Point source emissions were developed through a special inventory survey and also were estimated based on ambient data collected in the industrial source region. Underestimation in the emission inventory for VOC point sources was addressed by adding approximately 150 tons per day of reactive olefin emissions at point sources that the TCEQ identified as having highly reactive hydrocarbon emissions. These emissions were added to the facilities in amounts based on their emissions of NO_x, following a procedure established by the TCEQ. Details of the meteorological modeling and the VOC and NO_x emission inventory development are available at (http://www.tnrcc.state.tx.us/air/aqp/airquality_photomod.html#section4; http://www.tnrcc.state.tx.us/air/aqp/airquality_contracts.html#section3). Collectively, the versions of the base case emission inventories and meteorology used in this work are referred to as Base 5b.

In this work, emission events were added to the simulation at locations that were consistent with emission events observed by aircraft during this episode period. The PAPPTs described in Chapter 2 were applied to the regions in which the events occurred. As described in Chapter 2, the steps in the application of the PAPPT are (1) define the control volumes, (2) extract the mixing heights, (3) assemble the process rate data, and (4) assemble the reaction rate data. Steps 1 and 2 for this case study are described below; the information resulting from steps 3 and 4 is described in the Results section.

Figure 3-3 shows the location of the PAPPT control volumes used in this work for two different simulation days. Figure 3-3a shows three PAPPT control volumes for an

August 25 simulation day and Figure 3-3b shows two process control volumes for an August 30 simulation day. High ozone concentrations were observed on both days, but the meteorological conditions on the two days were different. On August 25, winds from the east in the late morning and early afternoon advected air from an industrial source region, referred to as the Ship Channel region (located in the center right portion of Figure 3-3a), over downtown Houston and the residential areas of west Houston. On August 30, winds from the north-northwest in the late morning and early afternoon advected air from the Ship Channel region over Galveston Bay.

Figures 3-3a and 3-3b define the horizontal dimensions of the PAPPT control volumes used in this work. The vertical dimension of the control volume is determined by the evolution of the mixing height. As described in detail in Chapter 2, the mixing height is determined by examining the vertical layer interface diffusivity or “ K_v ” values from the photochemical model. These values vary spatially and temporally due to the heterogeneity of terrain and meteorological conditions. An extraction program was written to extract from CAMx the K_v parameter, for each layer interface, for each grid cell within the control volume, as a function of time. Figures 3-4a through 3-4e show the temporal variation in the vertical height of the 3 control volumes used for the August 25 simulation and the two control volumes used for the August 30 simulation. The x-axis in the figure represents the hours of the simulation day and the modeling height is shown vertically.

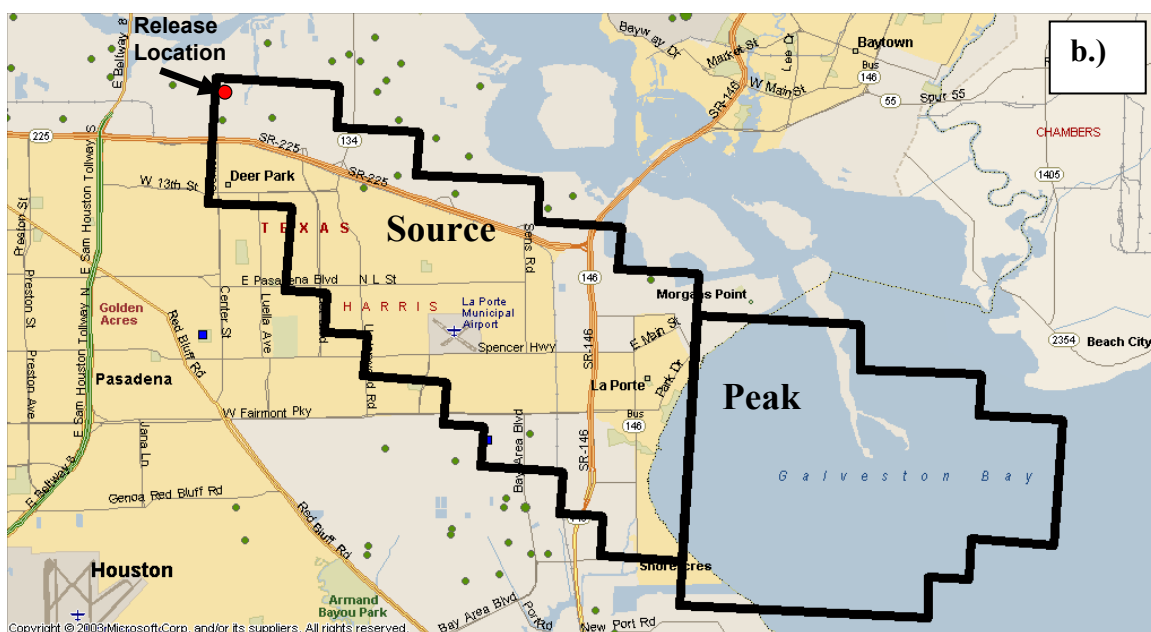
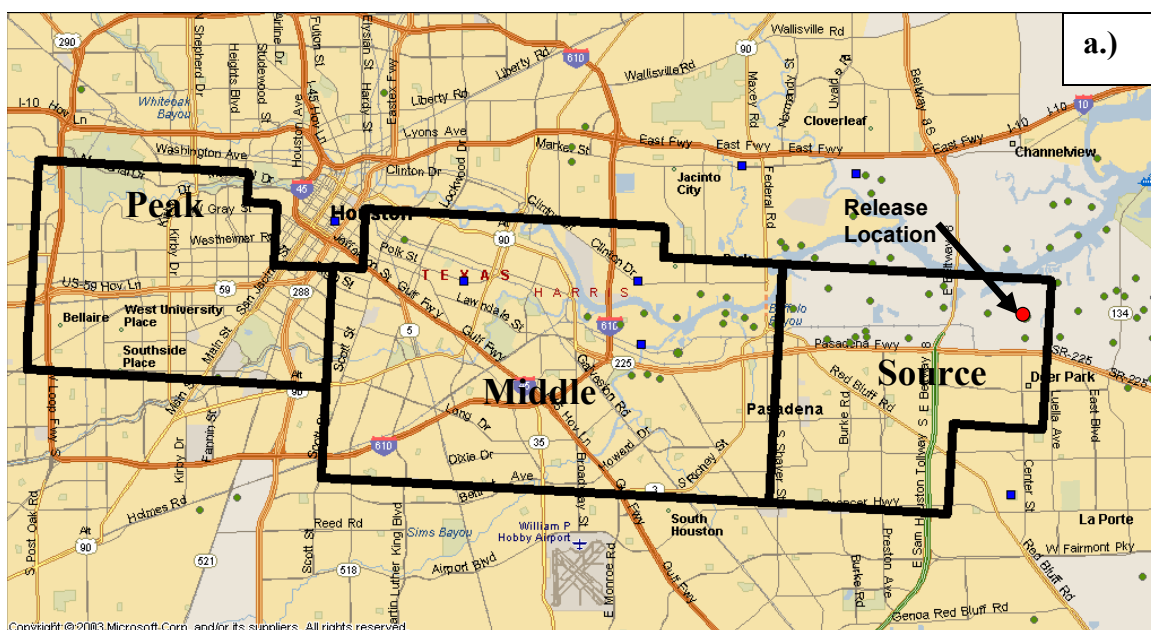


Figure 3-3. (a) Location of the three control volumes used for the PAPPT for the August 25, 2000 simulation day. (b) Location of the two control volumes used for the PAPPT for the August 30, 2000 simulation day. The red dot indicates the location where the simulated emission event was located.

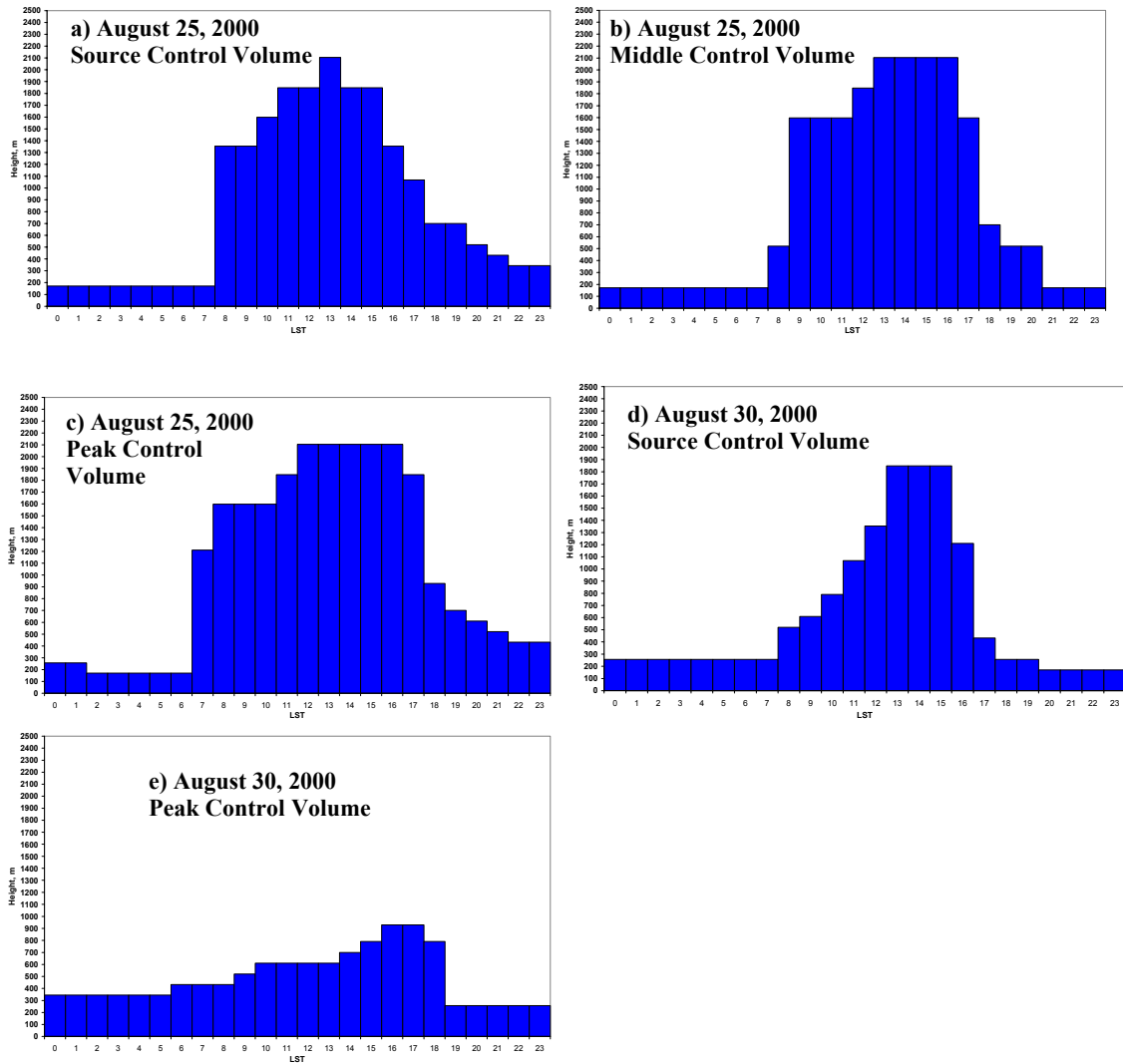


Figure 3-4. Control Volume Heights for the three control volumes on August 25, 2000 (a-c) and the two control volumes for August 30, 2000 (d-e). The x-axis represents the hours of the simulation day and the modeling height is shown vertically.

The spatial distributions of ozone concentrations in the Houston area on the two days that will be examined in detail in this work are shown in Figures 3-5a and 3-5b. These episode days occurred during an intensive air quality study period in the Houston Galveston area (www.utexas.edu/research/ceer/texaqs), and data collected by aircraft on these days indicated evidence of emission events at the location labeled “release location” in Figures 3-3a and 3-3b. The aircraft observations for August 30 are summarized in Figures 3-6a and 3-6b (data abstracted from NOAA, 2004). Figure 3-6a shows the flight track of the aircraft, the wind direction and the estimated release point. The estimated release point was based on the data shown in Figure 3-6b, which includes continuous observations of total oxides of nitrogen (NO_y), semi-continuous measurements of formaldehyde, and discrete canister samples that were analyzed post-flight for hydrocarbons. Also shown in Figure 3-6b are model predictions of ethylene and olefin concentrations at the vertical layer consistent with the aircraft’s elevation. With winds out of the northwest, the aircraft flight track detected NO_y plumes associated with the point sources labeled in the figure. For most of the flight track shown in the Figure, concentrations of ethylene and higher molecular weight olefins (largely propylene) were less than 20 ppb. However, a narrow plume of very high ethylene, propylene and NO_y concentrations were detected, with total olefin concentrations in excess of 100 ppb. A similar narrow hydrocarbon plume from the same source region also was detected during an aircraft flight on August 25th, however, the hydrocarbon plume was absent on aircraft fly-bys on other days.

The data taken on these aircraft flights, together with downwind ozone concentration data, suggest that emission events occurred on August 25th and August 30th near the location labeled as ‘release location’ in Figures 3-3a and 3-3b. The exact

magnitude of the event is not precisely known, therefore a variety of emission rates were used in this work to characterize the event. In addition, while the specific event detected on August 25 and 30, 2000 involved ethylene and propylene, the sources in the region also emit alkanes and aromatics and ground monitors in the region have detected elevated concentrations of alkanes and aromatics with frequencies similar to the detection of elevated concentrations of reactive olefins. Emission event reports submitted to the State of Texas (Murphy and Allen, 2005) indicate that this region has frequent emission events involving alkenes, alkanes and aromatics. The emission event reports indicate that many of the events are relatively short (a few hours or less) and that the events can lead to emission rates of up to 10,000-50,000 lbs/hr.

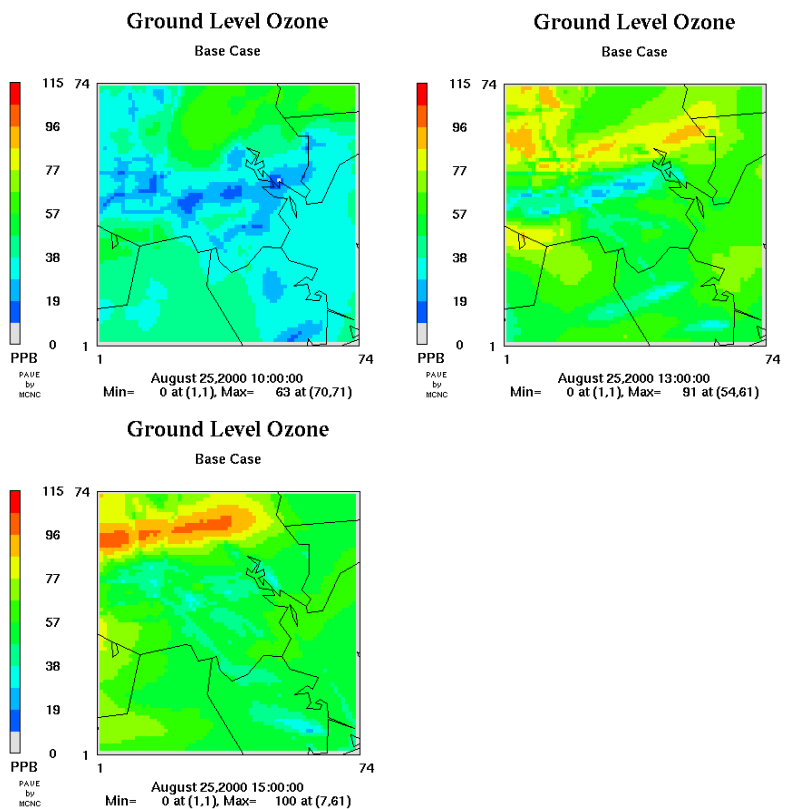


Figure 3-5a. Model predicted ground level ozone concentrations (ppb) for the Houston-Galveston (HG) domain (defined in Figure 3-2) on August 25, 2000.

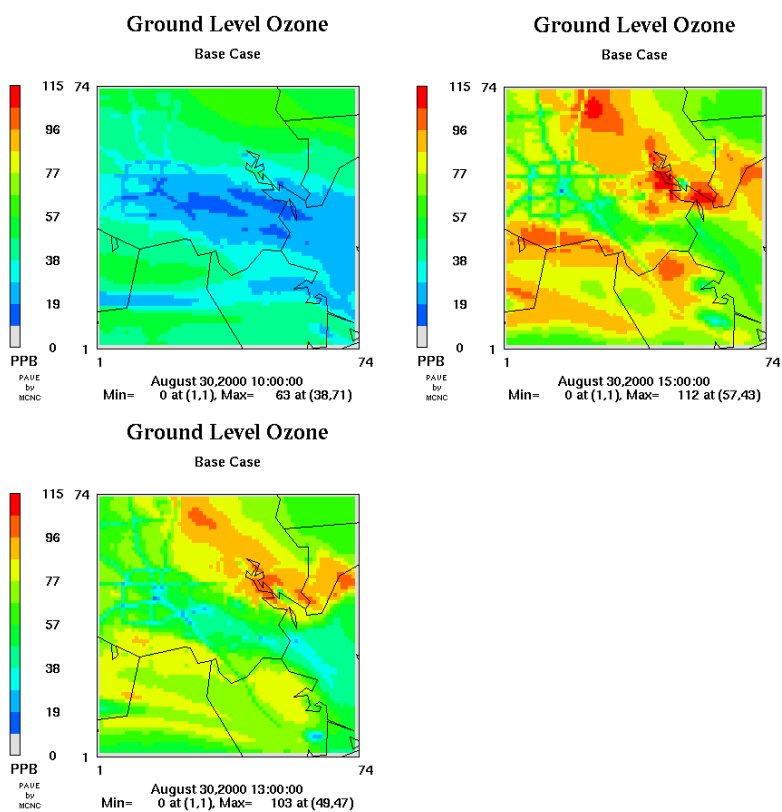


Figure 3-5b. Model predicted ground level ozone concentrations (ppb) for the Houston-Galveston (HG) domain (defined in Figure 3-2) on August 30, 2000.

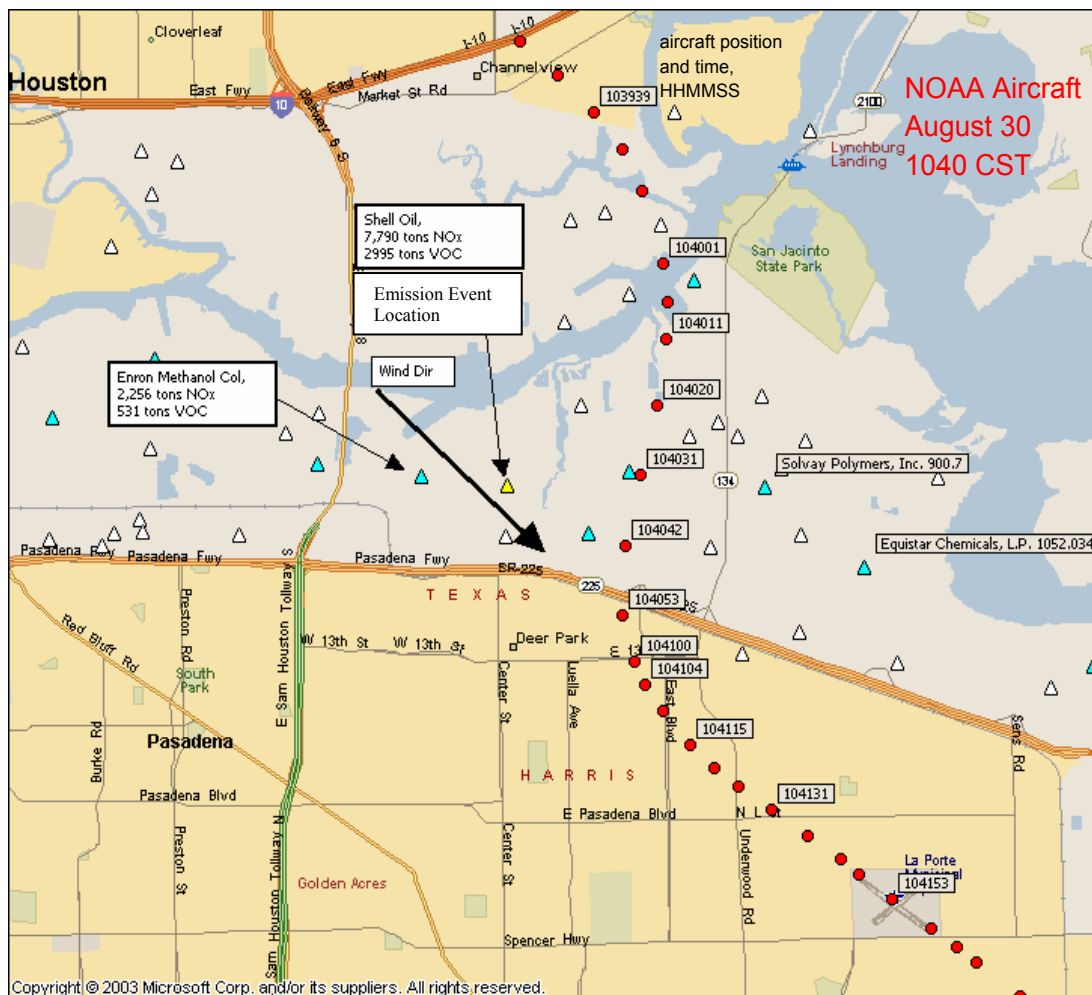


Figure 3-6a. Location of one of the elevated propylene and ethylene measurements made by a NOAA aircraft east of Houston during the August and September 2000 time period. The measurement was made on August 30, 2000. The site labeled “Emission Event Location” corresponds to the “release location” in the maps of Figure 3-3. The aircraft flight track is shown by red circles in the map; the wind direction (black arrow), industrial point sources (triangles), and the estimated release point (yellow triangle) also are shown.

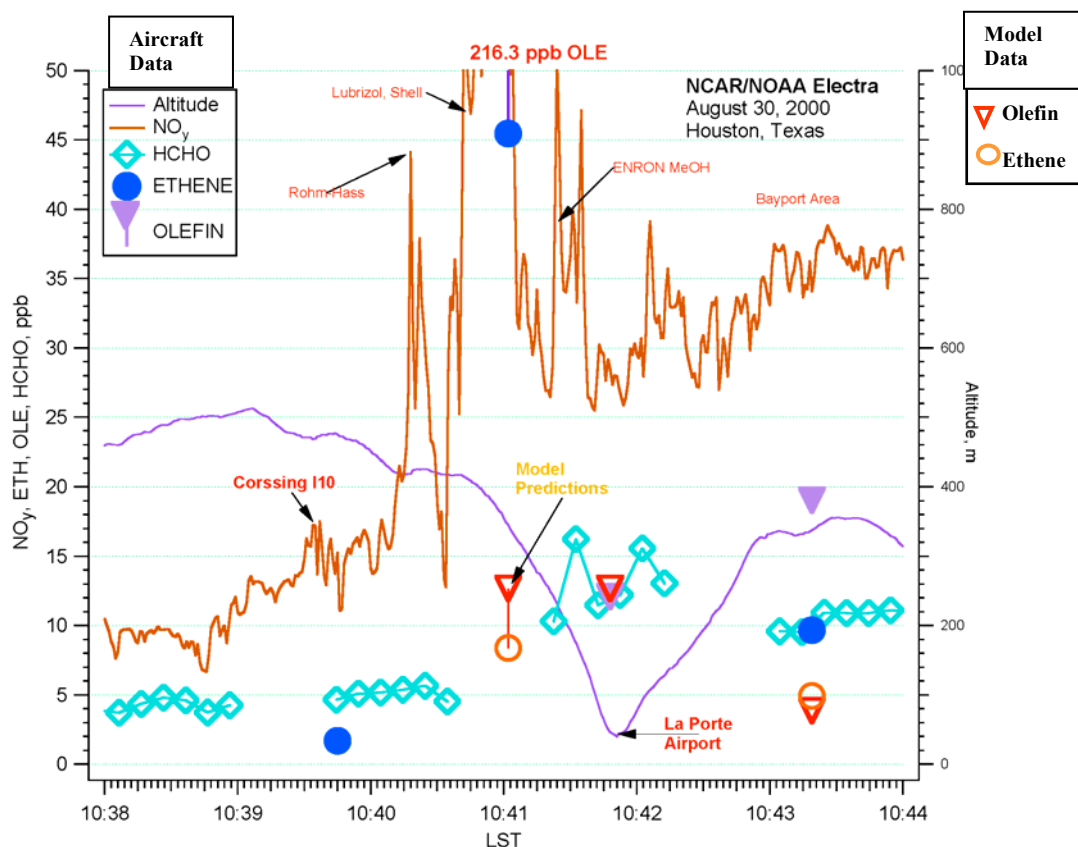


Figure 3-6b. Summary of aircraft measurements on August 30, 2000 at the location of the high ethylene and propylene concentration measurements; time stamps along the horizontal axis can be matched to time stamps on the aircraft flight track in (a). Observations and model predictions (using an inventory with HRVOC emissions enhanced by approximately 150 t/d, but with no emission events) are shown. Note that the hydrocarbon concentrations dissipate rapidly around the maximum, lasting for only a few minutes of flight time. Since the aircraft flew at a speed of approximately 100 m/sec, the hydrocarbon plume width can be assumed to be less than 10 km wide. Note that at this stage, the hydrocarbons are just beginning to react; formaldehyde concentrations are less than 15 ppb (data abstracted from NOAA, 2004).

To simulate the types of emission events suggested by the aircraft data, ground monitoring data and emission event reports, a 2 hour emission event beginning at 10 a.m. was introduced at the location defined in Figure 3-3. The sensitivity of ozone formation to plume composition was evaluated by examining four separate releases composed of all ethylene, all propylene, all xylene, and all n-pentane. Propylene was released at a rate of 5,819 pounds per hour, a rate that was selected to approximately match the aircraft data shown in Figure 3-6. The magnitudes of the other three hydrocarbon releases were selected to match the reactivity of the propylene release. Reactivity was assessed using a Maximum Incremental Reactivity (MIR) scale (Carter, 1994), that is being used by the State of Texas in a hydrocarbon emission trading program (TCEQ, 2004). Emission rates were 7,422 lbs/hr, 9,045 lbs/hr, and 44,004 lbs/hr for ethylene, xylene, and n-pentane respectively. The changes in atmospheric chemical and physical processes and the changes in pollutant concentrations that resulted from the addition of these event emissions were analyzed with the PAPPT. Table 3-1 summarizes the modeling scenarios that were examined.

The chemical mechanism used in CAMx is the Carbon Bond Mechanism version 4 (CBIV) with revised radical termination mechanism and isoprene chemistry (Gery *et al.*, 1989; Carter, 1994; Adelman, 1999). This mechanism is based on reactivity classes of species, although some species important to urban air chemistry are explicit. In the event emission scenarios ethylene is an explicit species in CBIV, categorized as ETH. Propylene is specified as one olefin (OLE) plus one paraffin (PAR). N-pentane is classified as 5 paraffins (5*PAR) and all xylene species are classified as XYL.

Date	Ethylene (ETH)	Propylene (OLE+PAR)	Xylene (XYL)	N-pentane (5*PAR)
8/25/2000	7,422 lbs/hr 2 hour release 10 a.m. – 12 p.m.	5,819 lbs/hr 2 hour release 10 a.m. – 12 p.m.	9,045 lbs/hr 2 hour release 10 a.m. – 12 p.m.	44,004 lbs/hr 2 hour release 10 a.m. – 12 p.m.
8/30/2000	7,422 lbs/hr 2 hour release 10 a.m. – 12 p.m.	5,819 lbs/hr 2 hour release 10 a.m. – 12 p.m.	9,045 lbs/hr 2 hour release 10 a.m. – 12 p.m.	44,004 lbs/hr 2 hour release 10 a.m. – 12 p.m.

Table 3-1. Modeling scenarios that were tested with the CAMx model including emission rates, duration, date, and release time. The Carbon Bond IV reaction classification for each species is listed in parentheses.

3.3 RESULTS

Figures 3-7a and 3-7b show changes in ozone concentration that resulted from the addition of the propylene emission event. Super-imposed on these ozone concentration difference plots are the horizontal dimensions of the PAPPT volumes. Peak ozone concentrations in the event plume are increased by up to 75 ppb on August 25 and 100 ppb on August 30. The plumes advect in different directions; the August 25 plume is transported to the west, and encounters significant NO_x emissions associated with Houston urban core. In contrast, the August 30 plume travels to the southeast, over Galveston Bay and encounters little additional NO_x after leaving the source region. For each date, the PAPPTs were used to examine process rate data, and reaction rate data. For the 25th, process analysis data are presented separately for the three regions defined in Figures 3-3a and 3-7a. For the 30th, the process analysis data are presented for the two regions defined in Figures 3-3b and 3-7b.

3.3.1 August 25, 2000

The path of the emission event plume was tracked using the ozone difference plot in Figure 3-7a. From this Figure it is evident that the plume tracks across the modeling domain remaining relatively intact, with little horizontal dilution of pollutants. The three control volumes identified in Figure 3-3a were chosen to capture the evolution of the plume as it aged and traversed the Houston urban core. These three control volumes (source, middle, and peak) cover the source of the hydrocarbon release near Galveston Bay, the plume as it crosses just south of the urban core and the peak ozone region over western Houston. It is within the context of these three control volumes that the description of the ozone impact of a hydrocarbon release is discussed.

A dramatic increase in ozone generation resulted in the source control volume, due to the emission event, for all hydrocarbon releases except for the n-pentane release. Ozone chemical production rates in the source control volume at hour 12 increased from 7 ppb/hr in the base case to 31 ppb/hr, 22 ppb/hr, 40 ppb/hr, and 12 ppb/hr in the propylene, ethylene, xylene, and n-pentane emission event cases, respectively. The resulting plume advected out of the source control volume and traveled west into the Houston urban core. By hour 15, the plume impacted the peak control volume increasing ozone concentrations there. The propylene, xylene, and ethylene releases all increased the ozone concentration in the peak control volume by 33 ppb.

The n-pentane release increased the ozone concentration by only 15 ppb. The xylene release generated the most ozone near the release point, but as the plume aged and traveled across urban Houston all emission event releases, except n-pentanes, added nearly identical amounts of ozone. Understanding the reasons for these similarities and differences between the emission events requires the physical and chemical rate information extracted by the PAPPT.

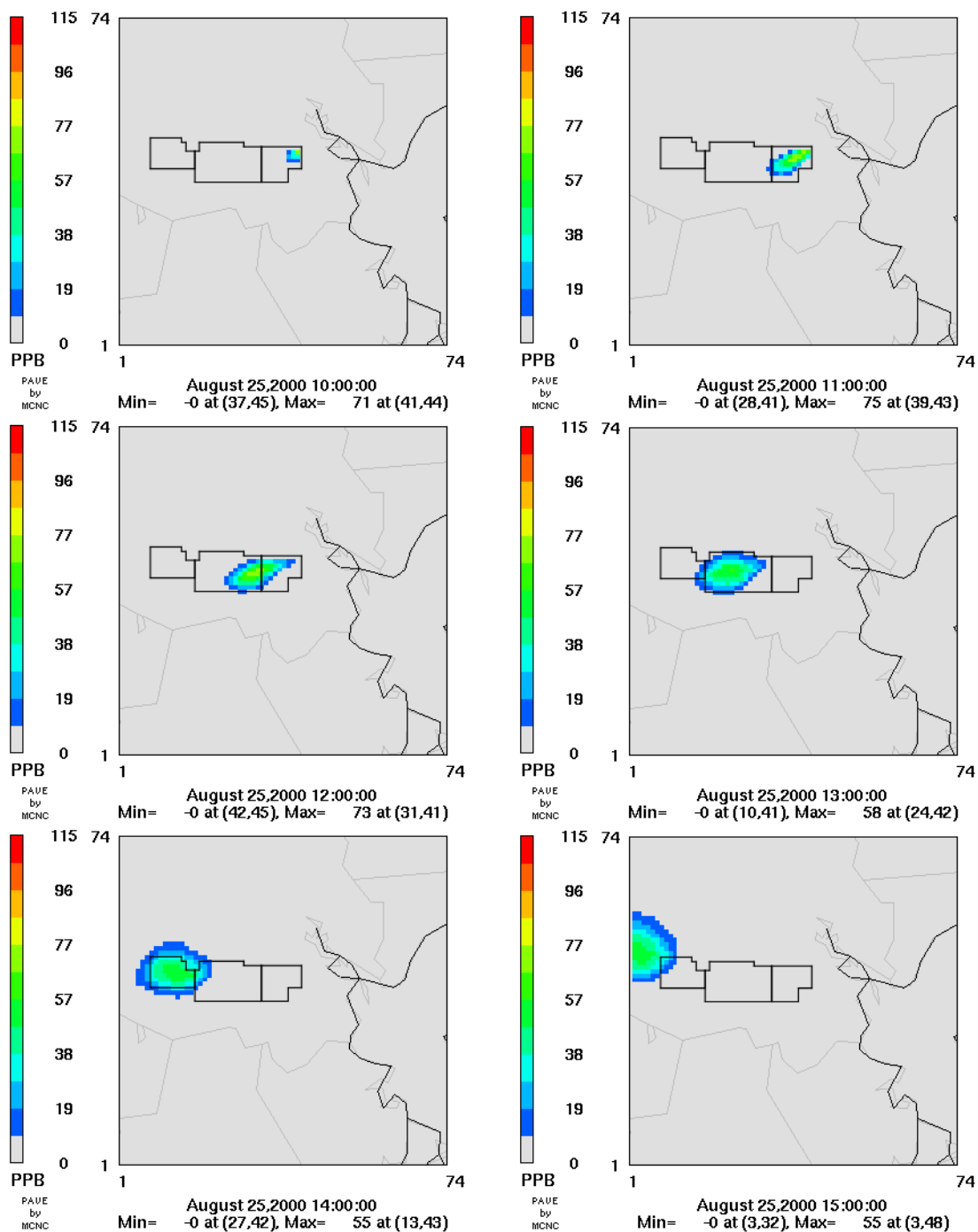


Figure 3-7a. Model output of ground level ozone concentrations (ppb) on August 25, 2000 from 10 a.m. – 3 p.m. The plots show the difference in ozone predictions between the propylene emission event case and the base case. The control volumes are outlined in black.

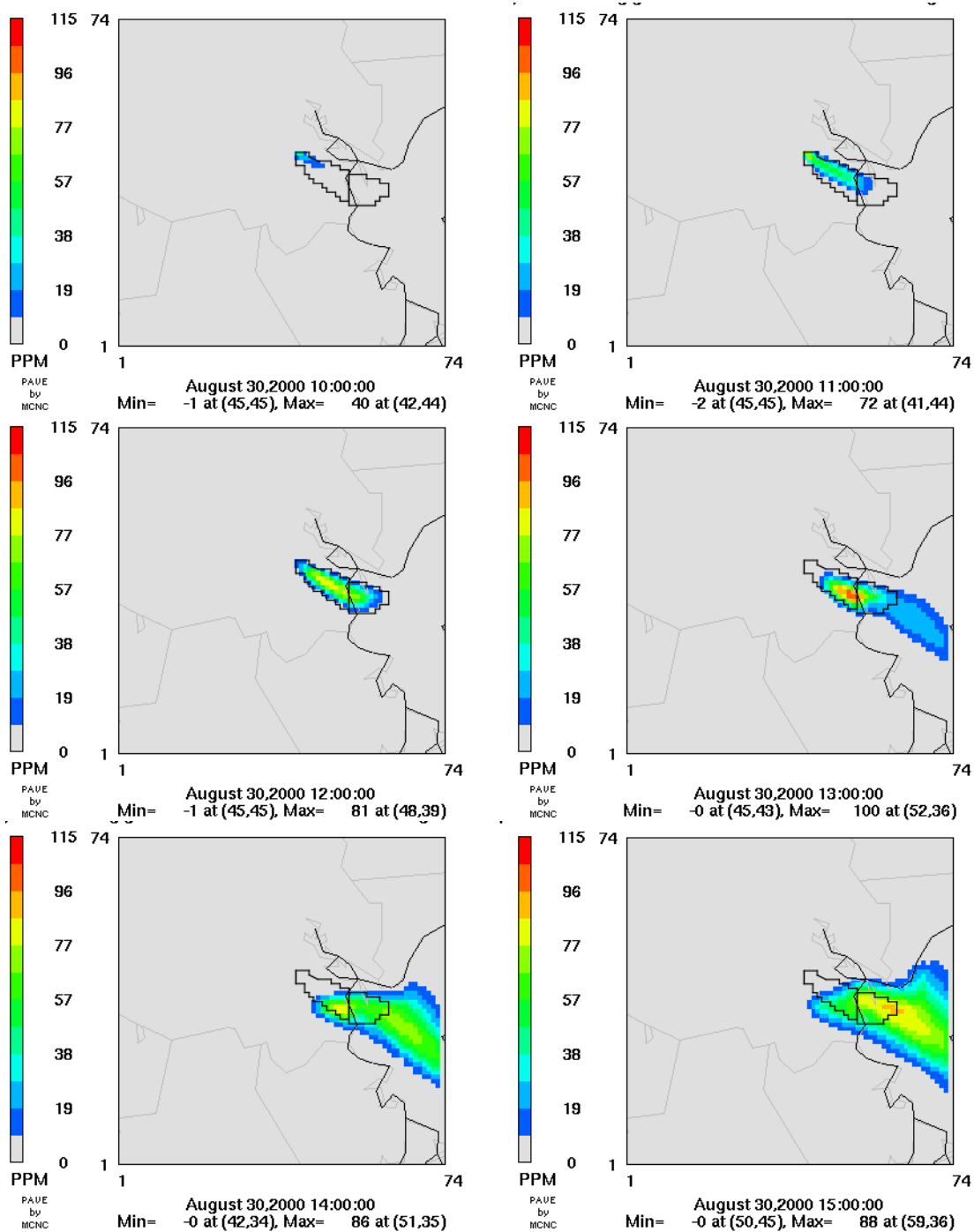


Figure 3-7b. Model output of ground level ozone concentrations (ppb) on August 30, 2000 from 10 a.m. – 3 p.m.. The plots show the difference in ozone predictions between the propylene emission event case and the base case. The control volumes are outlined in black.

The PAPPT is able to quantify the process rate data such as horizontal advection and chemical generation for each control volume. These data are presented in time series plots, as described in Chapter 2 of this thesis. Figure 3-8a-f and Figure 3-9a-f give these plots for the source, middle, and peak control volumes for the olefin (OLE) and ozone (O_3) species respectively, for the propylene emission event. OLE is a CBIV chemical mechanism classification used by the CAMx model to represent the reactivity class of alkenes such as propylene. The right column gives the time series plots for the propylene emission event scenario and the left column gives the time series for the base case. Figure 3-8b shows an increase in the olefin emission rate (pink line) from 1 ppb/hr to 30 ppb/hr at hour 10 coinciding with the emission event. At 11 a.m. the rate of chemical destruction of olefins jumps from -2 ppb/hr in the base case to -22 ppb/hr. The plume resulting from the propylene release leaves the source control volume at noon as horizontal advection rates (blue line) increase to -13 ppb/hr. These olefins are advected into the middle control volume at rates up to 6 ppb/hr at hour 12 as seen in Figure 3-8d. Within the same hour that these olefins are advected into the control volume, they are being chemically destroyed at rates of -4 ppb/hr. By hour 13 we see the plume horizontally advect into peak control volume at 1 ppb/hr in Figure 3-8f. These plots illustrate the path of the plume and the rate at which these olefins are destroyed in the model. The chemical destruction rates of olefin deplete olefin concentrations quickly enough so that by the time the plume reaches the peak control volume, only a small amount of the original olefin release remains. In the peak control volume an increase of less than 1 ppb/hr is seen in the horizontal advection rates between the base case and olefin emission event scenario.

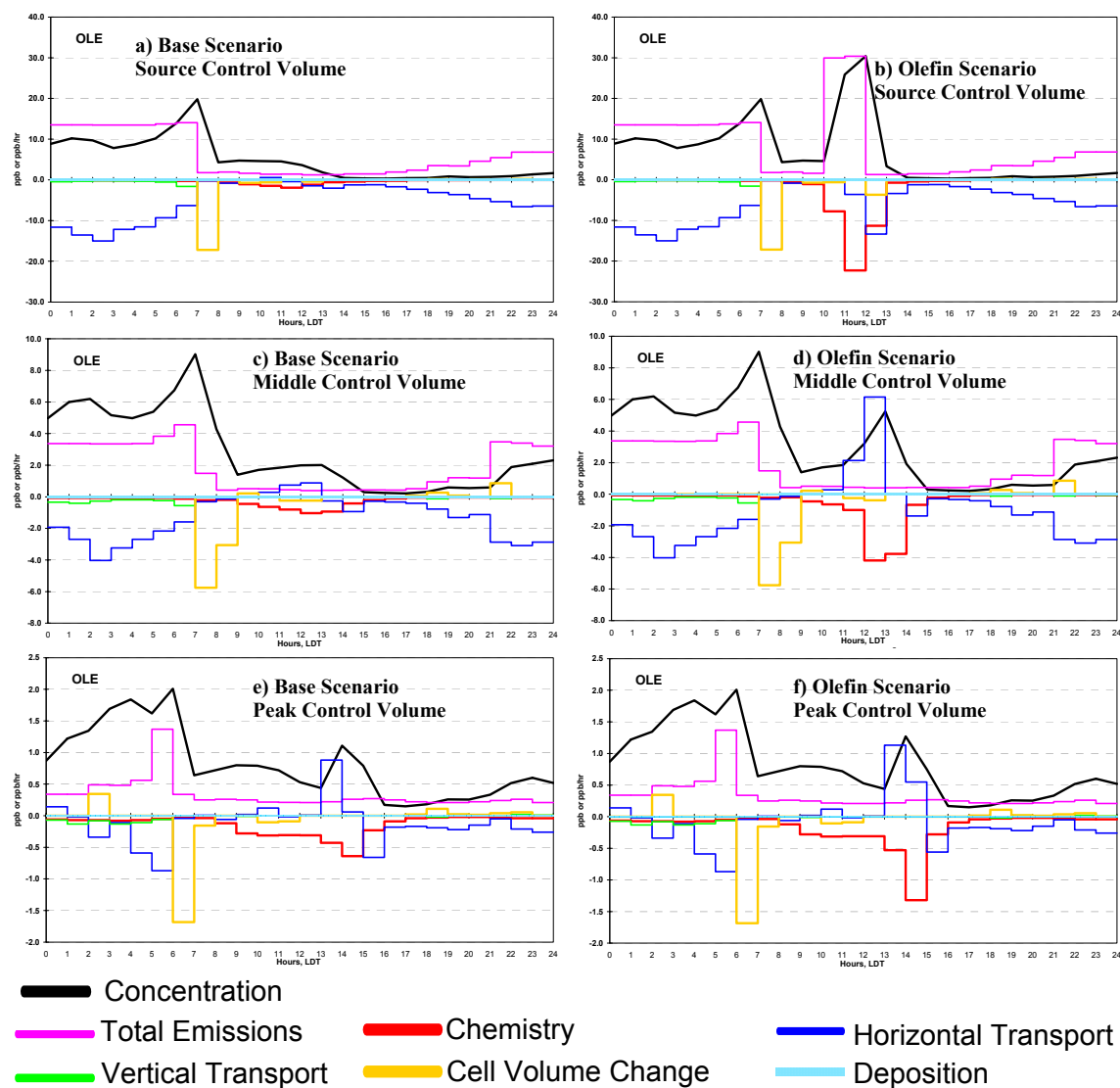


Figure 3-8. (a),(b) Evolution of olefin concentrations and rates of change of ozone concentration over the course of a 24-hour period in the source control volume on August 25, 2000 for the base and propylene event emission simulation respectively. (c),(d) Olefin concentration for the base and propylene event emission simulation for the middle control volume. (e),(f) Olefin concentration for the base and propylene event emission simulation for the peak control volume.

Figure 3-9a-b shows an ozone time series plot for the source control volume for the base case and olefin event emission scenario, respectively. Ozone concentrations at hour 12 increased from 41.6 ppb to 66.5 ppb as a result of the emission event. In the same hour the ozone chemistry generation rates increased from 6.7 ppb/hr to 31.4 ppb/hr. Most of the ozone that was generated as a result of the emission event was quickly advected horizontally out of the control volume. In hour 12, -39 ppb/hr of ozone were advected horizontally; an increase of 34 ppb/hr from the base case. That ozone was advected into the middle control volume at hour 12 with a horizontal advection rate of -18 ppb/hr (Figure 3-9d). At hour 13 ozone leaves the middle control volume at a rate of approximately -21 ppb/hr. There also is an increase in ozone chemical generation rates during hours 12-14; these rates nearly doubled when compared to the base case. This increase in production is due to the ozone precursors that are advected from the source control volume. Figure 3-9f shows an hourly ozone time series plot for the peak control volume. Ozone concentrations peaked at 155 ppb with chemistry generating up to 27 ppb/hr in hour 15. Although this region had less chemical ozone production than the source control volume, the peak ozone concentration was higher. This was the result of ozone being transported into the control volume during hours 12-14 at a rate of 55 ppb/hr.

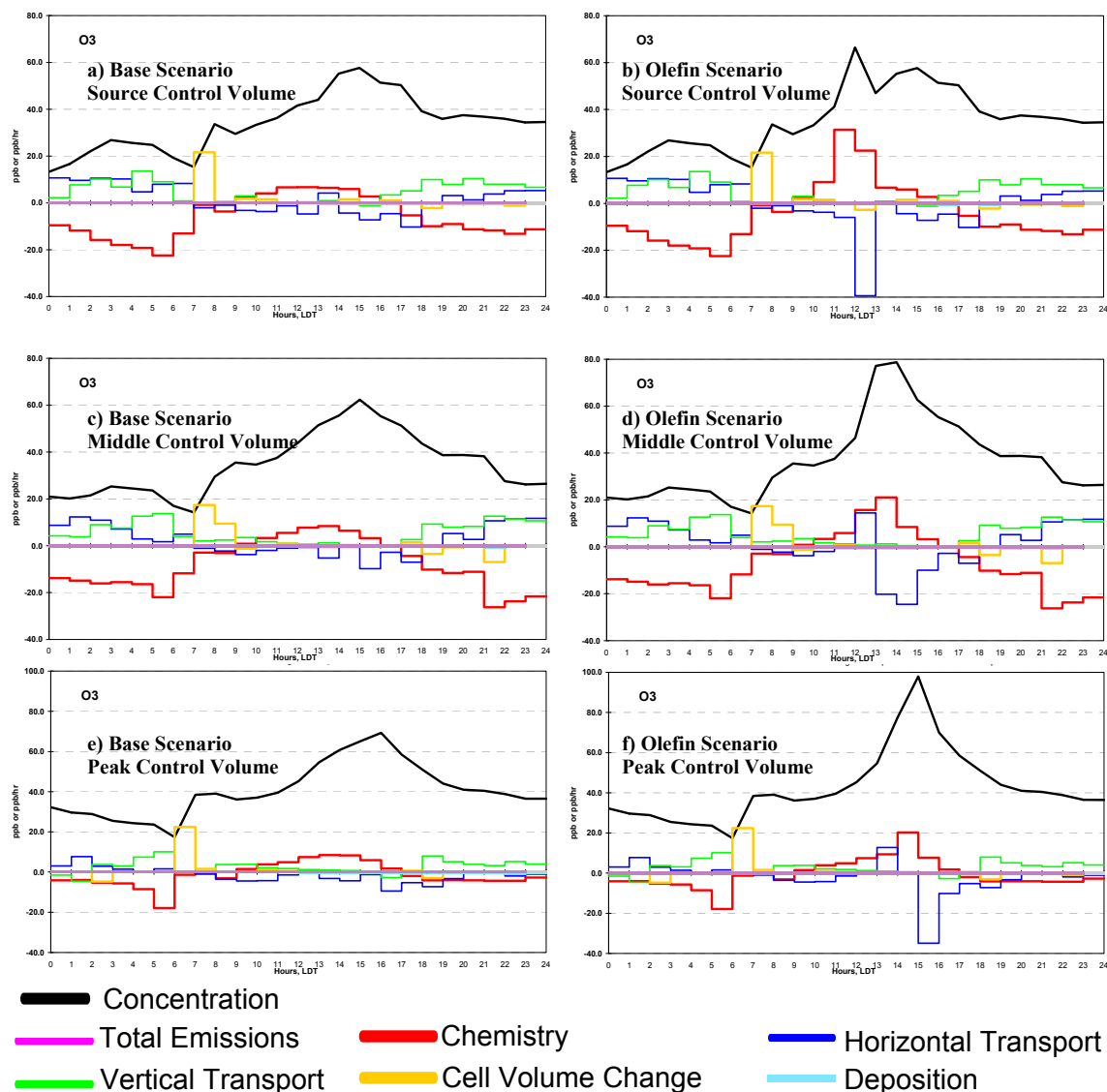


Figure 3-9. (a),(b) Evolution of ozone concentrations and rates of change of ozone concentration over the course of a 24-hour period in the source control volume on August 25, 2000 for the base and propylene event emission simulation respectively. (c),(d) Ozone concentration for the base and propylene event emission simulation for the middle control volume. (e),(f) Ozone concentration for the base and propylene event emission simulation for the peak control volume.

The PAPPT also can be used to describe the chemical cycles that characterize the emission events. Figures 3-10 and 3-11 are the chemical cycle diagrams for the source and peak control volumes. A detailed description of the chemical cycle diagrams can be found in Chapter 2. Figure 3-10 presents the cycle diagrams in the source control volume for the base case and propylene event emission scenarios. All values are aggregated for the hours where the emission event had the most critical impact, 10 a.m. – 1 p.m. The first parameter on the left side of the diagram gives the amount of new OH radicals from the photolysis of aldehydes and O₃. The amount of new OH radicals increased from 10.6 ppb to 17.4 ppb, mostly from increases in the photolysis of the aldehyde products resulting from the olefin chemistry. This increase in new OH radicals is significant because a fraction of the OH reaction pathways result in the reformation of OH, which is available to react again. This OH reaction and reformation can occur multiple times until the OH eventually reacts through a pathway that does not regenerate OH. In the PAPPT, OH reaction and reformation is quantified by the OH cycle values, which represent the average number of times each new OH cycles before being lost in termination reactions. This cycle number, in conjunction with the total number of VOCs reacted, is indicative of the reactivity of the hydrocarbons that are present in the atmosphere. The emission event scenario showed that 42.3 ppb more VOCs reacted with OH radicals and the OH cycles increased from 2.5 to 3.4. This is evidence of the dramatic increase of reactivity put into the system by the emission event.

The increase in the extent of reaction of new OH radicals is the cause of the increase of the total number of NO to NO₂ conversions occurring in the system. This parameter also is listed in Figure 3-10. In the propylene emission event, the number of conversions increased from 34.9 ppb in the base case to 90.2 ppb. The cycling of NO into

NO₂, with subsequent photolysis, ozone formation, and NO regeneration can occur multiple times until the NO eventually reacts through a pathway that does not regenerate NO or is transported away. Similarly to the OH cycle these processes are represented by a NO cycle value. This value represents the average number of times each NO will cycle through the system before being lost in termination reactions. The NO cycle value increased from 1.7 in the base case to 2.9 in the propylene emission event scenario. It is the lack of sufficient NO in the source control volume that is the cause of the horizontal advection of olefins seen in the time series plots. However, even in a NO_x limited regime, the highly reactive nature of the plume allows for extensive oxidation of NO molecules ultimately leading to significant increases in ozone formation. This is seen in the amount of ozone that is generated chemically in the source control volume. The amount of ozone that is generated as a result of chemical reactions increased from 18 ppb in the base case to 66 ppb in the propylene emission event case. The emission event created a transient ozone plume that transports a total of 49 ppb of ozone out of the control volume within the first three hours of the release. The data suggests a NO_x limited atmosphere in the source control volume and further reductions in ozone could be achieved with effective VOC controls.

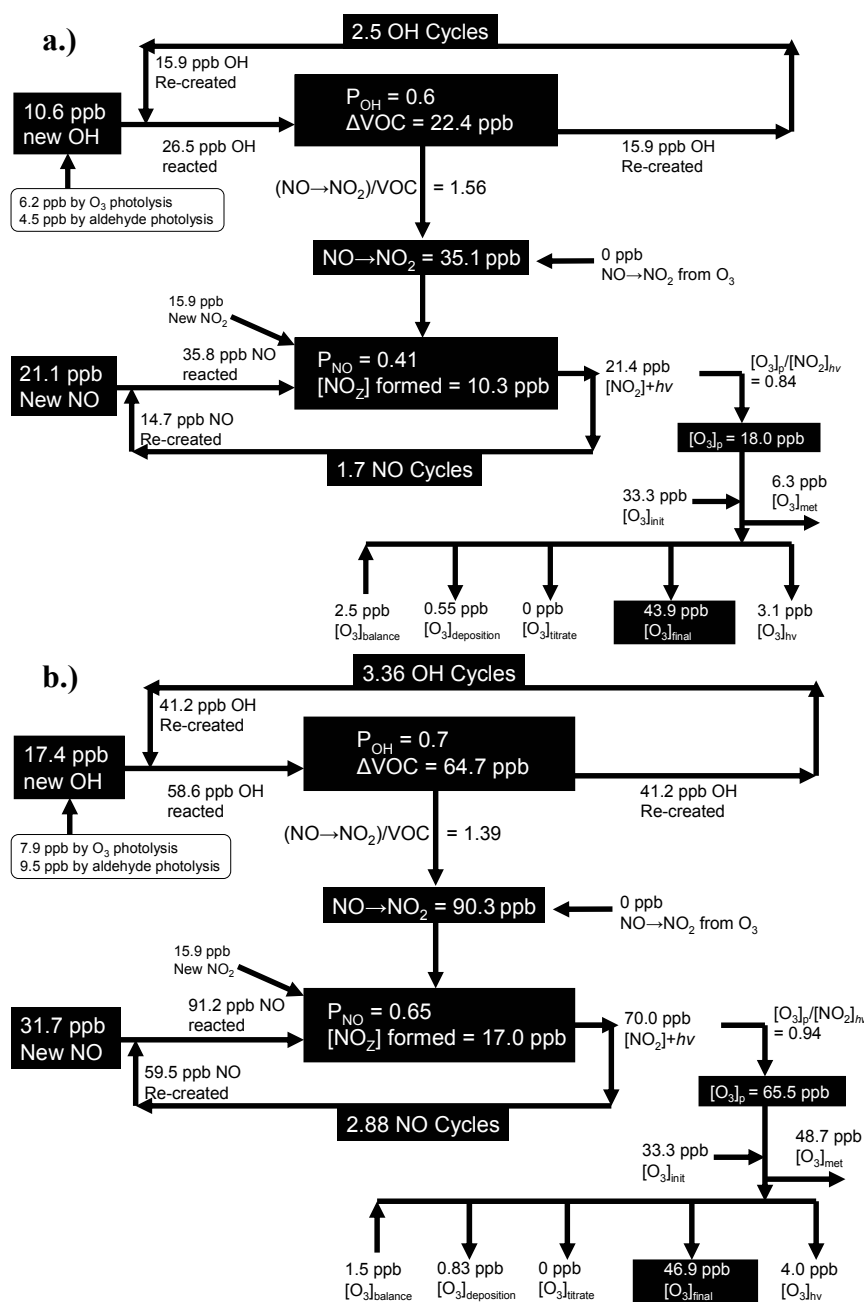


Figure 3-10. Cycle diagrams for simulation day August 25, 2000 for the hours 10 a.m. – 1 p.m. in the source control volume for the (a) base case and (b) propylene event emission scenario.

Figure 3-11 shows the cycle diagrams in the peak control volume for the base case and propylene emission event case. All values are aggregated for the hours where the emission event had the most impact on ozone concentrations, 1 p.m. – 3 p.m.. In this control volume 12.3 ppb of new OH radicals were created in the base case, 3.5 ppb less than in the propylene emission event scenario. The increase from new radicals in the peak control volume largely originated from the photolysis of ozone, instead of aldehydes. In contrast, the majority of new OH radicals originated from aldehydes in the source control volume. The base case OH cycle in the peak control volume was 2.61 compared to 2.77 in the propylene release case. The base case reacted 25.9 ppb of VOCs and the emission event 37.1 ppb. This resulted in 40.9 ppb and 57.1 ppb of NO to NO₂ conversions in the base case and the propylene emission event case respectively. The NO cycle values for the base case and emission event scenario were 1.95 and 2.51. The emission event case chemically generated 38 ppb of ozone, an increase of 15.2 ppb from the base case.

The sensitivity of ozone generation to plume composition was tested by simulating releases of several different hydrocarbons. Figure 3-12 presents some key chemical parameters extracted by the PAPPT for the August 25, 2000 base case. The four hydrocarbons that were compared were propylene, ethylene, xylene, and n-pentane. The chemical parameters are aggregated in the source control volume for hours 10 a.m. – 1 p.m., the middle control volume for hours 11 a.m. – 3 p.m. and for the peak control volume for hours 1 p.m. – 4 p.m. The first parameter on the left is the amount of new OH generated within each control volume. This parameter is vital in determining the amount of ozone that ultimately will be generated. In the source control volume, the largest increase was from the xylene release event. The production of new OH radicals is nearly doubled, increasing by 13.2 ppb when compared to the base case. In the other cases the

amount of new OH radicals increased by 6.8 ppb, 4.2 ppb, and 0.5 ppb for the propylene, ethylene, and n-pentane releases respectively. As the plume ages and travels into the middle and peak control volumes the percent difference in new OH radicals between the base case and xylene case diminishes. By the time the plume reaches the peak control volume there is only a 24% increase in new OH radicals in the xylene release. The xylenes ability to rapidly generate new OH radicals near the release point results in larger gains in every chemical parameter except total VOC reacted. However, this parameter does not count the secondary reactions that occur to the partially oxidized xylene products. These secondary reactions do generate aldehydes and ultimately become a source of new OH radicals. Since the OH radicals are counted, but the secondary reactions are not, the “VOC reacted” value is underestimated for xylenes. The differences in new OH radicals generated by xylene emission events, compared to the other events, disappears by the time the plume reaches the middle and peak control volumes. In the middle and peak control volumes, the ethylene emission event case dominates nearly all the chemical parameters.

The OH radical balance explains the differences in ozone formation and accumulation occurring in these control volumes. The PAPPT separates the source of new OH radicals into two categories, photolysis of ozone and photolysis of aldehydes. Those reactants that are able to quickly generate aldehydes will contribute new OH radicals early in the oxidation process. As the plume ages and these HRVOCs have reacted away, sources of new OH are dominated by ozone photolysis. Figure 3-11 shows these two sources of new OH radicals for August 25, 2000 for the (a) source control volume, (b) middle control volume and (c) peak control volume. In the source control volume, it is clear that in xylene emission event aldehydes were responsible for the

sizable increase in new OH radicals. However, once the HRVOCs are oxidized the majority of new OH radicals originate from the photolysis of ozone molecules. Approximately 60% of all new radicals originated from ozone reactions once the plume left the source control volume.

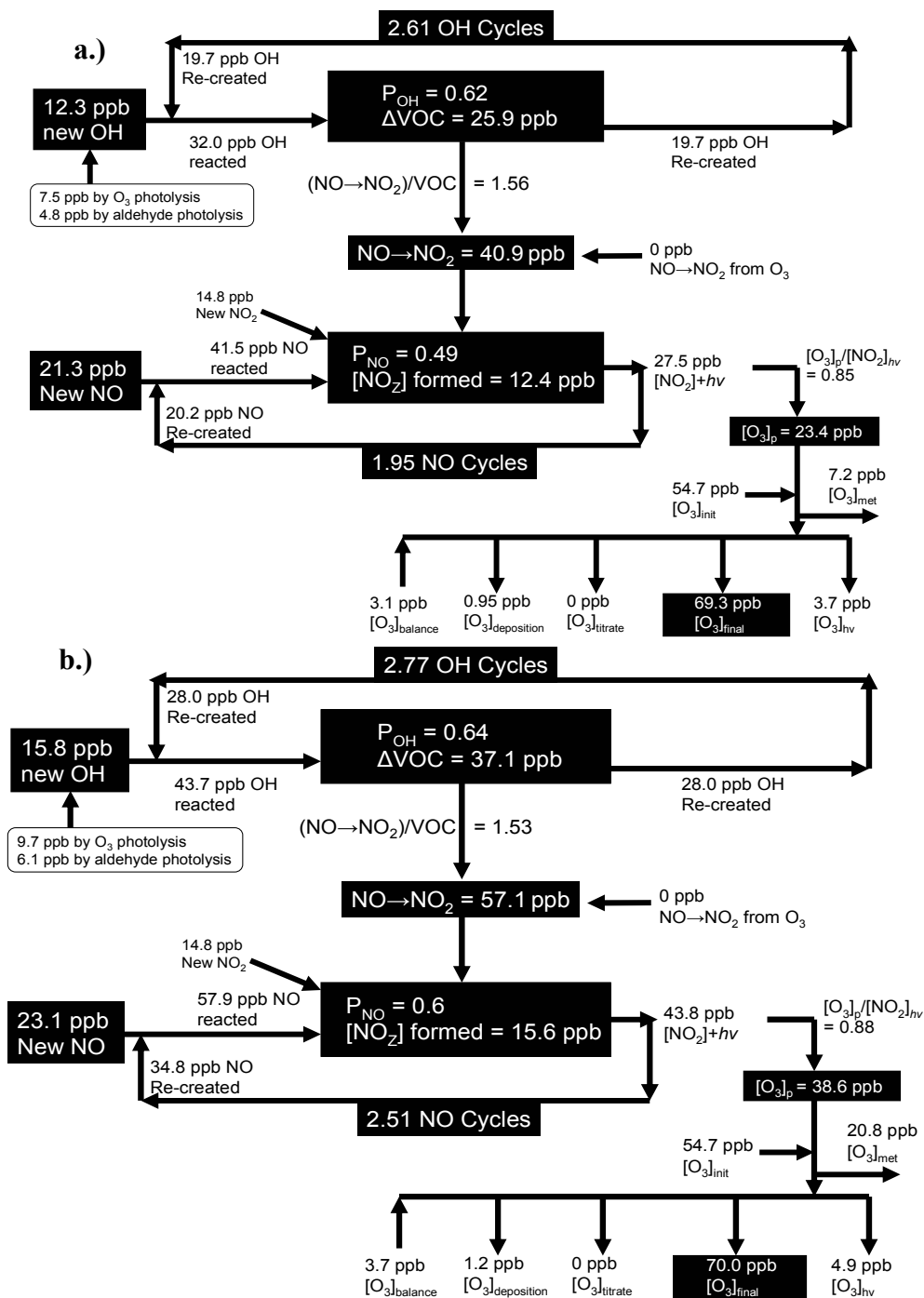
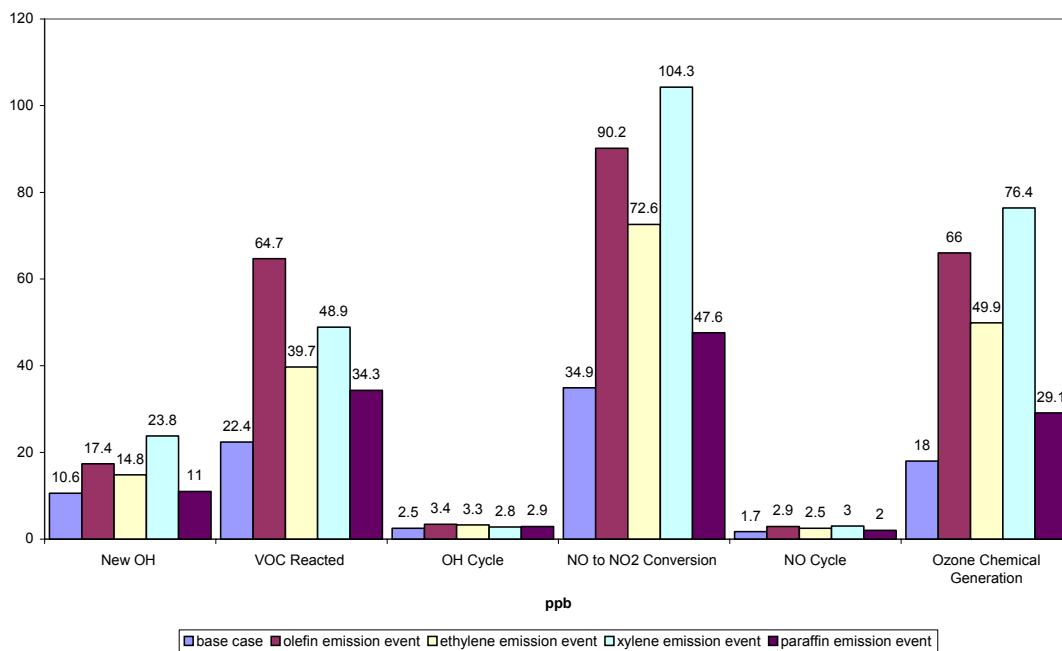


Figure 3-11. Cycle diagrams for simulation day August 25, 2000 for the hours 1 p.m. – 4 p.m. in the peak control volume for the (a) base case and (b) propylene event emission scenario.

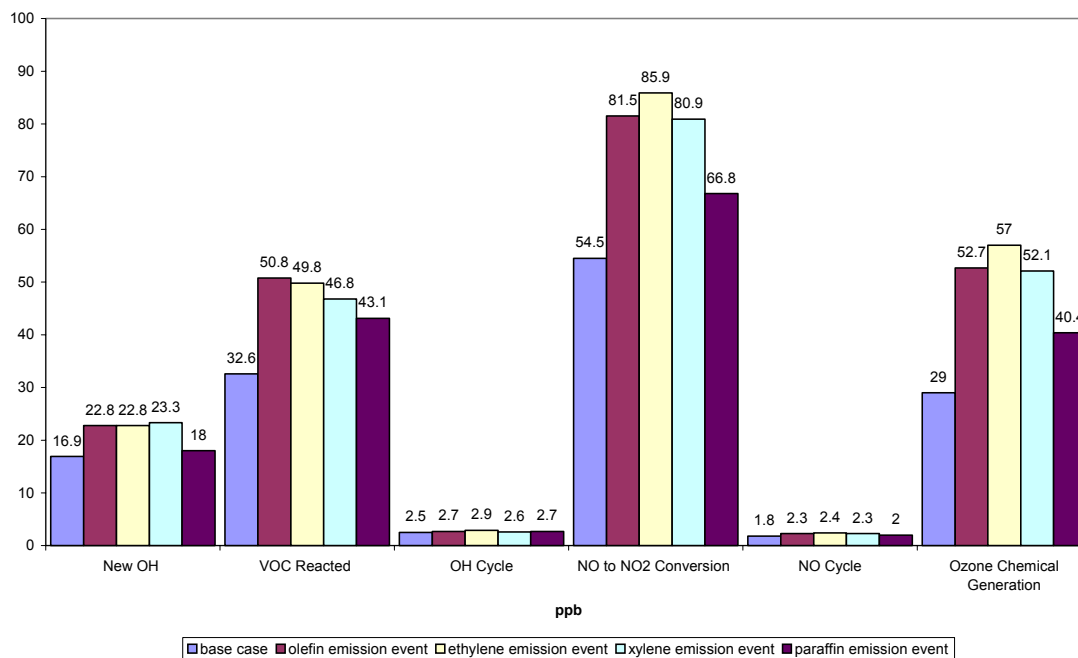
a.)

Source Region Chemical Parameters
Hours 10-13



b.)

Middle Region Chemical Parameters
Hours 11-15



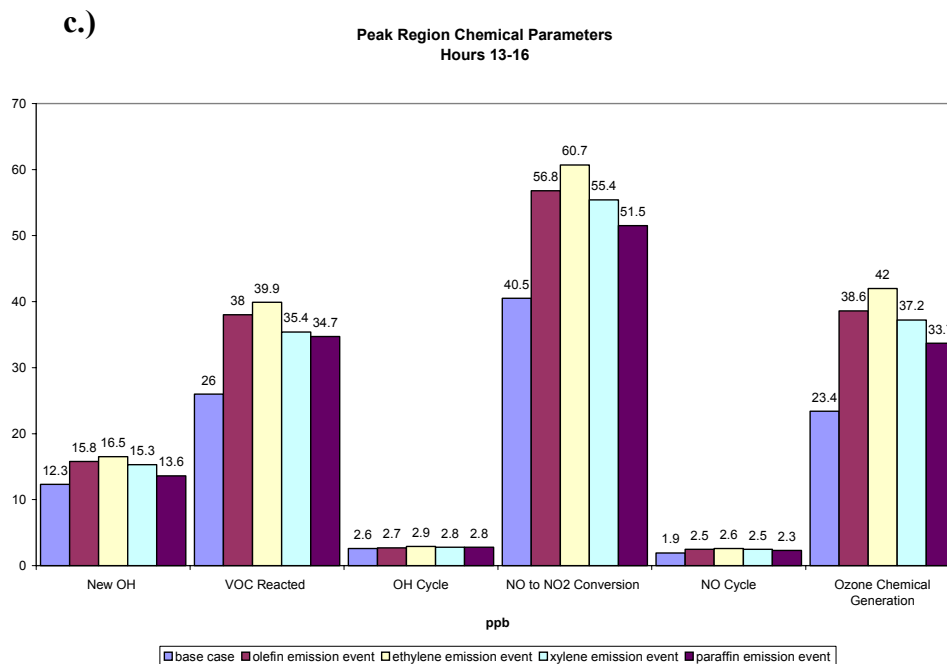
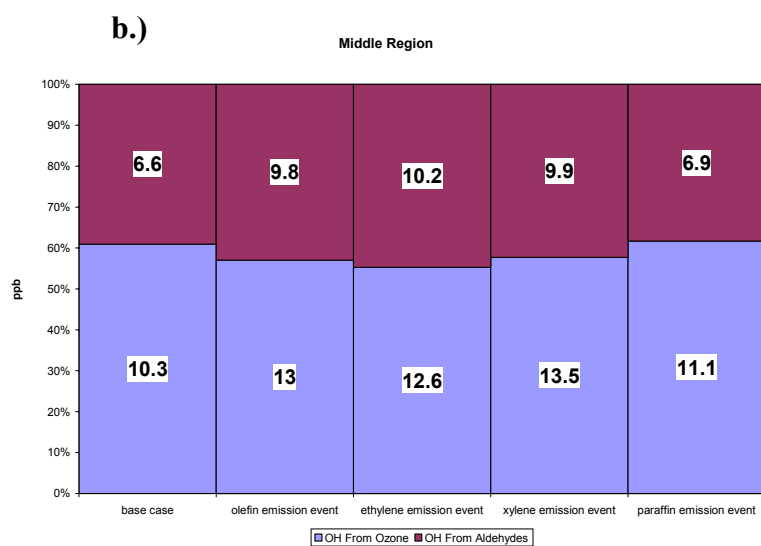
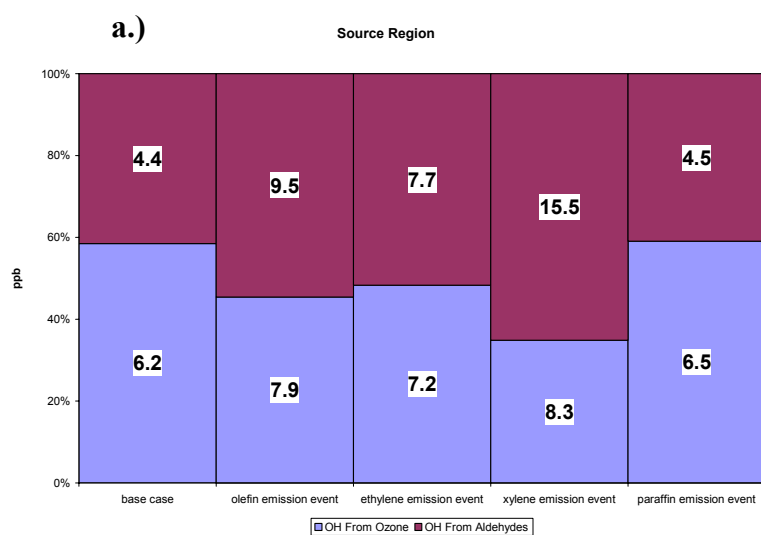


Figure 3-12. Key chemical parameters for the August 25, 2000 base case, propylene, ethylene, xylene, and n-pentane emission events for (a) the source control volume hours 10 a.m. – 1 p.m. and b) the middle control volume (c) the peak control volume hours 1 p.m. – 4 p.m.



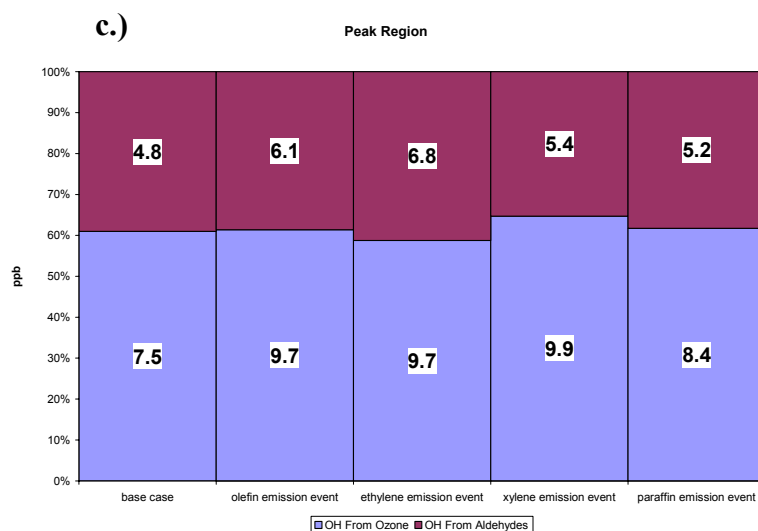


Figure 3-13. Sources of new OH radicals for August 25, 2000 for the (a) source region, (b) middle region, and (c) peak region.

3.3.2 August 30, 2000

Event emission releases on August 30th quickly generate large amounts of ozone that are then transported into Galveston Bay. This is clearly shown in the ozone difference plot in Figure 3-7b. As with the August 25th simulation day, a source control volume was chosen to capture the chemical activity occurring near the release point (source control volume, Figures 3-3b, 3-7b). A second control volume (peak) was chosen to investigate the chemistry occurring over Galveston Bay. It is within these two control volumes that the descriptions of the chemical characteristics of the release plume are discussed.

Ozone generation in the source control volume increased substantially for all hydrocarbon releases except for the n-pentane. Ozone chemical production rates in the source control volume at hour 11 increased from 6 ppb/hr in the base case to 31 ppb/hr,

19 ppb/hr, 39 ppb/hr, and 11 ppb/hr in the propylene, ethylene, xylene and n-pentane emission event cases, respectively. The propylene, xylene, and ethylene releases all increased the ozone concentration in the peak control volume by 35 ppb in hour 16. The n-pentane release increased the ozone concentration by only 20 ppb.

Figure 3-14 a-d and Figure 3-15a-d give the time series plots for the source and peak control volumes for the olefin (OLE) and ozone (O₃) species respectively. The right column gives the time series plots for the propylene emission event scenario. Figure 3-14b shows an increase in the olefin emission rate from 0.4 ppb/hr to 46 ppb/hr at hour 10 coinciding with the emission event. At 11 a.m. the rate of chemical destruction of the olefin species jumps from -0.5 ppb/hr in the base case to -23 ppb/hr. The plume resulting from the propylene event release leaves the source control volume with horizontal advection rates from -4 ppb/hr in hour 10 to -11 ppb/hr in hour 12. Within these same two hours olefins are being chemically destroyed at rates of nearly -10 ppb/hr. Although the chemical destruction rates of olefin are relatively fast, the wind velocities were sufficient to transport unreacted olefin into the peak control volume. These olefins contributed to the ozone generation rates there.

Figure 3-15a-b shows an ozone time series plot for the control volume in the source region for the base case and propylene event emission scenario. The effect of the propylene release is clearly illustrated by the increase in chemical generation of ozone at hour 11. During that hour the ozone chemistry generation rates increased from 2.8 ppb/hr to 31.1 ppb/hr. Most of that ozone was quickly transported out of the control volume. In hour 13, -62.3 ppb/hr of ozone were advected horizontally. Figure 3-15d shows an ozone time series plot for the peak control volume. Ozone concentrations peaked at 130 ppb in

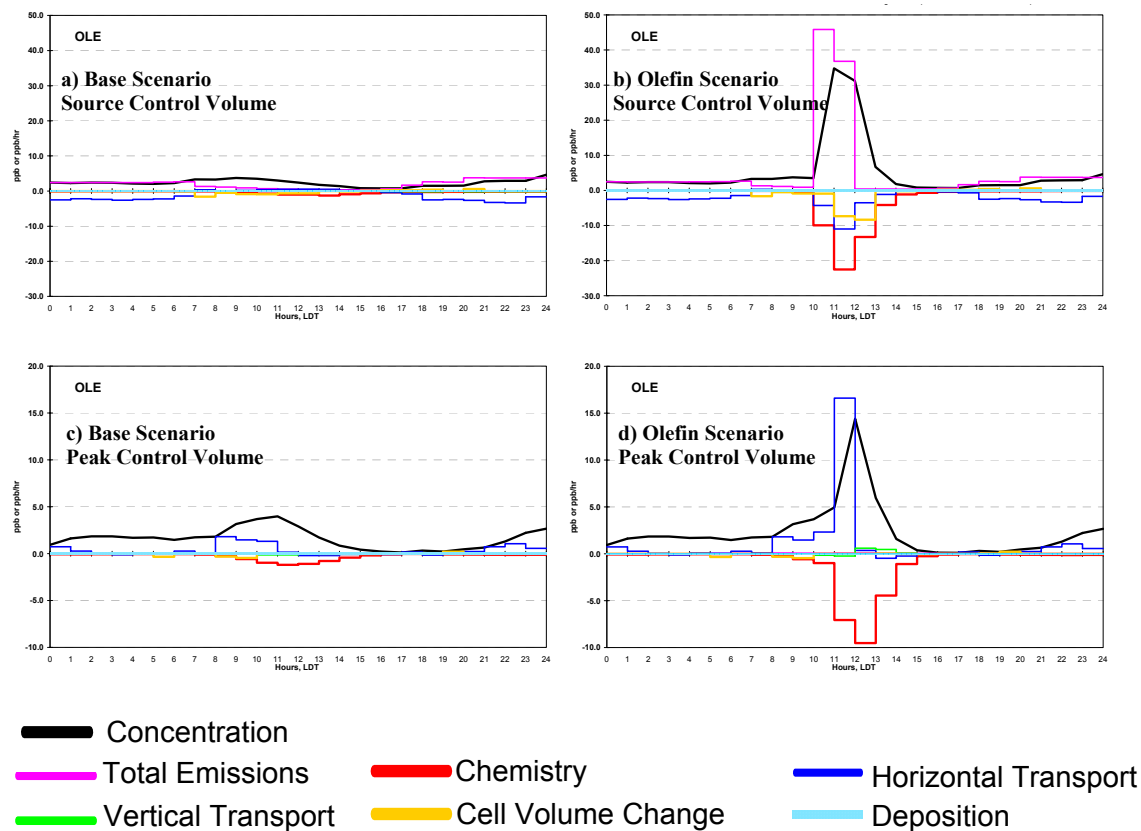


Figure 3-14. (a),(b) Evolution of olefin concentrations and rates of change of ozone concentration over the course of a 24-hour period in the source control volume on August 30, 2000 for the base and propylene event emission simulation respectively. (c),(d) Olefin concentration for the base and propylene event emission simulation for the peak control volume.

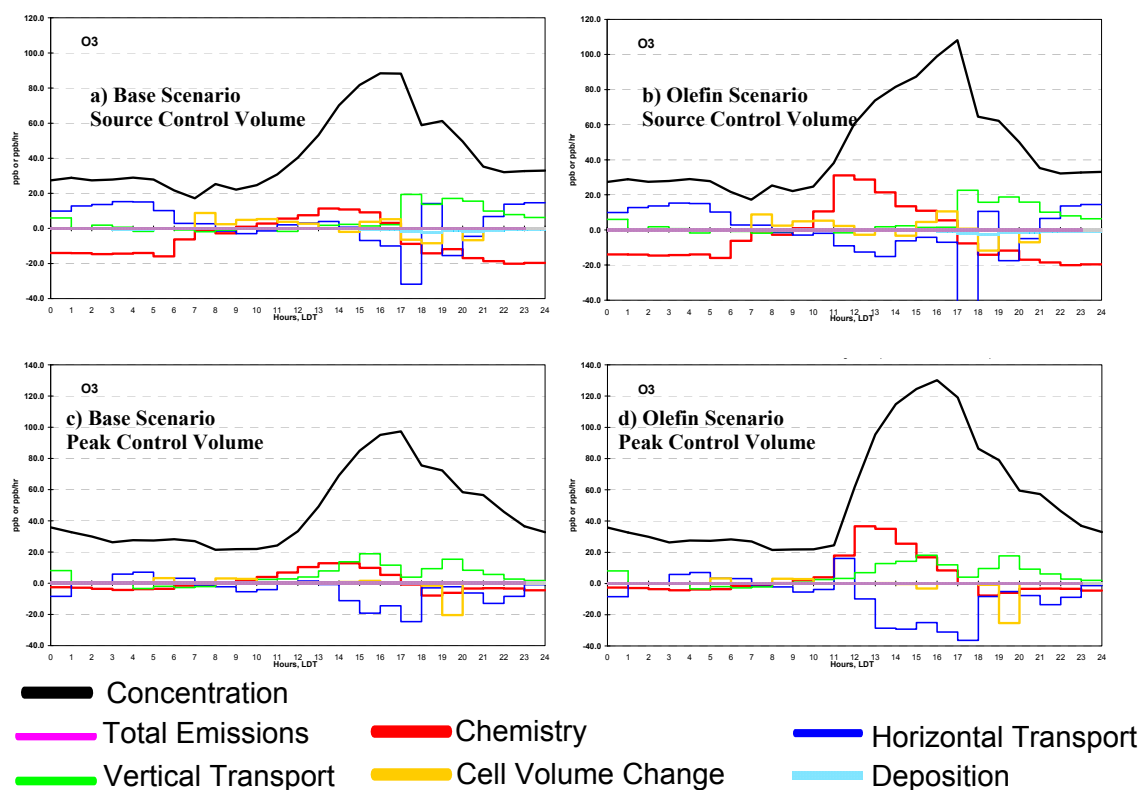


Figure 3-15. (a), (b) Evolution of ozone concentrations and rates of change of ozone concentration over the course of a 24-hour period in the source control volume on August 30, 2000 for the base and propylene event emission simulation respectively. (c),(d) Olefin concentration for the base and propylene event emission simulation for the peak control volume.

hour 16. Chemistry generation rates peaked at 36.6 ppb/hr at hour 12. The influx of ozone from the source control volume is evident at hour 11 with a horizontal transport rate of 16 ppb/hr.

Figures 3-16 and 3-17 are the chemical cycle diagrams for the source and peak control volumes. Figure 3-16 presents the cycle diagrams in the source control volume for the base case and propylene event emission scenarios. All values are aggregated for the hours where the emission event had the most critical impact, 10 a.m. – 1 p.m. The amount of new OH radicals increased from 8.9 ppb to 15.9 ppb mostly, from photolysis of the aldehyde products resulting from the olefin chemistry. The propylene emission event scenario reacted 52 ppb more VOCs; the OH cycles increased from 2.65 to 3.82. In the propylene emission event the number of NO to NO₂ conversions increased from 34.9 ppb to 90.2 ppb. The NO cycle value increased from 1.6 to 2.9 in the emission event scenario. The amount of ozone that is generated as a result of chemical reactions increased from 16 ppb to 73 ppb in the emission event case.

Figure 3-17 shows the cycle diagrams in the peak control volume for the base case and propylene emission event case. All values are aggregated for the hours where the emission event had the most critical impact, 1 p.m. – 3 p.m.. In this control volume 12.9 ppb of new OH radicals were created in the base case, 20.6 ppb in the propylene emission event scenario. The base case OH cycle in the peak control volume was 2.78 compared to 3.22 in the propylene release case. The base case reacted 28.2 ppb of VOCs and the emission event 57.6 ppb. This resulted in 48.3 ppb and 92.8 ppb of NO to NO₂ conversions in the base case and emission event case respectively. Once the plume entered the peak control volume it entered an area where no NO_x point sources existed.

Ozone chemistry was no longer inhibited by NO_x and NO cycles increased from 2.29 to 4.15 ultimately leading to higher ozone concentrations. The emission event case chemically generated 80 ppb of ozone, an increase of 44 ppb from the base case. The changes to ozone chemistry resulting from the various plume compositions were similar to the data in the August 25th simulation.

Figure 3-18 presents some key chemical parameters extracted by the PAPPT for the August 30, 2000 case. Four emission releases were compared; propylene, ethylene, xylene, and n-pentane. The chemical parameters for each scenario are given in the source control volume for hours 10 a.m. – 1 p.m. and for the peak control volume for hours 1 p.m. – 4 p.m. In the source control volume the largest increase in new OH radicals again comes from the xylene release emission event. The xylene species are able to produce more aldehyde products near the release point than the other species. It is this larger concentration of aldehydes that are responsible for a greater number of new OH radicals. As the plume ages and travels into the peak control volume the initial advantage in new OH radical generation by xylenes disappears. In the peak control volume the ethylene emission event case dominates nearly all the chemical parameters. Figure 3-19a-b shows the sources of new OH radicals for August 30, 2000 in the source control volume and the peak control volume. In the source control volume it is clear that in the xylene emission event aldehydes were responsible for the substantial increase in new OH radicals. However, once the HRVOCs are initially oxidized the fraction of new OH radicals originating from the photolysis of ozone molecules dominates. Approximately 60% of all new radicals originated from ozone reactions once the plume left the source control volume.

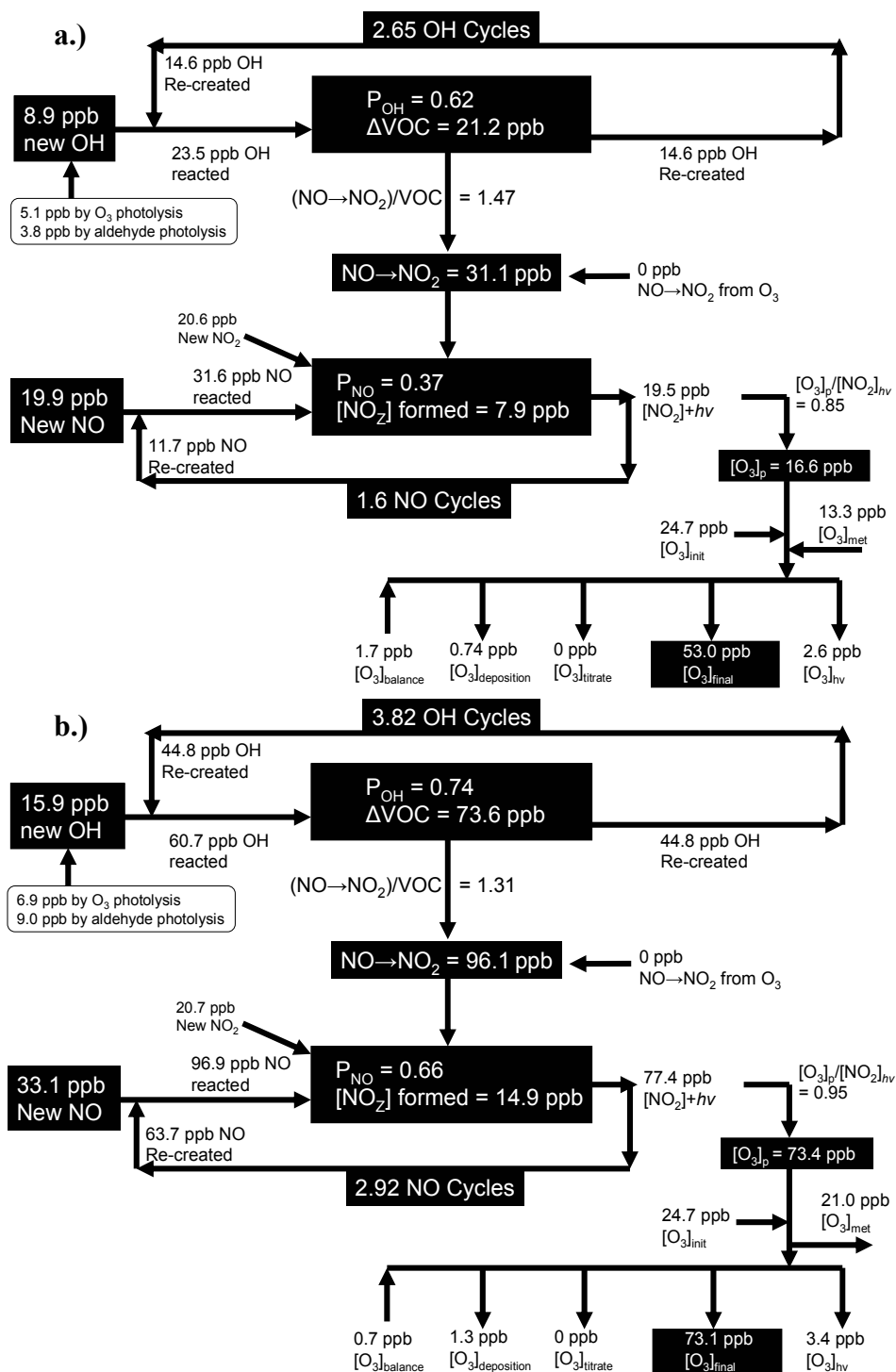


Figure 3-16. Cycle diagrams for simulation day August 30, 2000 for the hours 10 a.m. – 1 p.m. in the source control volume for the (a) base case and (b) propylene event emission scenario.

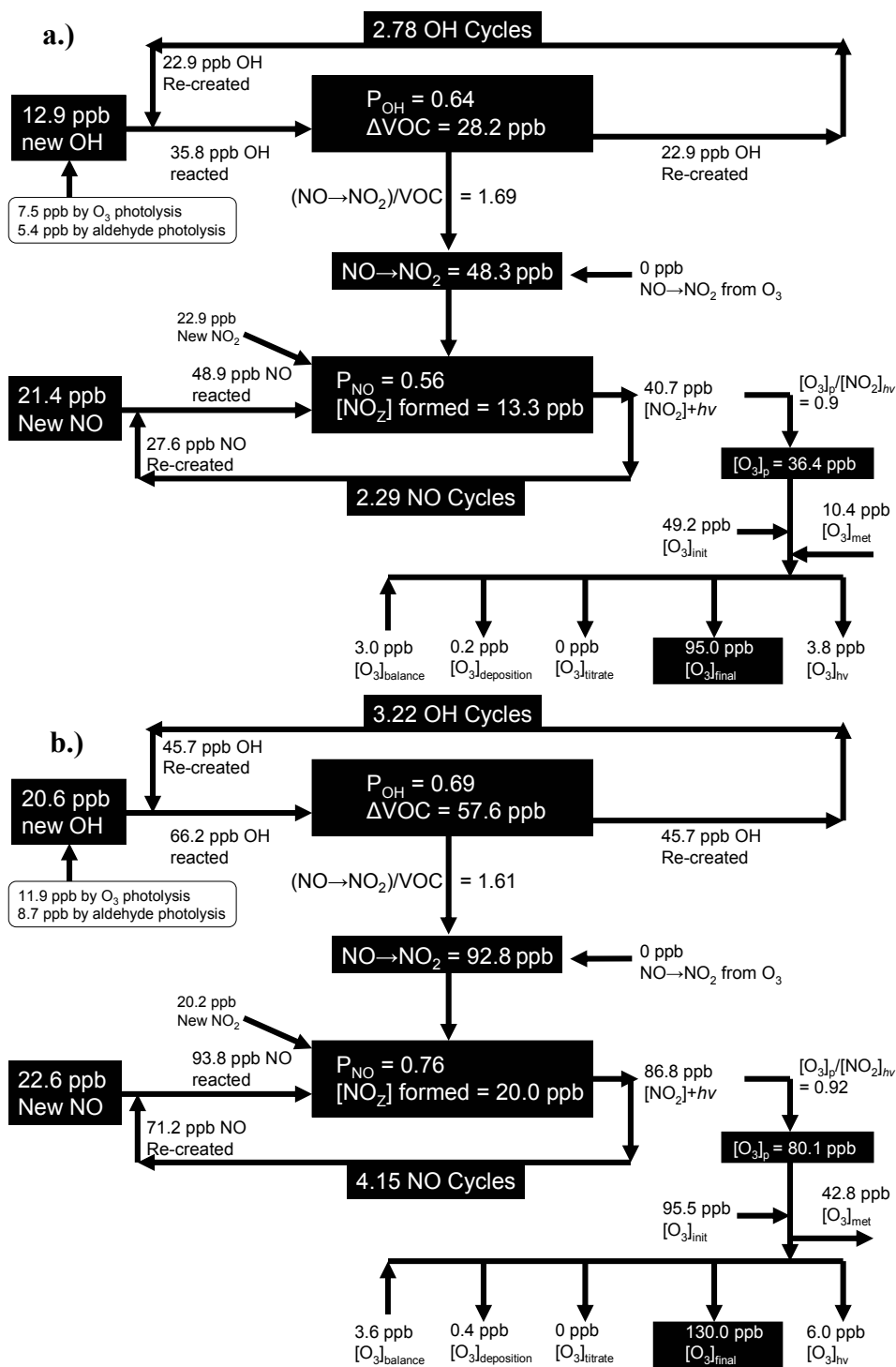


Figure 3-17. Cycle diagrams for simulation day August 30, 2000 for the hours 1 p.m. – 4 p.m. in the peak control volume for the (a) base case and (b) propylene event emission scenario.

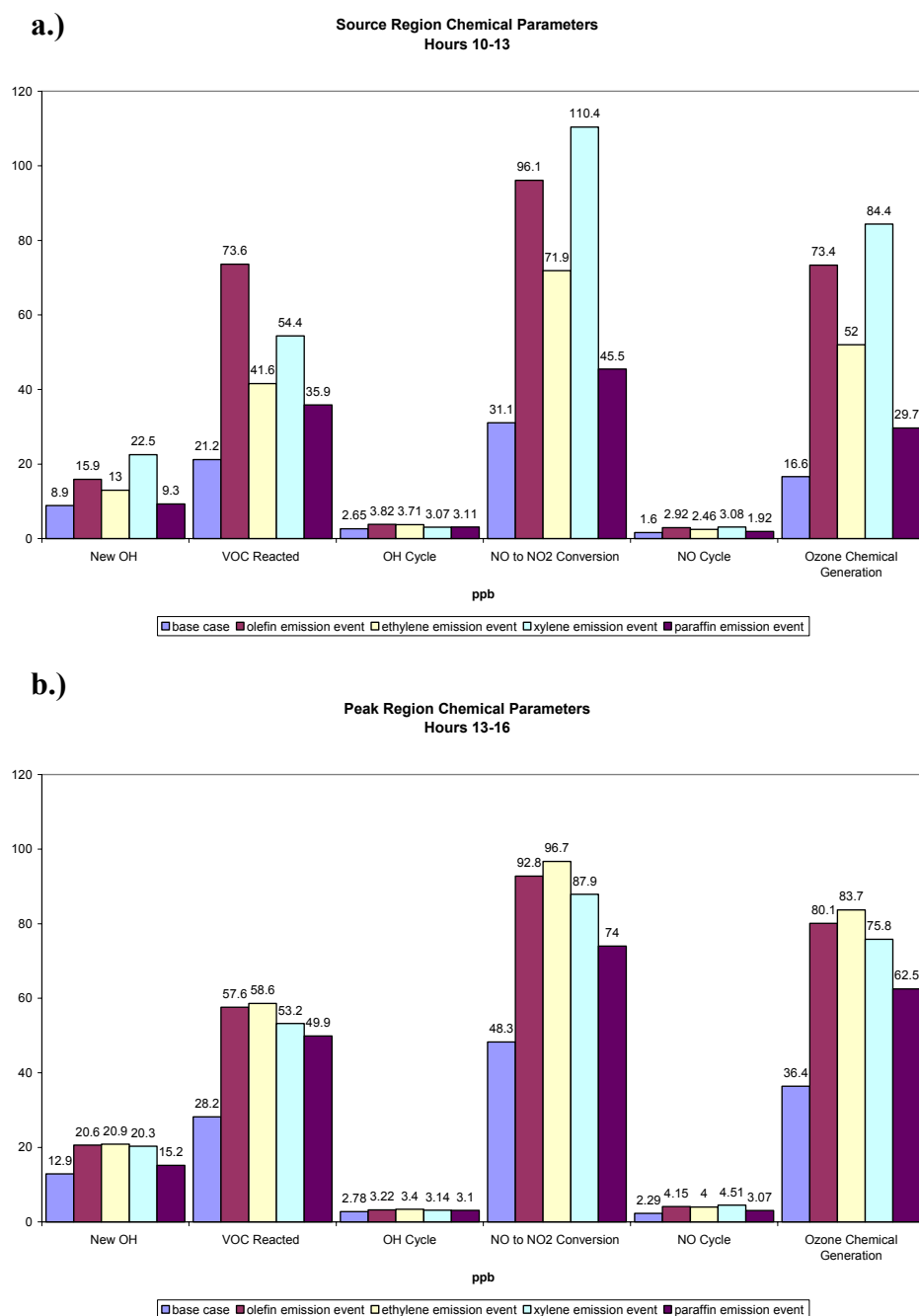


Figure 3-18. Key chemical parameters for the August 30, 2000 base case, propylene, ethylene, xylene, and n-pentane emission events for (a) the source control volume hours 10 a.m. – 1 p.m. and (b) the peak control volume hours 1 p.m. – 4 p.m.

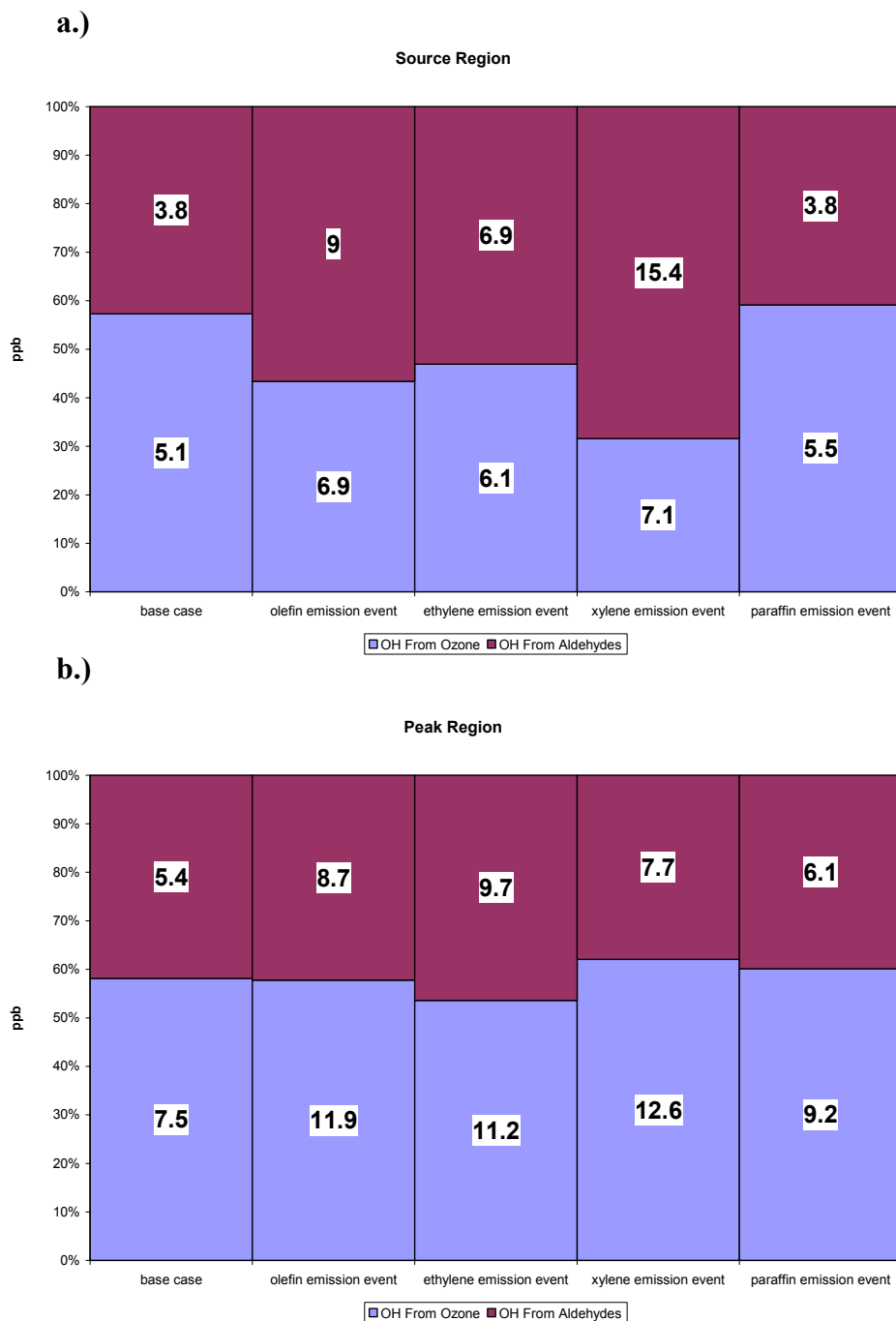


Figure 3-19. Sources of new OH radicals for August 30, 2000 for the (a) source control volume and (b) peak control volume.

3.4 CONCLUSION

The PAPPT described in Chapter 2 was used to examine the impact of emission events on ozone formation and accumulation processes in the Houston-Galveston area. Specifically, the effects of the composition of the emissions and plume trajectories were examined. Emission events involving ethylene, propylene, n-pentane, and xylene were modeled and plume processing over a NO_x rich environment was contrasted with plume processing over water. When MIR-weighted emissions were equal, each hydrocarbon, except n-pentane, contributed approximately the same increases in ozone concentrations downwind of the release point. However, the xylene case generated more ozone near the release point. Both NO_x rich and NO_x limited environments exhibited this pattern. In all of the simulations the OH radical balance provided key insights into ozone formation processes. Emissions that were able to quickly generate aldehydes created new OH radicals, which, in turn accelerated ozone formation. So, the species that had the greatest initial aldehyde yields also had the greatest initial ozone production. As the plume aged new OH was dominated by ozone photolysis and the behavior of all of the releases, except for the n-pentane, converged.

3.5 ACKNOWLEDGEMENTS

This work was made possible with funding from Houston Advanced Research Center (HARC, www.harc.edu). Aircraft data presented in this work were collected by the National Oceanic and Atmospheric Administration (NOAA, www.noaa.gov).

3.6 REFERENCES

- Murphy C., Allen D. T. 2005. "Hydrocarbon Emissions from Industrial Release Events in the Houston Galveston Area and their Impact on Ozone Formation." Atmospheric Environment In Press
- Kleinman L., Daum P., Imre D., Lee Y., Nunnermacker L., Springston S., Weinstein-Lloyd J., Rudolph J. 2002. "Ozone production rate and hydrocarbon reactivity in 5 urban areas: A cause of high ozone concentration in Houston." Geophysical Research Letters 30(12): 1639.
- Texas Commission on Environmental Quality (TCEQ) 2004. "The State Implementation Plan for the Control of Ozone Pollution: Attainment Demonstration for the Houston/Galveston Ozone Non-attainment Area." P.O. Box 13087, Austin, Texas 78711-3087, www.tceq.state.tx.us
- National Oceanic and Atmospheric Administration (NOAA). 2004. <ftp://ftp.al.noaa.gov>
- Carter W. P. 1994. "Development of ozone reactivity scales for volatile organic compounds." Journal of the Air and Waste Management Association Vol 44, 881-899.
- Gery M. W., Whitten G. Z., Killus J. P., Dodge M. C. 1989. "A Photochemical Kinetics Mechanism for Urban and Regional Scale Computer Modeling." Journal of Geophysical Research. 94, 925-956.
- Adelman Z. 1999. "A re-evaluation of the carbon bond IV photochemical mechanism." University of North Carolina at Chapel Hill, Department of Environmental Sciences and Engineering, School of Public Health.: 208 <http://airsite.unc.edu/>.

Chapter 4: Development and Evaluation of a Sub-Domain Model

4.1 INTRODUCTION

The Houston/Galveston region exceeds the National Ambient Air Quality Standards (NAAQSs) for ozone and has been designated as a severe ozone non-attainment area. Compared to other cities in the United States, Houston has a large concentration of industrial point sources, particularly chemical manufacturing facilities and petroleum refineries. Observational data collected during the 2000 Texas Air Quality Study showed that high concentrations (>200 ppb) of ozone, at times, formed rapidly in the plumes of these industrial facilities (Kleinman, et al., 2002). The data also showed that the emissions from the facilities can be episodic (Murphy and Allen, 2005). The largest of these episodic emission events can have emission rates of reactive hydrocarbons that exceed 10,000 pounds per hour; the events typically last only a few hours, can occur at all times of day, and can occur at any of dozens of facilities that are dispersed over a 10^4 - 10^5 km² region (Murphy and Allen, 2005). When large emission events occur, they dominate local emissions of ozone precursors, and therefore, in designing air quality management plans for attaining the NAAQSs for ozone, it is necessary to identify the limits that should be imposed on episodic emissions.

The previous chapter in this thesis examined the chemical and physical processes that control ozone formation during large industrial emission events by examining a small group of case studies. While this analysis provides important phenomenological information, it is limited in the sense that a small number of case studies cannot represent the diverse range of conditions associated with industrial emission events. The goal of the work presented in this chapter is to use the Process Analysis Post Processing Tools

(PAPPTs) to develop a sub-domain model that is capable of simulating the thousands of possible types of emission events. The sub-domain model could then assess the impacts of industrial emission events on ozone formation in southeast Texas.

4.2 METHODOLOGY

Thousands of possible combinations of emission events can exist with varying composition, duration, location, and timing. All these permutations may lead to different ozone formation and accumulation patterns. To consider the full range of possible permutations of emission event characteristics, it is necessary to construct computationally efficient photochemical models. These computationally efficient models would approximate, as closely as possible, the analysis that would be performed by a full 3-dimensional regional air quality model, but do so with a fraction of the computational effort of the full model.

Data in the previous chapter suggested that the impacts of emissions events are spatially isolated. Therefore, a horizontally stationary box model could be used to model the ozone formation processes focusing on the region near the release of the emission event. The stationary box model predictions could then be enhanced by incorporating data from the PAPPT described in previous chapters of this thesis. The combination of a stationary box model and the PAPPT data resulted in the synthesis of the sub-domain model, described in this chapter. The sub-domain model shares certain similarities with a conventional Eulerian box model. They both assume that the modeled air is completely mixed, and hence only one cell represents the entire volume being modeled. However, the sub-domain model allows the height of the modeled air mass to change as a function of time and allows for hourly variations in advection into and out of the sub-domain based on data imported from the full gridded model. It also imports all of the initial conditions and other key conditions of the photochemistry from the full gridded model. Allowing the vertical height of the sub-domain model to vary with time enables the sub-

domain model to simulate air within the planetary boundary layer at all times accounting for vertical entrainment and dilution due to mixing height change. Importing the initial conditions, boundary conditions, and other key conditions of the photochemistry from the full gridded model allows the sub-domain model to mimic, as closely as possible, the processes modeled by the full gridded model.

The first step in constructing the sub-domain model is to identify the geographical region, or sub-domain, to be modeled. A sub-domain shown in Figure 4-1, was used in this work. This sub-domain is identical to the PAPPT control volume used in chapter 3 of this thesis. The location was chosen because it is consistent with locations where significant numbers of emission events are reported (Murphy and Allen, 2005) and because aircraft detected evidence of emission events there. August 25, 2000 was chosen as the simulation day. On August 25, winds from the east in the late morning and early afternoon advected air from an industrial source region, referred to as the Ship Channel region (located in the center right portion of Figure 4-1), toward downtown Houston.

Figure 4-1 shows the horizontal dimension of the sub-domain; the temporal evolution of the vertical dimensions of sub-domains are determined by examining the vertical layer interface diffusivity or " K_V " values from the host 3-dimensional photochemical model, as described in chapters 2 and 3 of this thesis. These vertical dimensions of the sub-domains used in this work are the same as those reported for the PAPPT control volumes described in chapter 3.



Figure 4-1. Location of the PAPPT control volume used for August 25, 2000. The red dot indicates the location where the simulated emission event was located.

After the sub-domains' horizontal and vertical dimensions are defined, the initial and boundary conditions for the model are determined using the PAPPT. Table 4-1 lists the information used in the sub-domain model that is derived from the PAPPT output. Initial concentrations of all modeled species except fast reacting radicals are imported from the gridded model. Imported boundary conditions include emission rates, dry deposition velocity, horizontal and vertical advection rates, and entrainment/detrainment/dilution due to mixing height changes that occur at the beginning of each hour.

The rate at which emissions of various chemical species enter the sub-domain is calculated for each one-hour period of the simulation:

$$E = \frac{\sum_{\text{all } j} V_j \cdot \Delta C_{\text{emission},j}}{A \cdot \Delta t} \quad (\text{Equation 4-1})$$

where E is the emission rate (moles/m²/min) of a species during a one-hour period; $\Delta C_{\text{emission},j}$ is the change in concentration (moles/m³) due to emissions in grid cell j , extracted from the PAPPT output; V_j is the volume of the grid cell j (m³) in which the emissions occur; A is the surface area (at the surface) of the sub-domain (m²); Δt is the period for which the emission rate is calculated, i.e. 60 min. The summation is taken over all grid cells in the sub-domain.

Deposition velocity is calculated for each one-hour period of the simulation:

$$v_d = - \frac{h \cdot \sum_{\text{all } j} V_j \cdot \Delta C_{\text{deposition},j}}{\Delta t \cdot \sum_{\text{all } j} V_j \cdot \bar{C}_j} \quad (\text{Equation 4-2})$$

$$\bar{C}_j = \frac{1}{2} (C_{j,t=t_0} + C_{j,t=t_0+\Delta t}) \quad (\text{Equation 4-3})$$

where v_d is the dry deposition velocity of a species (m/sec) during a one-hour period imported from the gridded model; $\Delta C_{\text{deposition},j}$ is the change in concentration (moles/m³) due to deposition in grid cell j ; h is the height of the sub-domain for the hour being analyzed. The summation in the numerator is taken over all surface level grid cells in the sub-domain. In the denominator, \bar{C}_j is the time averaged concentration of the species in grid cell j . The form of Equation 4-2 is based on the definition of deposition velocity:

$$\left. \frac{\partial C}{\partial t} \right|_{\text{deposition}} = - \frac{v_d}{h} C \quad (\text{Equation 4-4})$$

For horizontal transport of species, only advection was considered, since diffusion played a minor role in overall transport of pollutants. The sub-domain model uses the

horizontal air exchange rate X_h (1/min) and the concentration of species in the upstream grid cells, C_{upwind} (moles/m³) to calculate advective influx of species. Efflux is product of X_h and the concentration within the sub-domain, C .

$$\left. \frac{\partial C}{\partial t} \right|_{\text{horizontal transport}} = -X_h \cdot C + X_h \cdot C_{\text{upwind}} \quad (\text{Equation 4-5})$$

Horizontal air exchange rates for the sub-domain were calculated for each hour by averaging the inflow across each of the external faces of the sub-domain:

$$X_h = \frac{\sum_{k \in \{\text{faces where air flows in}\}} a_k \cdot f_{\text{air},k}}{\sum_{\text{all } j} V_j \cdot \rho_j} \quad (\text{Equation 4-6})$$

where k is an index for the external faces of the sub-domain that experience inflow during the hour being considered; a_k is the area of the horizontal surface (m²), and $f_{\text{air},k}$ is flux of air at the face (moles/m²/min); ρ_j is the density of the air in cell j (moles/m³), V_j is the volume of the cell j (m³).

The time-averaged upwind concentration \bar{C}_{upwind} was calculated as the volumetric average of concentration of the species within the air that flows into the box. Specifically

$$\bar{C}_{\text{upwind}} = \frac{P}{R \cdot T} \cdot \frac{\sum_{k \in \{\text{faces where air flows in}\}} a_k \cdot f_k}{\sum_{k \in \{\text{faces where air flows in}\}} a_k \cdot f_{\text{air},k}} \quad (\text{Equation 4-7})$$

The bar in \overline{C}_{upwind} represents the fact that the concentration is time-averaged value for one hour; f_k is the flux of species k ; p is total pressure [Pa], R is the gas constant [J/mol/K], and T is temperature[K].

Calculations analogous to Equations 4-6 and 4-7 were made in order to calculate vertical advection. Vertical air exchange rate X_v (1/min) and aloft concentration \overline{C}_{aloft} are calculated based on the upper boundary of the sub-domain, however, it should be noted that the design of the sub-domain model, which defines the height of the sub-domain as the mixing height, makes the exchange of mass at the top boundary small.

Since the height of the sub-domain may change at the beginning of each hour, mass can be entrained or detrained at each hour. Chapter 2 of this thesis describes how entrainment and detrainment were calculated. The treatment of the detrainment term in the sub-domain model is slightly different. Unlike the PAPPT of the 3-D model, detrained air has the same concentration throughout the sub-domain. Therefore detrainment of mass does not change concentrations in the sub-domain, as it does in the gridded model. Entrainment of aloft air is treated in the same manner described in chapter 2.

The dark chemistry of the gridded and sub-domain models has identical reaction paths and rate expressions (temperature/pressure dependency). Temperature, atmospheric pressure, and water content of air in the sub-domain model were calculated based on a volumetric average of those in the gridded model. Photolysis rates in the sub-domain model were imported from the gridded model as a volumetric average of

photolysis rates in each grid cell, which was estimated as a function of solar zenith angle, altitude, total ozone column, surface albedo and atmospheric turbidity (Environ, 2004).

All of the parameters listed in Table 4-1 are updated at the beginning of every hour. The resultant system of ordinary equation was solved numerically. A FORTRAN code that implements the difference equations used the mechanism compiling code developed by Carter (2004), and used LSODE (Hindmarsh, 1980) to solve the ordinary differential equations.

Process	Parameters imported from gridded model
Initial Condition	
	Initial Concentrations
Physical Processes	
Emissions	Emission Rate
Dry Deposition	Deposition Velocity
Horizontal Advection	Horizontal Air Exchange Rate
	“Upwind” Concentration
Vertical Advection	Vertical Air Exchange Rate
	Aloft Concentration
Entrainment	Mixing heights before/after entrainment
	Aloft concentration
Dilution	Mixing heights before/after entrainment
Chemical Processes	
Dark Chemistry	Temperature
	Pressure
	Water Content
Photolysis	Photolysis Rate

Table 4-1. Processes modeled in the sub-domain model

A sub-domain model was developed to efficiently use computational resources in analysis of a stochastic emission inventory. The basic approach of the development of this tool was to extend the capability of a conventional box-model tool using output from a three-dimensional Eulerian model with the help of the PAPPT. The sub-domain model was customized to represent a particular part of the host Eulerian model. In this way the sub-domain model can replicate results from the three-dimensional model as closely as possible, yet is computationally efficient, and allows researchers to simulate large numbers of scenarios. The sub-domain model could then be used to identify emission events that lead to extreme values of ozone formation and accumulation and to establish general trends in the response of ozone formation and accumulation to variables such as event magnitude, timing, and location.

A 3-dimensional eulerian photochemical model with the PAPPT was used to evaluate, for selected cases, whether the trends and extreme values predicted by the sub-domain model were replicated by the 3-dimensional model. The 3-dimensional photochemical model and PAPPT used in this work was identical to the model formulation described in chapter 3. Briefly, model simulations were performed using the Comprehensive Air Quality Model, with extensions, version 4.03 (CAMx 4.03, <http://www.camx.com>). An August 22 - September 6, 2000 photochemical modeling episode was used. Results of the evaluation of the sub-domain model by the CAMx model are now presented.

4.3 RESULTS

The goal of this study is to evaluate the performance of the sub-domain model in representing the behavior of a full gridded model. This comparison was performed by evaluating the PAPPT output (see chapter 2 of this thesis) from the full gridded and sub-domain models for a base case simulation and a simulation with emission events added. Figure 4-2a-b compares the time series plot for ozone for both the full gridded model and the sub-domain model on the August 25, 2000 simulation day in the base case scenario. The sub-domain model is initialized with the conditions at 6:00 of the gridded model and simulation continued through 18:00. Therefore Figure 4-2b shows only the processes for 12 hours during the day. The black line indicates the mixing ratio of ozone, whereas the colored lines indicate the contribution of each process to the change in ozone concentration. Daily maximum ozone concentrations within the sub-domain were 57.7 ppb and 59.9 ppb for the gridded and sub-domain models, respectively. Both models show (1) large entrainment from aloft between 7:00 to 8:00, (2) chemical formation of ozone from 9:00 to 16:00 with a mild peak around noon, and (3) large losses of ozone between 12:00 to 15:00 due primarily to horizontal transport. The results show that both models predict similar results for final ozone concentrations and physical process rates.

Figures 4-2c-d are a demonstration of the effect of adding an emission event of 11,638 lbs of propylene at a constant rate of 5,819 lbs/hr from 10:00 - 12:00 at the location indicated in Figure 4-1. The thick lines show the results with the added propylene, while the thinner lines are the result without the emission event (i.e., identical to the results in Figure 4-2a-b) shown for reference purposes. To meet our purpose, the two models should respond to the perturbation in an identical manner.

Examination of the time series curves reveal that the sub-domain model ozone concentrations are smeared in time compared to the gridded model. In the gridded model's concentration of ozone, the difference between the two scenarios occurs mostly around 12:00, while the result from sub-domain model has a larger time window of a few hours. The horizontal advection illustrates this phenomenon in a more pronounced way. The gridded model shows a distinct spike of horizontally advection rates between 12:00 to 13:00. The sub-domain model smears this advection spike into a three-hour window spanning 11:00 to 14:00.

The discrepancy in the chemical process rates of the two models could be explained by how each model treats the transport of pollutants. The eulerian grid framework of the CAMx model allows the introduction of an emission event into a single grid cell within the PAPPT control volume. The emitted pollutants are then transported throughout the control volume via diffusion and exchange with other grid cells. This causes the model to behave similar to a plug-flow model when emissions are introduced. In contrast, the sub-domain model lacks the resolution of the grid frame work and emissions can not be introduced into a single grid. Instead, emissions are completely mixed throughout the control volume. As a result, pollutant concentrations are diluted and residence times are reduced.

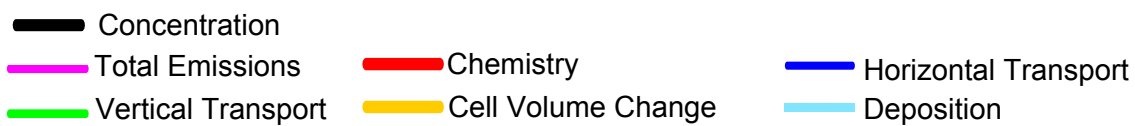
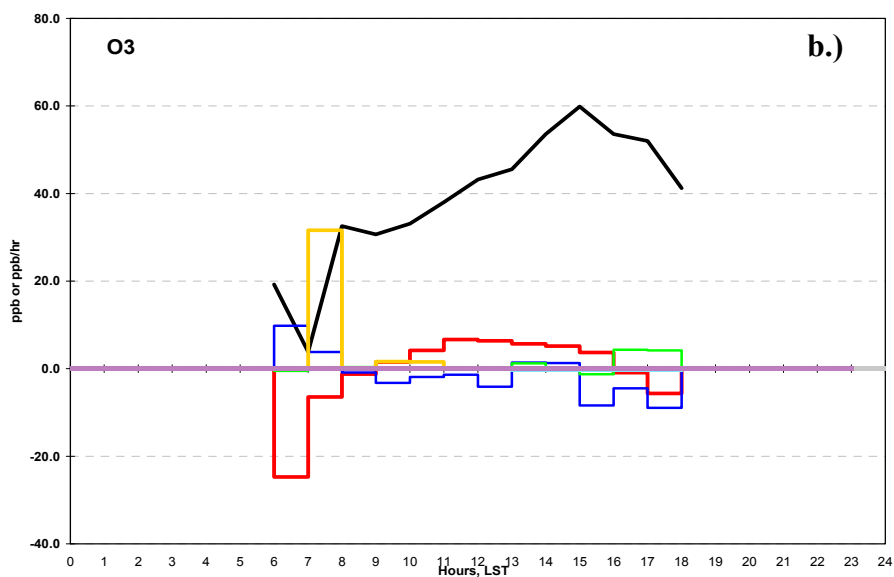
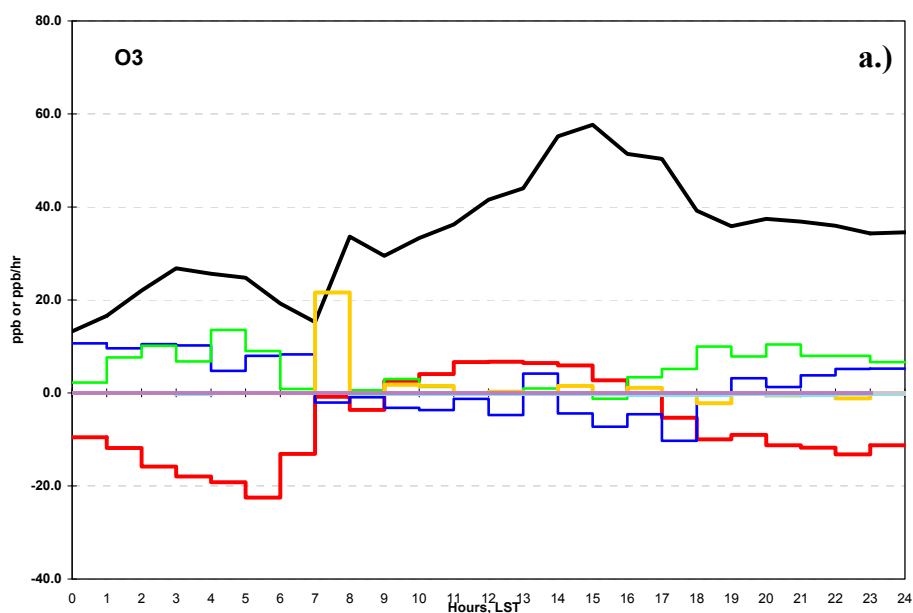


Figure 4-2. Evolution of ozone concentrations and rates of change of ozone concentration over the course of a 24-hour period in the PAPPT control volume on August 25, 2000 for the (a) full grid and (b) sub-domain model respectively.

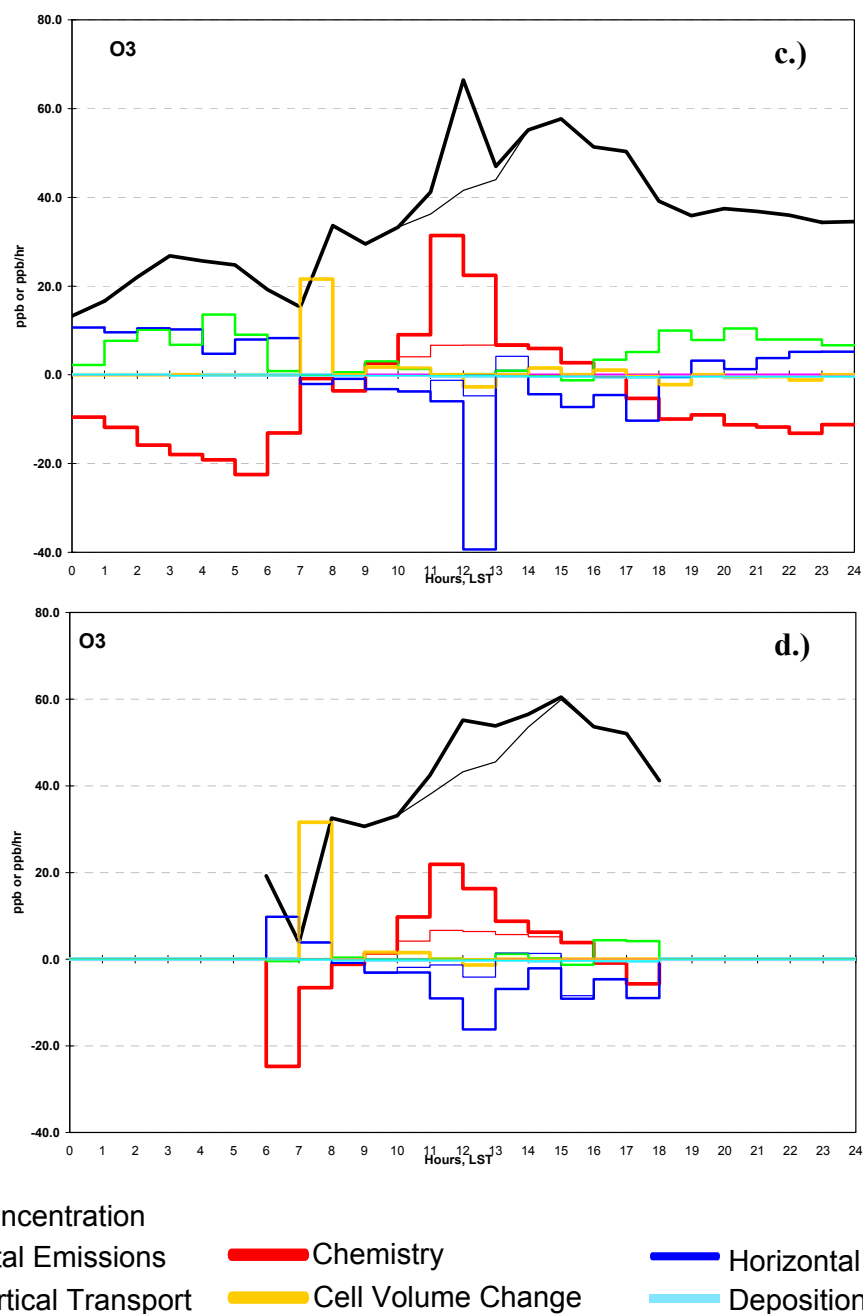


Figure 4-2. (c),(d) Evolution of ozone concentrations and rates of change of ozone concentration over the course of a 24-hour period in the control volume on August 25, 2000 for the (c) full grid and (d) sub-domain model respectively. Solid lines show the result with 11,638 lbs propylene added between 10:00 to 12:00. Thin lines were the results without addition.

Figure 4-3a-d compares the chemistry cycles of the two models. Chapter 2 of this thesis describes in detail the cycle diagrams created by the PAPPT. As seen in Figures 4-2c-d, the VOC emission event affects ozone chemistry primarily between 10:00 to 13:00 for gridded model, and 10:00 to 14:00 for the sub-domain model. To highlight the change in chemistry caused by the VOC emission event, the chemistry cycles focused only on the hours between 10:00 and 14:00.

When a comparison was made between the two unperturbed cases, Figures 4-3a-b, the chemistry cycle values match very closely. For example 14.4 ppb of new OH radicals were created in both the gridded model and the sub-domain model. The amount of reacted VOC was 29.7 ppb and 29.1 ppb, NO to NO₂ conversion was 47.3 and 45.8 ppb, and chemically produced O₃ was 24.7 and 23.5 ppb for the gridded model and the sub-domain model respectively. This demonstrates that the sub-domain model reproduces the processes contributing to species change in the model.

Figure 4-3c-d shows the full gridded and sub-domain model cycle diagrams for the emission event simulation. The gridded model generated 2.4 ppb more OH radicals, reacted 14.2 ppb more VOCs, converted 16.9 ppb more NO to NO₂, and ultimately generated 14.3 ppb more of O₃. The gridded model reacted a larger amount of VOC in the control volume than the sub-domain model. The differences between the two models

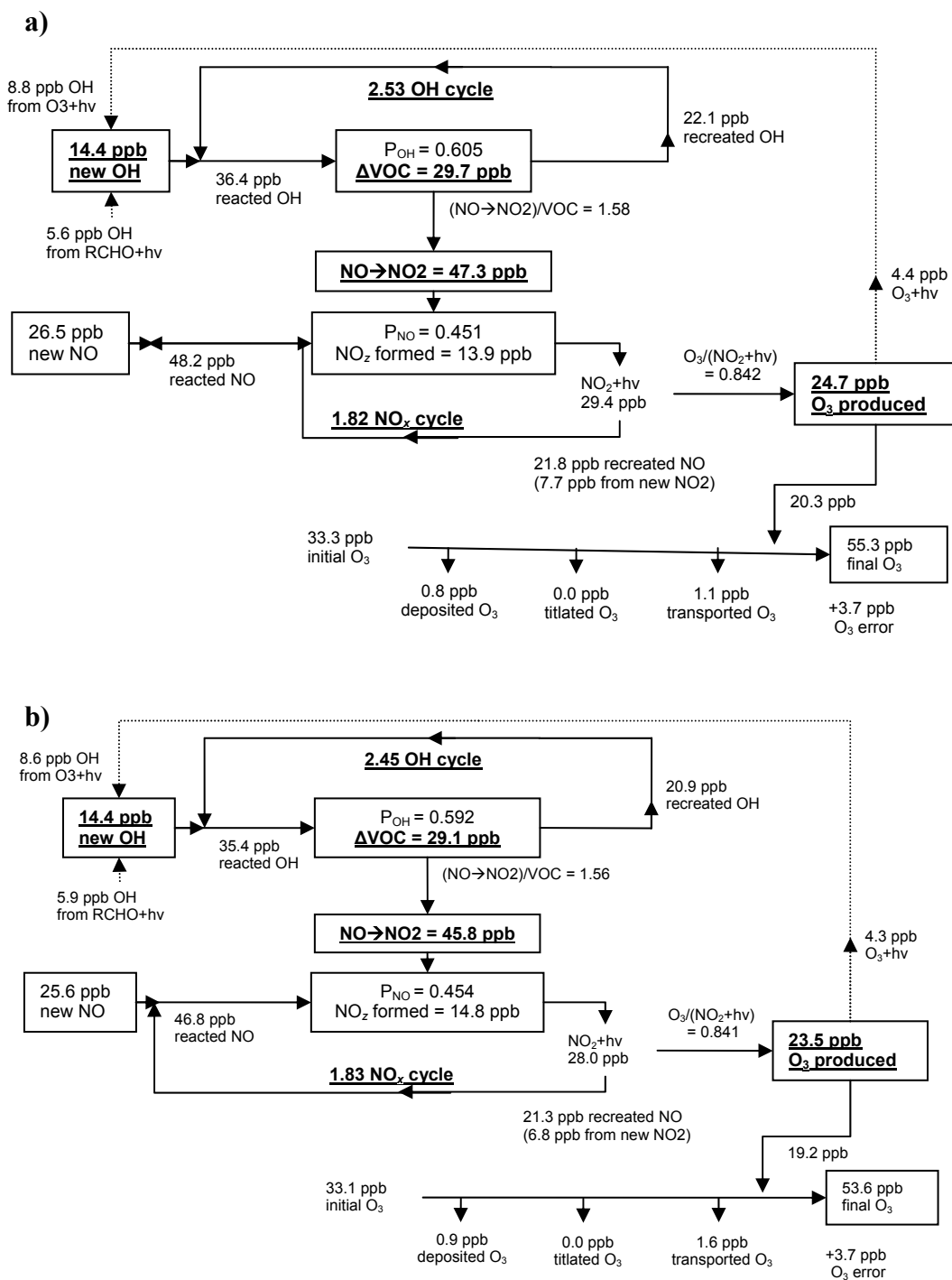


Figure 4-3. Chemistry cycle diagram for a 4-hour period (10:00 to 14:00) in the control volume on August 25, 2000 for the (a) full grid, and (b) sub-domain models respectively.

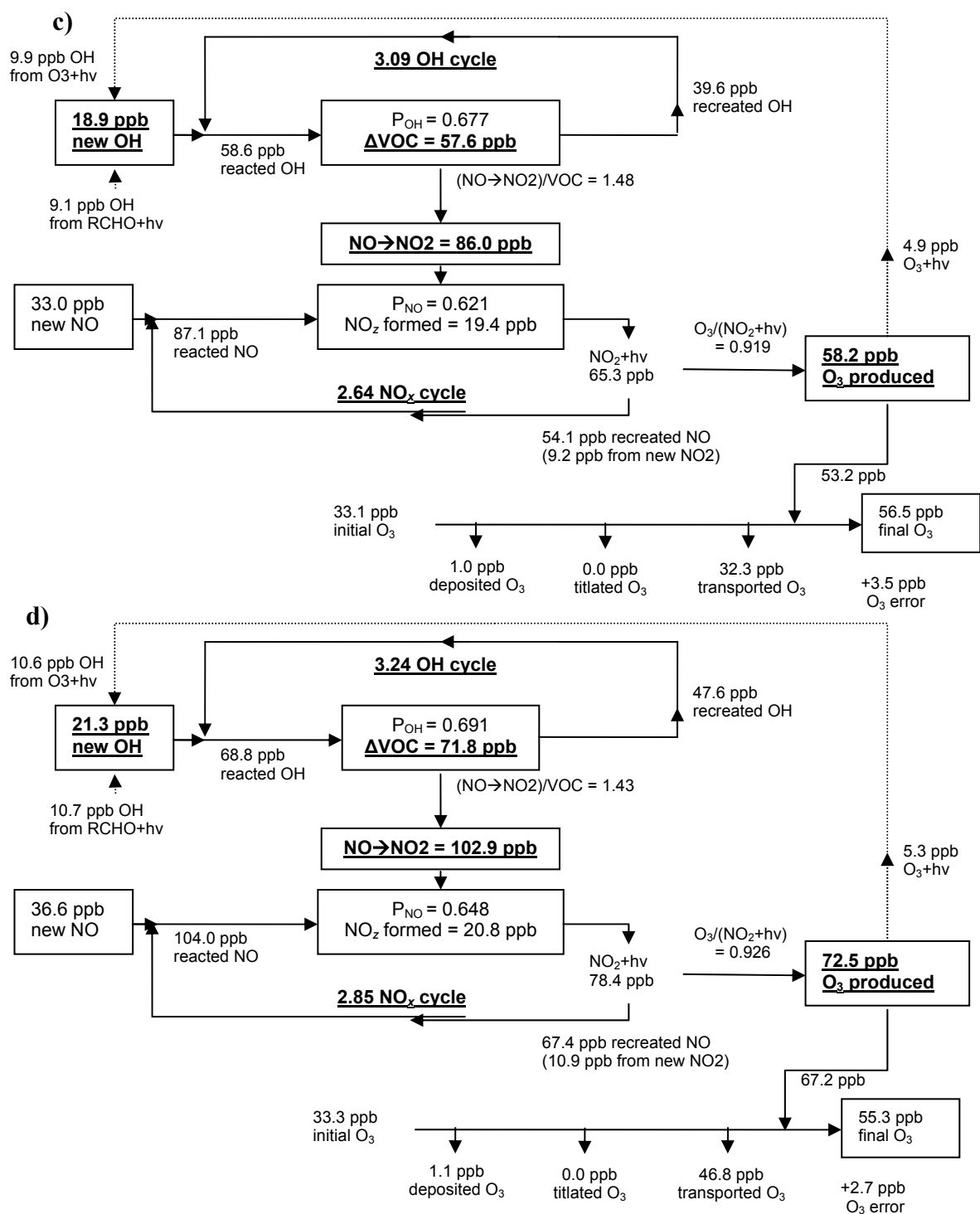


Figure 4-3. Chemistry cycle diagram for a 4-hour period (10:00 to 14:00) in the control volume on August 25, 2000 for the emission event simulation for the (c) full grid, and (d) sub-domain models respectively.

are more pronounced when large concentration gradients are introduced into the control volume. This suggests that the differences in the transport treatments by each model described earlier in this chapter could be the reason for these discrepancies.

4.4 CONCLUSION

The PAPPT was used to develop a simplified sub-domain model to produce similar predictions to a full 3-D gridded model. The PAPPT also was used to compare the physical and chemical processes of both the sub-domain and full grid CAMx model. Time series plots revealed that the sub-domain model smeared pollutant concentrations in time when compared to the gridded model. The chemical process rates, quantified in the cycle diagrams, showed similar values between each model in the base case. However, the differences between the two models become more pronounced when large concentration gradients were introduced into the control volume. In the emission event scenario the gridded model was able to react a larger amount of VOC in the control volume than the sub-domain model.

The discrepancy in the chemical process rates of the two models could be explained by how each model treats the transport of pollutants. The eulerian grid framework allows for greater resolution for the introduction of an emission event into a smaller control volume. In contrast, the sub-domain model's lacks the resolution of a grid frame work and emissions are completely mixed into the entire control volume. As a result, pollutant concentrations are diluted and residence times are reduced. For the sub-domain model this results in the reduction of the amount of time for VOC to react and ultimately generate ozone within the PAPPT control volume.

4.5 REFERENCES

- Kleinman L., Daum P., Imre D., Lee Y., Nunnermacker L., Springston S., Weinstein-Lloyd J., Rudolph J. 2002. "Ozone production rate and hydrocarbon reactivity in 5 urban areas: A cause of high ozone concentration in Houston." *Geophysical Research Letters* 30(12): 1639.
- Murphy C., Allen D. T. 2005. "Hydrocarbon Emissions from Industrial Release Events in the Houston Galveston Area and their Impact on Ozone Formation." *Atmospheric Environment* In Press
- ENVIRON. 2004. CAMx Users Guide, v4.00. 2004. www.camx.com
- Carter W. P. 2004. "SAPRC-99 Mechanism Files and Associated Programs and Examples." <http://pah.cert.ucr.edu/~carter/SAPRC99.htm> last accessed 2005-02-23.
- Hindmarsh A. C. 1980. "Isode and Isodi, two new initial value ordinary differential equation solvers." *ACM-Signum newsLetters*, vol. 15, no. 4, pp. 10-11.

Chapter 5: Wildfires in eastern Texas in August and September 2000: Emissions, aircraft measurements and impact on photochemistry

5.1 INTRODUCTION

Outdoor fires can emit substantial amounts of particular matter (PM), carbon monoxide (CO), non-methane hydrocarbons (NMHCs), nitrogen oxides (NO_x), and ammonia (NH₃) into the atmosphere (Sandberg, 1999). In Texas, emissions of CO and fine particulate matter (particulate matter with diameters less than 2.5 µm, PM_{2.5}) from fires account for 10% and 1%–2% of total annual statewide emissions, respectively (Dennis *et al.*, 2002). On days and seasons when large fire events occur, these percentages can be much higher, and fires can dominate emissions and impact air quality over substantial areas (Liu, 2004).

The air quality impacts of fires are often estimated based on predicted emissions. Fire emission predictions are based on estimates of area burned, fuel mass burned per area and emissions per mass of fuel combusted. Significant uncertainties can arise in estimating each of these parameters, thus the emission estimates can be uncertain. Dennis *et al.* (2002) estimated uncertainties of approximately a factor of two in area burned and fuel loadings. Additional uncertainties in assessing the air quality impacts of fires are due to uncertainties in emission factors, which depend on the nature of the combustion (smoldering versus flaming) and the plume rise of the fire.

Work has already been done evaluating some of these uncertainties associated with estimating fire emissions. Junquera (2004) developed a model ready fire emission data file so that predicted emissions could be compared with observations made during a

large air quality field program, conducted in southeast Texas during the summer of 2000. This chapter will use the fire emission inventory in a 3-D model to characterize the photochemistry occurring in the wildfire plumes during the study period. This analysis will be accomplished by utilizing the PAPPT described in previous chapters.

5.2 METHODOLOGY

Junquera (2004), estimated emissions from wildfires for the regional domain shown in Figure 5-1. Wildfire emissions were estimated for the months of August and September 2000. These dates allowed for direct comparison with observed data from the Texas Air Quality Study (TexAQS) conducted from August 15 – September 15, 2000. The wildfire emissions inventory was merged with an existing inventory of emissions from point, area, and mobile sources obtained from the Texas Commission on Environmental Quality (TCEQ) as part of the Houston/Galveston Air Quality Science Evaluation (TCEQ, 2003). The modeling domains used by the TCEQ have a horizontal resolution of 16-by-16 kilometers (East Texas subdomain), 4-by-4 kilometers (HGBPA subdomain), or 1-by-1 kilometers (HG subdomain) (Figure 5-1).

The emissions data were input into the Comprehensive Air Quality Model with extensions (CAMx) version 3.11, a 3-dimensional eulerian photochemical grid model (ENVIRON, 2000). This allowed for more detailed assessments of the air quality impacts of fires predicted by the photochemical model. CAMx was used to examine the spatial dispersion of fire emissions, the impact of fire emissions on ozone formation, and other photochemical processes. The results section will describe the CAMx simulations and the impact of the fires on air pollutants. The physical and chemical processes occurring within the modeled fire plumes were evaluated with the PAPPT.

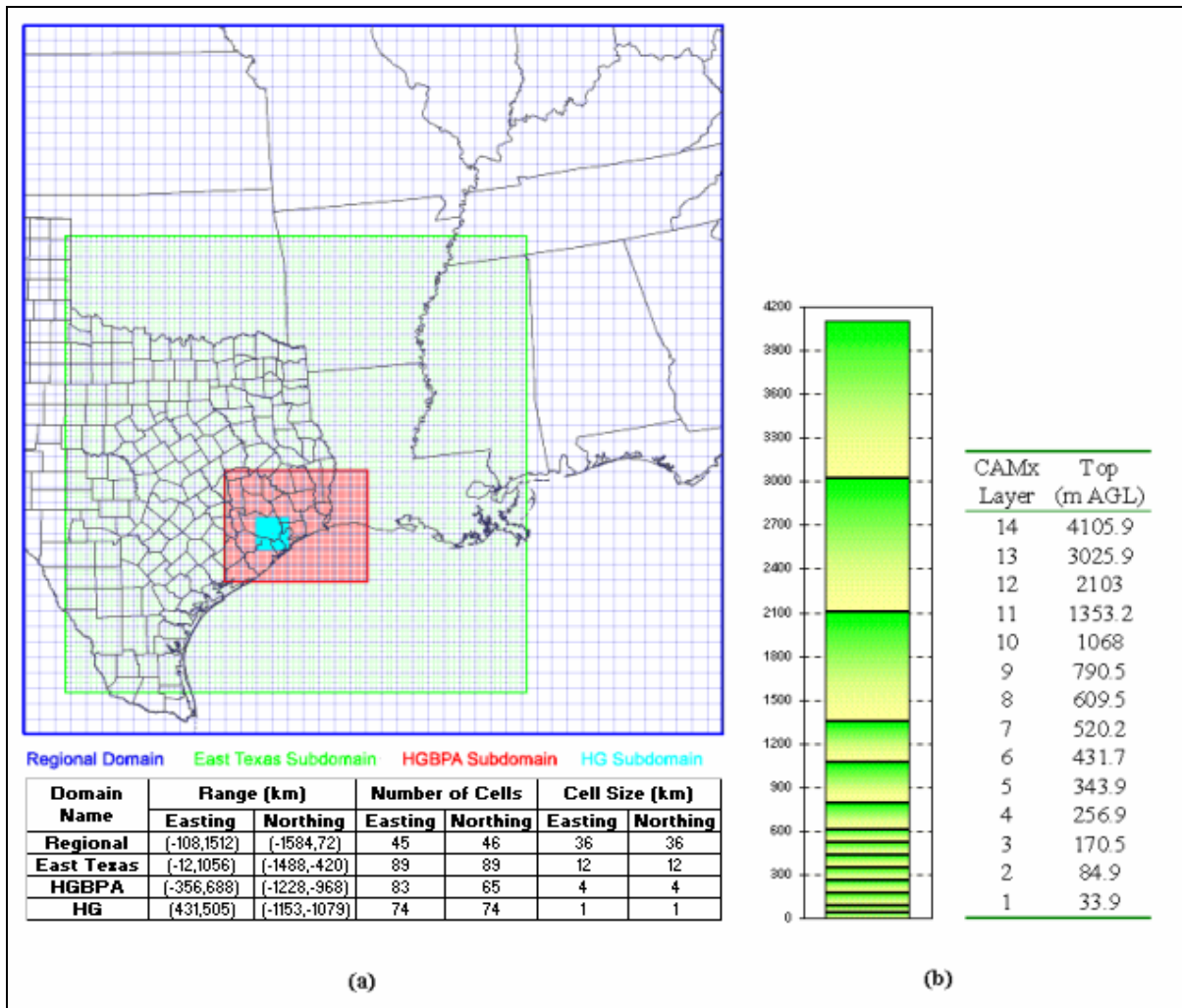


Figure 5-1. Horizontal and vertical structure of the modeling domain for the study. Fire emissions during the study period were estimated for the regional domain, with special attention paid to the Houston-Galveston, Beaumont Port Arthur (HGBPA) sub-domain. Emissions were assumed to enter a variety of vertical layers in an air quality model (Comprehensive Air Quality Model with extensions, CAMx).

5.3 RESULTS

In August and September 2000, 518 km² (128,000 acres) were burned in wildfires in Texas and 389 km² (95,000 acres) burned in the HGBPA domain (Table 5-1). In the HGBPA domain, 2% of the fires were larger than 3.24 km² (800 acres) and accounted for 56% of the total area burned, and 74% of the fires were smaller than 0.405 km² (100 acres) and burned only 5 percent of the total area. Figure 5-2 shows wildfire locations and acreage burned from August 22nd to September 6th. Estimated emissions of CO, NMHCs, PM_{2.5}, and NO_x in the HGBPA domain are shown in Figure 5-3. Figure 5-3 also shows the daily average emissions of CO, NMHCs, and NO_x from light duty gasoline vehicles (LDGV) in the Houston-Galveston area. Figure 5-3 shows that emissions of CO and NMHCs from fires exceeded emissions from LDGV on some days. The highest emissions during this period were approximately 3,700 short tons/day, 250 short tons/day, 340 short tons/day, and 50 short tons/day for CO, NMHC, PM_{2.5}, and NO_x, respectively.

Period	Regional Domain	Texas	HGBPA Domain
August & September	971 (240,000)	518 (128,000)	389 (96,100)
September 2 – 8	386 (95,300)	251 (62,000)	262 (64,700)

Table 5-1: Burned area in km² (acres) during the study period; September 2–8 was characterized by the highest wildfire intensity.

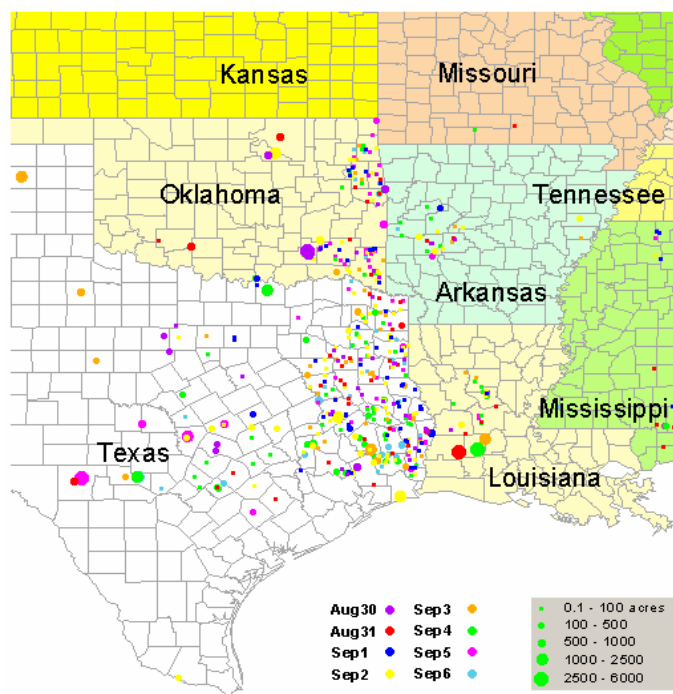
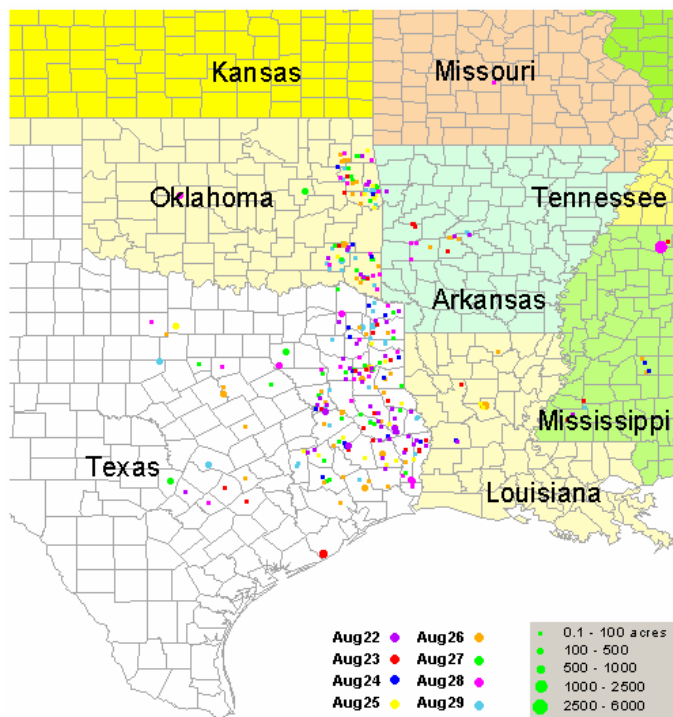


Figure 5-2. (a) Wildfires during the period from August 22–August 29, 2000. (b) Wildfires during the period from August 29–September 6, 2000.

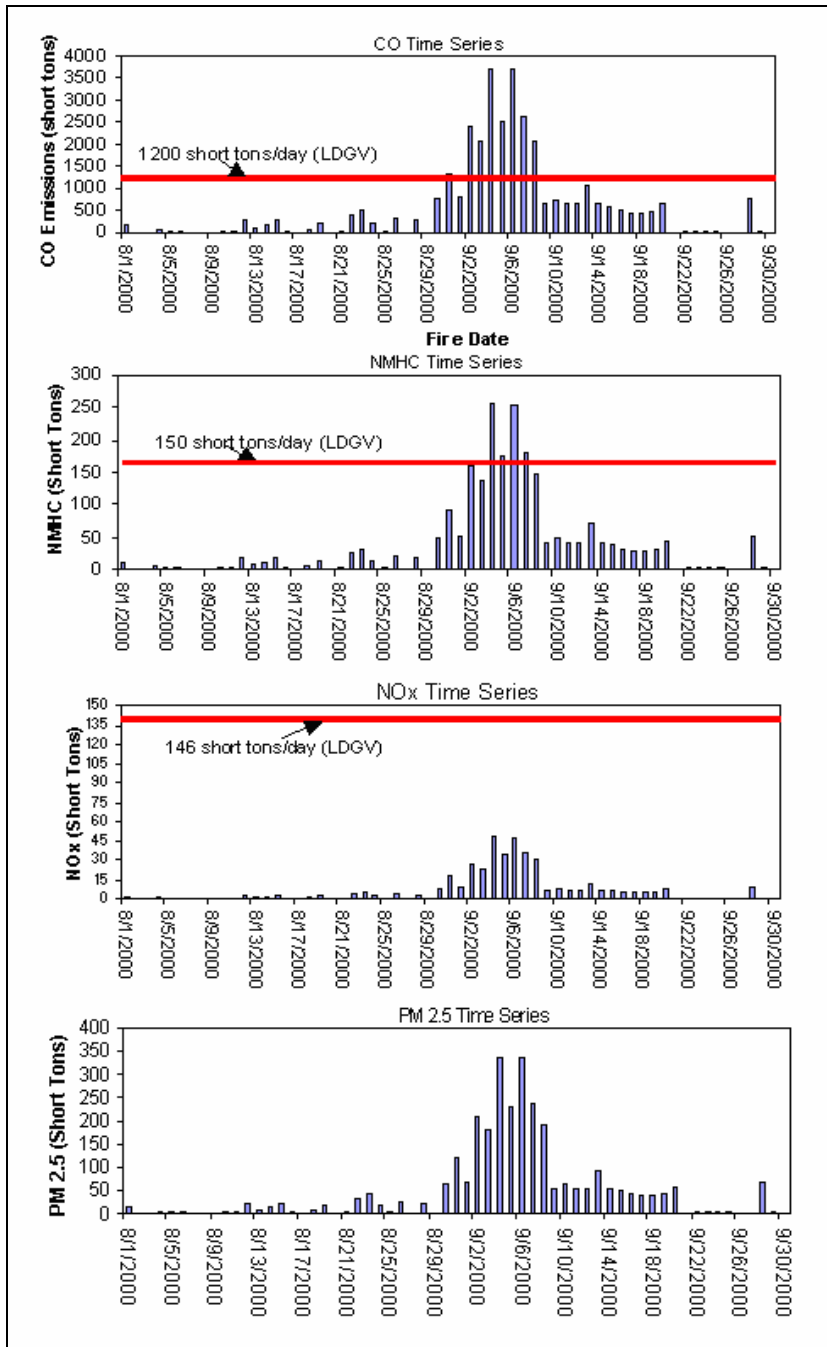
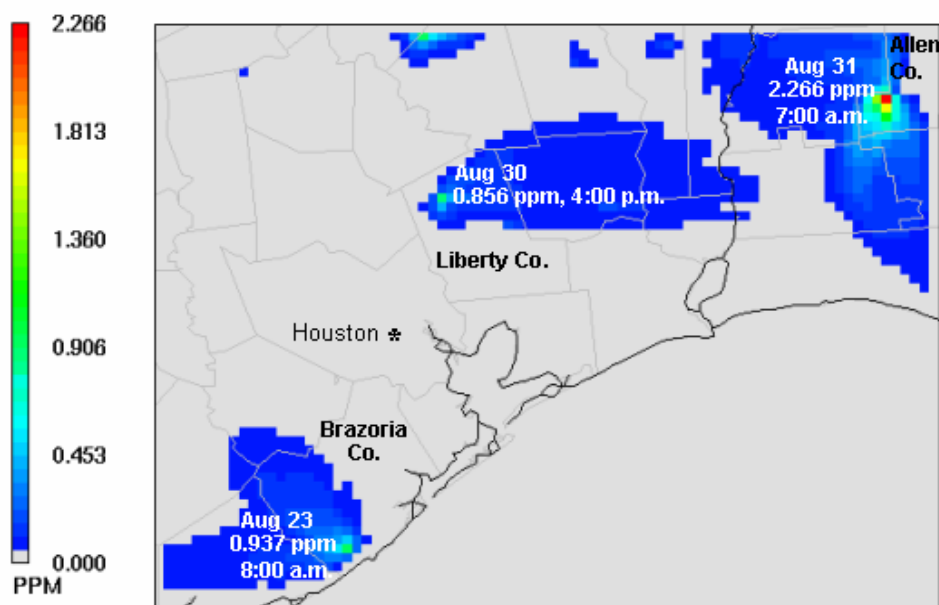


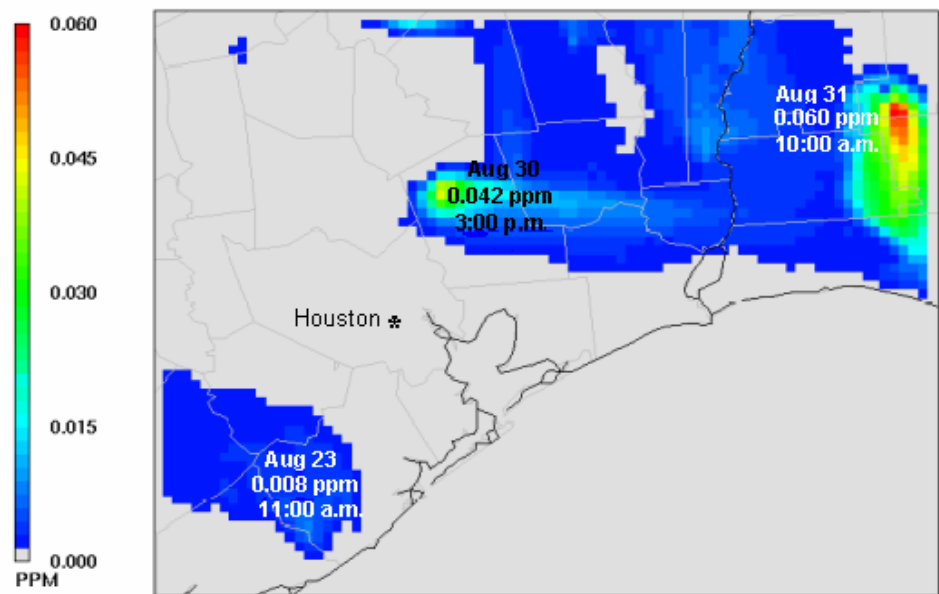
Figure 5-3: Emissions of CO, NMHCs, NO_x, and PM_{2.5} from wildfires in the HGBPA domain during August and September 2000. Emissions of CO and NMHC from wildfires exceeded emissions from Light Duty Gasoline Vehicles, LDGV (indicated by horizontal line) on some days.

Junquera (2004) used a variety of ambient measurements to evaluate the performance of the emission estimates. These included total aerosol concentrations (as characterized by aerosol backscatter) as a function of elevation measured by a National Oceanic and Atmospheric Administration (NOAA) aircraft with downward-looking aerosol and ozone Light Detection and Ranging (lidar). Gas phase air pollutant concentrations also were measured by a second NOAA operated aircraft. Details of the aircraft measurements and operation are described elsewhere (NOAA, 2003; NCAR, 2002). Comparison of aircraft measurements and emission estimates demonstrated that, within the uncertainty limits of the tools, emission estimates were accurate (Junquera, 2004).

The newly developed fire emission inventory allowed for more detailed assessments of the air quality impacts of fires. CAMx simulations were performed both with and without the emissions from fires included. The difference between these simulations characterizes the impact of the fires. Figures 5-4 and 5-5 show two difference plots (concentrations predicted by the simulation including fire emissions minus concentrations predicted by simulation without fire emissions) for CO and ozone. Figure 5-4 shows, for each grid cell, the maximum difference in CO and ozone concentrations throughout the period from August 22nd to August 31st. Figure 5-5 shows the same data for September 6th. CO is shown because, as a slow-reacting species, it characterizes the dispersion of the fire emissions. A 4-km² (1000-acre) fire in Liberty County, 80 km (50 miles) northeast of Houston, caused a peak CO concentration of 856 ppb on August 30. In Allen County, Louisiana, a 16-km² (4000-acre) fire burned on August 31st causing a peak CO concentration of 2.266 ppm. On August 23rd, a 3-km² (750-acre) fire in Brazoria County, 97 km (60 miles) south of Houston, caused a 937-ppb peak CO



(a)



(b)

Figure 5-4: Difference plots (concentrations predicted by the simulation including fire emissions – concentrations predicted by simulation without fire emissions) for CO (a) and ozone (b). The figure shows, for each grid cell, the maximum difference in CO and ozone concentrations throughout the period from August 22nd to August 31st.

concentration and a 60 km fire plume with a northwest direction. The same fires caused localized increases in O₃ concentrations of 8 ppb, 42, ppb, and 60 ppb, on August 23rd, 30th, and 31st, respectively. The results of the simulations reported in Figure 5-4 indicate that for wildfires less than 10,000 acres, the greatest enhancements of CO and ozone concentrations due to the fire emissions are confined to regions within 10-100 km of the fire.

The CAMx model has the capability of performing a more detailed analysis of the physical and chemical processes influencing the formation and accumulation of ozone and other photochemical pollutants, using the PAPPTs described in previous chapters. The PAPPTs were applied on two simulation days, August 30 and September 6, 2000. On August 30th an isolated rural wildfire northeast of Houston, shown in Figure 5-4, was advected over relatively limited number of NO_x sources. The September 6th fire plumes, shown in Figure 5-5, were advected toward the Houston urban core. These two days provide distinct environmental conditions for ozone generation. The processes influencing ozone production in both scenarios were examined with the PAPPT.

The PAPPT allows quantitative tracking of individual physical and chemical process that contribute to changing pollutant concentrations. The processes tracked include horizontal and vertical pollutant fluxes crossing cell boundaries, chemical production and consumption rates, emission rates, and deposition rates. These rates are aggregated over a collection of vertical and horizontal grid cells defined as a control volume. Figures 5-6a-b show the horizontal dimensions of the control volume used for this analysis. The location of each control volume was chosen to capture the largest

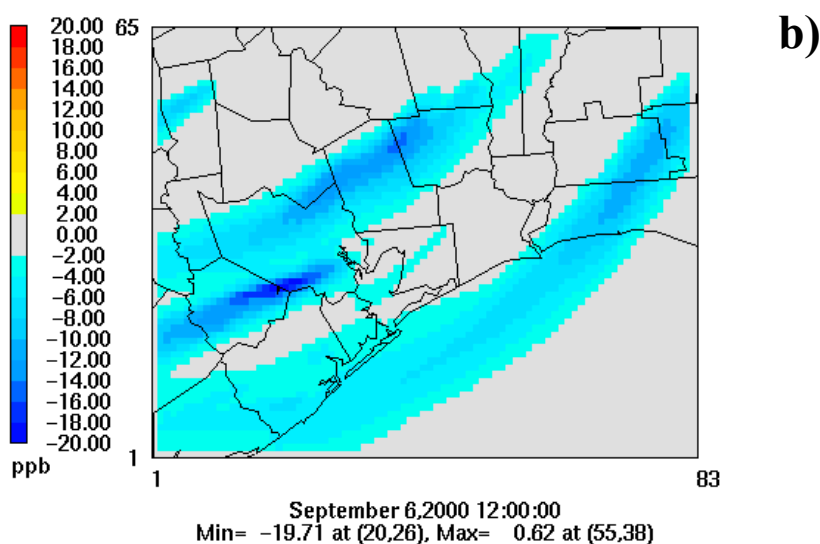
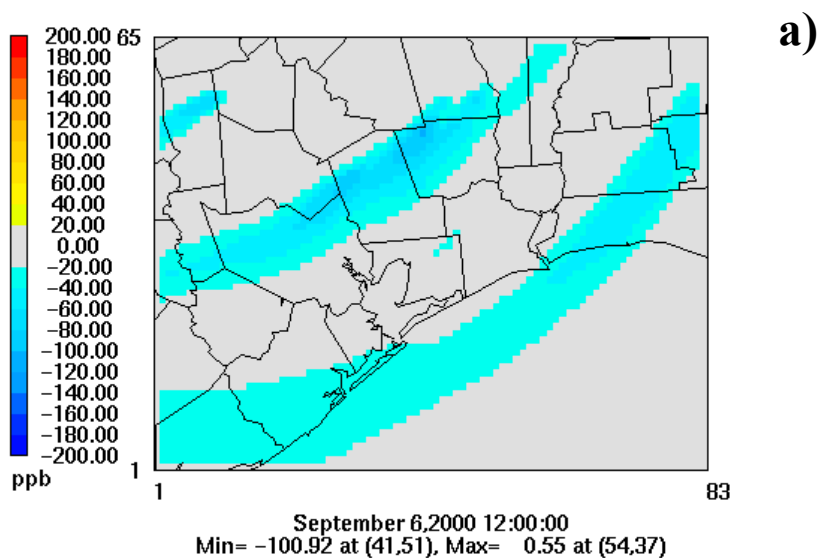


Figure 5-5. Difference plots (concentrations predicted by the simulation without fire emissions – concentrations predicted by simulation including fire emissions) for CO (a) and ozone (b). The figures are for September 6, 2000 hour 12; the time of the largest increase in ground level ozone concentrations due to fires.

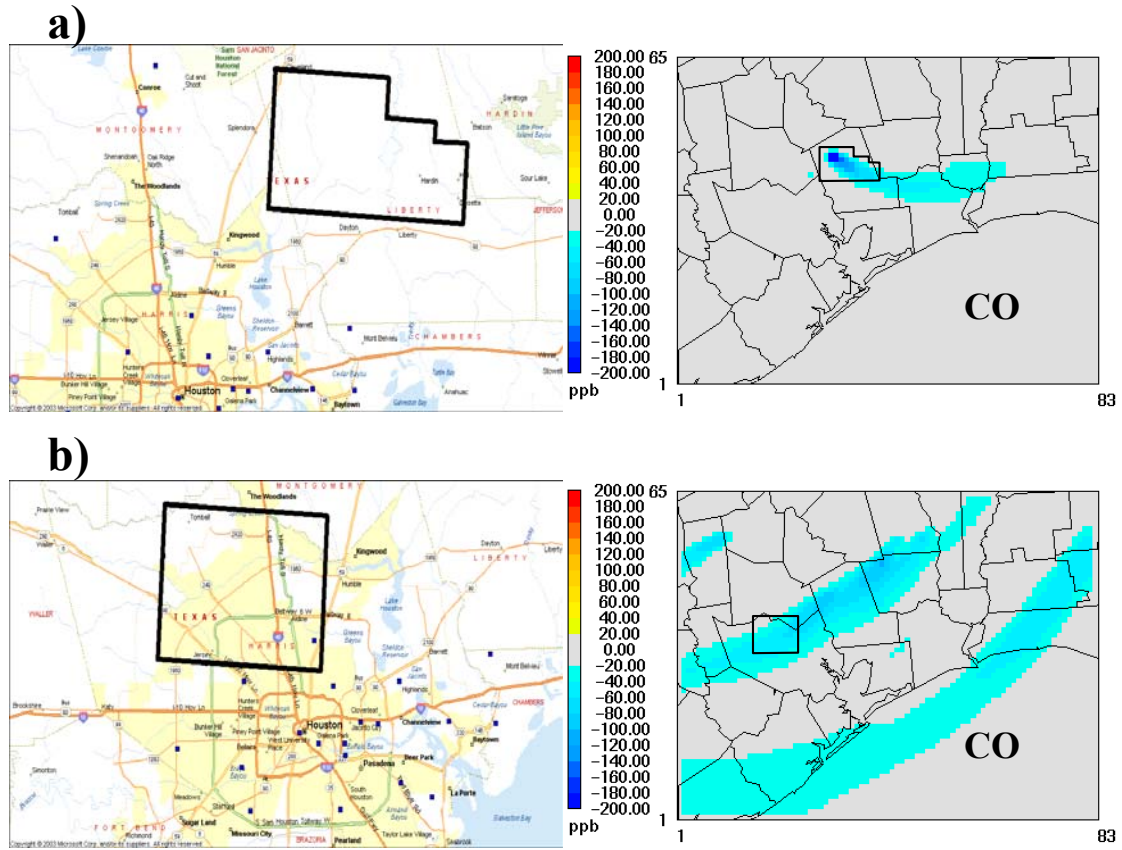


Figure 5-6. Location of PAPPT control volumes on (a) August 30, 2000 and (b) September 6, 2000.

increases in ground level ozone concentrations due to wild fire sources. The height of the control volume tracked the mixing height, as described in previous chapters.

Hourly VOC/NO_x ratios based on cell concentrations for each control volume are shown in Figures 5-7a and b. Ratios during daylight hours peaked at 64 at hour 17 on August 30th and 30 at hour 18 on September 6th. These values are typical of a photochemical environment where ozone production is limited by NO_x availability. The increased number of non-wildfire (urban) NO_x sources located in the September 6th control volume provided additional NO_x and reduced VOC/NO_x ratios. Figures 5-10a and 5-10b identify the specific VOCs that reacted to produce ozone within the control volumes, during hours 13-16 on August 30th and hours 10-13 on September 6th. The August 30th control volume generated 12 ppb of ozone compared to 27 ppb on September 6th. The August 30th control volume is located in a rural region where the majority of ozone formation chemistry, 63%, is due to reactions of isoprene. In the emission inventory developed for this work, the fires had very low rates of isoprene emissions, compared to other reactive hydrocarbons, so the bulk of the ozone formation reactions are due to isoprene emissions from the forests downwind of the fires. On September 6th, the fire, and the control volume, is located closer to Houston and is impacted by anthropogenic sources. Isoprene reactions account for only 33% of total ozone production. A more detailed analysis of the ozone chemistry is provided by reviewing several additional parameters, shown in Figure 5-9. Each parameter has been summed over the same hours used in the analyses presented in Figure 5-8. The increased anthropogenic sources on September 6th increased the extent of VOC reactions by 12 ppb. The September 6th control volume also had 21 ppb more NO to NO₂ conversions

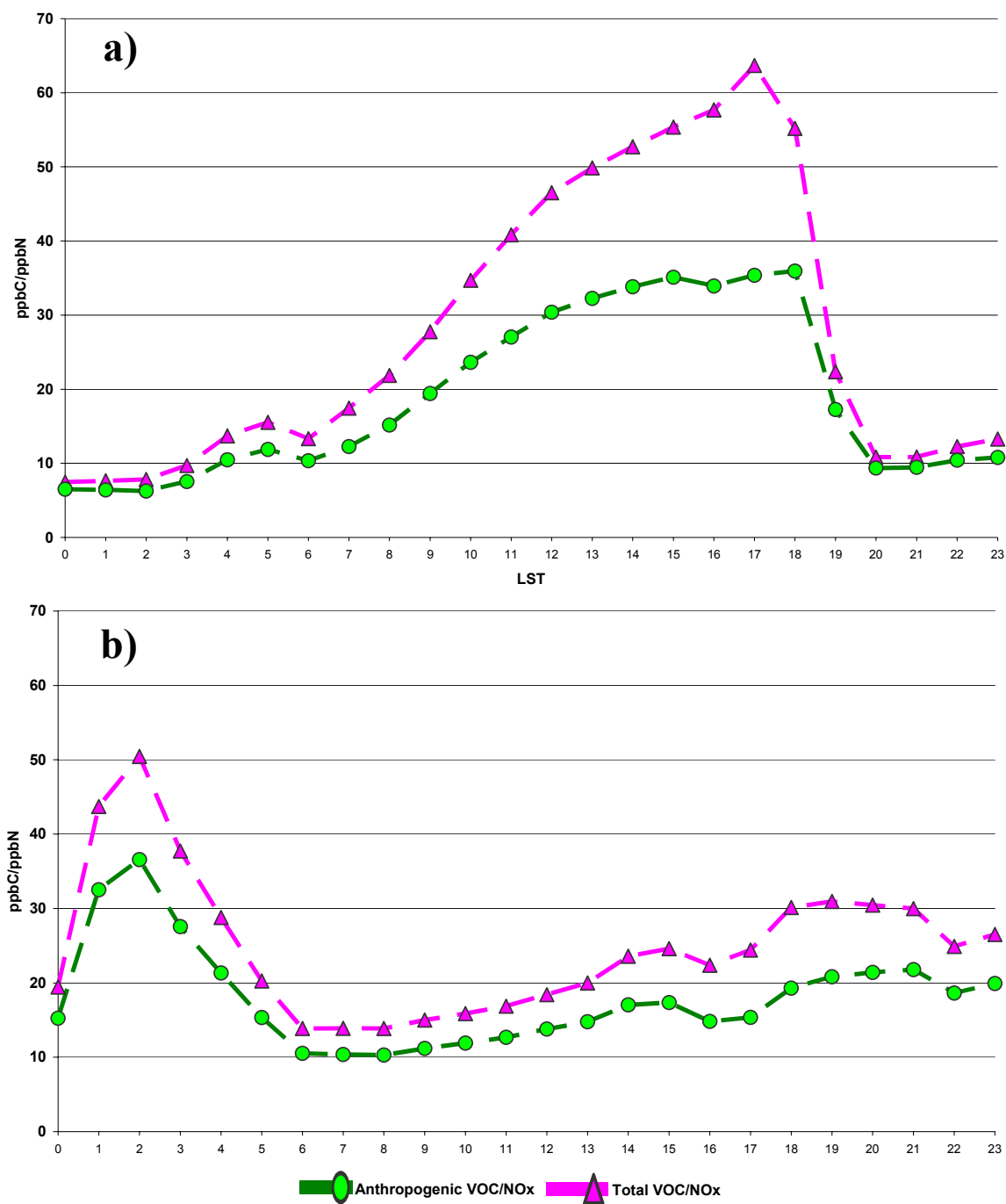
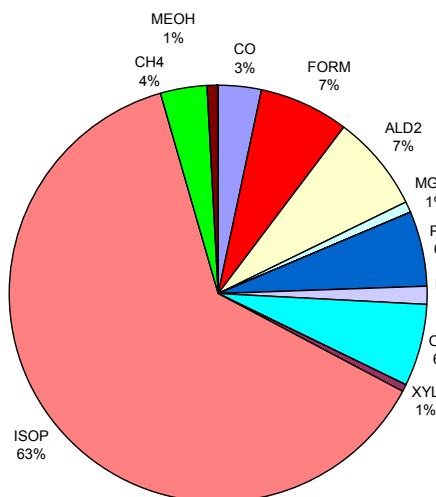


Figure 5-7. Time series of the VOC to NO_x ratios based on cell concentrations for the (a) August 30, 2000 and (b) September 6, 2000 control volumes.

a)

Ozone Produced (11.9 ppb) by each VOC



b)

Ozone Produced (27.3 ppb) by each VOC

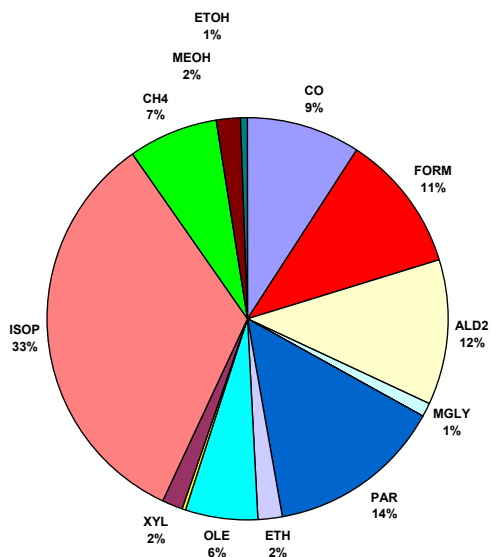


Figure 5-8. Origin of chemically produced ozone by each volatile organic carbon (VOC) for (a) August 30, 2000 hours 13-16, and (b) September 6, 2000 hours 10-13 control volumes.

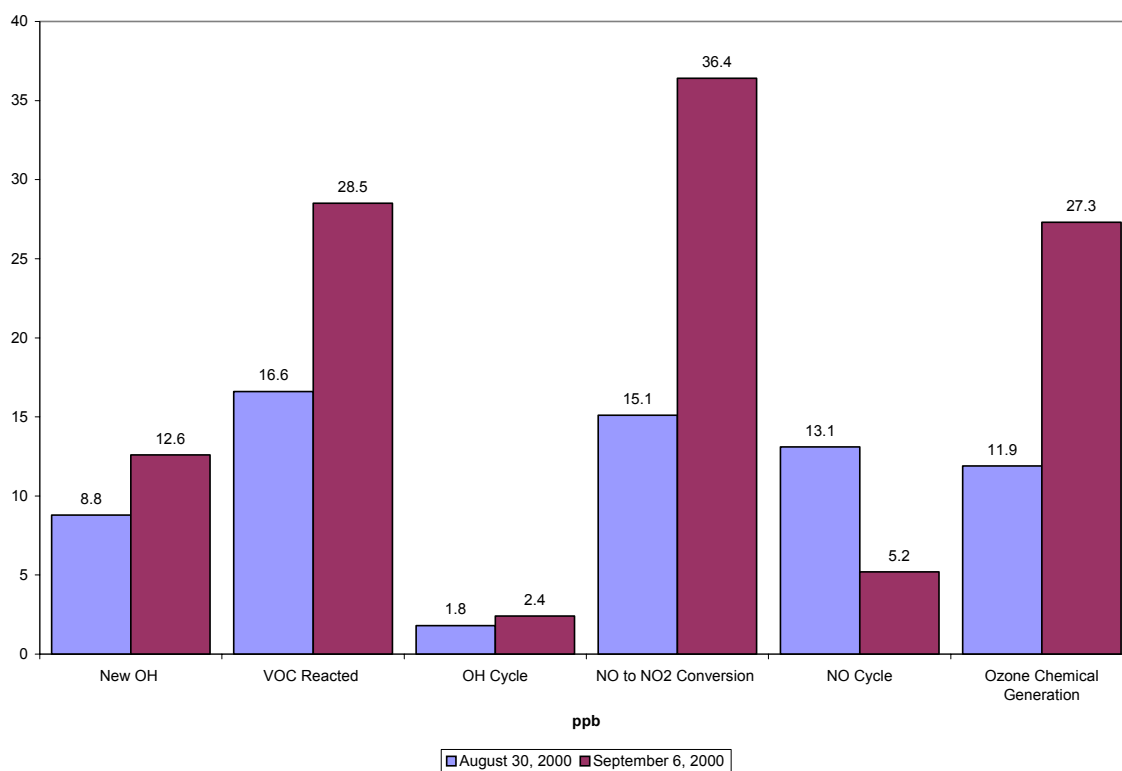


Figure 5-9. Key parameters for the chemistry occurring in the control volumes for August 30, 2000 (hours 13-16), and September 6, 2000 (hours 10-13).

resulting in the production of 15 ppb more of ozone. Under the chemical conditions presented here sources of NO_x play a significant role in determining ozone productivity.

5.4 CONCLUSION

Emissions from wildfires can have a significant impact on regional air quality. This work showed that the photochemistry occurring in the wildfire plumes is limited by NO_x availability and therefore, wildfire plumes that are advected over urban areas and anthropogenic NO_x sources can have significantly different photochemical impacts than wildfire plumes that do not encounter additional NO_x sources.

5.5 REFERENCES

- Sandberg D. V., Hardy C. C., Ottmar R. D., Snell J. A. K., Acheson A., Peterson J. L., Seamon P., Lahm P., Wade D. 1999. "National strategy plan: Modeling and data systems for wildland fire and air quality." U.S. Department of Agriculture, Forest Service, Pacific Northwest Research Station, 60 p.
- Dennis A., Fraser M., Anderson S., and Allen D. T. 2002. "Air Pollutant Emissions Associated with Forest, Grassland and Agricultural Burning in Texas." *Atmospheric Environment* 36, 3779 – 3792.
- Liu Y. 2004. "Variability of wildland fire emissions across the contiguous United States." *Atmospheric Environment* 38, 3489 – 3499.
- Junquera V. 2004. "Inventory of emissions of gaseous compounds and particulate matter from wildfires in east Texas in August and September 2000 and comparison with aircraft measurements." M.S. Thesis, University of Texas at Austin.
- Texas Commission on Environmental Quality (TCEQ). 2003. Houston/Galveston Air Quality Science Evaluation. Air Quality Modeling Files. CAMx Modeling Files. Files last updated December 2003. www.tceq.state.tx.us
- ENVIRON. 2000. User's Guide Comprehensive Air Quality Model with Extensions (CAMx) version 3.10, ENVIRON International Corporation. Novato, California.
- [National Center for Atmospheric Research](http://www.nacar.org) (NCAR). 2002. Project #2000-828 AESOP/TEXAQS-2000, Texas Air Quality Study, NSF/NCAR L-188 Electra (N308D). National Center for Atmospheric Research, Atmospheric Technology Division, Research Aviation Facility. Web site last updated August 2002. <http://raf.atd.ucar.edu/Projects/AESOP>
- National Oceanic and Atmospheric Administration (NOAA). 2003. "Texas Air Quality Study 2000 Airborne Lidar Aerosol Data." National Oceanic and Atmospheric Administration, Environmental Technology Laboratory, Optical Remote Sensing Division. Web page last modified August 2003. http://www.etl.noaa.gov/et2/data/data_pages/texaqs/air_aerosol.html

Chapter 6: Comparisons of Modeled and Observed Isoprene Concentrations in Southeast Texas

6.1 INTRODUCTION

Emissions of biogenic volatile organic compounds (BVOCs), including isoprene (C_5H_8), and monoterpenes ($\text{C}_{10}\text{H}_{16}$), are approximately 30 TgC yr^{-1} in the continental U.S., an amount larger than emissions from all anthropogenic VOC sources. (Guenther *et al.*, 2000). These emissions are not uniformly distributed, and so, in some regions, BVOCs are a major component of the total VOC inventory, while in other regions they are minor contributors. In eastern Texas, the emission inventory for reactive hydrocarbons is dominated by hydrocarbons originating from vegetation. Model predicted summertime biogenic emission rates (primarily isoprene) are over 10,000 metric tons day^{-1} (approximately 10 gigagrams day^{-1}) (Wiedinmyer *et al.*, 2001a) for the region. Anthropogenic emission rates in this same area were only a fifth of that amount, approximately 2,000 metric tons day^{-1} . However, the complex spatial distribution of biogenic emissions complicates the impact these hydrocarbons will have on atmospheric chemistry. For example, in the heavily forested areas of eastern Texas, biogenic emissions overwhelm anthropogenic emissions and dominate hydrocarbon chemistry. In contrast, anthropogenic emissions dominate in highly urbanized areas, such as the Houston urban core. Between each of these extremes lie a number of transition zones where both biogenic and anthropogenic emissions are significant fractions of the emission inventory. In these zones the relative roles of biogenic and anthropogenic emissions in ozone formation and other photochemical processes depends on meteorological conditions. Thus, in eastern Texas, accurate characterization of biogenic emissions is an important element in developing air quality improvement plans.

Accurate prediction of biogenic emissions relies on accurate characterizations of land covers (leaf biomass densities by species), surface temperatures, and photosynthetically active radiation (PAR). Land cover data for Texas has been reported by Wiedinmyer *et al.* (2001a) at a spatial scale of 1 kilometer. The accuracy of the biogenic emission estimates were assessed by comparing isoprene concentrations observed in aircraft and ground measurements to isoprene concentrations predicted using the emission inventory coupled with a photochemical model (Song *et al.*, 2005). The PAPPT was then used to quantify the chemical and physical processes leading to the predicted isoprene concentrations. The insight into these processes revealed by the PAPPT provided better understanding of the phenomena leading to discrepancies between observed and predicted isoprene values.

6.2 METHODOLOGY

Isoprene emission rates and atmospheric concentrations were predicted in this work with two separate publicly available models. Emission rates were calculated with the Global Biosphere Emissions and Interactions System (GloBEIS) model. Atmospheric concentrations based on these emission rates were calculated with the Comprehensive Air Quality Model with extensions (CAMx, ENVIRON, 2004). The GloBEIS program prepares hourly gridded, speciated biogenic emissions in a format suitable for use by CAMx. CAMx is an EPA-approved eulerian photochemical grid model that simulates emission, chemical transformation, horizontal advection and diffusion, vertical transport and diffusion, dry deposition, and wet deposition of species in the atmosphere. The Texas Commission on Environmental Quality (TCEQ) has chosen the GloBEIS emission estimation tool and the CAMx photochemical grid model for air quality planning and attainment demonstrations of Federal air standards. As a result, the TCEQ has developed all of the input data necessary to run the models. The CAMx model also has the capability to use the Process Analysis Post-Processing Tools (PAPPTs) described in previous chapters. This capability was used in evaluating the comparisons between observed and predicted concentrations that are the focus of this work. A brief overview of each of the models and the data they require are presented here.

The TCEQ, the National Center for Atmospheric Research (NCAR), and ENVIRON International, Inc. developed the GloBEIS biogenic emissions model. The source code and documentation for GloBEIS is publicly available and is described in detail by Yarwood *et al.* (1999a,b). Biogenic emissions are influenced primarily by vegetation type and density, solar radiation, cloud cover, and ambient temperature.

GloBEIS therefore requires data characterizing land use/land cover, ambient temperatures, and solar radiation or cloud cover across a region and time period of interest. Vegetation characteristics were based on a landuse/land-cover database developed by Wiedinmyer *et al.*, (2001a) for the state of Texas. In previous analyses, the GloBEIS computer model has given reasonable predictions of the spatial distribution and magnitude of isoprene emissions in Texas, when used in conjunction with this database (Wiedinmyer *et al.*, 2001b). The land-cover database contains several hundred land-cover categories and encompasses the state of Texas with a resolution of approximately one kilometer. Meteorological data for GloBEIS were extracted from several sources. Surface temperatures were developed by spatially interpolating temperatures measured by National Weather Service (NWS) and other weather stations throughout southeast Texas (Vizuite *et al.*, 2002). The University of Maryland and the National Oceanic and Atmospheric Administration (NOAA) for the Global Energy and Water Cycle Experiment (GEWEX) Continent Scale International Project (GCIP) provided the estimates of Photosynthetically Active Radiation (PAR) fluxes (TCEQ, 2004). All wind speed and humidity data were derived from the NCAR/Penn State Mesoscale Model version 5, MM5. The CAMx photochemical modeling episode spans August 22 - September 6, 2000. The modeling domain was a nested regional/urban scale 36-km/12-km/4-km/1km grid, shown in Figure 6-1.

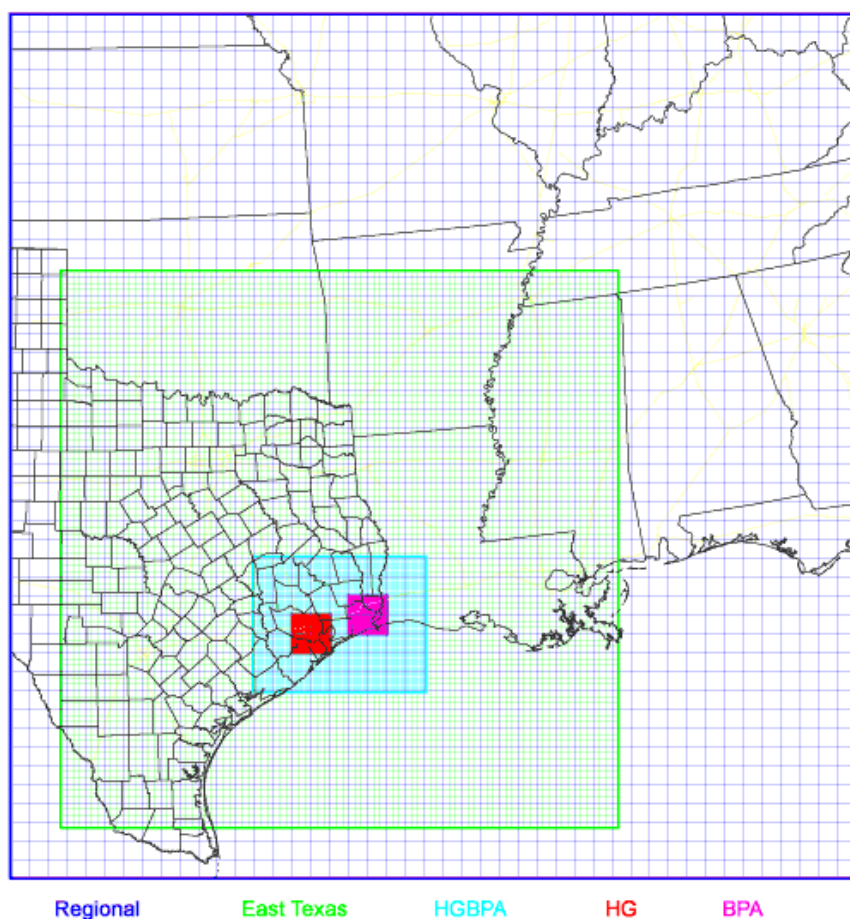


Figure 6-1. Modeling domain used in the study. The Regional, East Texas, Houston-Galveston-Beaumont-Port Arthur (HGBPA), Houston Galveston (HG), and Beaumont-Port Arthur (BPA) nested domains had 36, 12, 4 and 1 km resolution, respectively.

Meteorological inputs for the CAMx model were prepared based on the results from MM5. Emission inventories were assembled by the TCEQ in accordance with EPA guidance with some adjustments to the point source data based on ambient observations. A MOBILE6-based inventory was developed for on-road mobile source emissions; emissions for non-road mobile and area sources were developed using emission factors

and the U.S. EPA's NONROAD model, using local activity data when available. Details of the meteorological modeling and the VOC and NO_x emission inventory development are available at (http://www.tnrc.state.tx.us/air/aqp/airquality_photomod.html#section4; http://www.tnrc.state.tx.us/air/aqp/airquality_contracts.html#section3). These versions of the emission inventories and the meteorology used in this work are referred to as Base 5b.

The chemical mechanism used in CAMx is the Carbon Bond Mechanism version 4 (CBIV) with revised radical termination mechanism and isoprene chemistry (Gery *et al.*, 1989; Carter, 1994; Adelman, 1999). This mechanism is based on reactivity classes of species, although some species important to urban air chemistry, such as isoprene, are explicit. Isoprene chemical pathways in the mechanism include reactions with OH·, O₃, and NO₃. Rate constants for these reactions have been optimized based on chamber experiments (Carter, 1996). The values used in the model are 1.476×10^5 for the OH radical reaction, 1.9×10^{-2} for O₃ and 996 ppm min⁻¹ for NO₃ at 298 K.

An air quality field study was conducted in conjunction with the dates of the modeling episode and provided an extensive ambient data set for performance evaluations. The Texas Air Quality Study (TexAQS, 2000) was designed to improve the understanding of the factors that control the formation and transport of air pollutants along the Gulf Coast in southeastern Texas and the Houston area. The study, conducted in August and September 2000, included six weeks of intensive sampling by as many as 300 researchers who collected samples of gaseous and particulate air pollutants. Also included in the study were specially equipped aircraft that could detect air pollutants with high temporal and spatial resolution and at very low concentrations. The aircraft data

collected during the study provides the opportunity for comparison of observed and predicted biogenic concentrations in the modeling layers above the ground.

The National Center for Atmospheric Research (NCAR) Electra aircraft and the Brookhaven National Laboratory G-1 aircraft (BNL G-1) provided the majority of the aircraft-based isoprene measurements during TexAQS. Samples were collected onboard the aircraft in canisters for subsequent laboratory analysis. The Electra aircraft sampled at 600 m-700 m above ground level (AGL) in the late morning to early afternoon. Air samples typically filled sampling canisters within 10 seconds at aircraft speeds of approximately 100 m s^{-1} . Isoprene concentrations were measured using flame ionization and mass spectrometric detection methods. If either method yielded results above the detection limit, approximately 1 ppt, the average of both results was used. If only one method yielded a value above detection limit the value above the detection limit was used (Sueper, 2003). The BNL G-1 aircraft flew a total of 18 flights during the study period. Canister samples were taken during daylight hours at altitudes between 400 and 600 m AGL. The samples were subsequently analyzed by gas chromatography (BNL, 2000). Sampling times were 10 seconds. In addition to canister measurements, continuous measurements were made with a Proton Transfer Reaction Mass Spectrometer (PTR-MS) onboard the Electra aircraft. The PTR-MS system was operated by the University of Innsbruck and monitored selected VOCs on a time-shared basis for 2 seconds, respectively, once every 4-20 seconds.

The aircraft observations allow for model evaluation of isoprene predictions at various altitudes and locations. However, the data are limited to the times and locations of the flight path. Additional model evaluation in this work included comparisons to

continuously collected, one-hour averaged ground measurements. These ground measurements were provided by the extensive network of ambient monitoring stations throughout the Houston-Galveston area (TCEQ, 2004). As part of TexAQS, gas chromatography autosamplers (auto-GC) were sited at four monitoring stations located in La Porte, Clinton, Deer Park, Bayland Park, and Aldine. The ground data, along with canister samples, and the PTR-MS data, were used to evaluate model performance in predicting isoprene concentrations.

Canister samples that are collected by aircraft are likely to contain isoprene emitted by sources immediately below the aircraft and by sources transported in from other areas. As a result, observed isoprene concentrations cannot be directly compared with model predictions. Instead, a weighted average of isoprene concentrations spanning several model grid cells was used. The model grid cells were chosen by the path of the aircraft during a 2-minute total period before, during, and immediately after sample collection. Typically, an aircraft would transect up to six grid cells within 2 minutes of the collection of the air samples. A composite model prediction was obtained by weighting the isoprene concentration for each grid cell by the length of time that the aircraft spent in the grid cell during the 2-minute period selected for analysis. Ground measurements were compared to the modeled, 1-hour averaged isoprene concentrations in the grid cell containing the measurement location.

6.3 RESULTS

Comparisons of predicted isoprene concentrations to aircraft canister measurements are summarized in Tables 6-1 and 6-2 (Song, 2005). The mean value of isoprene concentrations measured by the aircraft was 0.35 ppb. The corresponding modeled values averaged 0.28 ppb. Mean normalized bias and mean normalized gross errors were -7% and 77% for the NOAA dataset and 85% and 147% for the BNL dataset. If the sample sets were restricted to measured concentrations above 0.1 ppb or 0.2 ppb, there was little change in the biases, but the normalized gross errors of NOAA dataset were reduced to 52% and 34% respectively. Restricting sample sets to measured concentrations above 0.1 ppb or 0.2 ppb reduced the normalized gross errors of the G-1 dataset to 70% and 85%, respectively. A total of 59 measurements were made by the NOAA Electra aircraft; 24 of these measurements had agreement between modeled and predicted values within a factor of two. The BNL G-1 aircraft had 52 total measurements and 22 measurements showed agreement within a factor of two of predicted values.

Model performance also was evaluated with semi-continuous measurements of isoprene concentrations made onboard the NOAA aircraft by PTR-MS. The measurements of isoprene from the PTR-MS were compared with modeled 1-hour average isoprene concentrations as shown in Table 6-3 and Figure 6-2 (Song, 2005). The resolution for the model predicted isoprene concentrations shown in Figure 6-2 is 4 km. The data suggest that modeled isoprene concentrations aloft in urban areas (Harris County) under-predict observed concentrations by approximately a factor of two. The PTR-MS data generally were consistent with model predictions in rural regions north of Houston (non-Harris County).

Ground layer isoprene concentrations predicted by the model were compared to measurements made at ground monitor sites located at various mixed urban, industrial and residential sites in the Houston-Galveston area. Auto-GC instruments measured hourly isoprene concentrations in Clinton, La Porte, Aldine, Deer Park, and Bayland Park. The measurements for the Clinton site are presented in Figure 6-3 along with model concentrations from the 4 km grid cell containing the monitoring site. Other ground sites showed similar patterns. Modeled isoprene concentrations were a factor of two or three greater than observed isoprene concentrations at all the urban ground sites.

Taken together, these results initially present an ambiguous picture of modeled isoprene concentrations. Modeled ground level isoprene concentrations are a factor of 2-3 higher than observed values; in contrast, modeled concentrations aloft are generally consistent with aircraft canister and PTR-MS data, except over urban Houston, where modeled aloft concentrations are lower than observed values. The PAPPT was used to examine possible explanations for these ambiguities.

Date of sample collection	Number of pairs	Mean (ppb)		Mean _{pred} /Mean _{obs}	MNB (%)	MNGE (%)
		Observed	Predicted			
8/25	14	0.37	0.33	0.9	1.7	77.
8/27	17	0.38	0.33	0.9	21.	86.
8/28	18	0.36	0.28	0.8	-34.	67.
8/30	10	0.27	0.13	0.5	-16.	80.
Total	59	0.35	0.28	0.8	-6.7 %	77. %

Samples with measured isoprene concentrations above 0.1 ppb

Date of sample collection	Number of pairs	Mean (ppb)		Mean _{pred} /Mean _{obs}	MNB (%)	MNGE (%)
		Observed	Predicted			
8/25	9	0.51	0.50	1.0	48.	74.
8/27	11	0.53	0.44	0.8	-12.	29.
8/28	8	0.67	0.59	0.9	-5.3	63.
8/30	4	0.43	0.24	0.6	1.7	39.
Total	32	0.54	0.47	0.9	8.4	52.

Samples with measured isoprene concentrations above 0.2 ppb

Date of sample collection	Number of pairs	Mean (ppb)		Mean _{pred} /Mean _{obs}	MNB (%)	MNGE (%)
		Observed	Predicted			
8/25	4	0.96	0.76	0.8	-23.	33.
8/27	6	0.77	0.68	0.9	-10.	27.
8/28	5	0.78	0.87	1.1	-18.	35.
8/30	1	1.19	0.30	0.3	-75.	75.
Total	16	0.85	0.74	0.9	-11.	34.

$$\text{Mean Normalized Bias (MNB)} = \frac{1}{N} \sum_{i=1}^N \left(\frac{\text{Pred.} - \text{Obs.}}{\text{Obs.}} \right) \cdot 100\%$$

$$\text{Mean Normalized Gross Error (MNGE)} = \frac{1}{N} \sum_{i=1}^N \left(\frac{|\text{Pred.} - \text{Obs.}|}{\text{Obs.}} \right) \cdot 100\%$$

Where N is the number of observations

Table 6-1. Statistical summary of the comparison of predicted isoprene concentrations and NOAA aircraft observations

Date of sample collection	Number of pairs	Mean (ppb)		Mean _{pred} /Mean _{obs}	MNB (%)	MNGE (%)
		Observed	Predicted			
8/26	25	0.38	0.39	1.0	61.	138.
8/29	27	0.23	0.25	1.1	108.	156.
Total	52	0.30	0.32	1.1	85.	147.

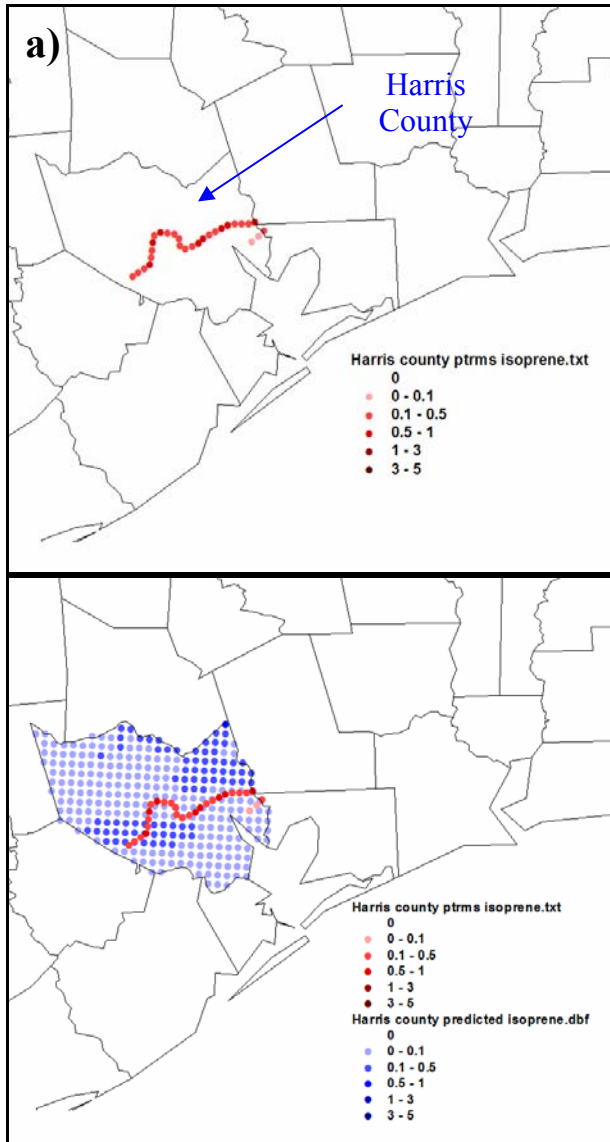
Samples with measured isoprene concentrations above 0.1 ppb

Date of sample collection	Number of pairs	Mean (ppb)		Mean _{pred} /Mean _{obs}	MNB (%)	MNGE (%)
		Observed	Predicted			
8/26	12	0.64	0.71	1.1	53.	133.
8/29	17	0.32	0.31	1.0	20.	77.
Total	29	0.45	0.47	1.0	34.	100.

Samples with measured isoprene concentrations above 0.2 ppb

Date of sample collection	Number of pairs	Mean (ppb)		Mean _{pred} /Mean _{obs}	MNB (%)	MNGE (%)
		Observed	Predicted			
8/26	7	0.77	1.12	1.5	133.	187.
8/29	7	0.46	0.46	1.0	0.8	68.
Total	14	0.62	0.79	1.3	67. %	127. %

Table 6-2. Statistical summary of the comparison of predicted isoprene concentrations and BNL G-1 aircraft observations



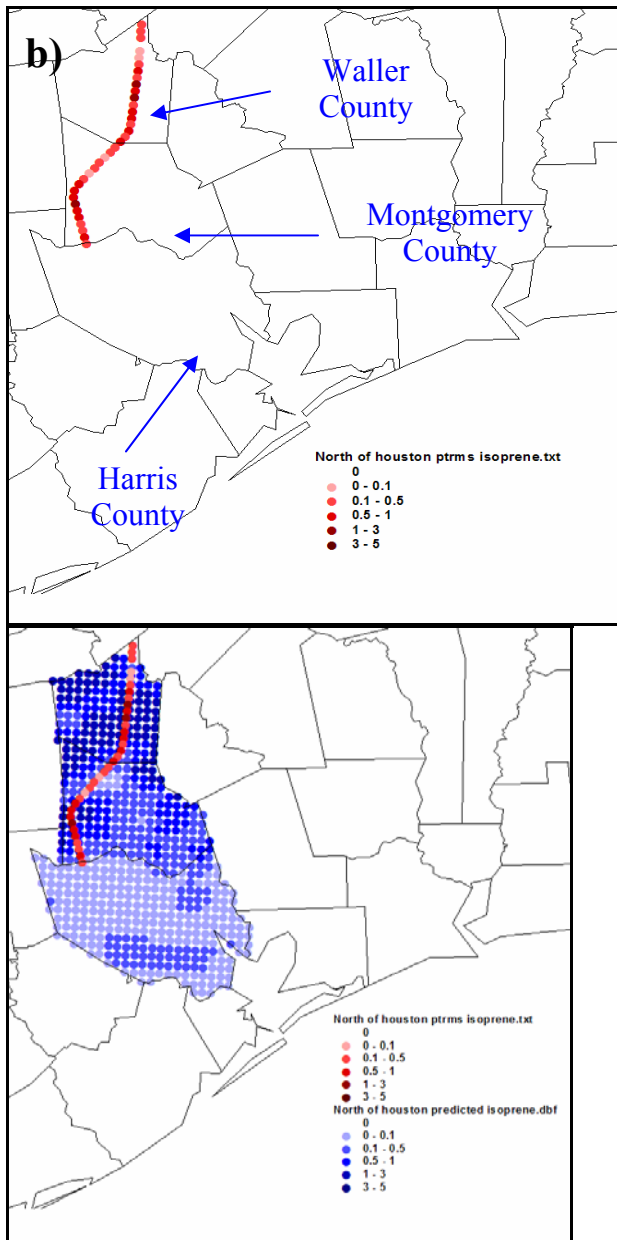


Figure 6-2. NOAA/NCAR PTR-MS data values for observed isoprene concentrations and the corresponding model predicted isoprene concentrations in the vertical layer and 1 km grid cell where the measurement was taken. (a) Flight path over the Houston urban core in Harris County at 2:00 pm on August 25, 2000, and (b) flight path in a rural region north of Houston at 12:00 pm on August 25, 2000

Samples with both observed and predicted isoprene concentrations above 0.1 ppb						
Date of sample collection	Number of pairs	Mean (ppb)		Mean _{pred} /Mean _{obs}	MNB (%)	MNGE (%)
		Observed	Predicted			
8/25	53	0.44	0.28	0.6	-6.	65.
8/27	32	0.43	0.29	0.7	12.	82.
8/28	25	0.38	0.22	0.6	6.	67.
8/30	31	1.10	0.35	0.3	-45.	68.
Total	141	0.57	0.29	0.5	-8.	70.

Table 6-3a. Statistical summary of the comparison of predicted isoprene concentrations and NOAA/NCAR aircraft PTR-MS observations, for Harris County

Samples with both observed and predicted isoprene concentrations above 0.1 ppb						
Date of sample collection	Number of pairs	Mean (ppb)		Mean _{pred} /Mean _{obs}	MNB (%)	MNGE (%)
		Observed	Predicted			
8/25	133	0.72	0.95	1.3	58.	81.
27	177	0.84	0.62	0.8	-1.	54.
28	180	0.75	0.98	1.3	74.	109.
30	41	0.81	1.49	1.8	101.	126.
Total	531	0.78	0.89	1.1	47.	85.

Table 6-3b. Statistical summary of the comparison of predicted isoprene concentrations and NOAA/NCAR aircraft PTR-MS observations, not in Harris County

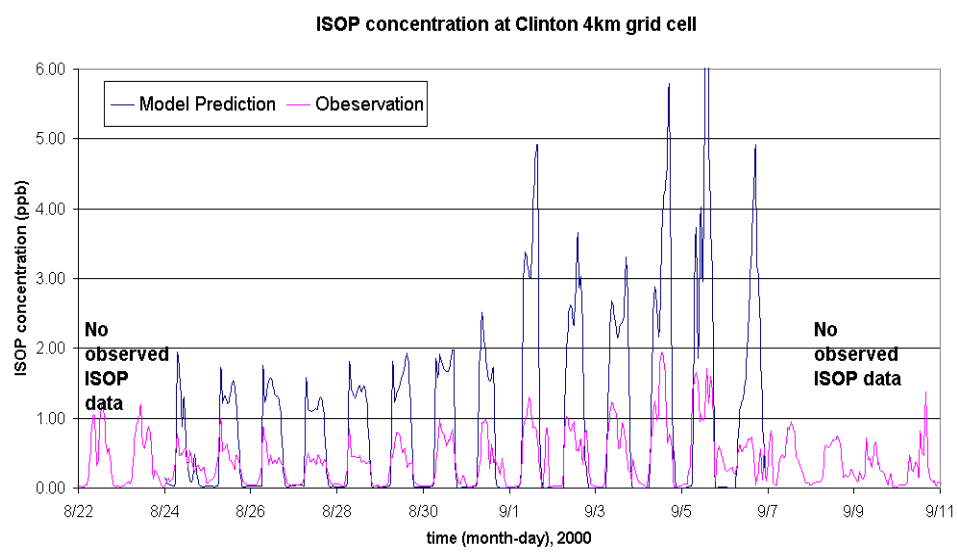


Figure 6-3. Time series of modeled and observed isoprene concentrations in the grid cell containing the auto-GC at Clinton during the August 22-September 6, 2000 CAMx episode.

6.4 DISCUSSION

Performance evaluations indicated that the model over-predicted isoprene concentrations at ground level for all urban sites and under-predicted isoprene aloft over urban areas. The model was, however, consistent with observations aloft over rural areas. Understanding the differences between modeled and measured isoprene concentrations requires a detailed understanding of the model's physical and chemical processes at the measurement locations. The PAPPT described in earlier chapters of this work was used for this analysis. The PAPPT provides hourly model estimates of the rates of individual chemical and physical processes, such as horizontal and vertical pollutant fluxes crossing cell boundaries, chemical production and consumption rates, emission rates, deposition rates, and initial and final concentrations. The PAPPT aggregates concentrations and magnitudes of process rates over a collection of vertical and horizontal grid cells defined as a control volume. The mass within each grid cell in the control volume is aggregated at each hour. The exchanges among cells within the control volume are summed to produce only exchanges at the faces of the aggregated control volume. The concentrations and magnitudes of process rates are therefore an average over the aggregated control volume.

The model processes that lead to predicted isoprene concentrations were investigated for the Clinton monitor site (an urban location) on the August 30, 2000 simulation day. The control volume was confined to the grid cell occupied by the Clinton monitor. A second control volume was chosen to match a rural grid cell where aircraft measurements were consistent with predicted isoprene concentrations on August 25, 2000. This control volume was located 83 km north of the Houston urban core in the Sam Houston National Forest. The PAPPT was applied using three separate vertical heights

for the Clinton site. The PAPPT aggregates processes occurring at various altitudes, and so these three scenarios represent average rates of processes over the Clinton site, where the averaging is done over three different vertical heights. Figures 6-4a-c show the time series plots of isoprene accumulation and loss processes on August 30, 2000 for the three different vertical heights. Figures 6-5a-b show the time series plots of isoprene accumulation and loss processes on August 25, 2000 for two vertical heights at the rural site in the Sam Houston National Forest.

Figure 6-4a presents a time series plot for isoprene at the Clinton monitor in the first vertical modeling layer (33.9 m AGL). In the first layer emissions (pink line), vertical transport (green line), and chemistry rates (red line) dominate the physical processes. The emission rates are positive since they represent isoprene entering the volume; the chemical reaction and vertical transport rates are negative since they represent losses from the volume. Nearly all the emitted isoprene is transported vertically out of the top of the first layer with rates peaking at over 100 ppb/hr at hour 15. Only 10%-20% of the emitted isoprene reacts in the first layer. Figure 6-4b shows the processes occurring when the first three vertical layers of the model are aggregated (170.6 m AGL). Similar to the first layer figure, the emission rates, vertical transport out of the grid cells, and chemical losses are the dominant processes affecting isoprene concentrations. In contrast to the 10%-20% of isoprene that had reacted in the first layer, at mid-afternoon, over the first 3 layers, half of the isoprene has reacted. This means that if vertical mixing in the first three layers is more extensive than predicted by the model, ground level isoprene concentrations would be lower, consistent with observations. Figure 6-4c shows that throughout the first nine vertical layers (699.7 m AGL, the approximate altitude of most of the aircraft observations) at mid-afternoon (the time of

most of the aircraft flights), accumulation and loss of isoprene are dominated by emission and chemical loss processes. By the time the isoprene has been transported vertically to 600-700 m AGL, more than 90% of the initial emissions have reacted. In all of these cases (Figures 6-4a-c), horizontal transport of isoprene into the control volume is approximately equal to horizontal transport out of the control volume. Net horizontal transport, shown in the Figures, is small. These accumulation and loss processes identified at the Clinton monitor are consistent with processes at the other urban monitors.

Figure 6-5a presents a time series plot for isoprene at the Sam Houston National Forest site averaged over the first three vertical modeling layers (170.6 m AGL). The first layer was not considered because it was largely within the canopy. The emission rates, vertical transport out of the grid cells, and chemical losses are the dominant processes affecting isoprene concentrations in the first three layers. The fraction of isoprene lost to reactions in the first three layers at mid-afternoon is less than that for the urban site (~30% vs. ~50%). Figure 6-5b shows that throughout the first nine vertical layers (699.7 m AGL, the approximate altitude of most of the aircraft observations) vertical transport of isoprene is still significant (roughly a third to one half of the rate of chemical loss). In contrast, the vertical transport rates at urban sites were considerably smaller when compared to chemical reaction rates.

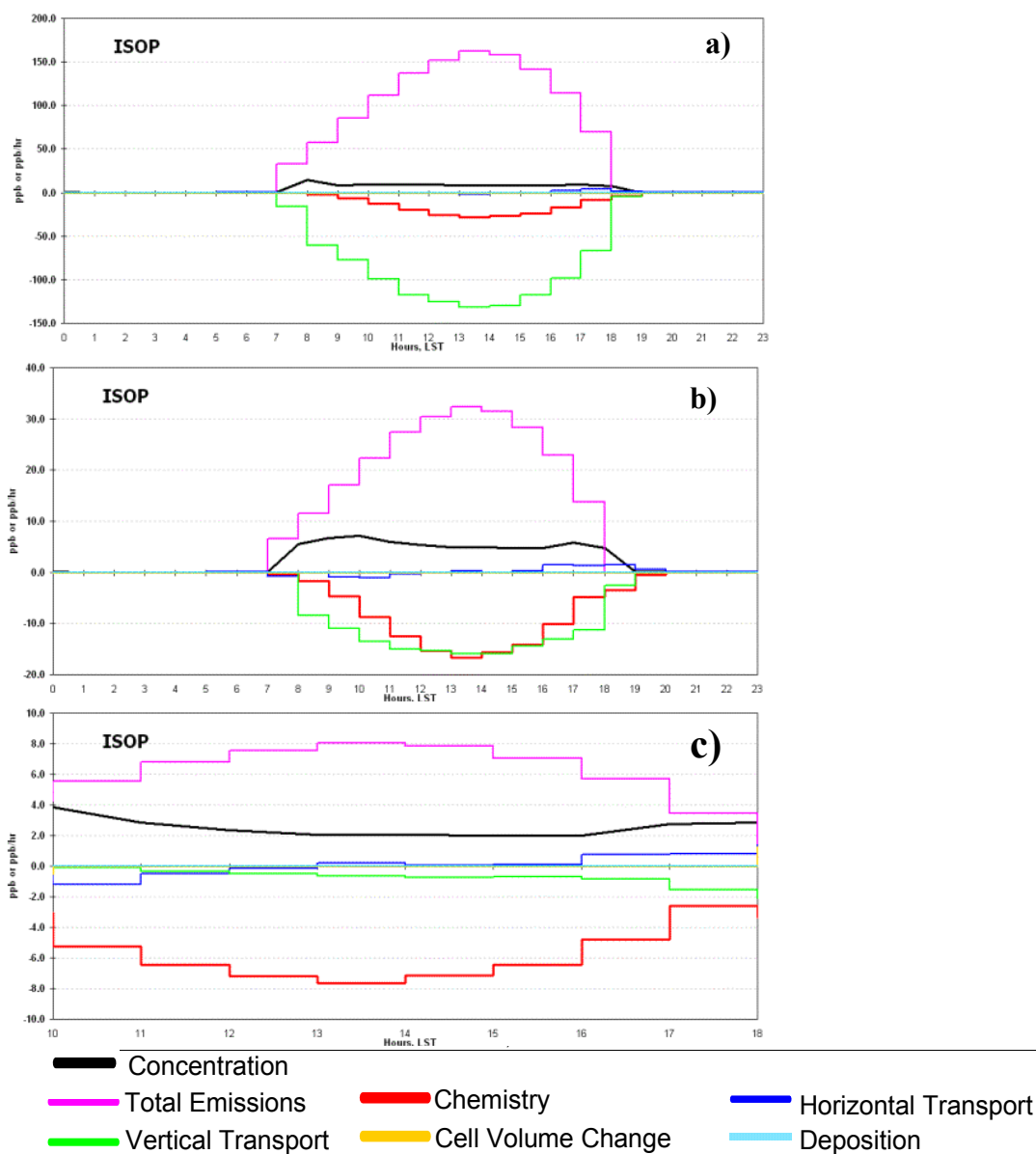


Figure 6-4. PAPPT time series of isoprene accumulation and loss processes in the (a) first vertical layer, (b) first three vertical layers, and (c) first nine vertical layers of the grid cell column containing the Clinton monitoring station on August 30, 2000. Only the period of the day when the mixing height is within layer 9 is shown in (c). In these diagrams, process rates are reported as ppb/hr of change in isoprene concentration and the isoprene concentration is reported as ppb. The sum of the process rates in each hour equals the hourly change in isoprene concentration.

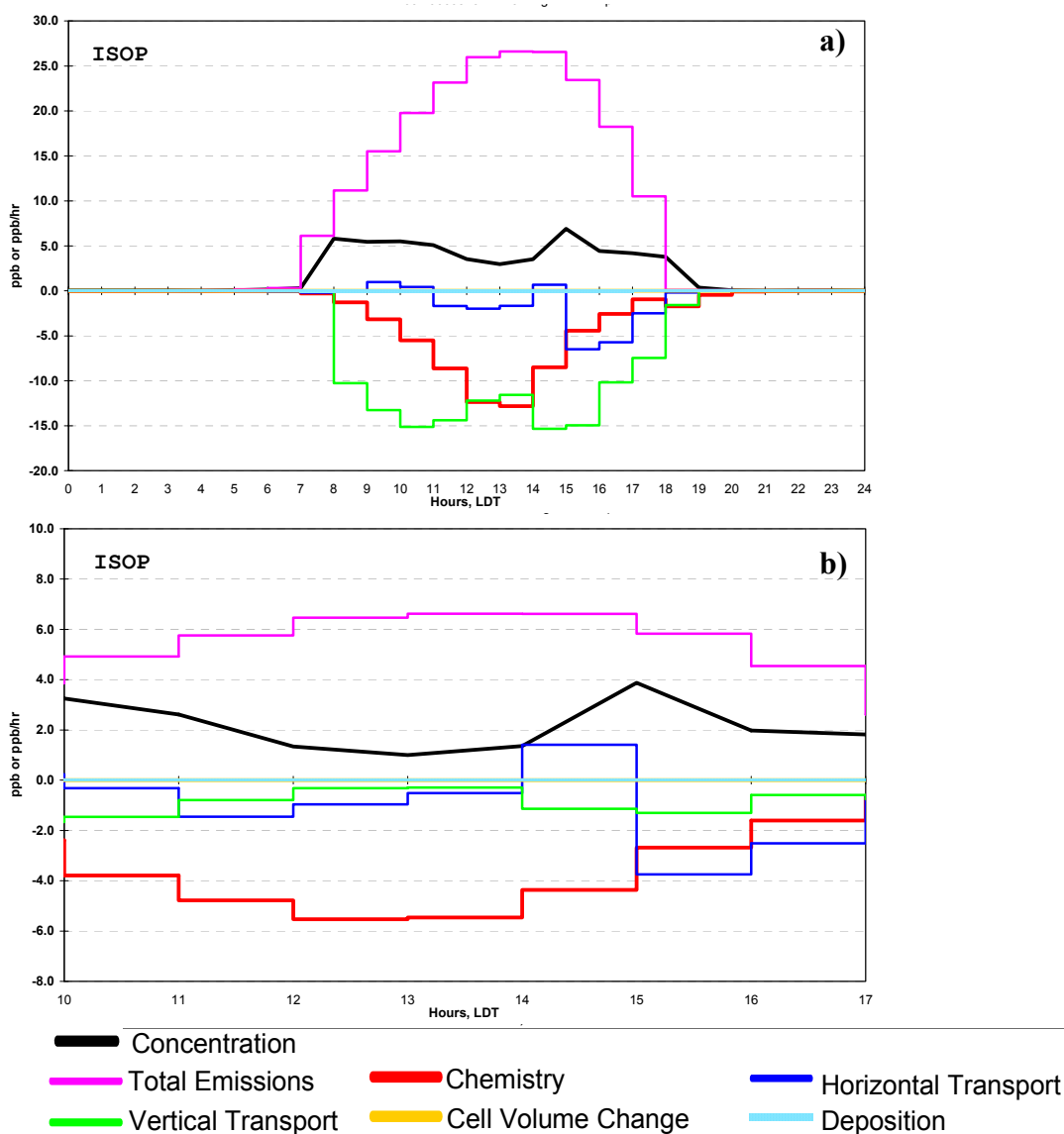


Figure 6-5. PAPPT time series of isoprene accumulation and loss processes in the (a) first three vertical layers, and (b) first nine vertical layers of the grid cell column containing the site in the Sam Houston National Forest on August 25, 2000. In these diagrams, process rates are reported as ppb/hr of change in isoprene concentration and the isoprene concentration is reported as ppb. The sum of the process rates in each hour equals the hourly change in isoprene concentration.

Thus, the PAPPT indicate that the balance between chemical reaction and vertical transport rates, predicted by the model, is weighted heavily toward chemical reaction in the near-ground layers at urban sites. In contrast, at rural sites, the modeled chemical reaction rates were not as large relative to the vertical transport rates predicted by the model. This suggests that the concentrations of isoprene predicted by the model will be very sensitive to vertical transport rates. To test this hypothesis, a model simulation was performed in which all of the vertical diffusivities in the model were increased by a factor of 5. This simulation was not intended to represent actual conditions, but instead was intended to determine whether the predicted isoprene concentrations would be sensitive to vertical mixing parameters. The results are summarized in Figures 6-6 and 6-7. Figure 6-6a shows ground level isoprene concentrations in the Houston-Galveston domain (shown in red in Figure 6-1). Figure 6-6b shows the vertical profile of isoprene concentrations along the gray horizontal line in Figure 6-6a. Both Figure 6-6a and 6-6b are for the base case simulation, with no changes to the vertical transport parameters. The Figures show that isoprene concentrations decrease rapidly with vertical height (shown as vertical layer numbers in the diagram), consistent with the PAPPT results.

Figure 6-7 shows the change in ground level concentrations of isoprene and the change in vertical distribution of isoprene concentrations if the parameter characterizing vertical mixing between grid cells (K_v) is uniformly increased by a factor of 5. Ground level concentrations decrease fairly uniformly and aloft concentrations are increased. The magnitudes of the increases of concentrations aloft and the decreases of isoprene concentration at ground level are of the same order of magnitude (up to 0.5 ppb) as the mean concentrations observed aloft. These results suggest that quantitative comparisons

between measured and predicted isoprene concentrations will be quite sensitive to vertical mixing assumptions made in the modeling.

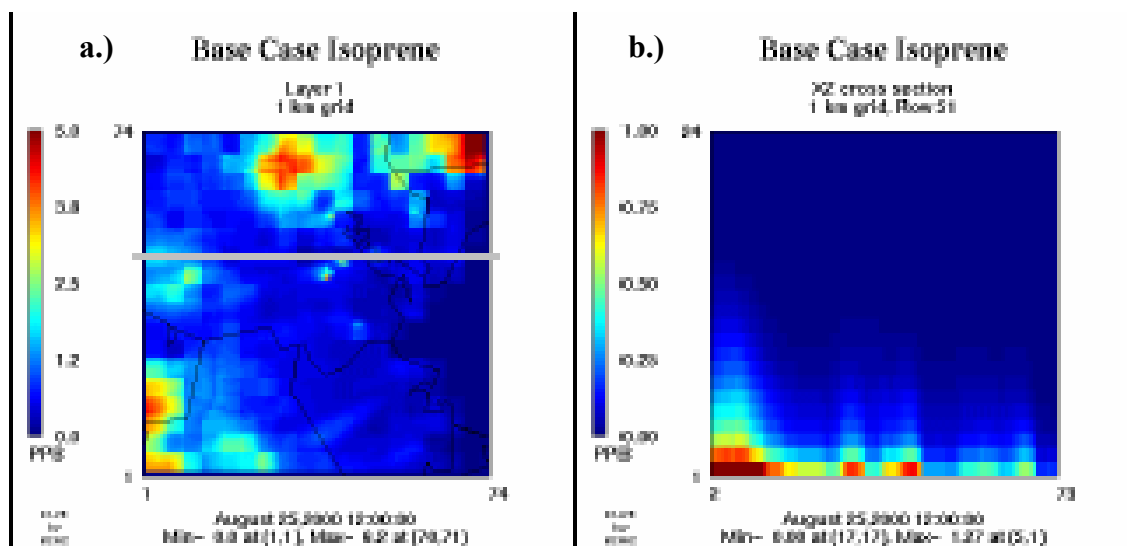


Figure 6-6. (a) Ground level isoprene concentrations in the Houston-Galveston domain (shown in red in Figure 6-1). (b) Vertical profile of isoprene concentrations along the gray horizontal line in Figure 6-6a. The vertical axis is reported as vertical layer number; the horizontal axis is reported as horizontal grid cell, numbered from west to east.

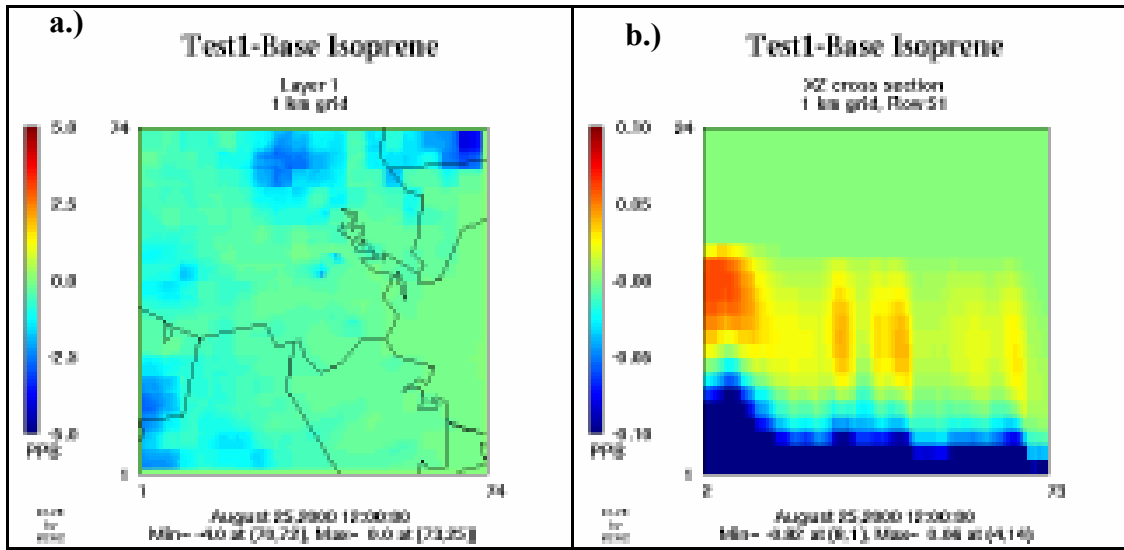


Figure 6-7. (a) Difference in ground level isoprene concentrations in the Houston-Galveston domain (shown in red in Figure 6-1) between the case with K_v values increased by a factor of 5 minus the base case. (b) Difference in vertical profile of isoprene concentrations along the gray horizontal line in Figure 6-6a (case with K_v values increased by a factor of 5 - base case). The vertical axis is reported as vertical layer number; the horizontal axis is reported as horizontal grid cell, numbered from west to east.

6.5 CONCLUSION

Predicted isoprene concentrations were compared to observations from a variety of measurement sources. These sources included canister samples and PTR-MS data from aircraft flying transects in the Houston area and surrounding region. Continuous measurements also were evaluated from ground sites dispersed at various locations around the Houston urban core. The performance evaluations indicated that the model over-predicted isoprene concentrations for all ground sites used in the study. The model under-predicted aircraft measurements of isoprene concentrations in urban areas but was able to match aloft observations in rural areas. The PAPPT was employed to determine the physical and chemical processes influencing predicted isoprene concentrations. The accumulation and loss of isoprene were dominated by emission, vertical transport, and chemical loss processes and were found to be dependent on vertical mixing parameters. Future work should focus on characterizing the uncertainty associated with emission rates, vertical mixing, and chemical loss processes. These factors will be important in understanding the differences between modeled and measured isoprene concentrations in southeastern Texas.

6.6 ACKNOWLEDGEMENTS

The authors thank investigators at the National Oceanic and Atmospheric Administration and the Department of Energy (Brookhaven National Laboratory) for providing isoprene concentration data collected by aircraft. The authors also thank the Texas Commission on Environmental Quality for providing model input files and isoprene concentration data from ground sites.

6.7 REFERENCES

- Guenther A., Geron C., Pierce T., Lamb B., Harley P., Fall R. 2000. "Natural emissions of non-methane volatile organic compounds, carbon monoxide, and oxides of nitrogen from North America." *Atmospheric Environment* 34, 2205–2230.
- Wiedinmyer C., Guenther A., Estes M., Strange I., Yarwood G., Allen D. T. 2001a. "A land use database and examples of biogenic isoprene emission estimates for the state of Texas, USA." *Atmospheric Environment* 35, 6465-6477.
- Song J., Vizuite W., Chang S., McDonald-Buller E., Kimura Y., Yarwood G., Allen D. T. 2005. "Comparisons of Modeled and Observed Isoprene Concentrations in Southeast Texas." Submitted to *Journal of the Air & Waste Management Association*
- ENVIRON. 2004. CAMx Users Guide, v4.00. 2004. www.camx.com
- Yarwood G., Wilson G., Shepard S., Guenther A. 1999a. "User's Guide to the Global Biosphere Emissions and Interactions System – Version 3.1." 101 Rowland Way, Suite 220, Novato, California, available at: <http://www.globeis.com>
- Yarwood G., Wilson G., Emery C., Guenther A. 1999b. "Development of the GloBEIS – A State of the Science Biogenics Emissions Modeling System." Final Report to the Texas Natural Resource Conservation Commission, 12100 Park 35 Circle, Austin, Texas 78753.
- Wiedinmyer C., Friedfeld S., Guenther A., Fraser M., Allen D.T. 2001b. "Measurement and Analysis of Atmospheric Concentrations of Isoprene and its Reaction Products in Central Texas," *Atmospheric Environment*, 35, 1001-1013 (2001b).
- Vizuite W., Junquera V., McDonald-Buller E., McGaughey G., Yarwood G., Allen D.T. 2002. "Effects of Temperature and Land Use on Predictions of Biogenic Emissions in Eastern Texas." *Atmospheric Environment* 36, 3321-3337.
- Texas Commission on Environmental Quality (TCEQ). 2004. "The State Implementation Plan for the Control of Ozone Pollution: Attainment Demonstration for the Houston/Galveston Ozone Non-attainment Area." P.O. Box 13087, Austin, Texas 78711-3087, www.tceq.state.tx.us
- Adelman Z. 1999. "A re-evaluation of the carbon bond IV photochemical mechanism." University of North Carolina at Chapel Hill, Department of Environmental Sciences and Engineering, School of Public Health.: 208 <http://airsite.unc.edu/>.
- Carter W. P. 1994. "Development of ozone reactivity scales for volatile organic compounds." *Journal of the Air and Waste Management Association* 44, 881-899

Gery M. W., Whitten G. Z., Killus J. P., Dodge M. C. 1989. "A Photochemical Kinetics Mechanism for Urban and Regional Scale Computer Modeling." *Journal of Geophysical Research* 94, 925-956

Carter W. P. 1996. "Condensed atmospheric photooxidation mechanisms for isoprene." *Atmospheric Environment* 30 (24), 4275-4290

Texas Air Quality Study (TEXAQS). 2000. available at:
<http://www.utexas.edu/research/ceer/texaqs/index.html>

Sueper D. 2003. Personal communication, March 13, 2003

Brookhaven National Laboratory. 2000. Available at:
ftp://aerosol.das.bnl.gov/pub/Houston00/HYDROCARBONS_V1.txt

Chapter 7: Summary of Findings

Photochemical air quality grid models, commonly used in the development and evaluation of air quality regulations, calculate the rates of atmospheric processes that control air pollutant concentrations. These models typically output only the spatial and temporal distribution of species concentrations. In this work, Process Analysis Post Processing Tools (PAPPT) were developed and applied to the outputs of simulations from the Comprehensive Air Quality Model with extensions (CAMx). These tools have been formulated to allow for horizontally irregular control volumes and dynamic vertical mixing heights. The use of the tool was demonstrated through the analysis of ozone formation processes in a Central California Ozone Study September episode. The PAPPT revealed the processes that contributed to model under-prediction of ozone generation in the Fresno area.

The PAPPT was then used to examine the impact of industrial emission events on ozone formation and accumulation processes in the Houston-Galveston area. Emission event releases of ethylene, propylene, n-pentane, and xylene were modeled and compared in a NO_x rich and NO_x limited environment. The propylene emission event released 5,819 lbs/hour for two hours; this emission rate was selected to approximately match observed aircraft data. Event emissions involving the three other hydrocarbons were designed to match the reactivity of the propylene release. Emission rates were 7,422 lbs/hr, 9,045 lbs/hr, and 44,004 lbs/hr for ethylene, xylene, and n-pentane respectively. Each hydrocarbon release, except n-pentane, contributed approximately the same increases in ozone concentrations downwind of the release point. However, the xylene case generated more ozone near the release point. Both NO_x rich and NO_x limited

environments exhibited the same pattern. In all of the simulations the OH radical balance indicated that the formation of new OH radicals near the release point from aldehyde photolysis controlled the initial ozone formation. Once the hydrocarbons in the release events were oxidized and the plume aged, the majority of new OH radicals originated from the photolysis of ozone molecules and the amount of ozone formed due to the releases converged, except for the n-pentane release.

The PAPPT was used to develop a simplified sub-domain model that could mimic predictions from a full 3-D gridded model. The PAPPT was useful in comparing the physical and chemical processes of both the sub-domain and full grid CAMx model. Time series plots revealed that the sub-domain model smeared pollutant concentrations in time when compared to the gridded model. The differences between the two models become more pronounced when large concentration gradients were introduced into the control volume. The discrepancy in the chemical process rates of the two models could be explained by how each model treats the transport of pollutants. The eulerian grid framework allows for greater resolution for the introduction of an emission event into a smaller control volume. In contrast, the sub-domain model lacks the resolution of a grid frame work and emissions are completely mixed into the entire control volume. As a result, pollutant concentrations are diluted and residence times are reduced. For the sub-domain model this results in the reduction of the amount of time for VOC to react and ultimately generate ozone within the PAPPT control volume.

The PAPPT was applied in an investigation of wildfire air pollutants based on a recently developed wildfire emission inventory developed for the CAMx model. The estimated emissions from fires were used, together with the CAMx photochemical model,

to characterize the extent of dispersion of the fire emissions and the photochemistry associated with the fire emissions. Although the dispersion and photochemical impacts varied from fire to fire, for wildfires less than 10,000 acres, the greatest enhancements of CO and ozone concentrations due to the fire emissions generally were confined to regions within 10-100 km of the fire. Within 10 km of these fires CO concentrations can exceed 2 ppm and ozone concentrations can be enhanced by 60 ppb. The extent of photooxidant formation in the plumes was limited by NO_x availability and isoprene emissions from forested areas downwind of the fires provided most of the hydrocarbon reactivity in the plumes.

The PAPPT also was utilized in an effort to accurately characterize biogenic emission inventories for the Houston-Galveston region. To evaluate the biogenic emissions estimates in southeastern Texas, isoprene concentrations recorded using ground and aircraft measurements were compared to model predictions. The photochemical and biogenic emission estimation models employed in the comparison were the Comprehensive Air Quality Model with extensions (CAMx) and the Global Biosphere Emissions and Interactions System (GloBEIS), respectively. Ground level isoprene concentrations predicted by the models were typically 2-3 times higher than observed concentrations, but mean predicted concentrations aloft generally were consistent with mean observations. These results were analyzed further by tracking individual physical and chemical process that contribute to changing isoprene concentrations in the model with the PAPPT. The analysis revealed that the model predicts very rapid chemical consumption of isoprene in the first hundred meters above ground level. The balance between vertical transport rates and chemical reaction rates in the model had a significant impact on both ground level and aloft concentrations.

Increasing the ground level mixing in urban areas explained many of the discrepancies between observations and modeled values.

Chapter 8: Future Work

The work that has been presented in the previous chapters has focused on the gas phase organic and inorganic chemical reactions that cycle carbon, nitrogen, sulfur, and other materials through the atmosphere. A process analysis post processing tool (PAPPT) was linked to a photochemical air quality model that determines the roles of individual physical and chemical processes in determining the concentrations of atmospheric air pollutants. The PAPPT was developed to quantify the source contributions and formation processes for a grid cell or collection of grid cells in a photochemical grid model. As illustrated in previous chapters, a detailed evaluation of the chemical and physical processes in the model leads to a better understanding of the atmospheric processes that contribute to poor air quality. In the future, the PAPPT could be extended and applied to other photochemical air quality models such as the SARMAP Air Quality Model (SAQM) or the Community Multiscale Air Quality (CMAQ). The tool also could be incorporated into indoor air quality models. Understanding the formation processes of indoor air pollutants would allow a more accurate and complete depiction of human exposure to air pollutants. These models also could provide insight into the exposure building occupants face if a chemical or biological attack occurs.

The PAPPT also could be incorporated into regional air quality models that predict aerosol concentrations. These models predict concentrations based on an emission inventory and a complex network of source emissions, atmospheric transport, chemistry, and removal processes. The PAPPT could examine the effects that altering the emission inventory would have on these networks. For example, the PAPPT could determine the relative importance of the deposition process versus emissions as climate changes land

cover. Comparing the sensitivity of these processes to changes in climate and inventory will improve the understanding of the complex relationships that lead to aerosol formation.

Once it is incorporated into an aerosol model the PAPPT could investigate aerosol formation processes. A large source of atmospheric particles is secondary organic aerosols (SOA). Estimations of global formation rates of SOA range from 13-24 Tg/yr (Griffin *et al.*, 1999) to 30-270 Tg/yr (Andreae *et al.*, 1997). This amount of aerosol is similar in magnitude to the estimates of carbonaceous aerosol emitted globally to the atmosphere from fossil fuel and biomass combustion (Liousse *et al.*, 1996). Sesquiterpenes, a biogenic hydrocarbon, may play a significant role in secondary organic aerosol (SOA) formation because of its SOA yield of nearly unity. Work has been completed that estimates the emissions of isoprene, monoterpenes, and sesquiterpenes in southeast Texas (Vizuite *et al.*, 2004). Results from that work showed that in the eastern half of Texas, sesquiterpenes may play a very significant, but poorly understood role in SOA formation.

The eastern Texas air shed could be used as a case study in conjunction with the PAPPT to examine the potential role of sesquiterpenes in SOA formation. Model results could be compared with aircraft observations taken from flight paths that coincided with areas of high sesquiterpene emissions. Analysis of modeling runs and observed data would focus on reducing the high uncertainty associated with the magnitude of sesquiterpene emissions. This improved understanding of sesquiterpene emission estimates would be incorporated into the biogenic model, resulting in an emission

inventory that includes sesquiterpenes. With this inventory the impact on aerosol formation pathways could be quantified with the PAPPT.

In the near future satellite imaging will play an important role in producing a reliable set of observed data, at multiple scales, to compare with air quality model output. Advances in satellite imaging will provide new opportunities to view flux data for a number of pollutants. This provides another area of opportunity for the PAPPT to be utilized. For example, these data could provide observed fluxes of aerosols entering the United States from biomass burning in Mexico. The PAPPT could be used to compare the observed satellite fluxes from these fires in Mexico to the processes that are occurring in the model.

8.1 REFERENCES

- Griffin R. J., Cocker III D. R., Seinfeld J. H. 1999. "Estimate of global atmospheric organic aerosol from oxidation of biogenic hydrocarbons." *Geophysical Research Letters*, 26(17), 2721-2724
- Andreae M. O., Crutzen P. J. 1997. "Atmospheric aerosols: Biogeochemical sources and role in atmospheric chemistry." *Science*, 1052-1058
- Liousse C., Penner J. E., Chuang C., Walton J.J., Eddleman H., Cachier H. 1996. "A global three-dimensional model study of carbonaceous aerosols." *Journal Geophysical Research*, 101(D16), 19411- 19432
- Vizuite W., Junquera V., Allen D. T. 2004. "Sesquiterpene emissions and secondary organic aerosol formation potentials for southeast Texas." *Aerosol Science & Technology*, 38 (S1):167-181

Appendices

APPENDIX A – PROCESS ANALYSIS POST PROCESSING TOOL OUTPUT FOR AUGUST 25, 2000

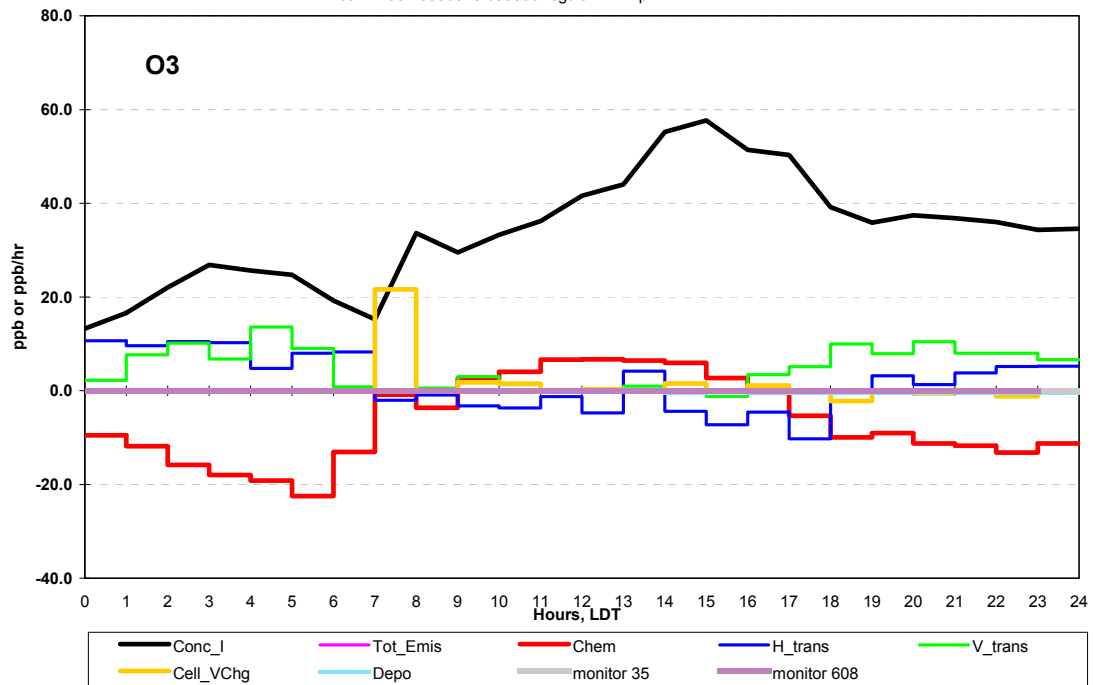
A.1 Introduction

The following plots are the time series and cycle diagrams produced by the Process Analysis Post Processing Tool for the August 25, 2000 simulation day. Data for the source, middle, and peak control volumes for the base case and the emission event scenarios are presented. Details of the simulation scenarios and control volumes are described in Chapter 3. Time series plots were included for the following CBIV species: O₃, OLE, PAR, XYL, and ETH.

Source Control Volume

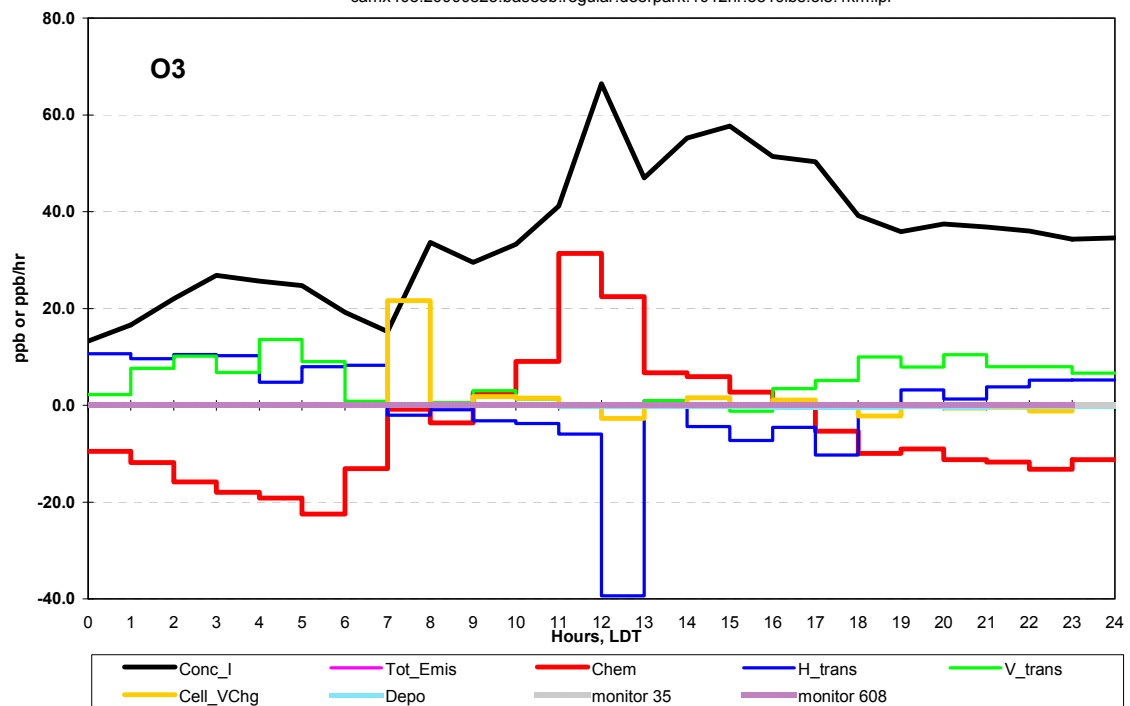
camx403.20000825.base5b.regul

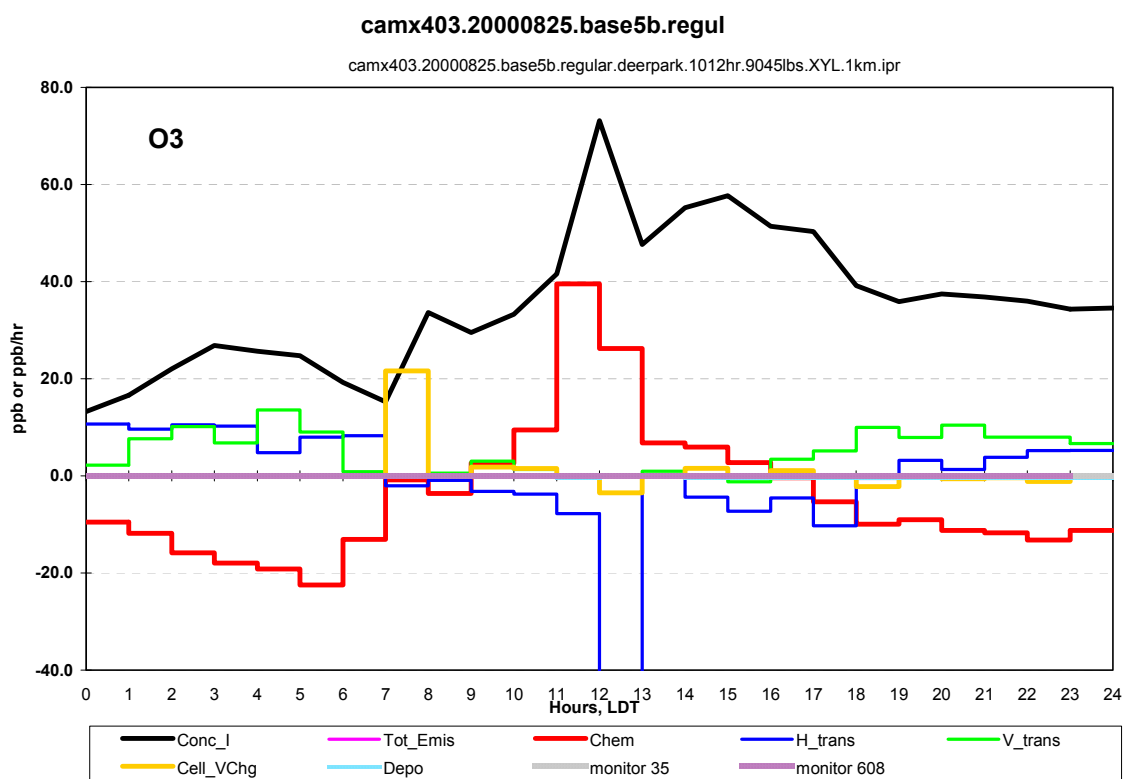
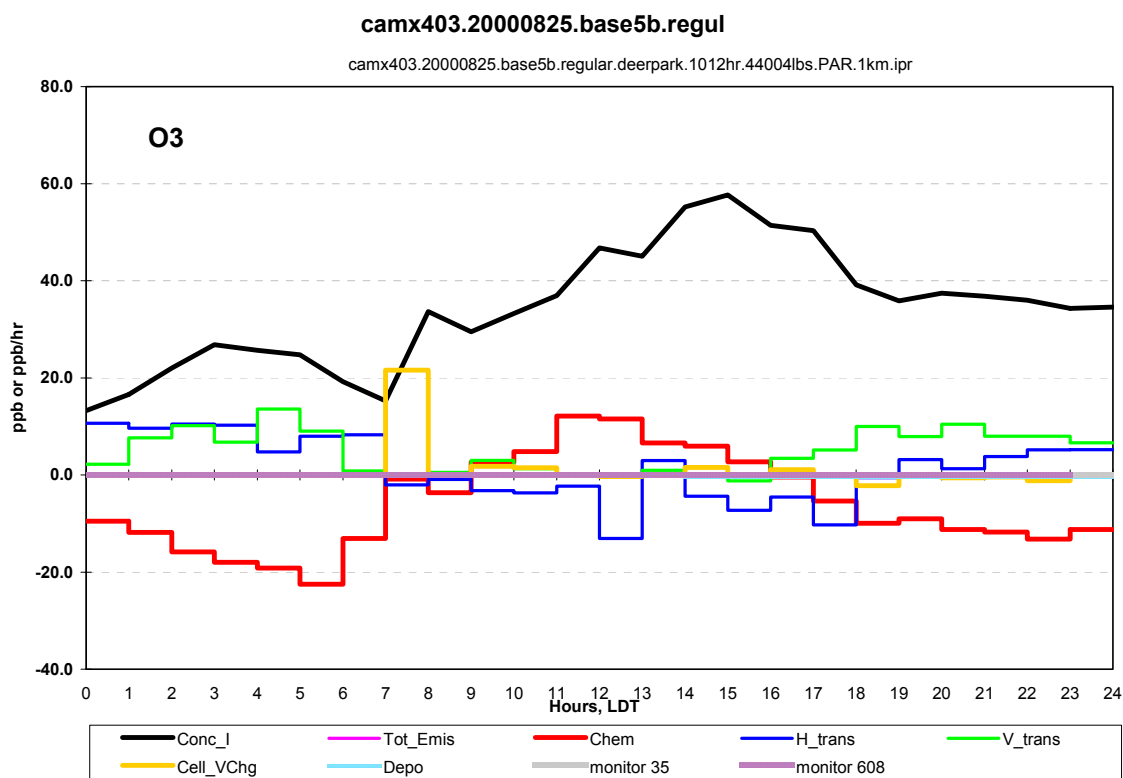
camx403.20000825.base5b.regular.1km.ipr

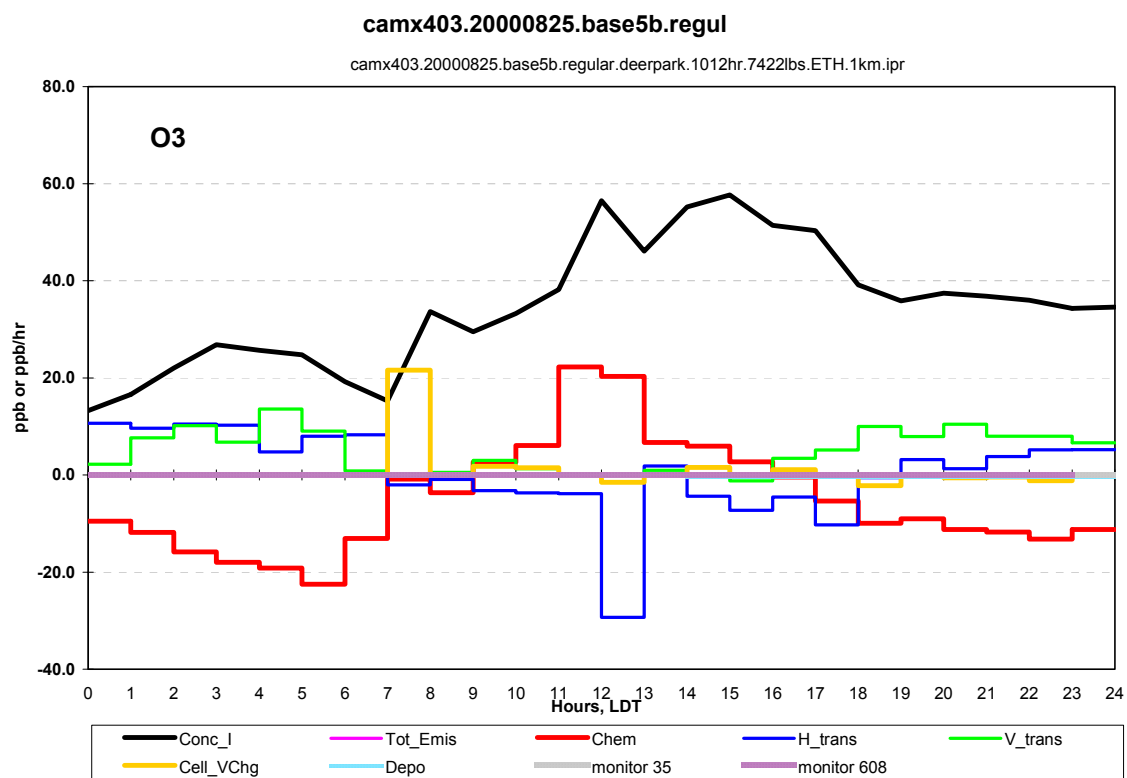


camx403.20000825.base5b.regul

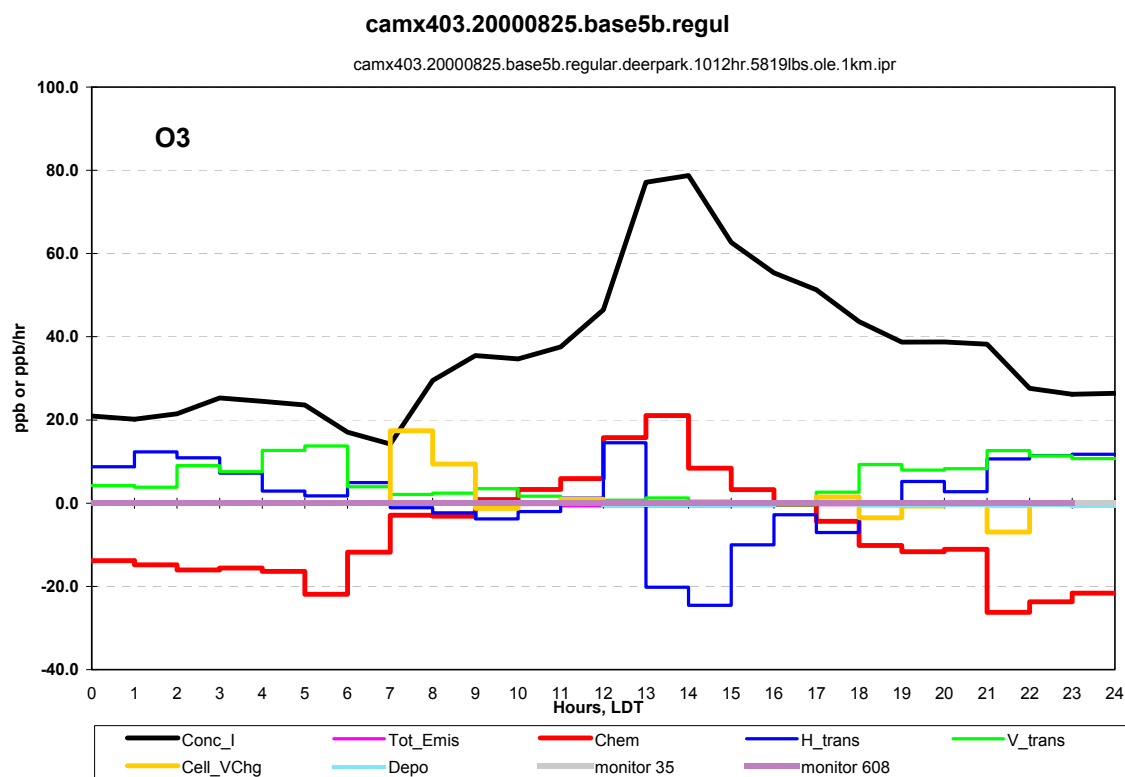
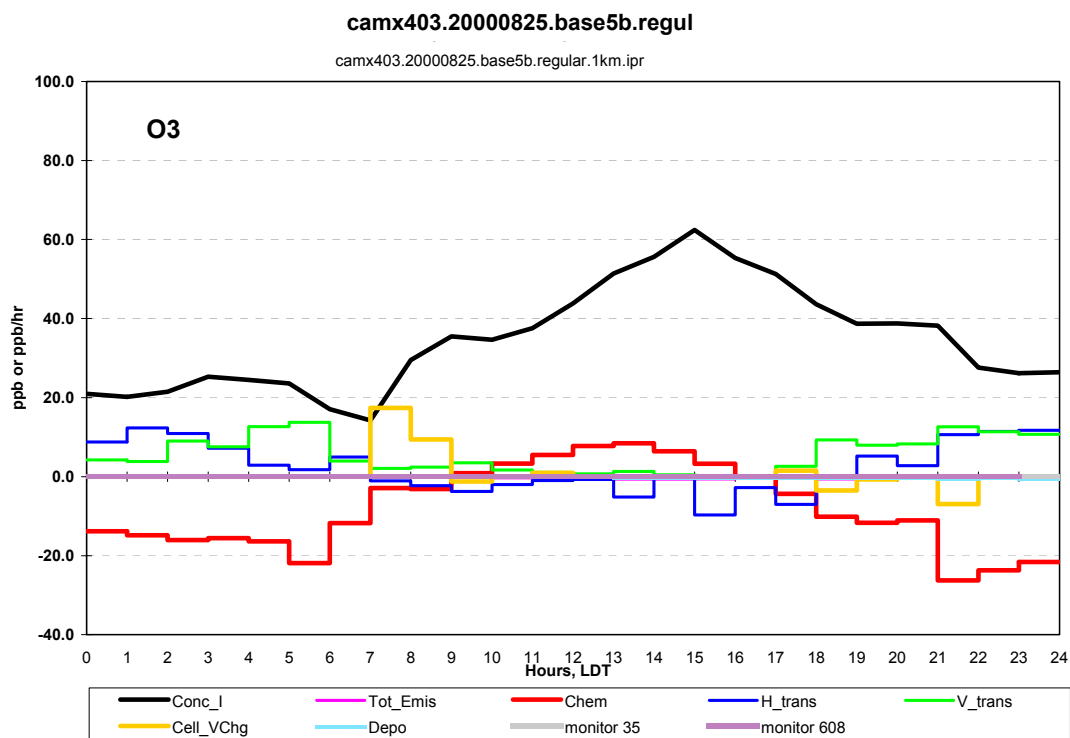
camx403.20000825.base5b.regular.deerpark.1012hr.5819lbs.ole.1km.ipr





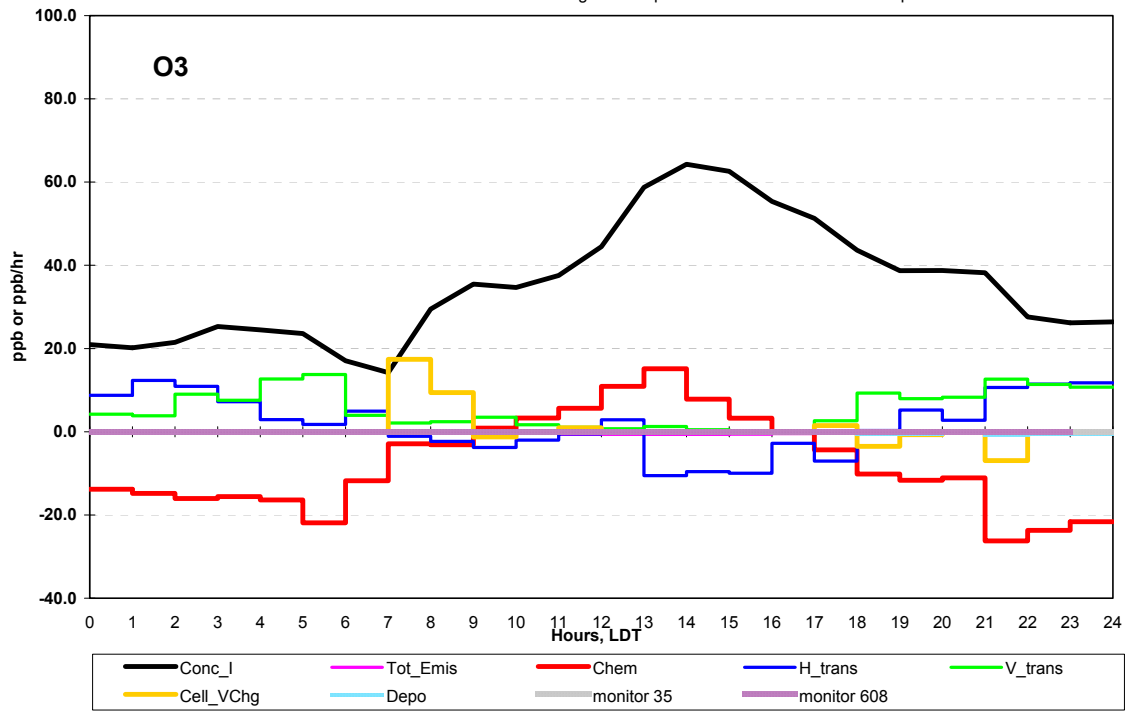


Middle Control Volume



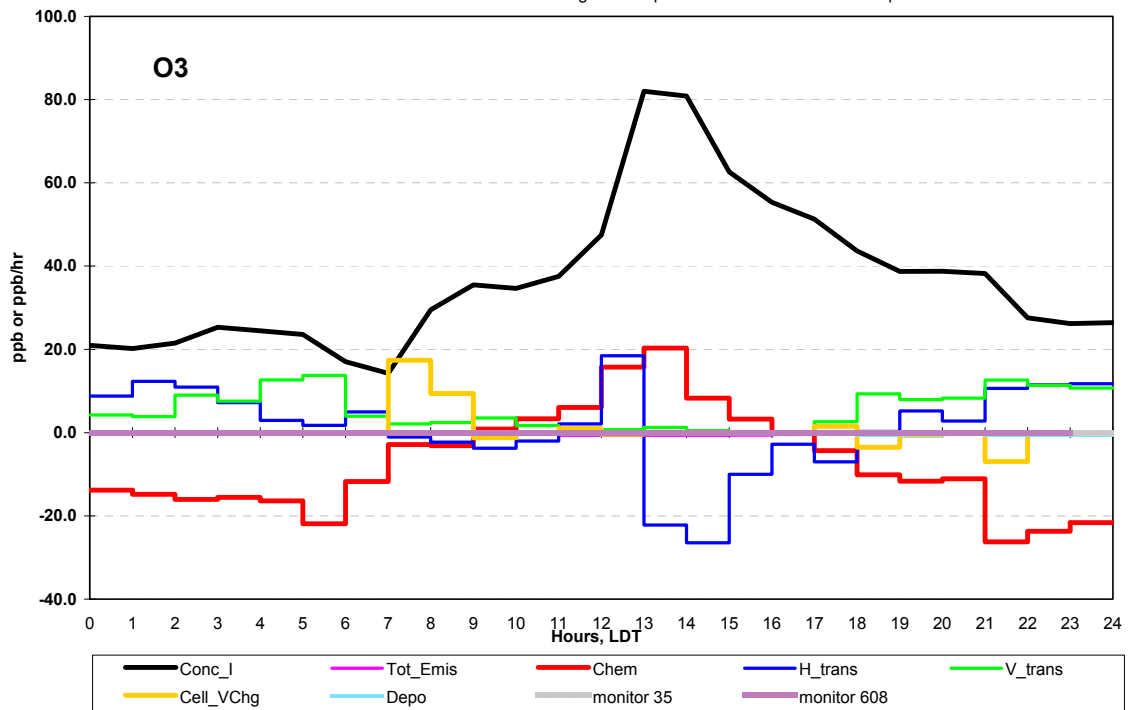
camx403.20000825.base5b.regul

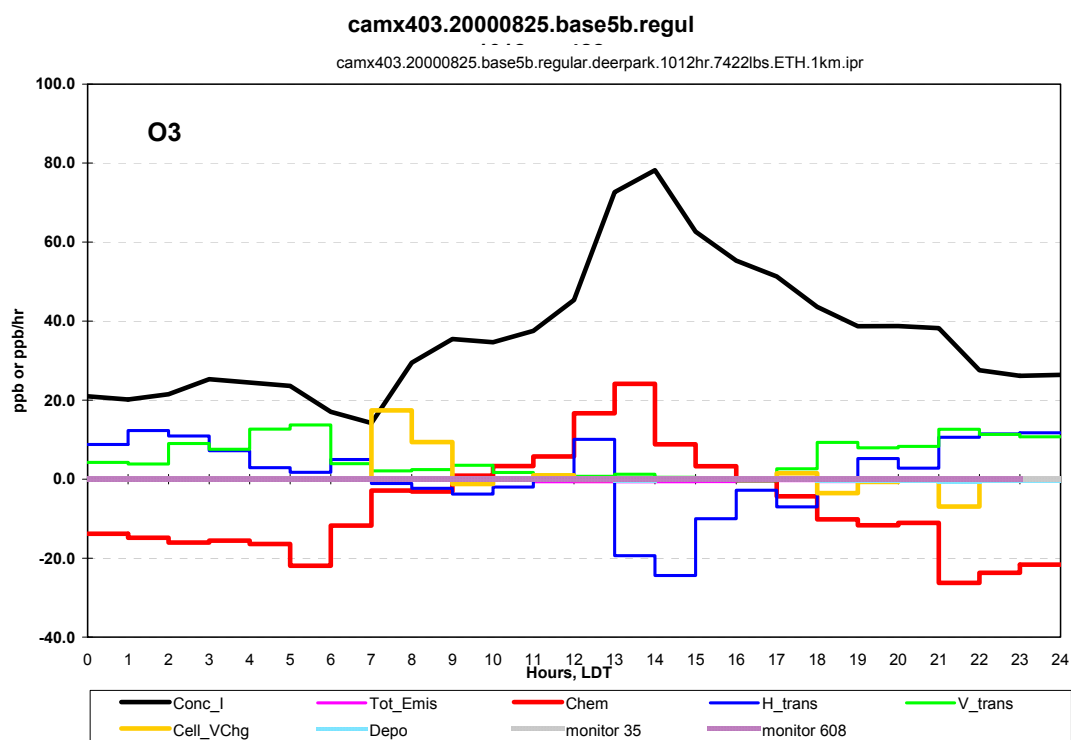
camx403.20000825.base5b.regular.deerpark.1012hr.44004lbs.PAR.1km.ipr



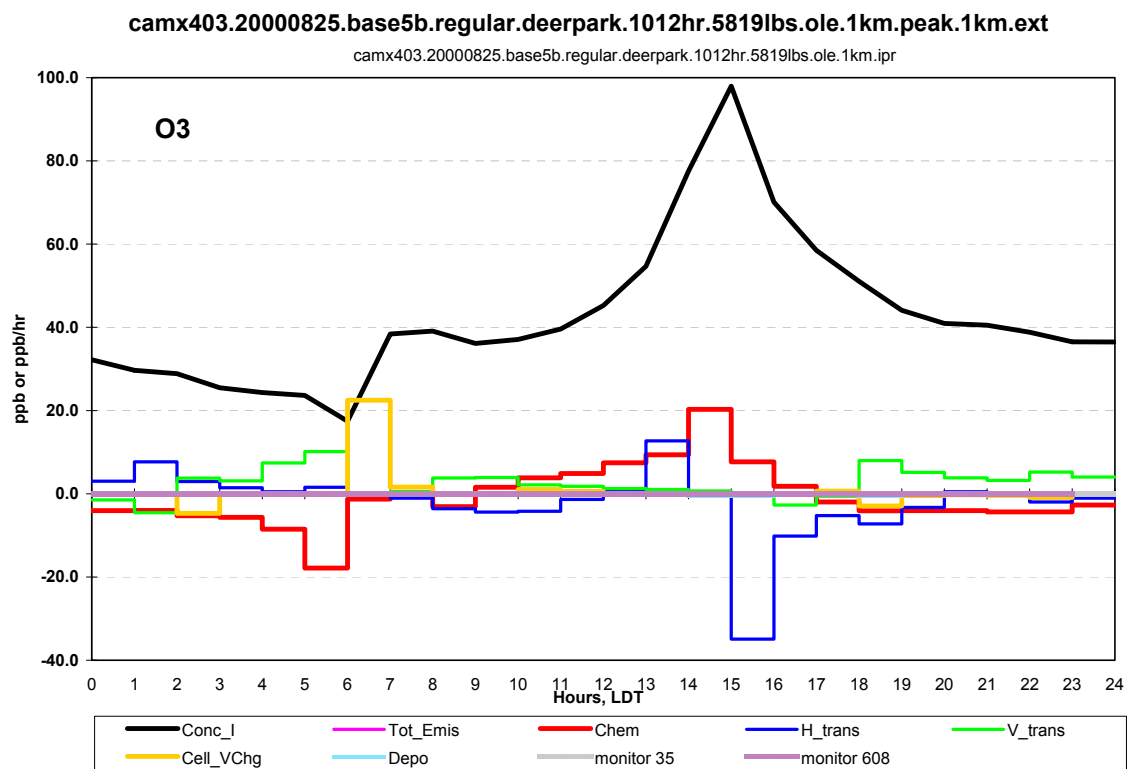
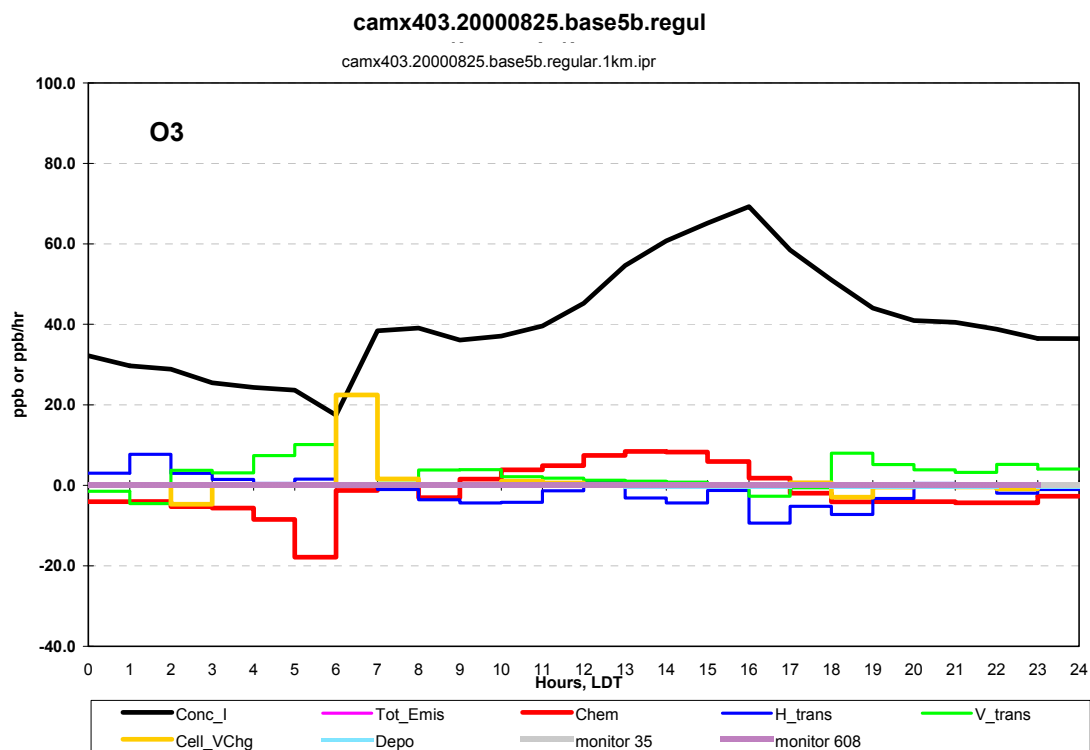
camx403.20000825.base5b.regul

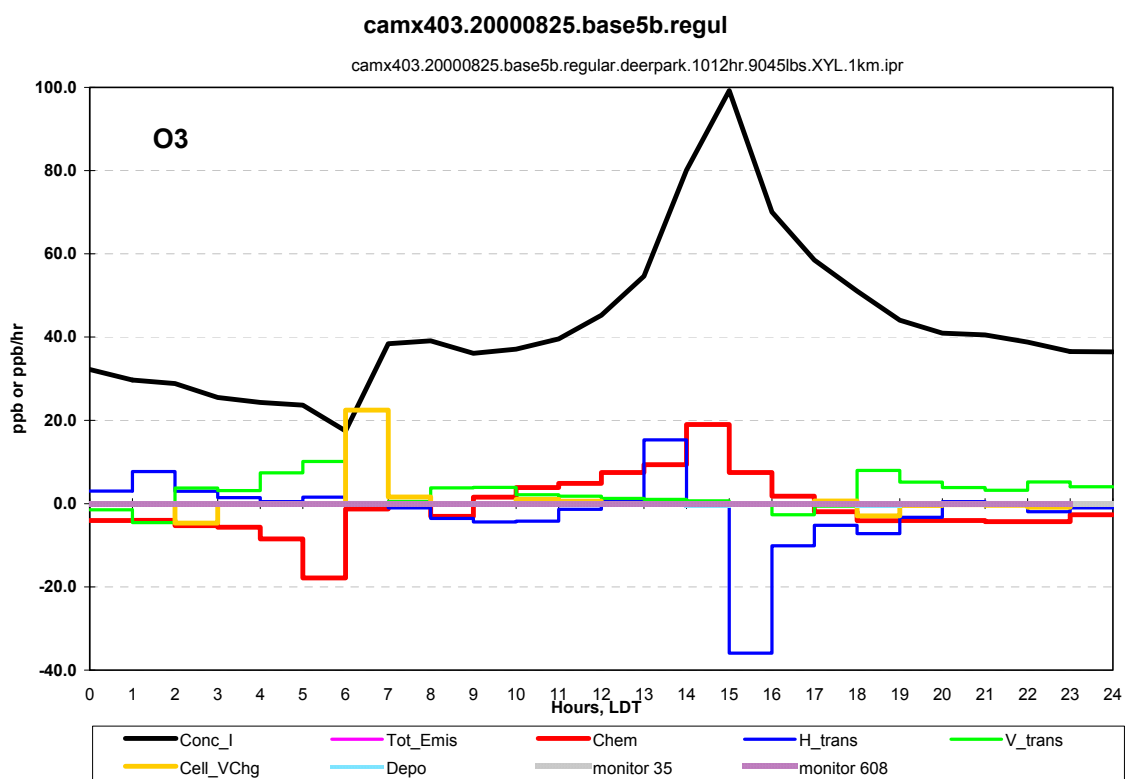
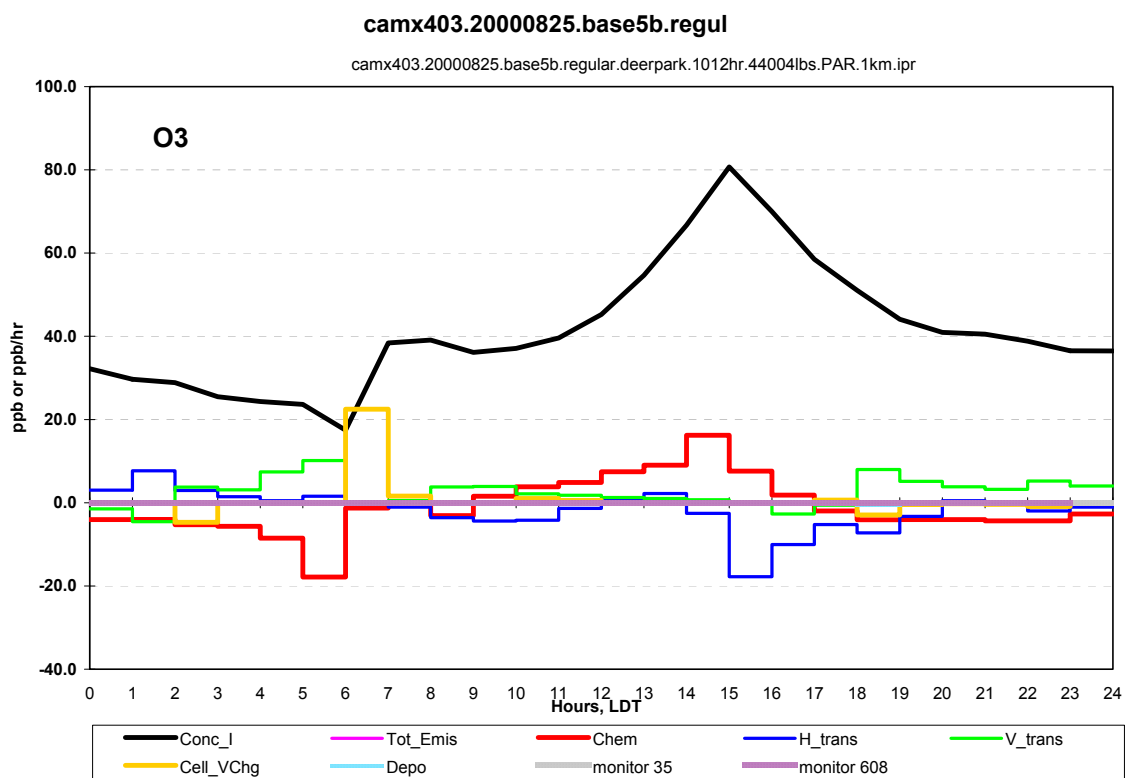
camx403.20000825.base5b.regular.deerpark.1012hr.9045lbs.XYL.1km.ipr

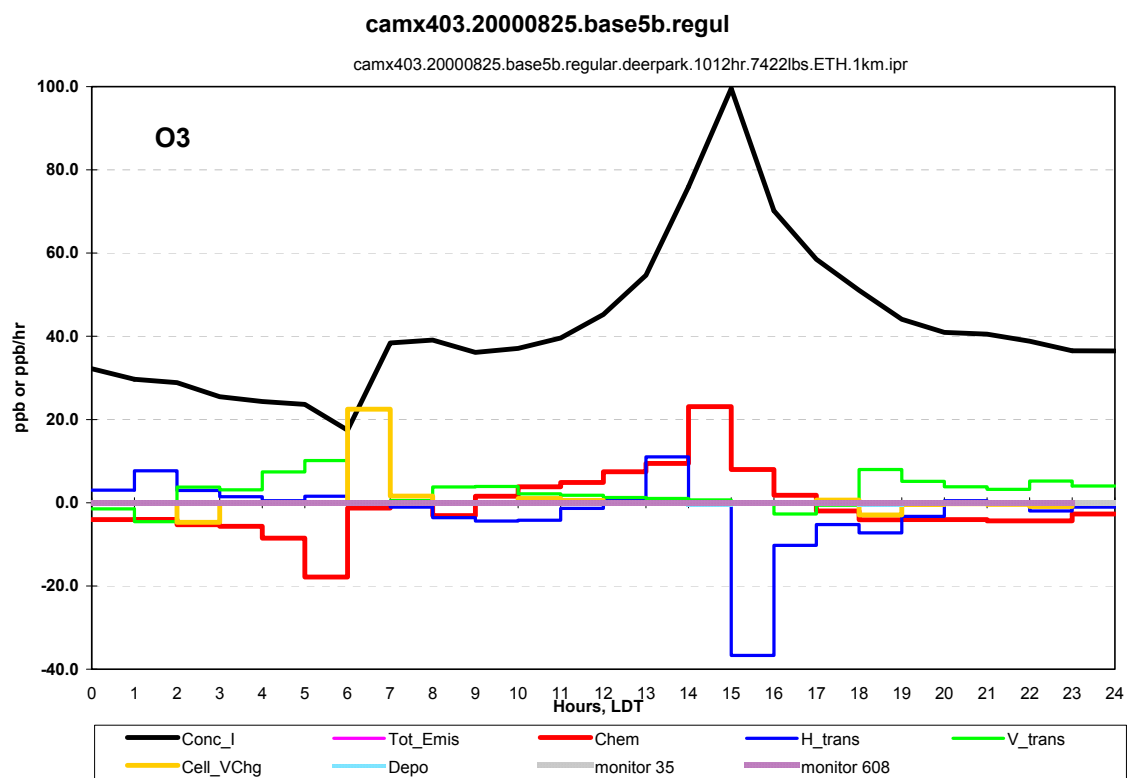




Peak Control Volume



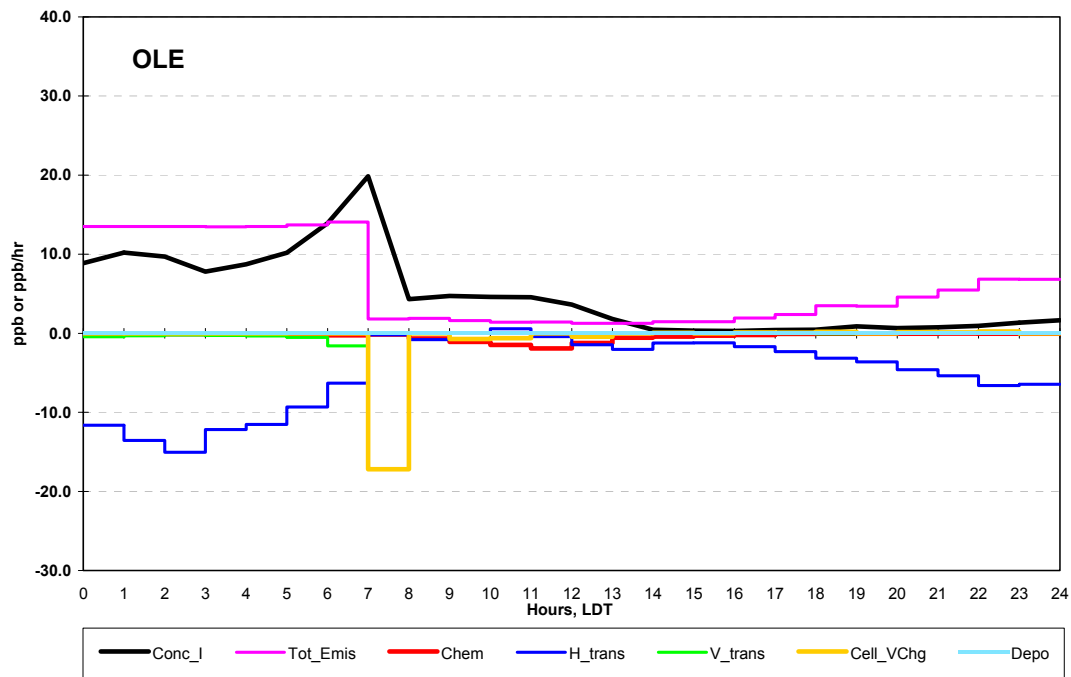




Source Control Volume

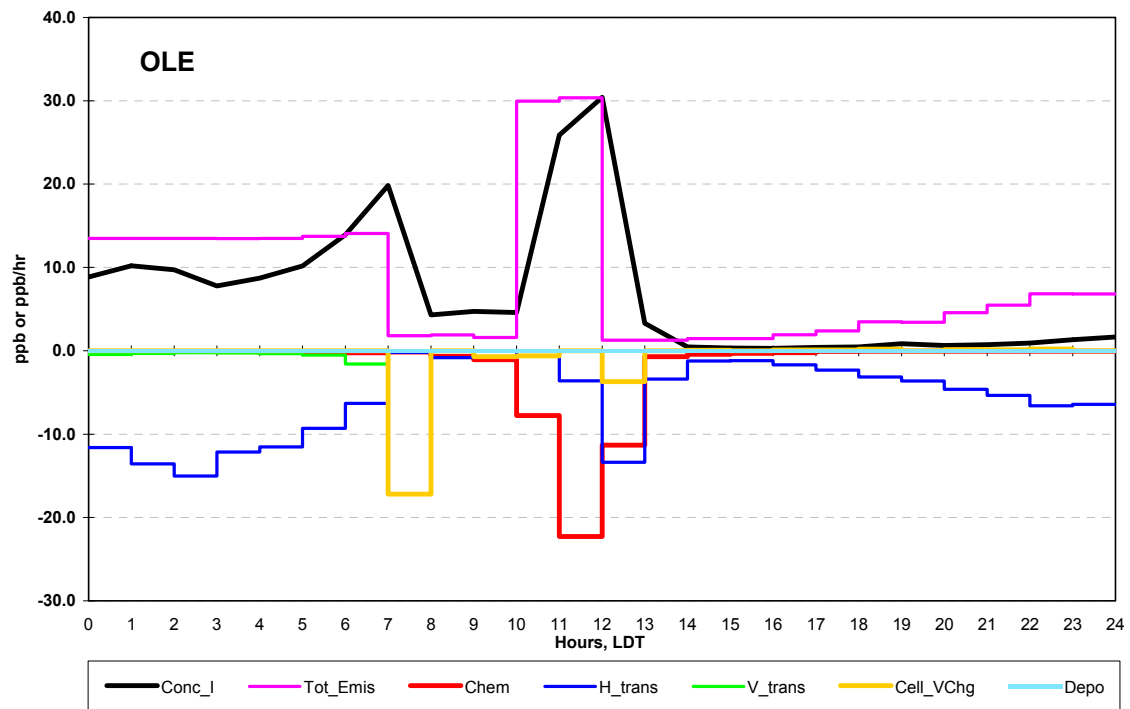
camx403.20000825.base5b.regul

camx403.20000825.base5b.regular.1km.ipr

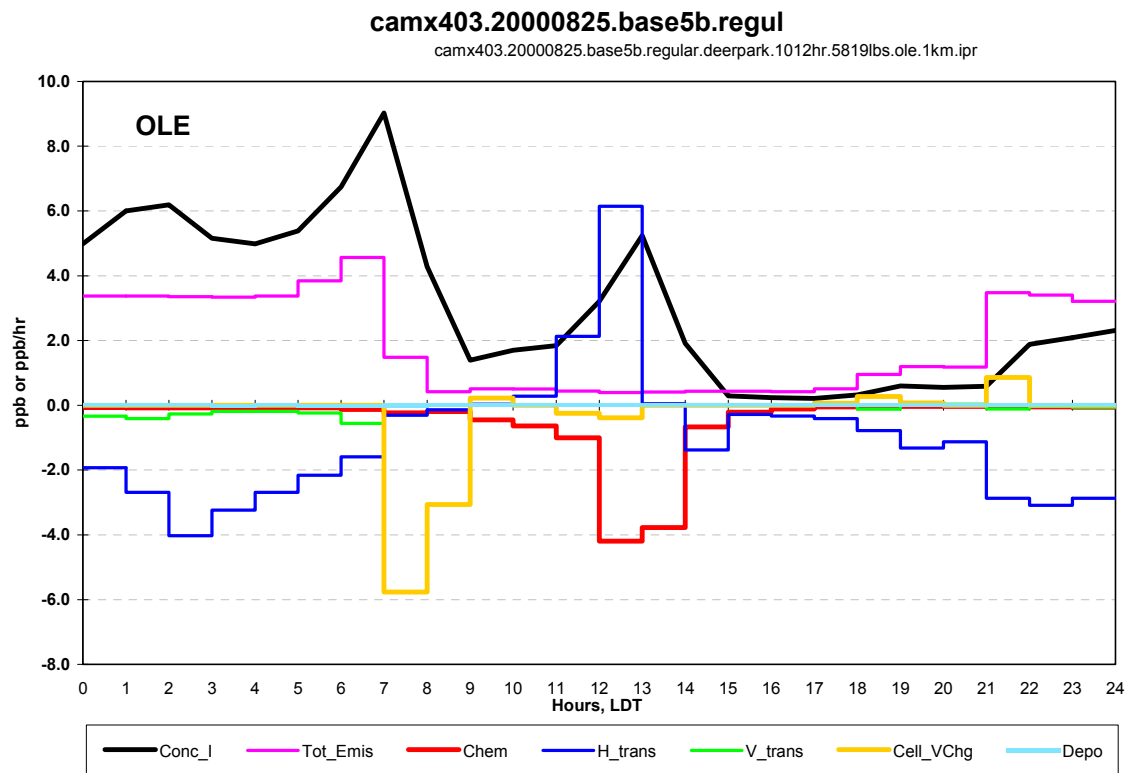
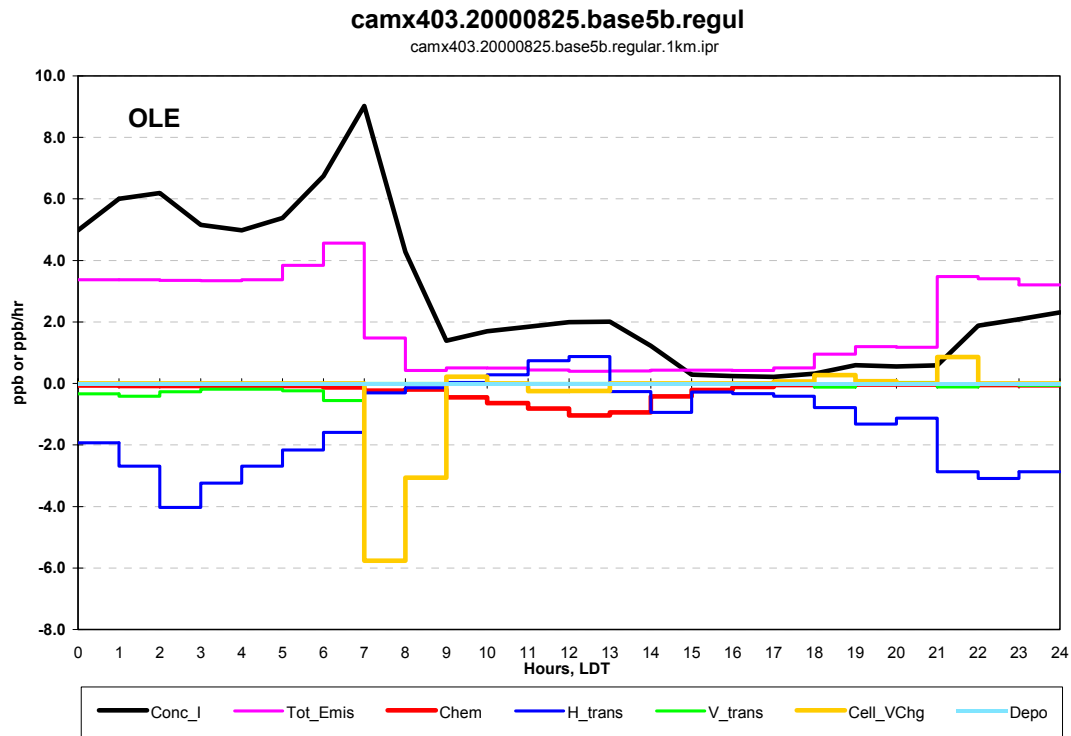


camx403.20000825.base5b.regul

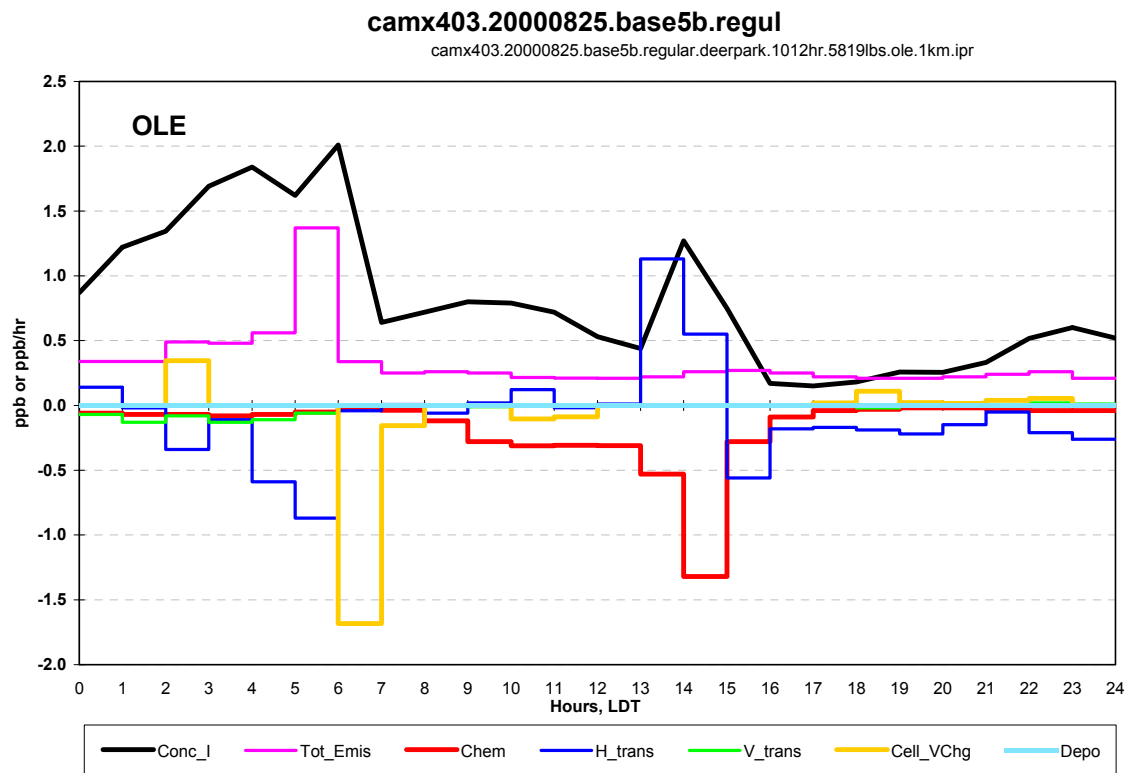
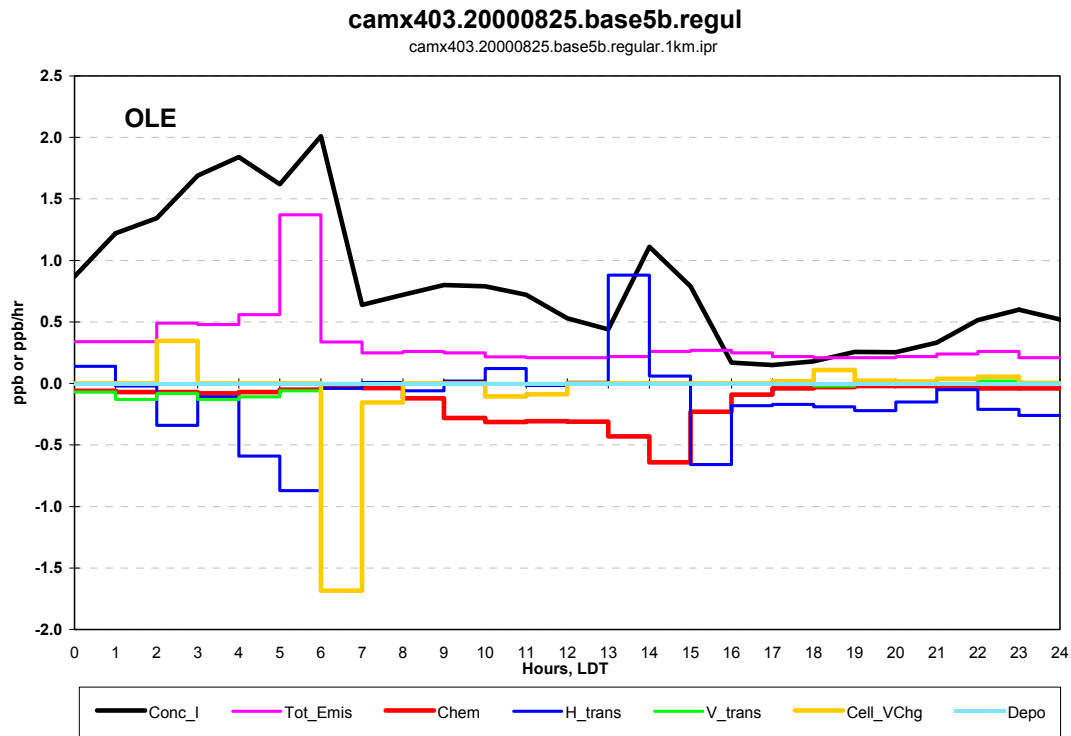
camx403.20000825.base5b.regular.deerpark.1012hr.5819lbs.ole.1km.ipr



Middle Control Volume



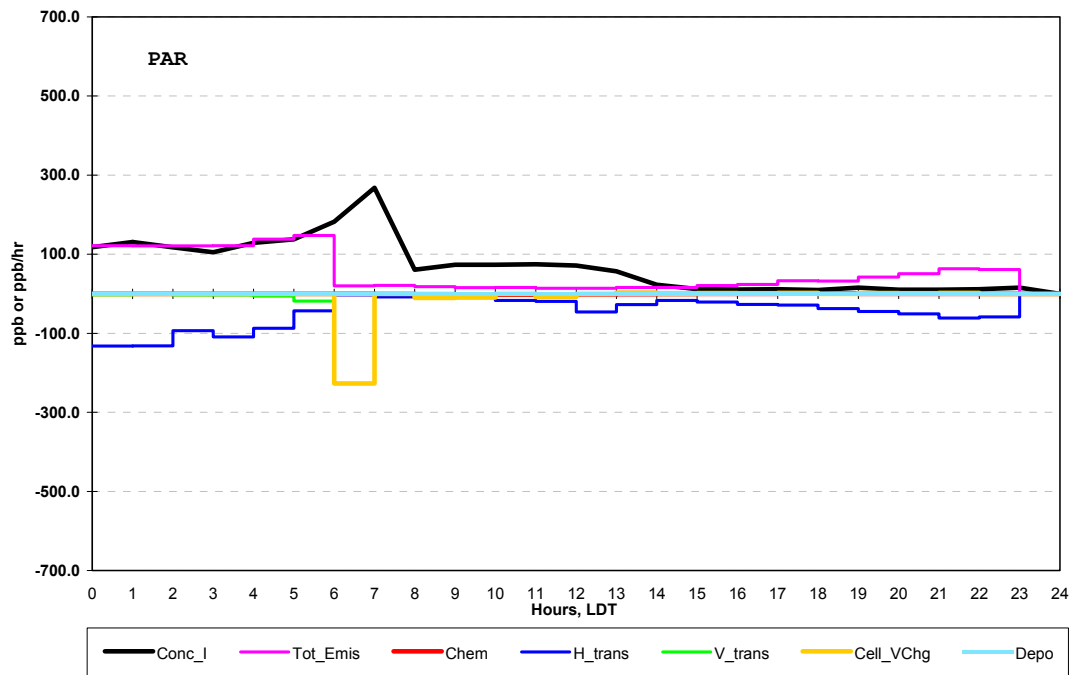
Peak Control Volume



Source Control Volume

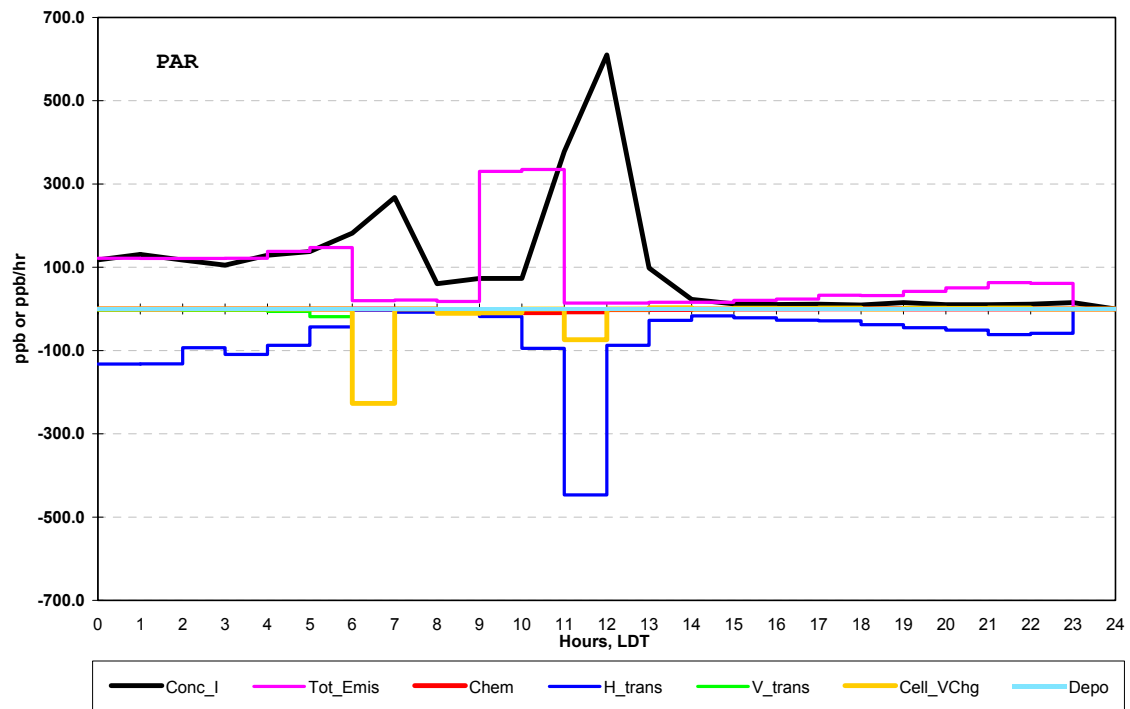
camx403.20000825.base5b.regul

camx403.20000825.base5b.regular.1km.ipr



camx403.20000825.base5b.regul

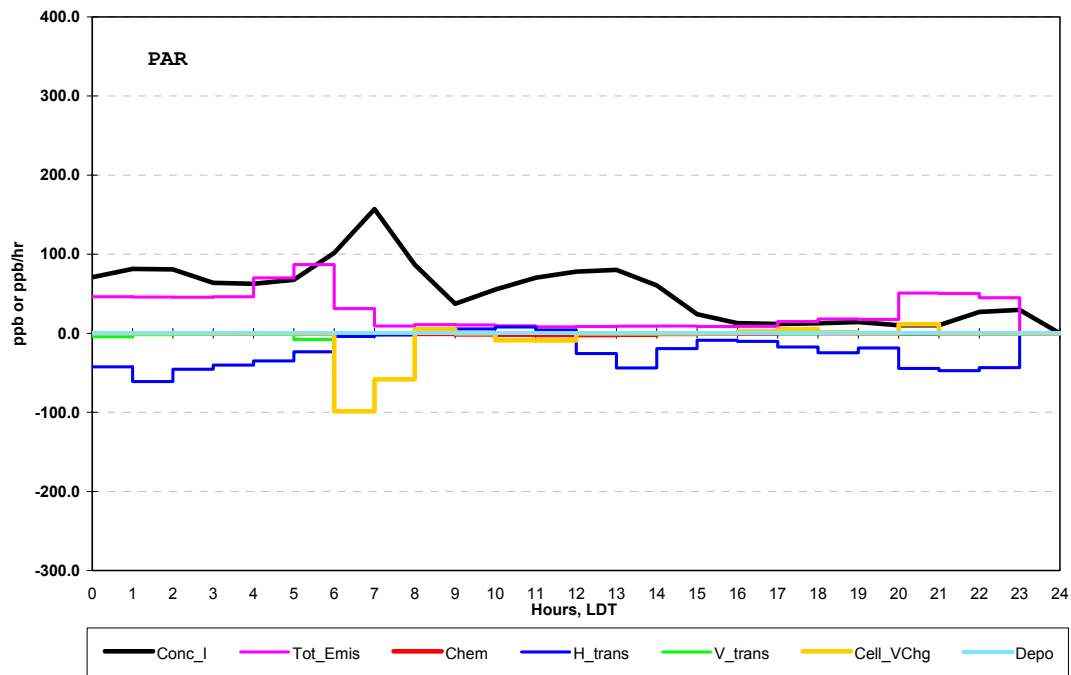
camx403.20000825.base5b.regular.deerpark.1012hr.44004lbs.PAR.1km.ipr



Middle Control Volume

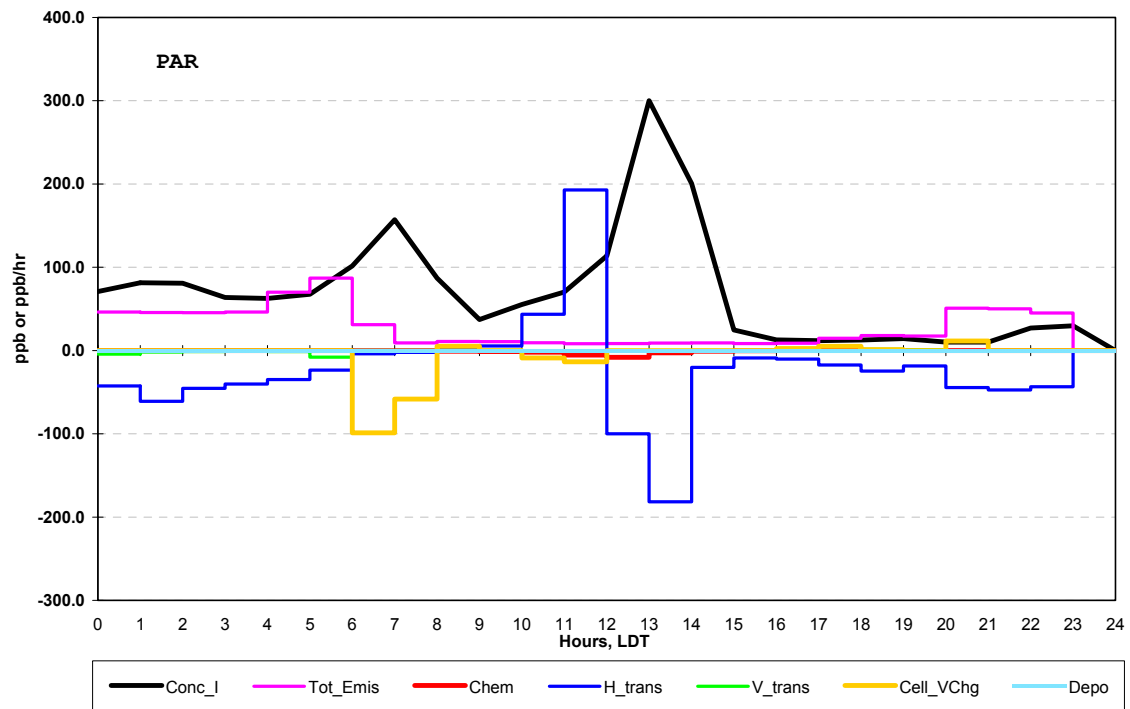
camx403.20000825.base5b.regul

camx403.20000825.base5b.regular.1km.ipr



camx403.20000825.base5b.regul

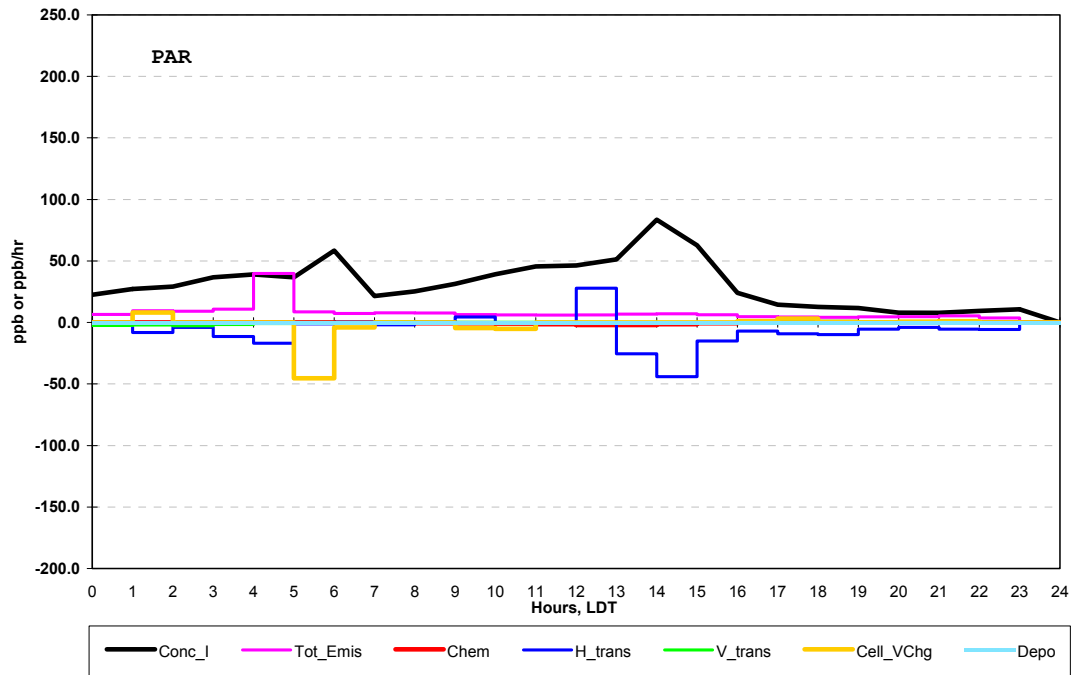
camx403.20000825.base5b.regular.deerpark.1012hr.44004lbs.PAR.1km.ipr



Peak Control Volume

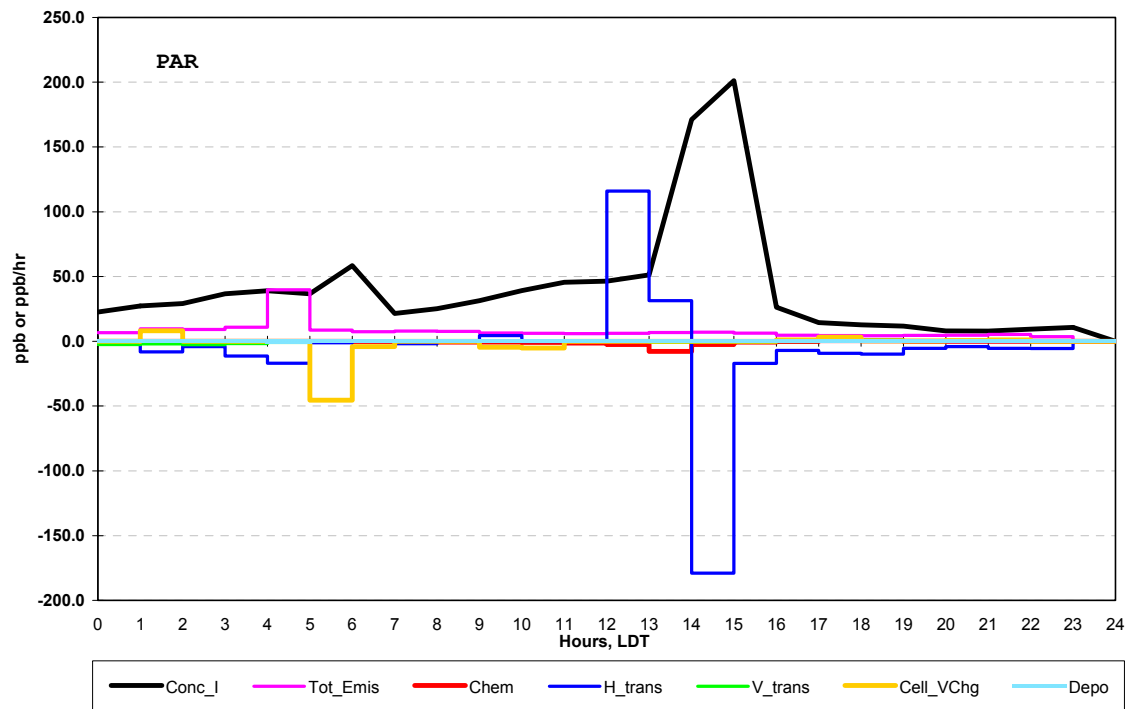
camx403.20000825.base5b.regul

camx403.20000825.base5b.regular.1km.ipr



camx403.20000825.base5b.regul

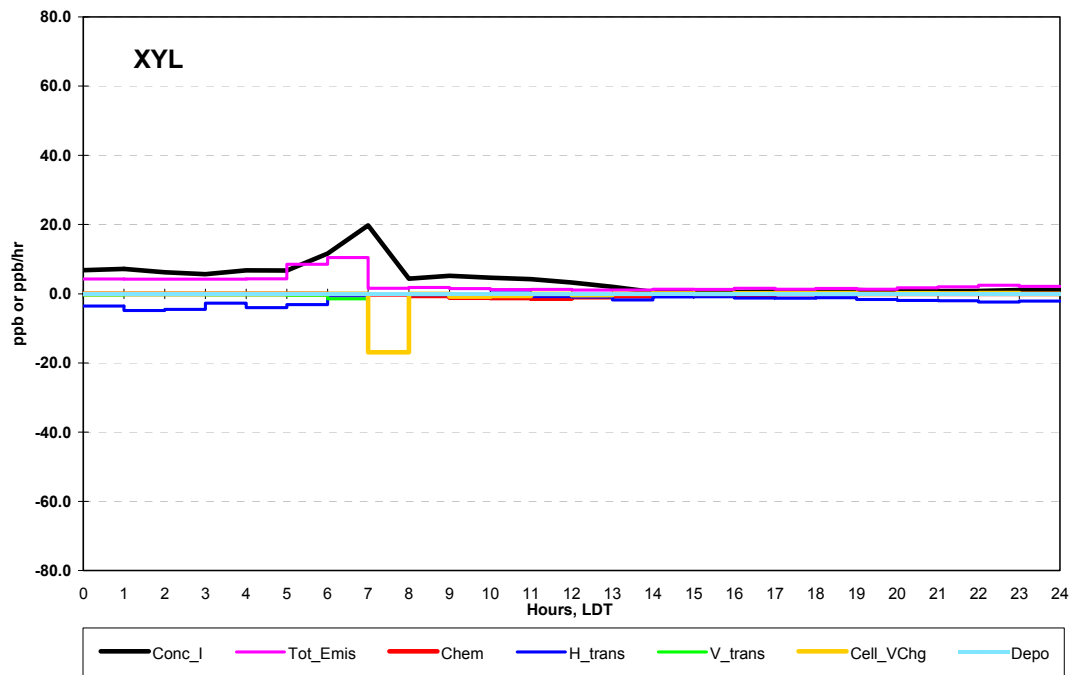
camx403.20000825.base5b.regular.deerpark.1012hr.44004lbs.PAR.1km.ipr



Source Control Volume

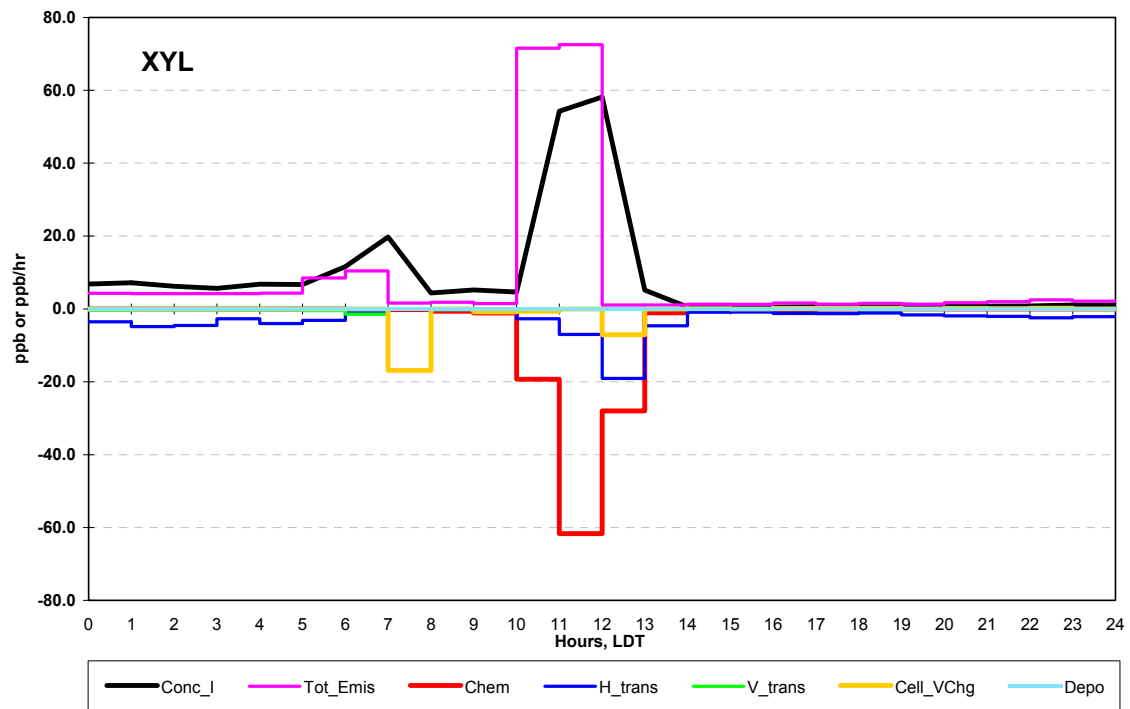
camx403.20000825.base5b.regul

camx403.20000825.base5b.regular.1km.ipr

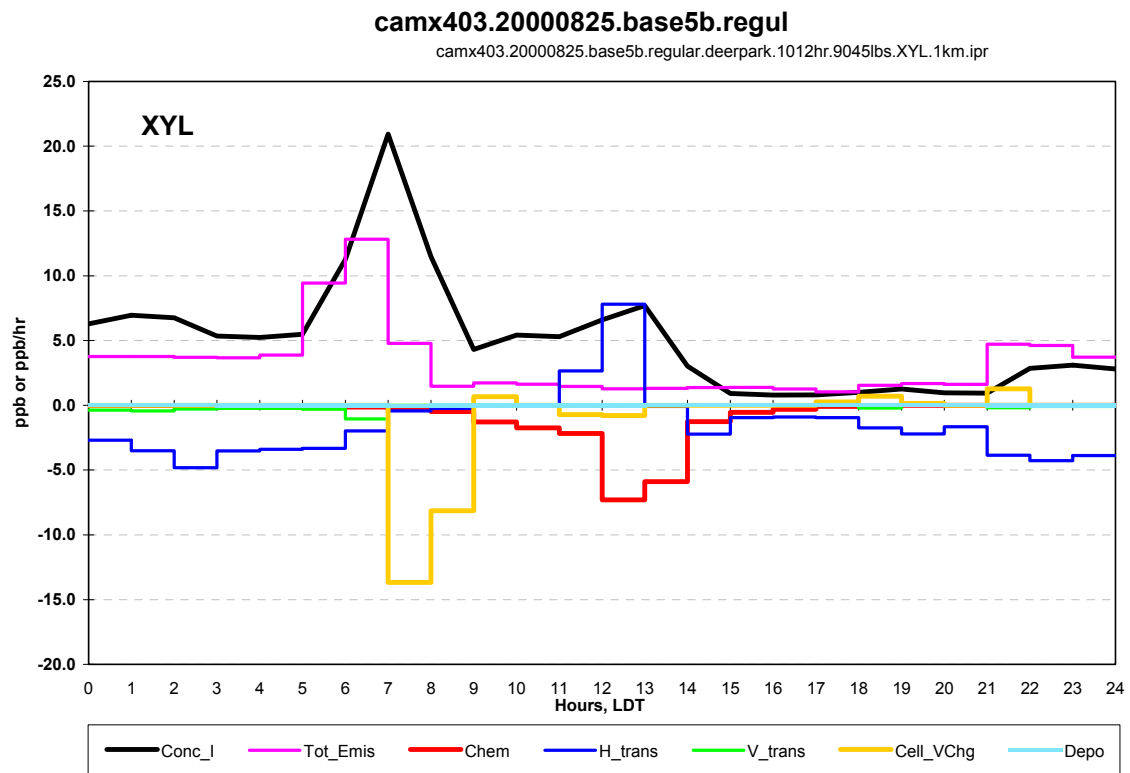
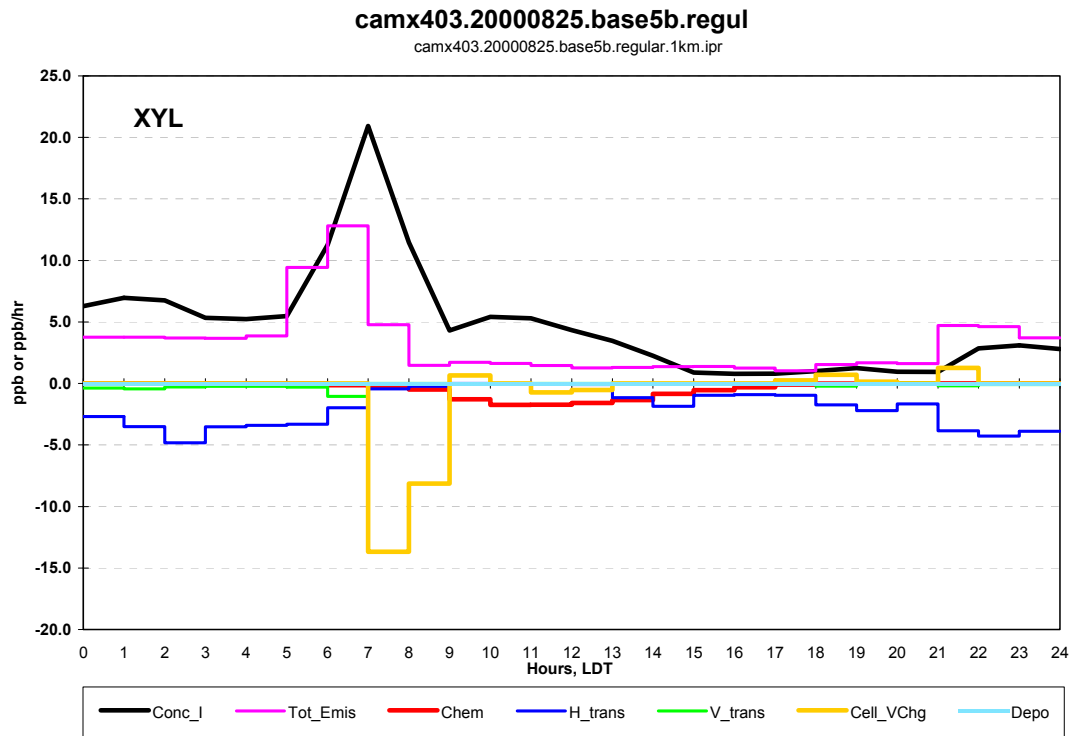


camx403.20000825.base5b.regul

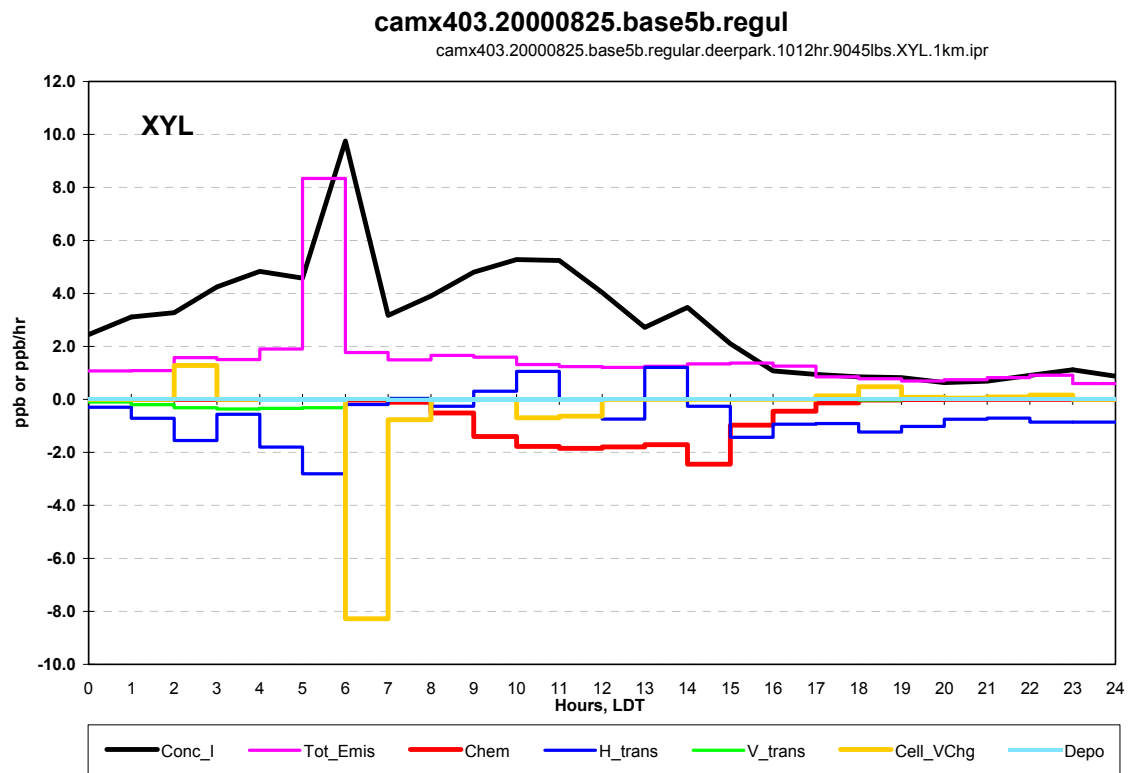
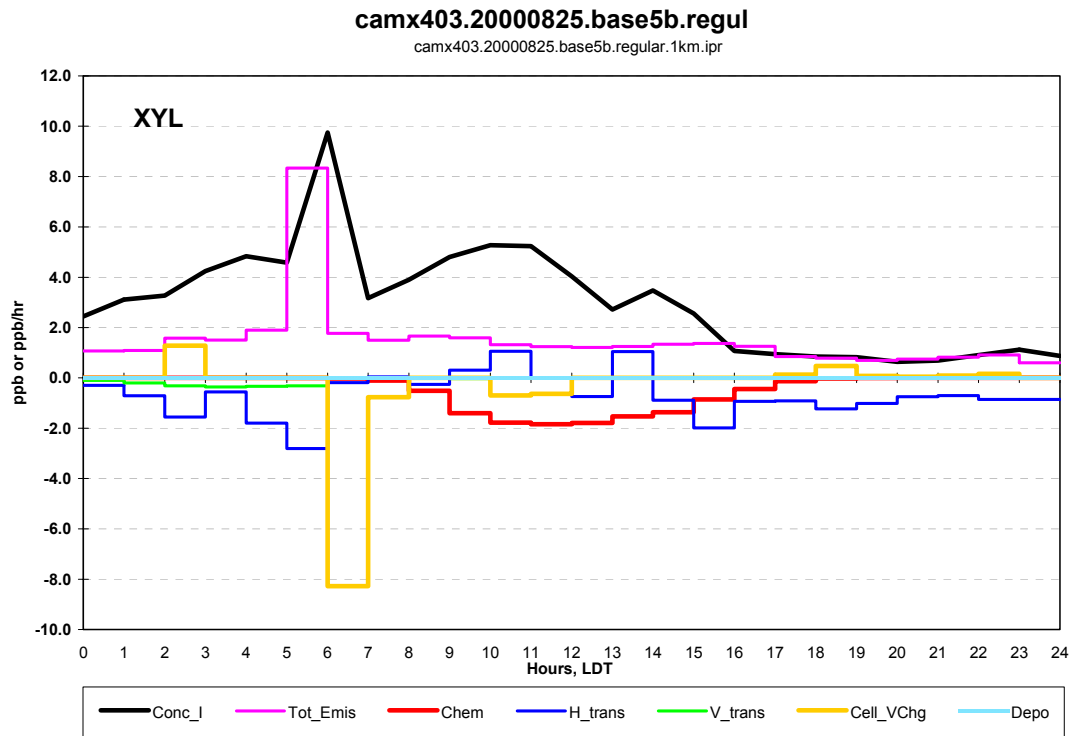
camx403.20000825.base5b.regular.deerpark.1012hr.9045lbs.XYL.1km.ipr



Middle Control Volume



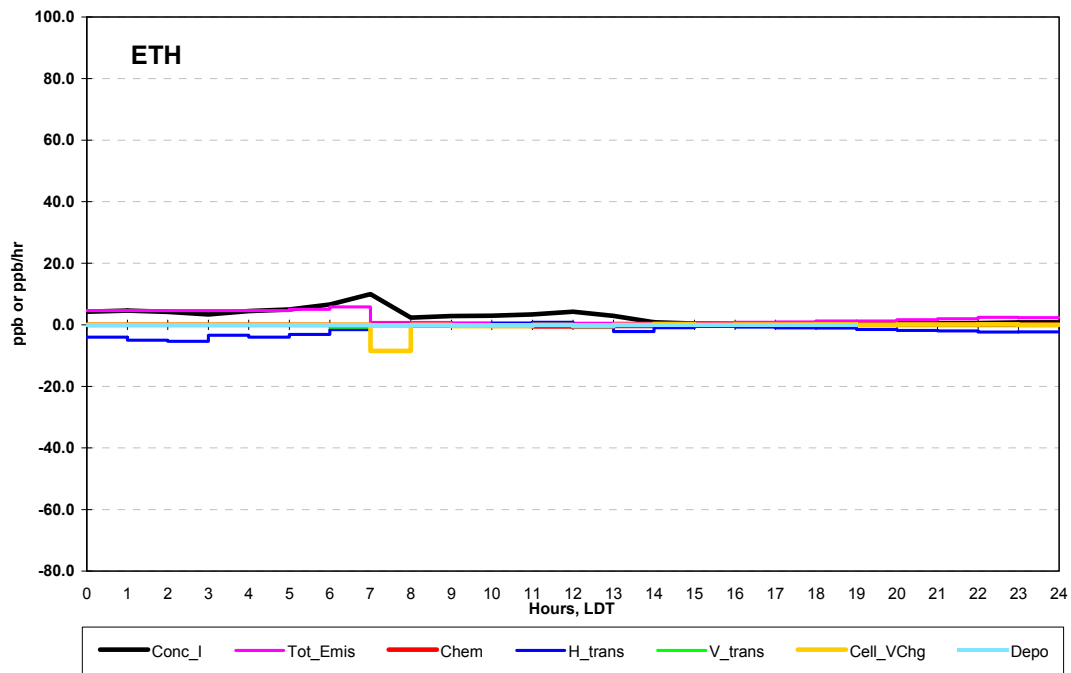
Peak Control Volume



Source Control Volume

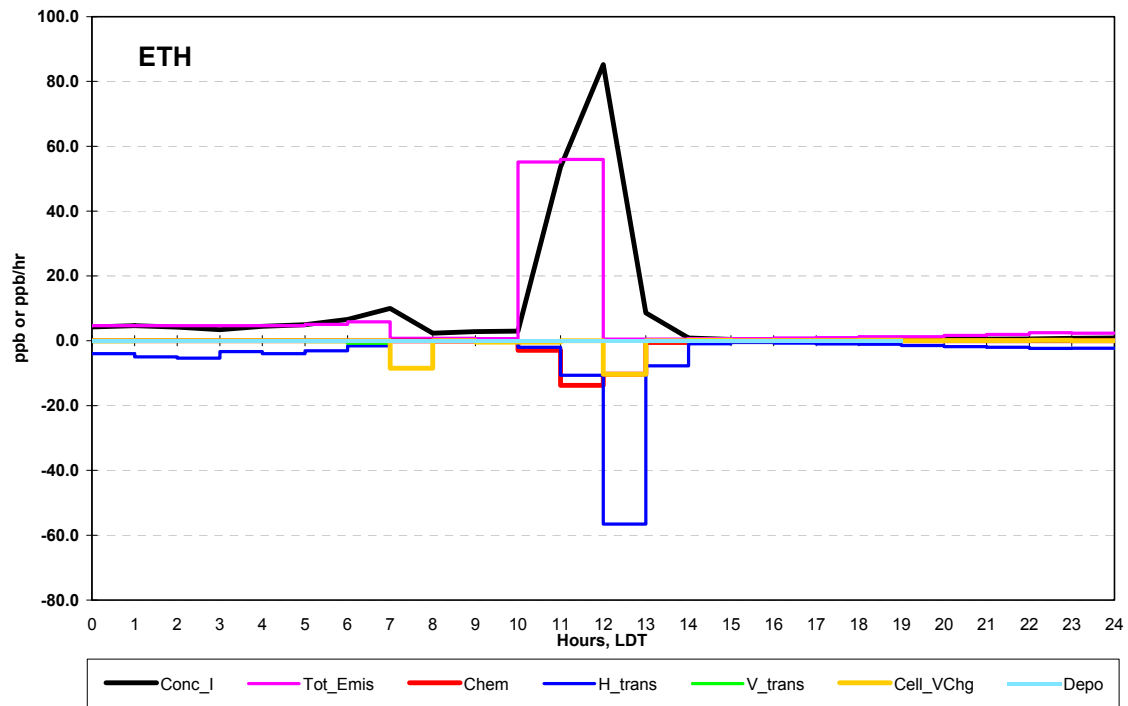
camx403.20000825.base5b.re

camx403.20000825.base5b.regular.1km.ipr



camx403.20000825.base5b.re

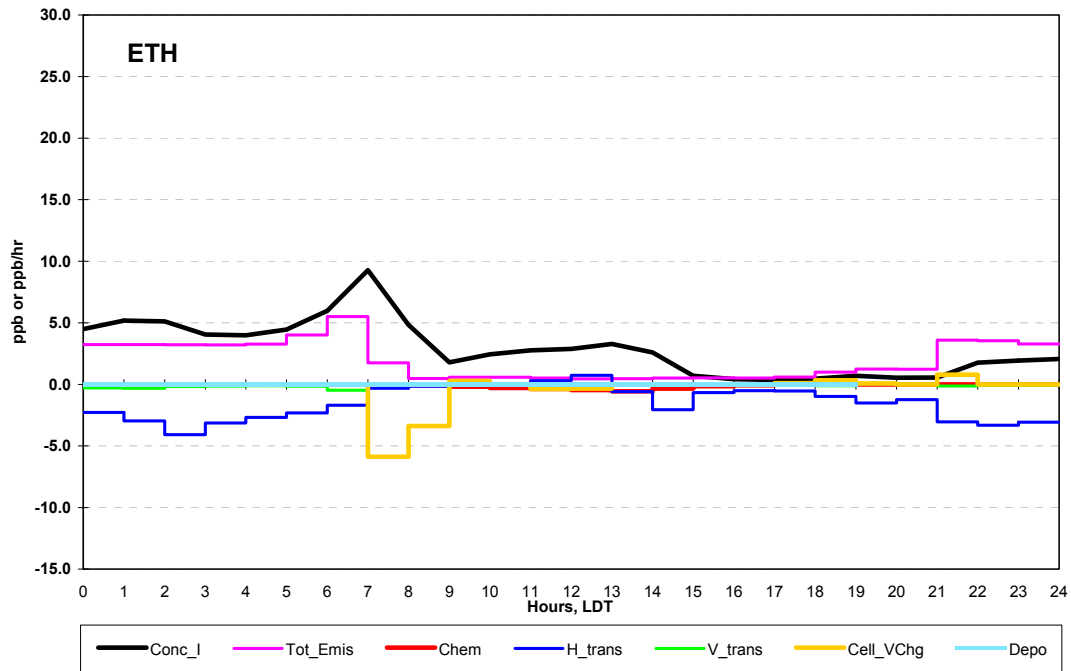
camx403.20000825.base5b.regular.deerpark.1012hr.7422lbs.ETH.1km.ipr



Middle Control Volume

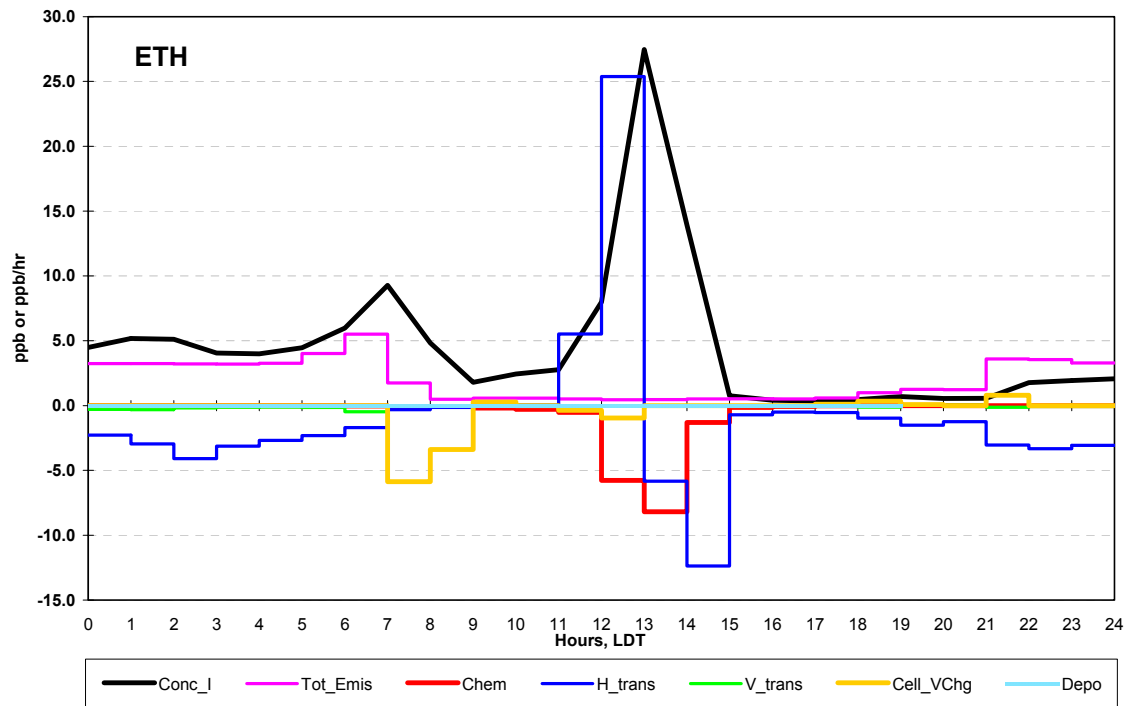
camx403.20000825.base5b.re

camx403.20000825.base5b.regular.1km.ipr

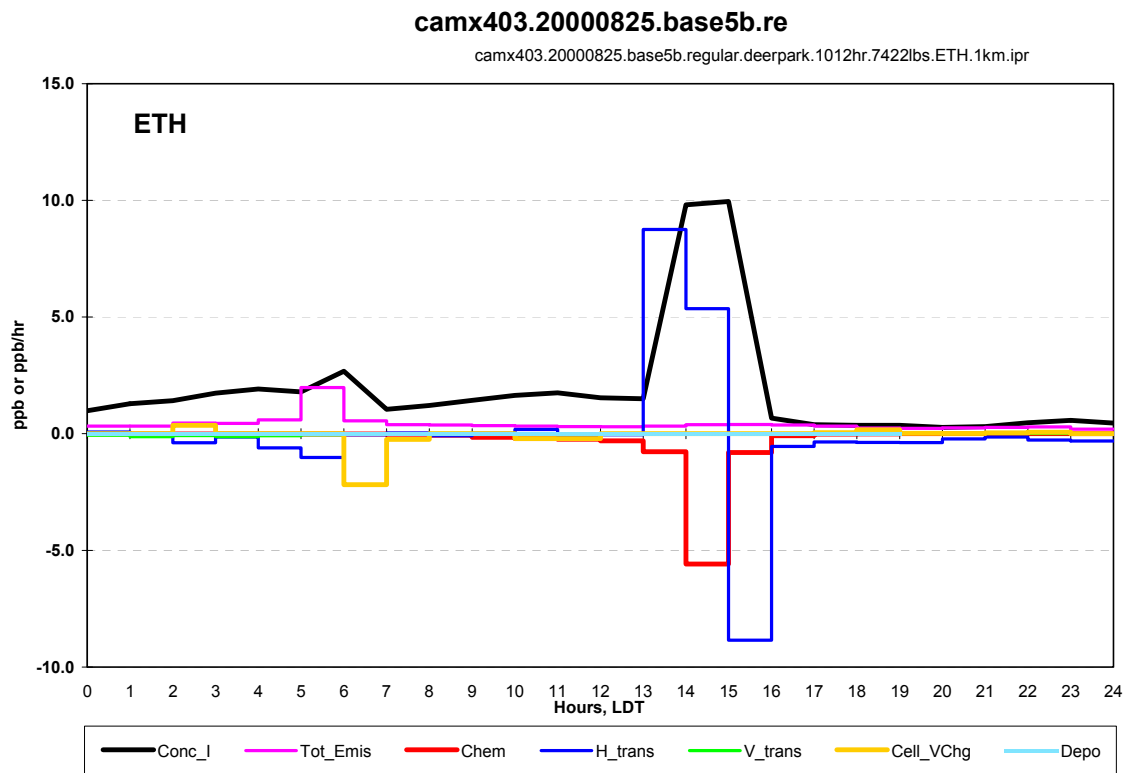
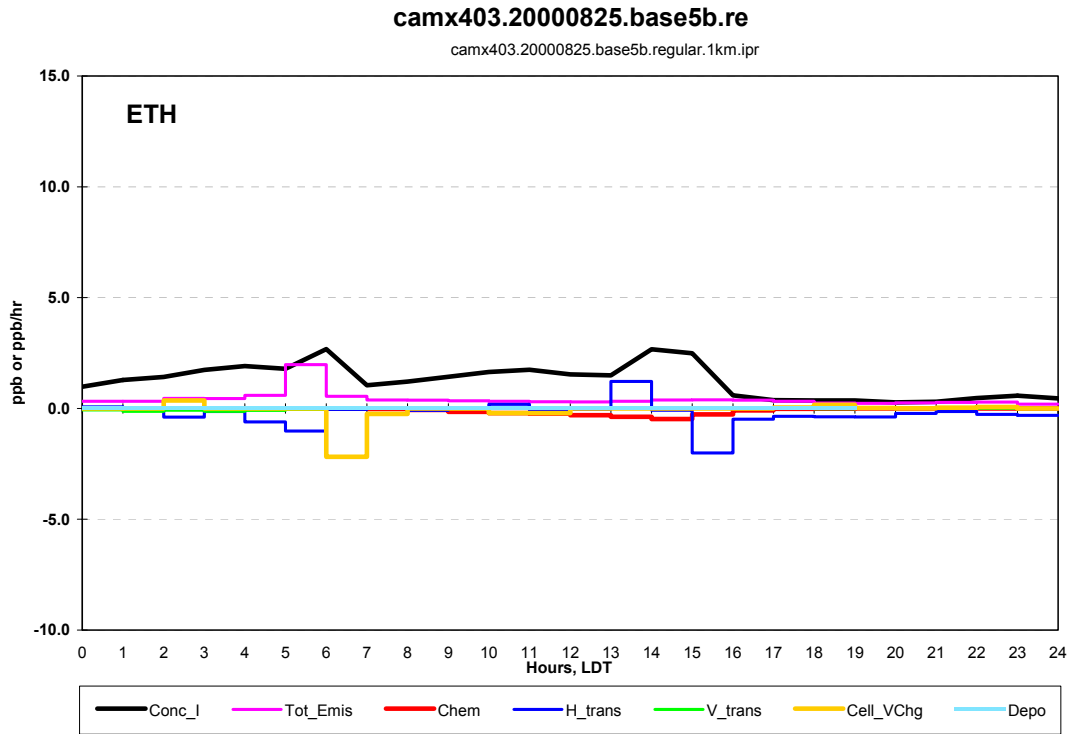


camx403.20000825.base5b.re

camx403.20000825.base5b.regular.deerpark.1012hr.7422lbs.ETH.1km.ipr

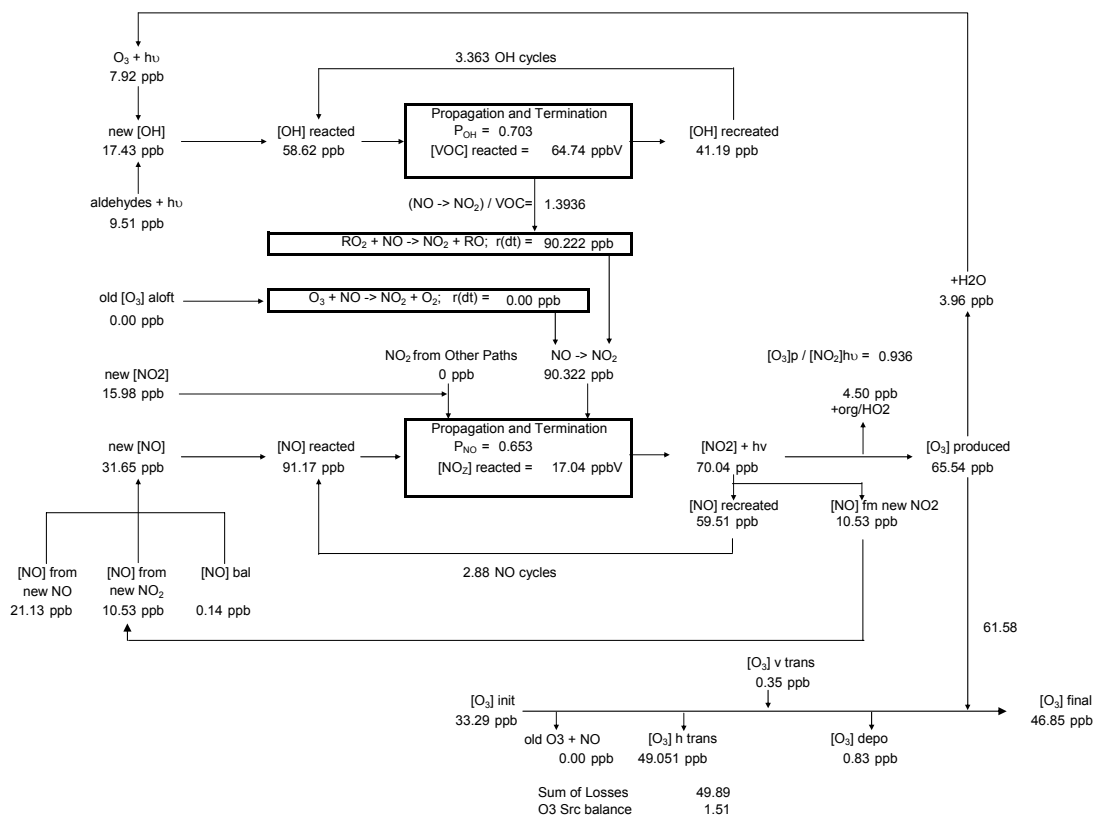


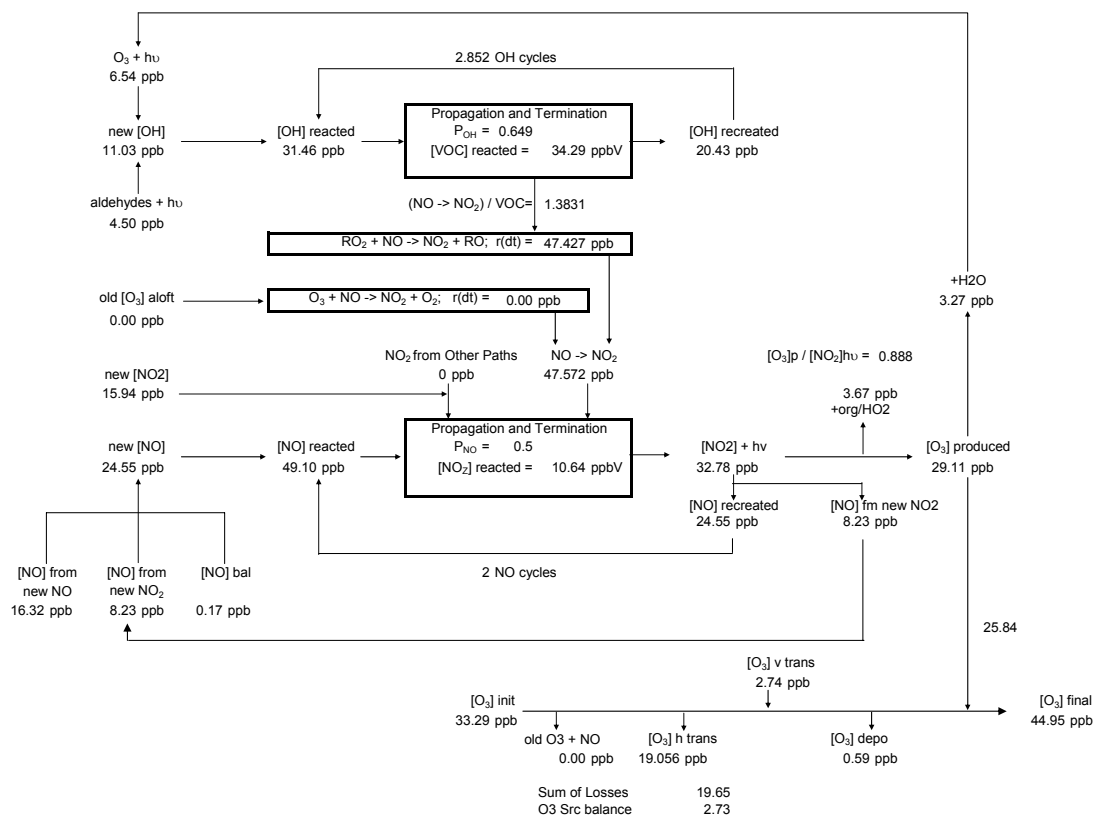
Peak Control Volume

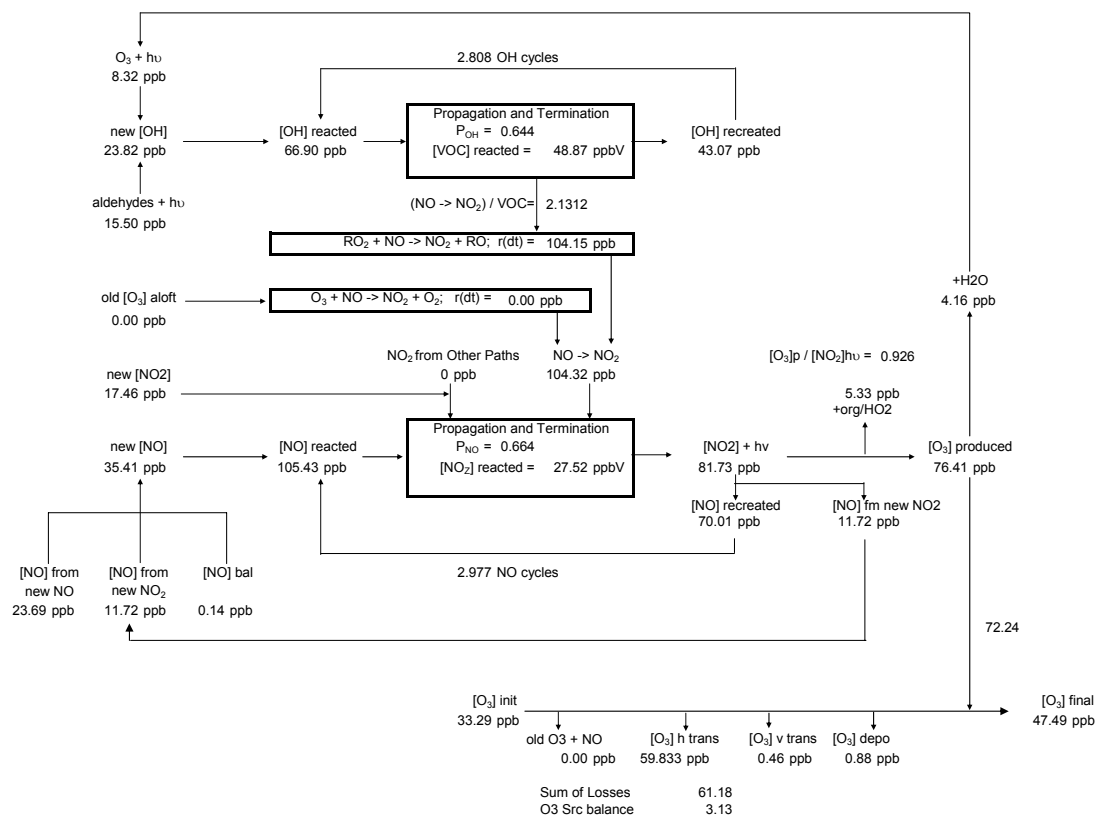


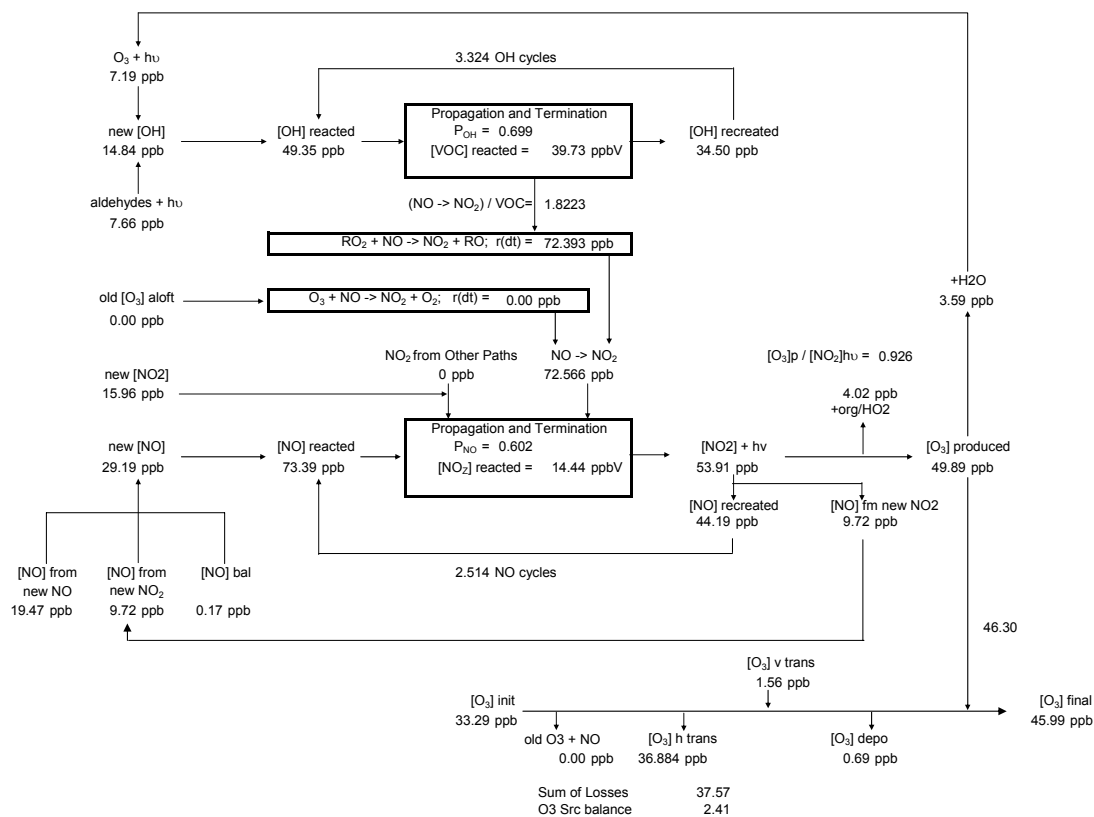
camx403.20000825.base5b.regular.1km.ipr
camx403.20000825.base5b.regular.1km.irr





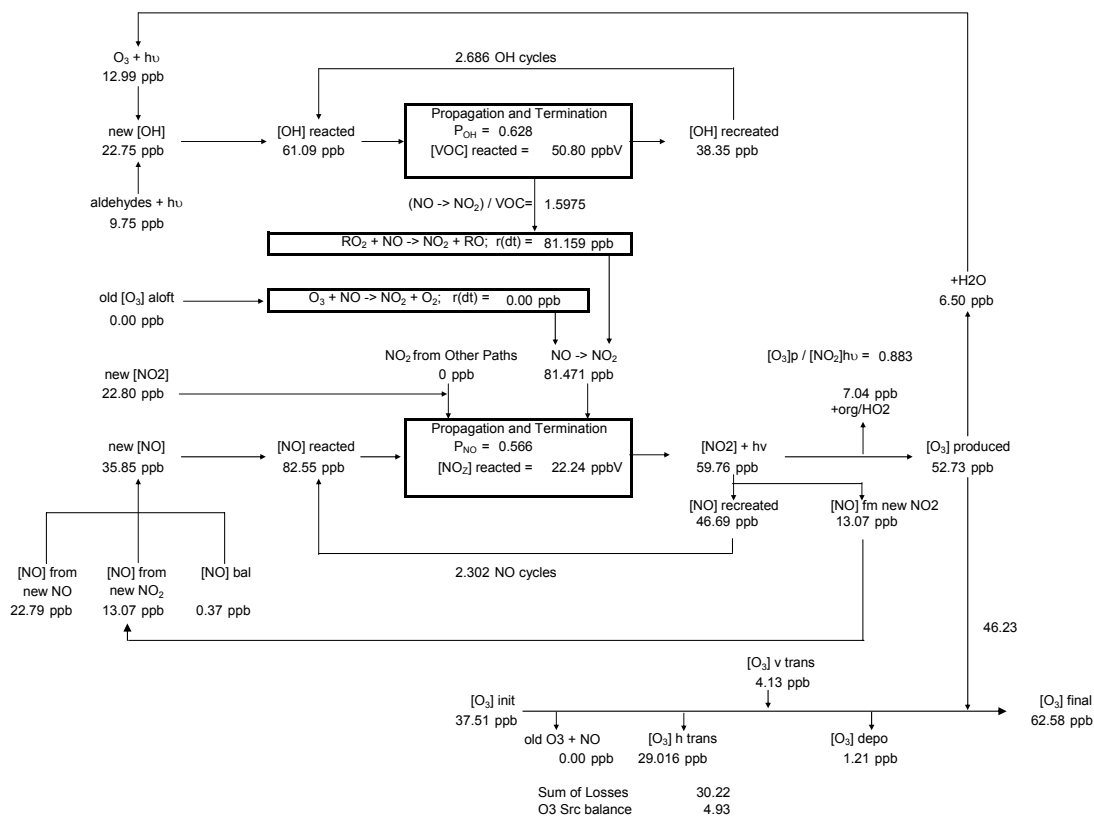




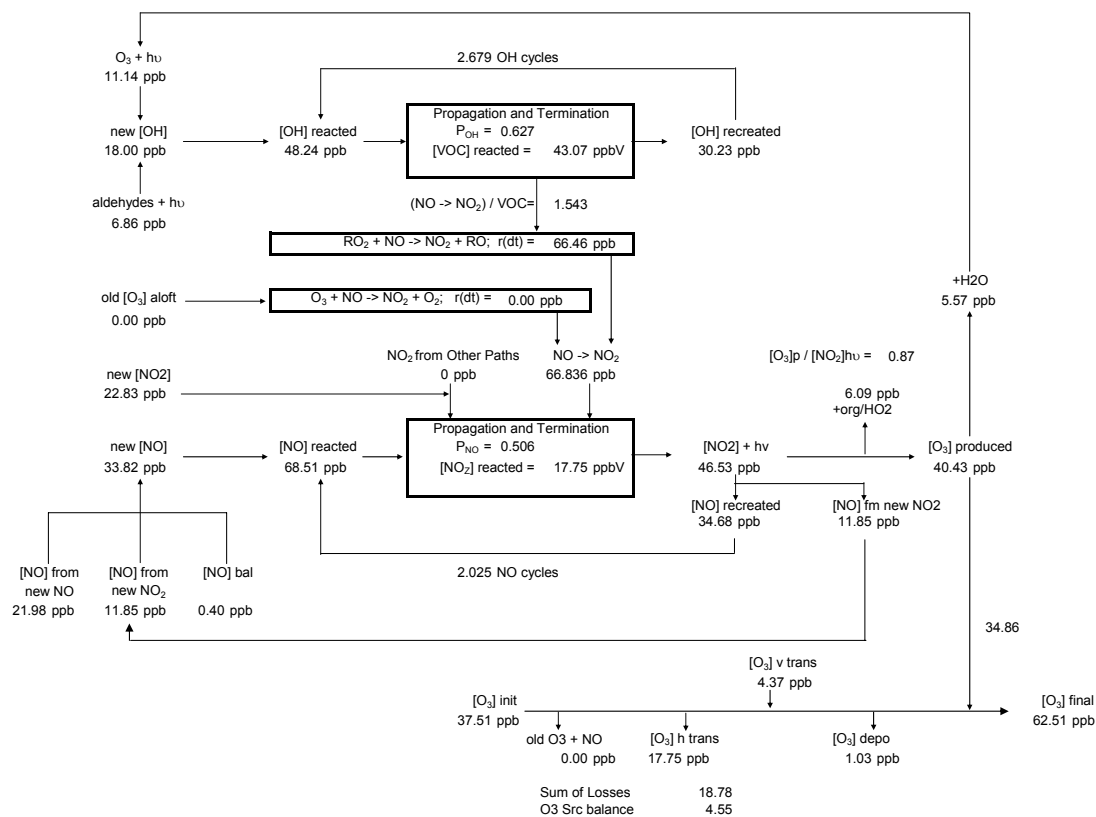


camx403.20000825.base5b.regular.1km.ipr
camx403.20000825.base5b.regular.1km.irr

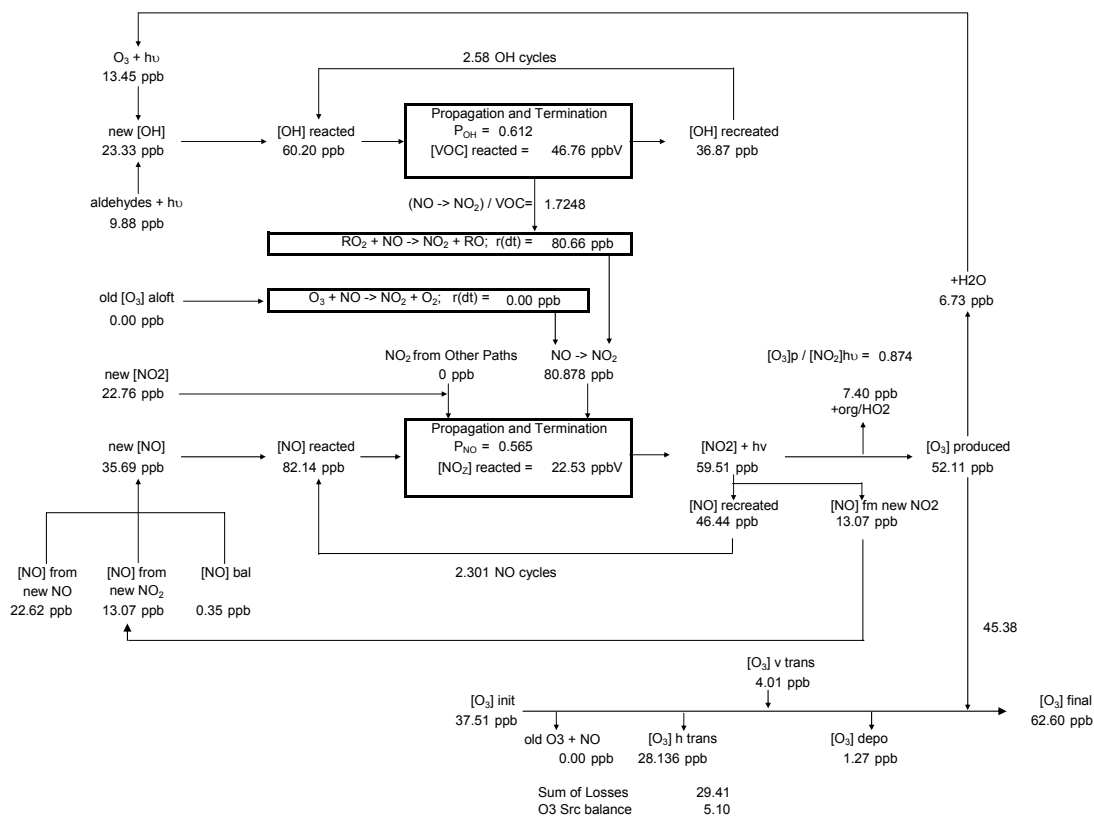


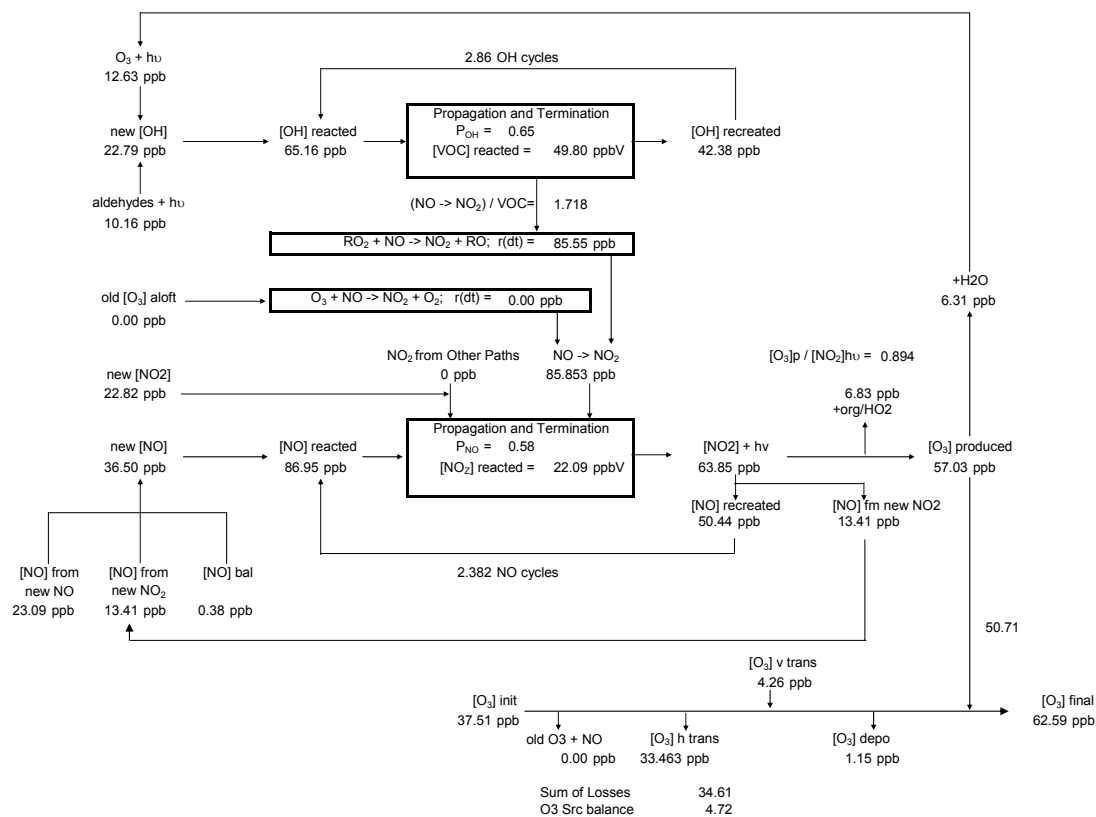


camx403.20000825.base5b.regular.deerpark.1012hr.44004lbs.PAR.1km.ipr
camx403.20000825.base5b.regular.deerpark.1012hr.44004lbs.PA **Radical Cycle/ NO Cycle/ Ozone**



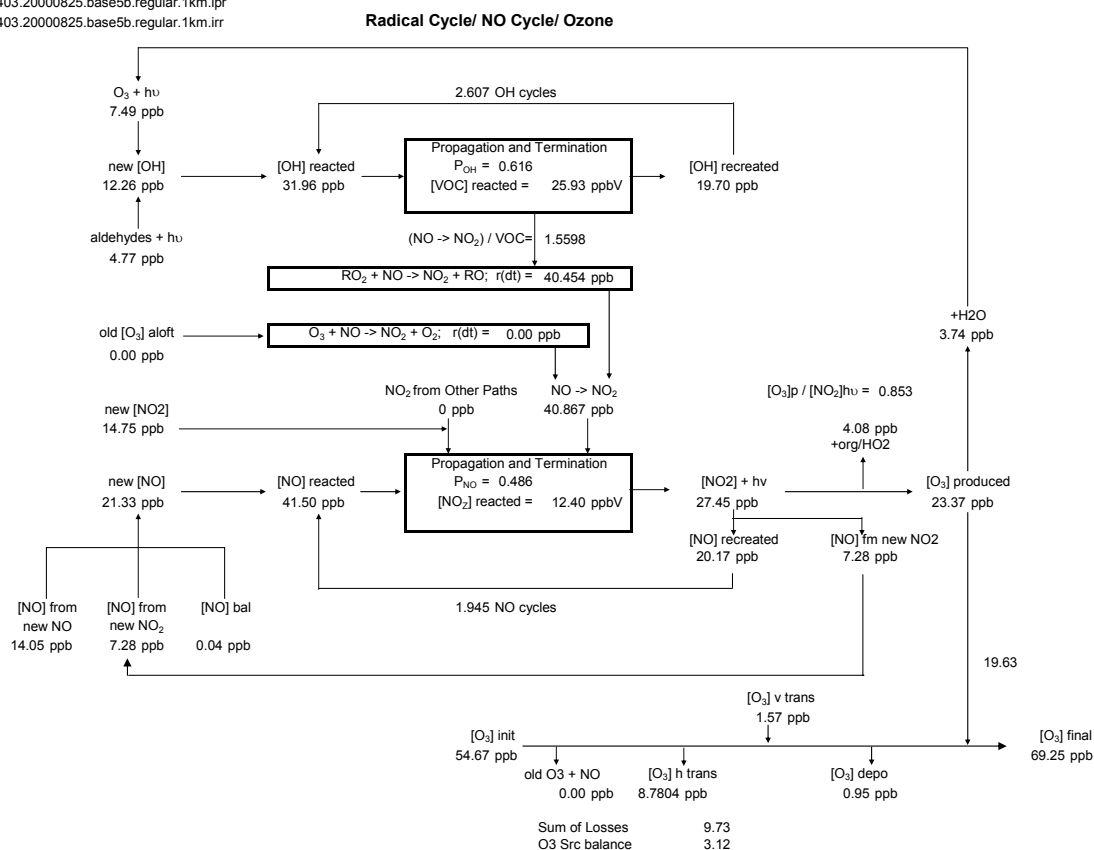
camx403.20000825.base5b.regular.deerpark.1012hr.9045lbs.XYL.1km.ipr
camx403.20000825.base5b.regular.deerpark.1012hr.9045lbs.XYL **Radical Cycle/ NO Cycle/ Ozone**

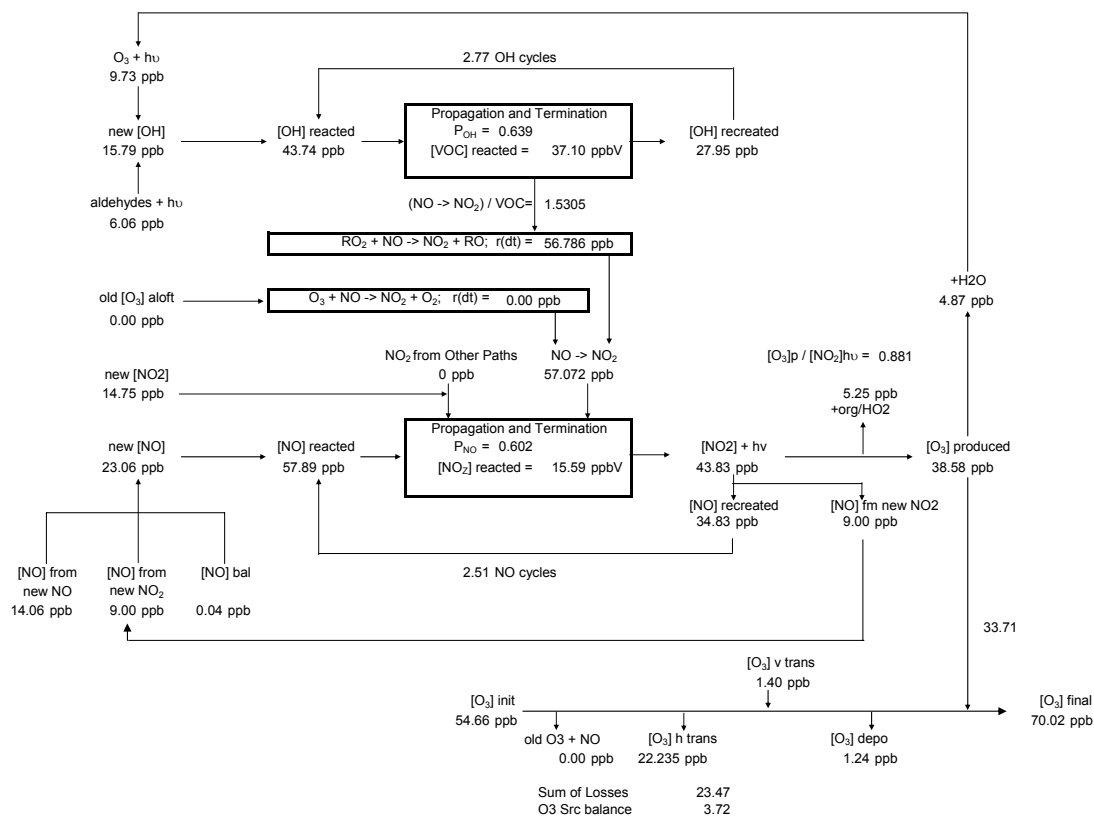


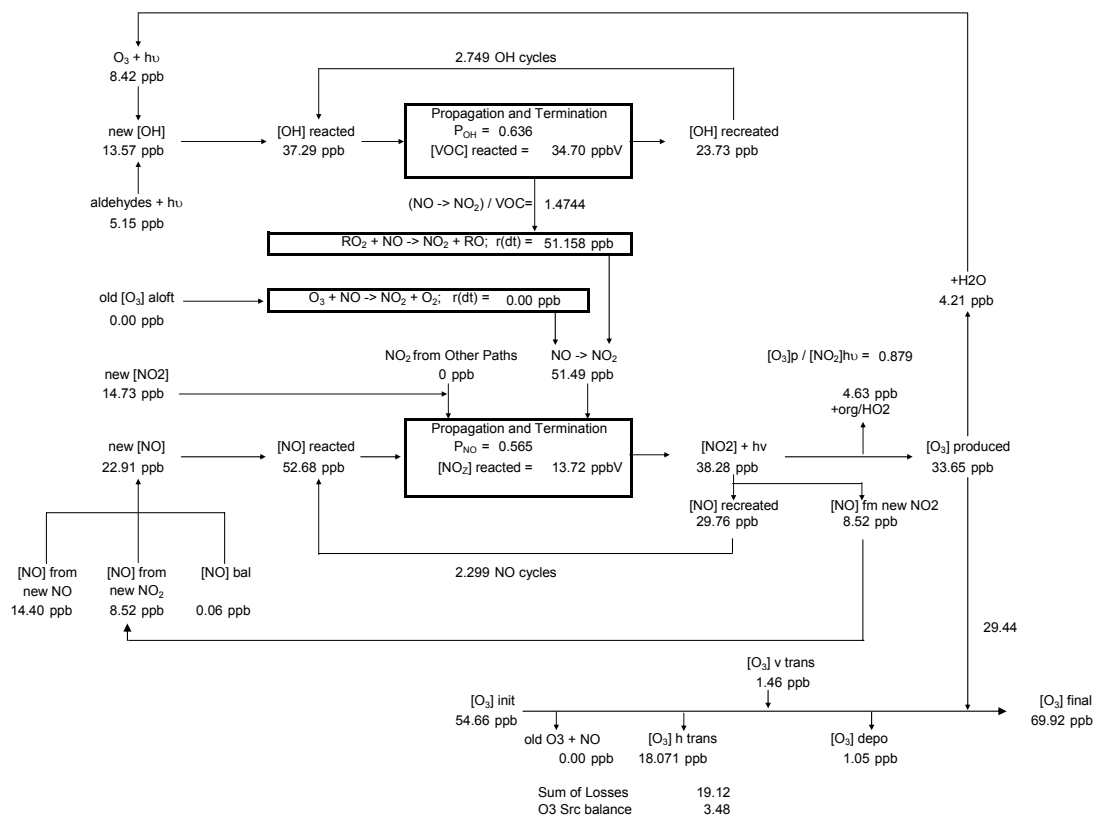


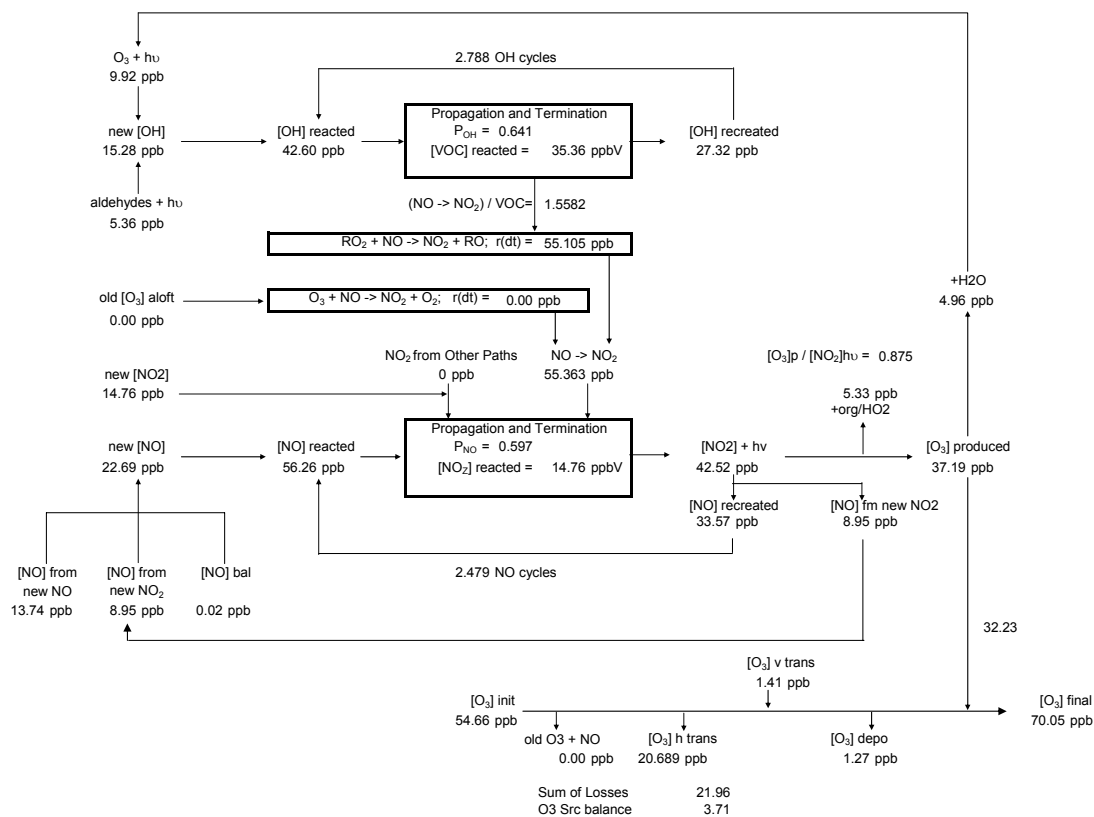
Peak Control Volume

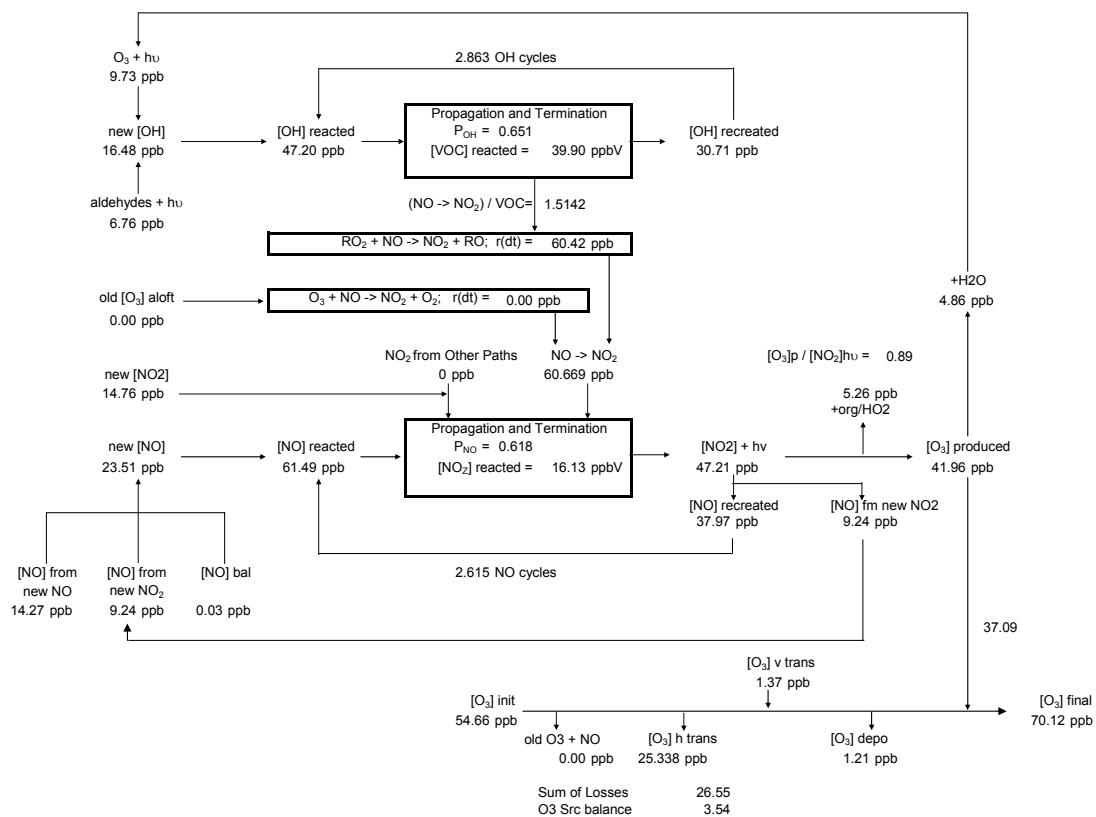
camx403.20000825.base5b.regular.1km.ipr
camx403.20000825.base5b.regular.1km.irr











APPENDIX B – PROCESS ANALYSIS POST PROCESSING TOOL OUTPUT FOR AUGUST 30, 2000

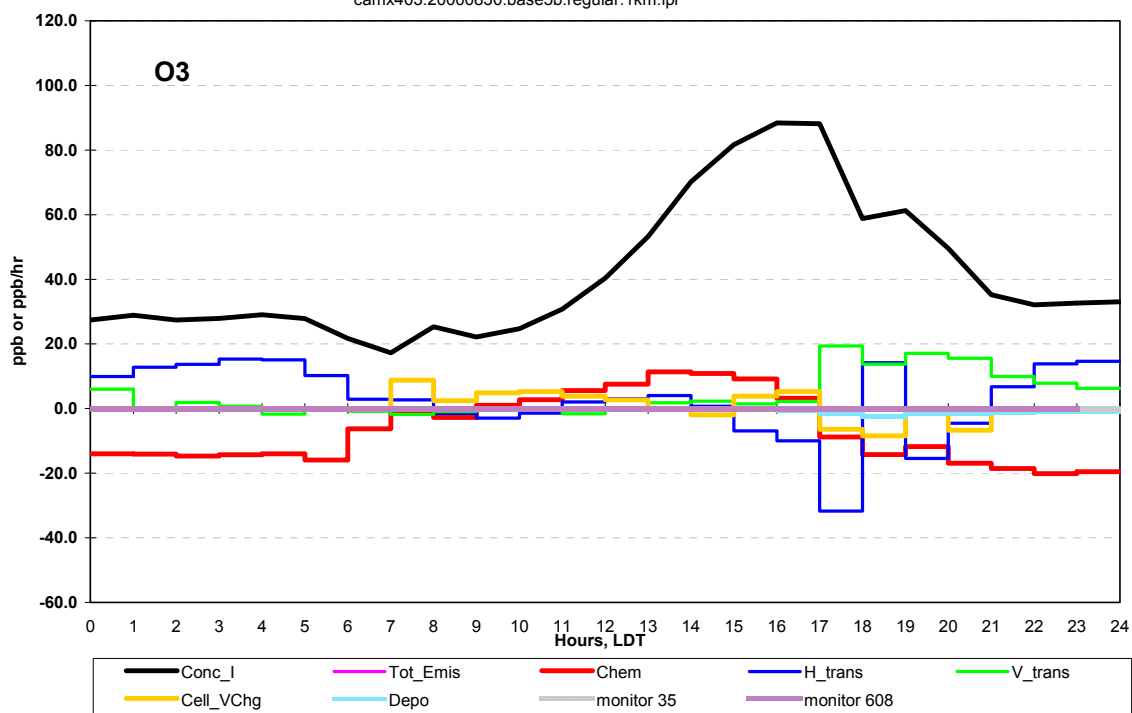
B.1 Introduction

The following plots are the time series and cycle diagrams produced by the Process Analysis Post Processing Tool for the August 30, 2000 simulation day. Data for the source and peak control volumes for the base case and the emission event scenarios are presented. Details of the simulation scenarios and control volumes are described in Chapter 3. Time series plots were included for the following CBIV species: O₃, OLE, PAR, XYL, and ETH.

Source Control Volume

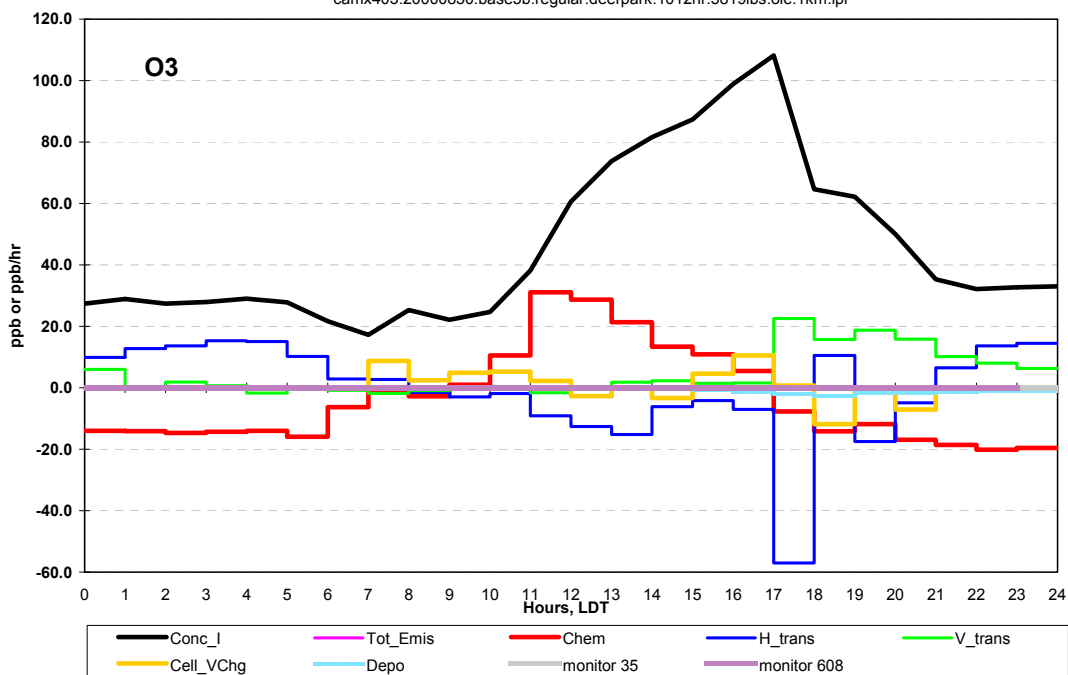
camx403.20000830.base5b.regul

camx403.20000830.base5b.regular.1km.ipr



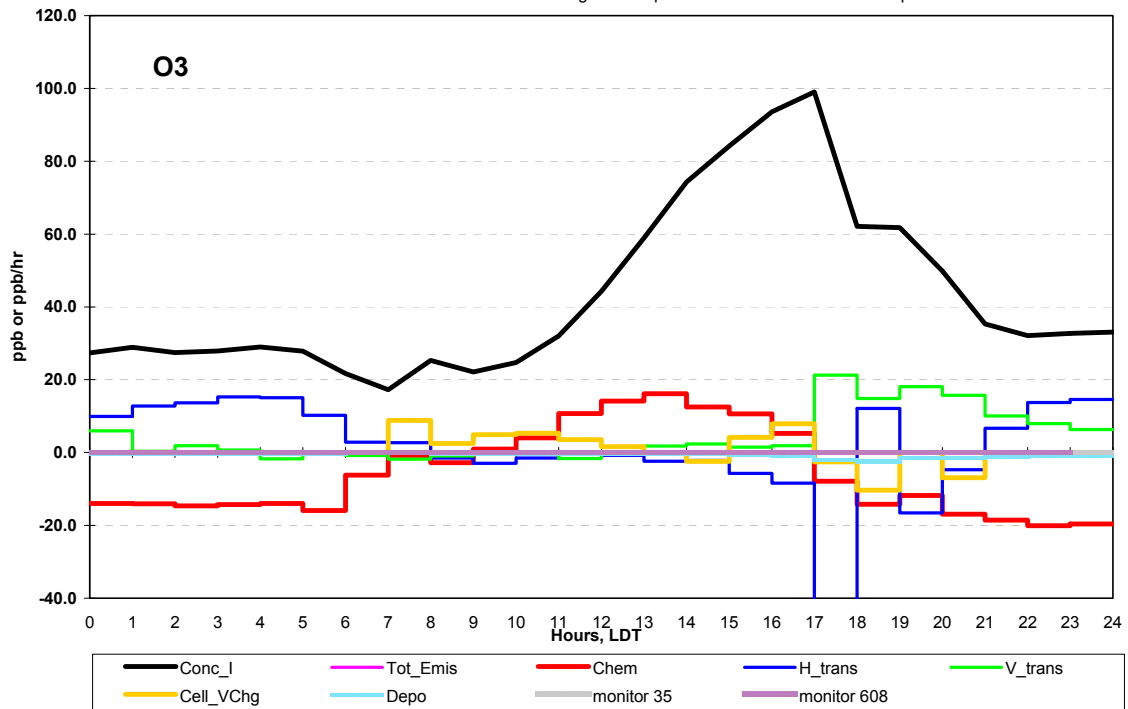
camx403.20000830.base5b.regul

camx403.20000830.base5b.regular.deerpark.1012hr.5819lbs.ole.1km.ipr



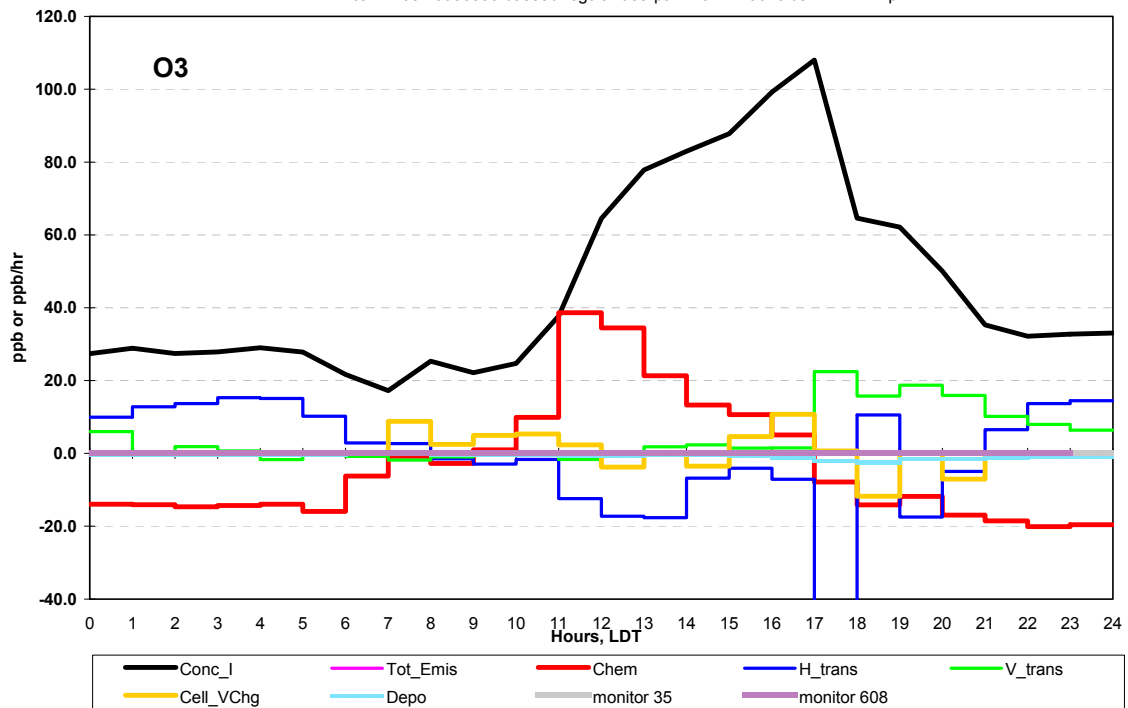
camx403.20000830.base5b.regul

camx403.20000830.base5b.regular.deerpark.1012hr.44004lbs.PAR.1km.ipr



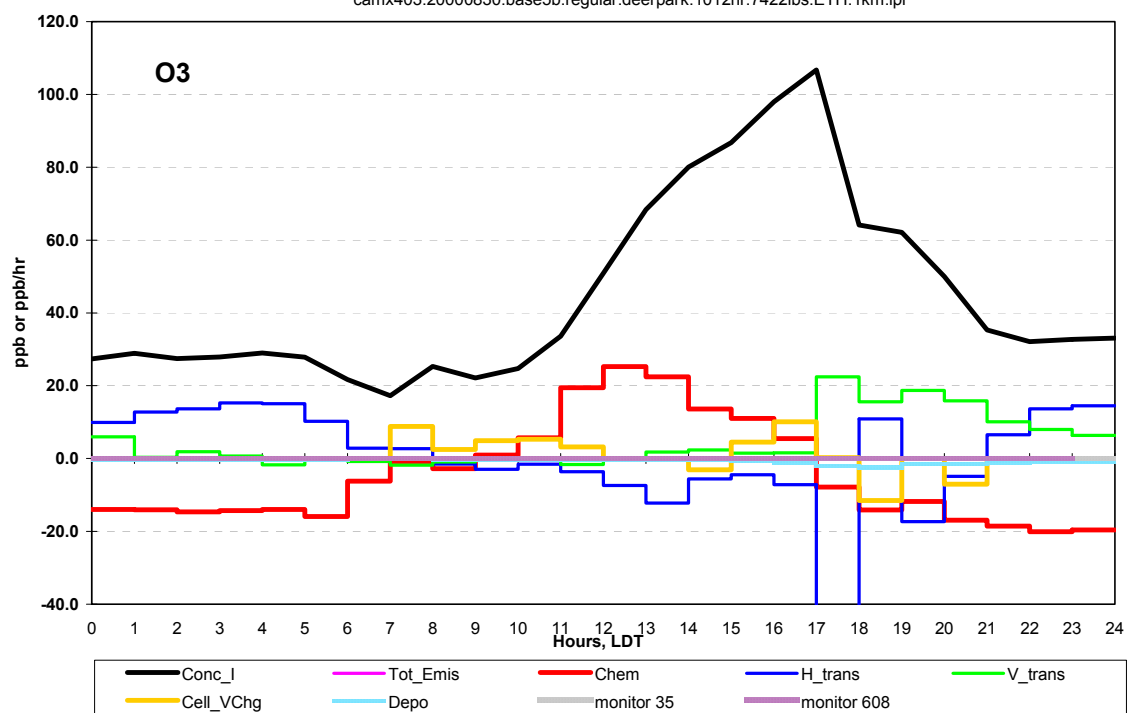
camx403.20000830.base5b.regul

camx403.20000830.base5b.regular.deerpark.1012hr.9045lbs.XYL.1km.ipr

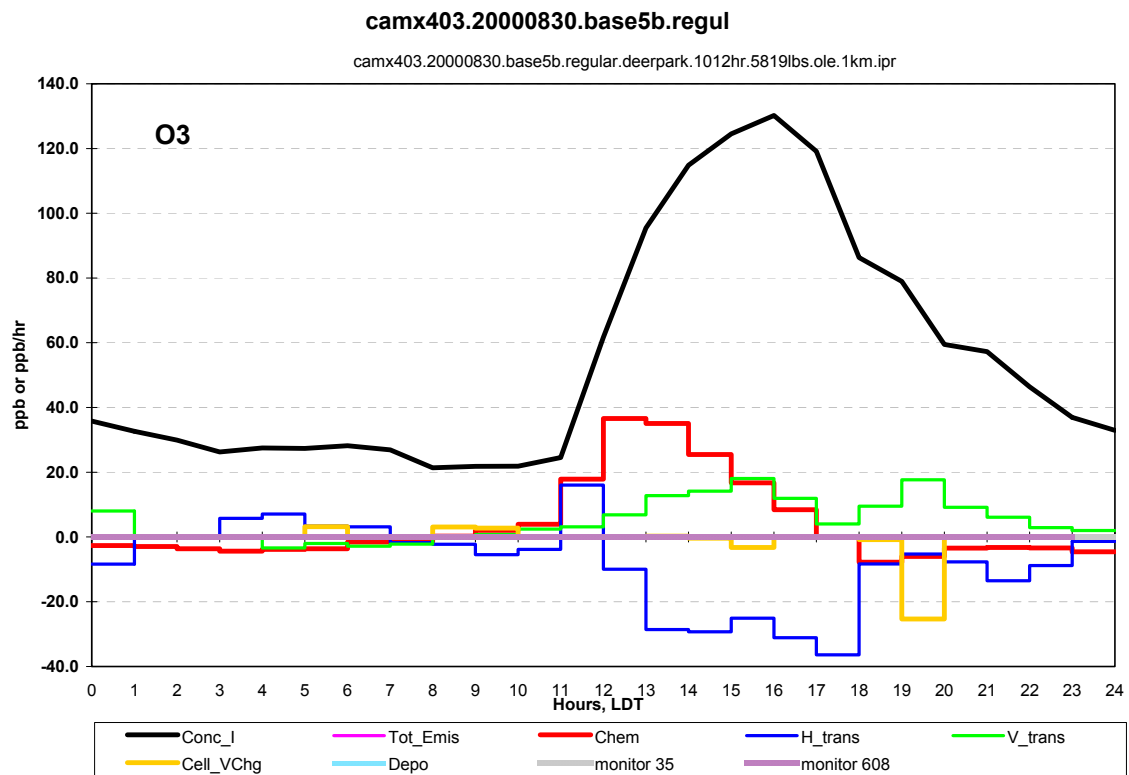
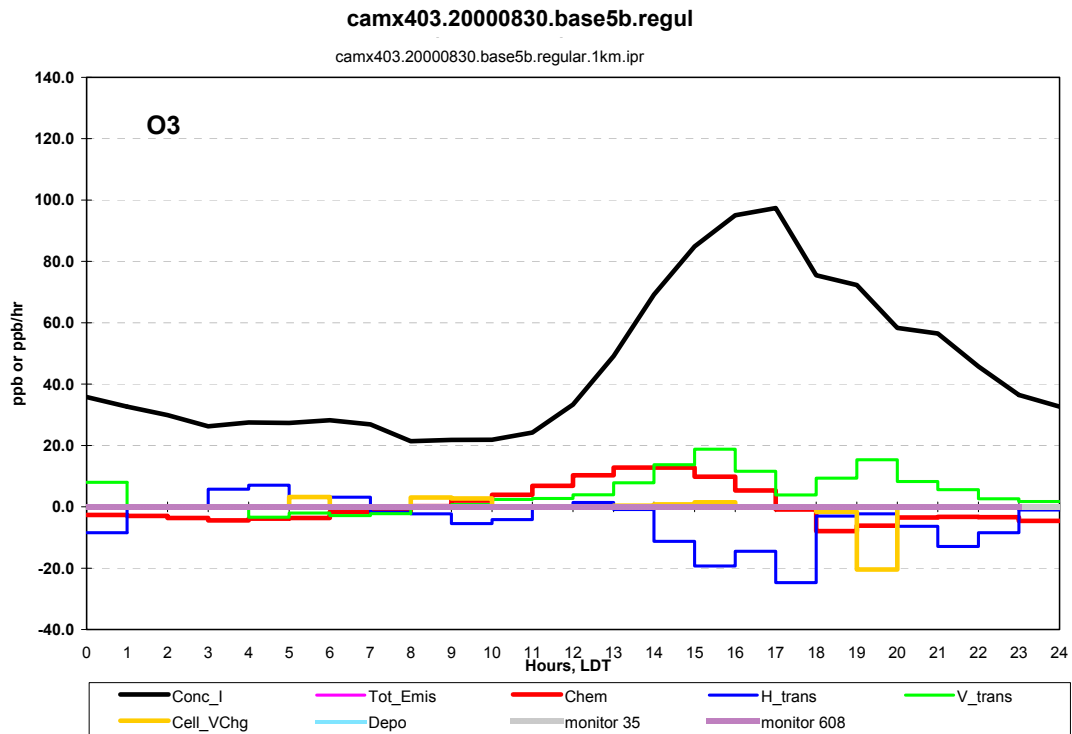


camx403.20000830.base5b.regul

camx403.20000830.base5b.regular.deerpark.1012hr.7422lbs.ETH.1km.ipr

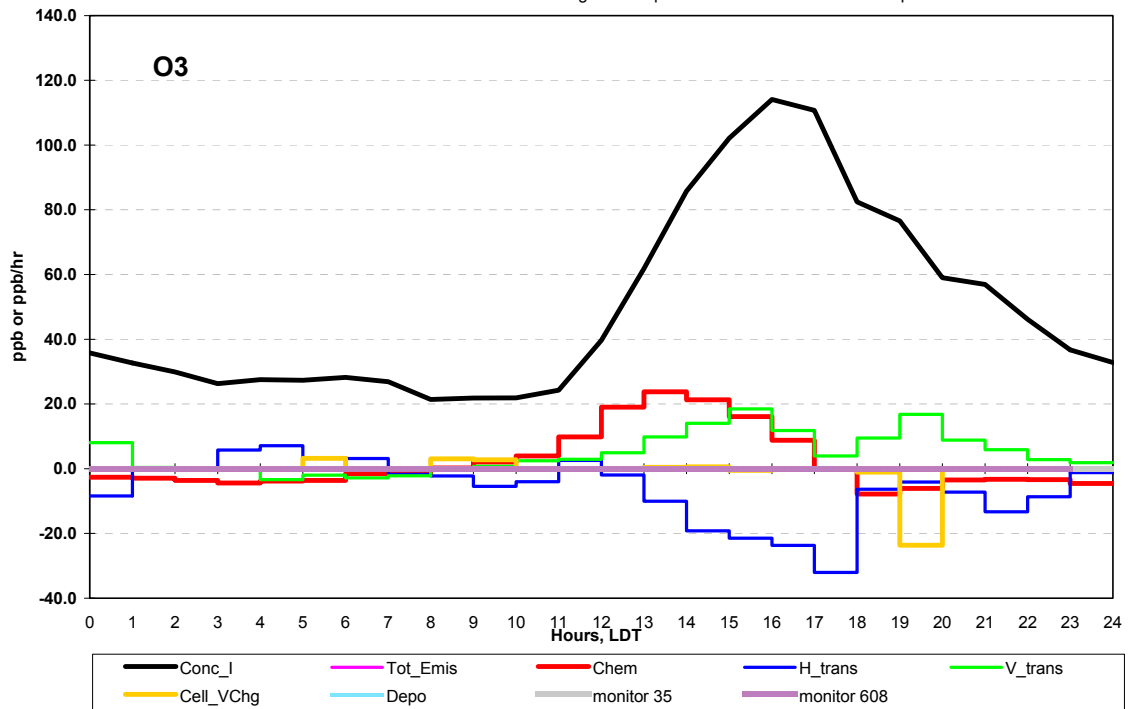


Peak Control Volume



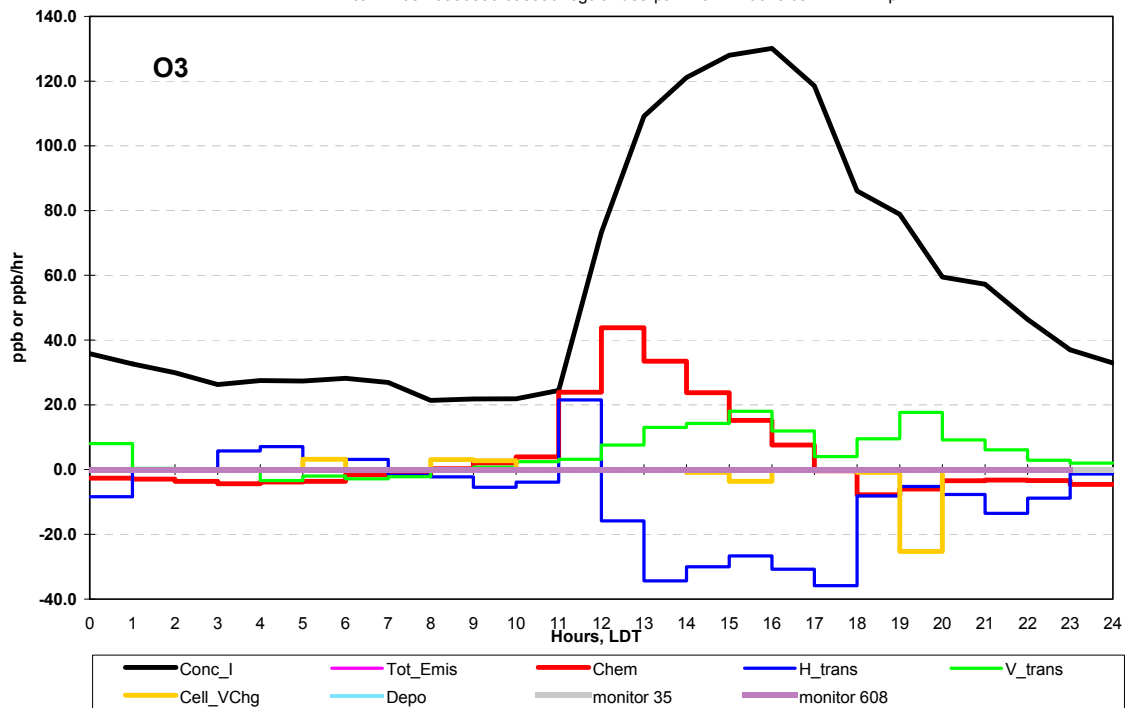
camx403.20000830.base5b.regul

camx403.20000830.base5b.regular.deerpark.1012hr.44004lbs.PAR.1km.ipr



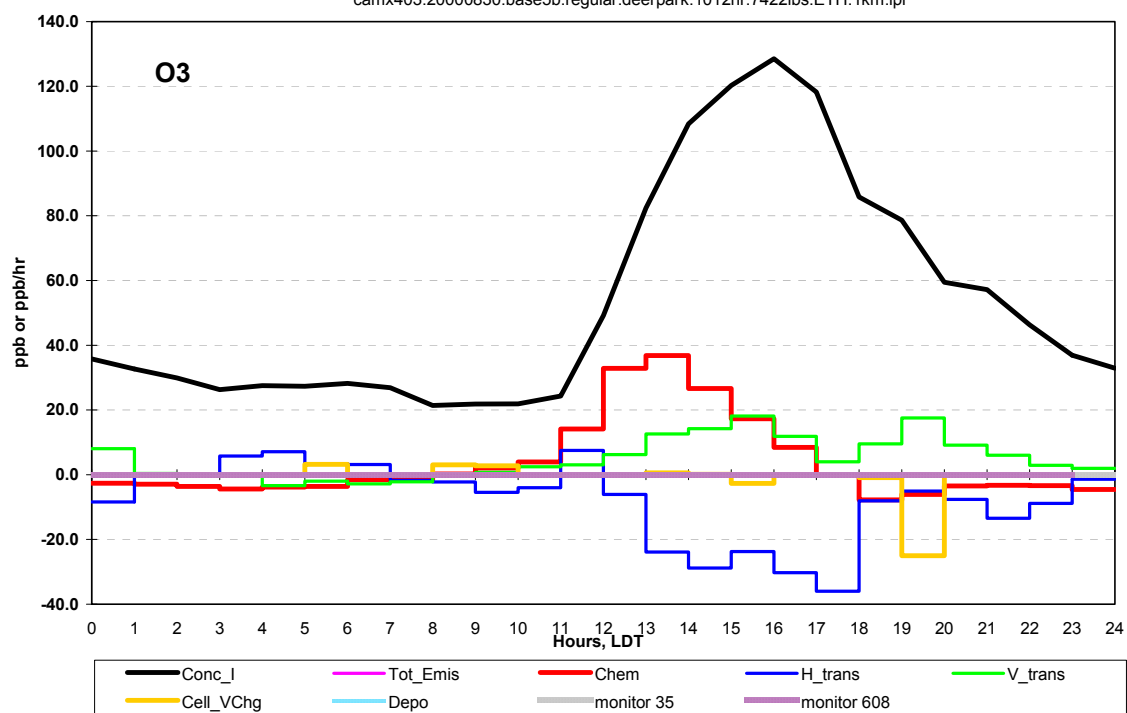
camx403.20000830.base5b.regul

camx403.20000830.base5b.regular.deerpark.1012hr.9045lbs.XYL.1km.ipr



camx403.20000830.base5b.regul

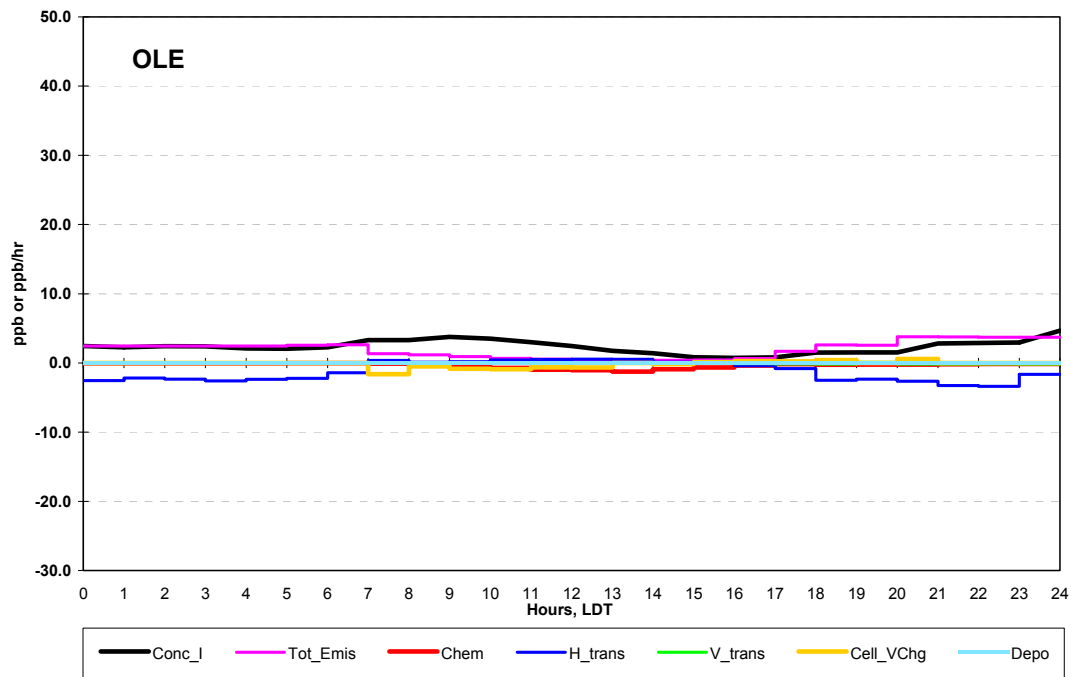
camx403.20000830.base5b.regular.deerpark.1012hr.7422lbs.ETH.1km.ipr



Source Control Volume

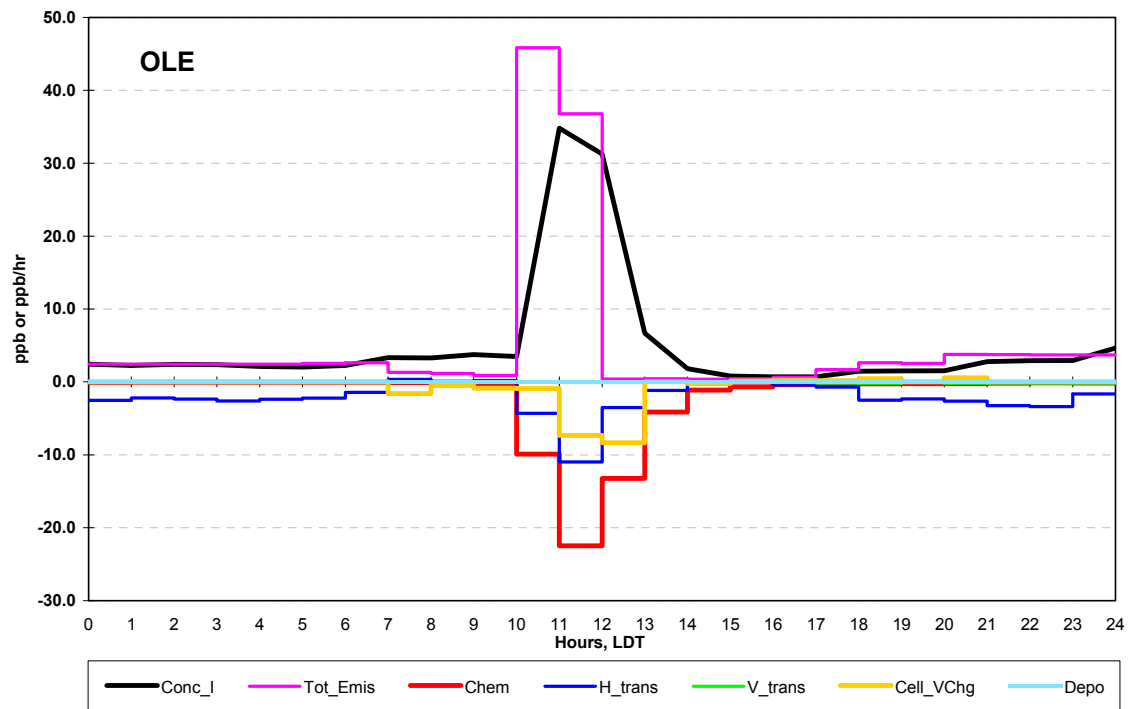
camx403.20000830.base5b.regul

camx403.20000830.base5b.regular.1km.ipr

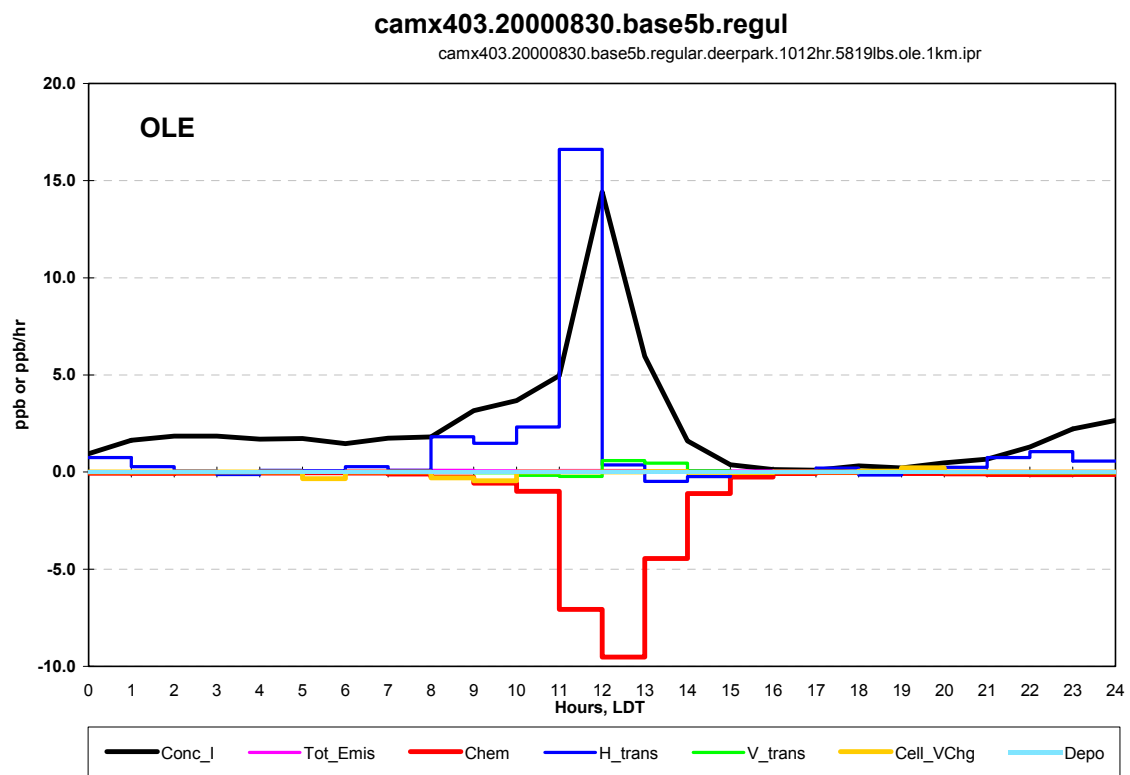
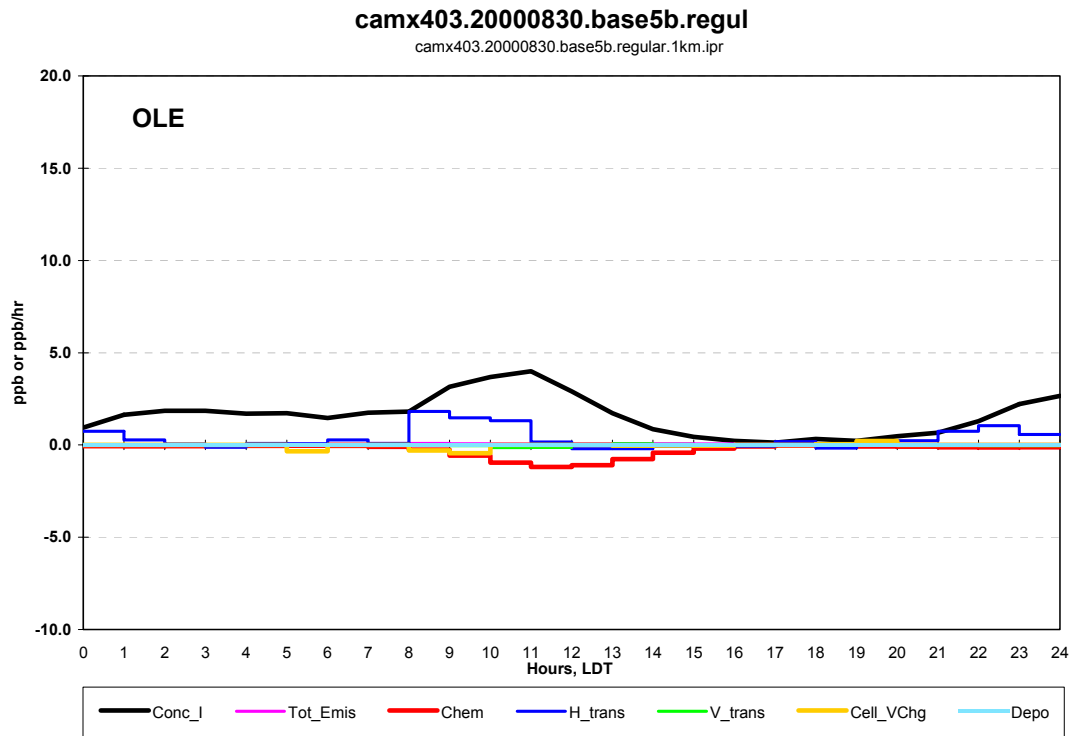


camx403.20000830.base5b.regul

camx403.20000830.base5b.regular.deerpark.1012hr.5819lbs.ole.1km.ipr



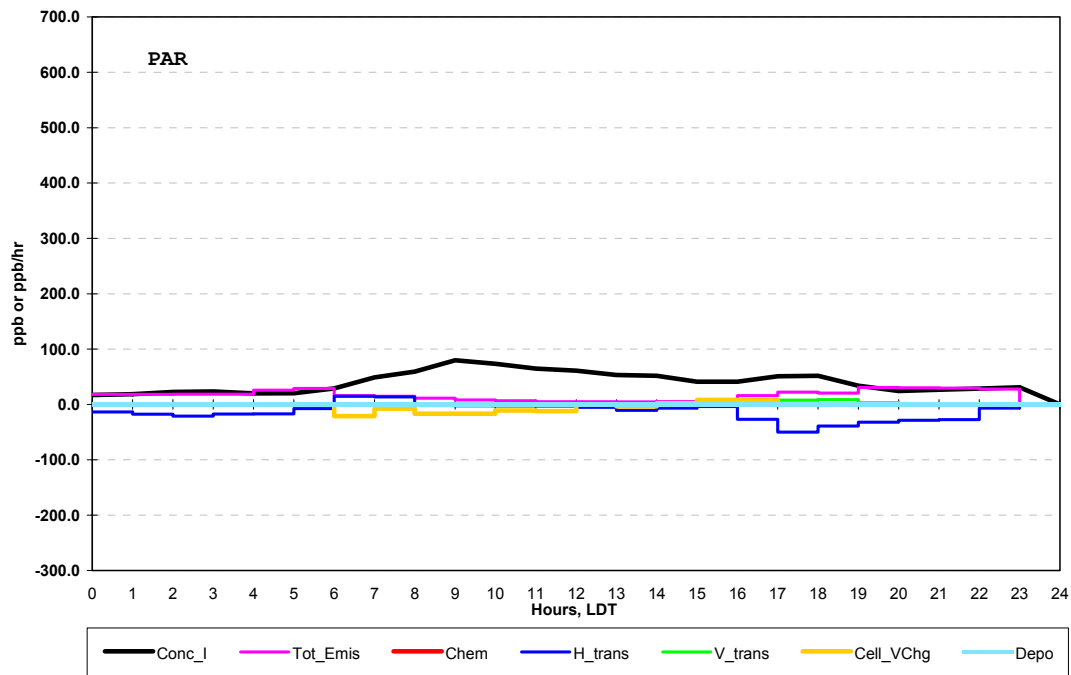
Peak Control Volume



Source Control Volume

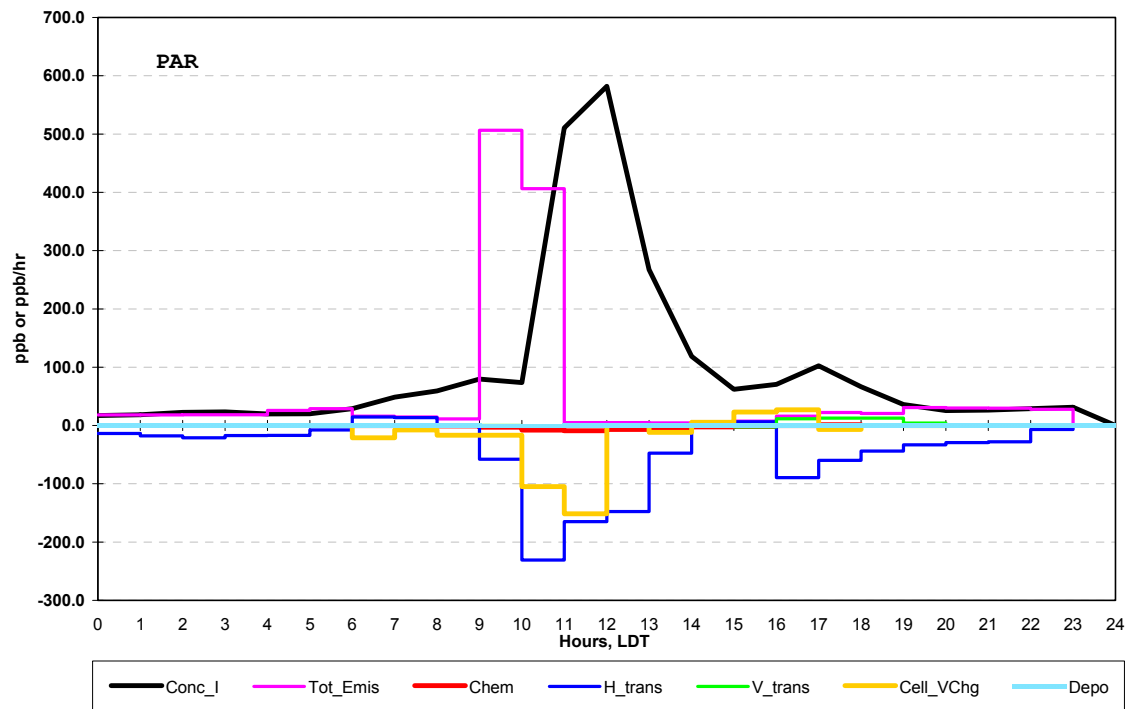
camx403.20000830.base5b.regul

camx403.20000830.base5b.regular.1km.ipr



camx403.20000830.base5b.regul

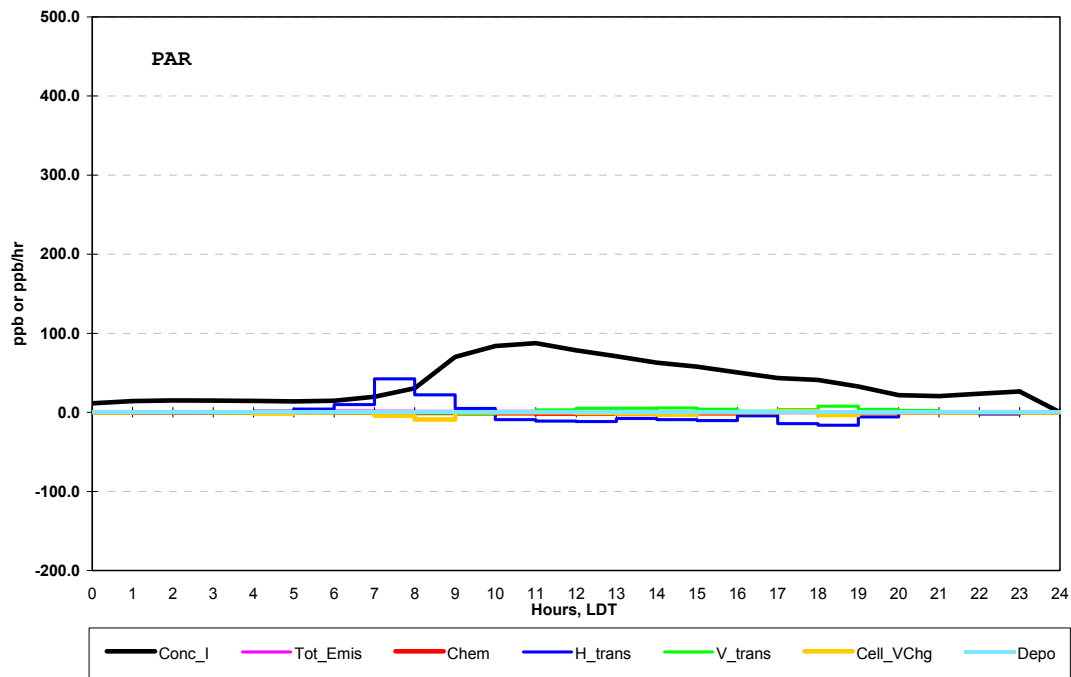
camx403.20000830.base5b.regular.deerpark.1012hr.44004lbs.PAR.1km.ipr



Peak Control Volume

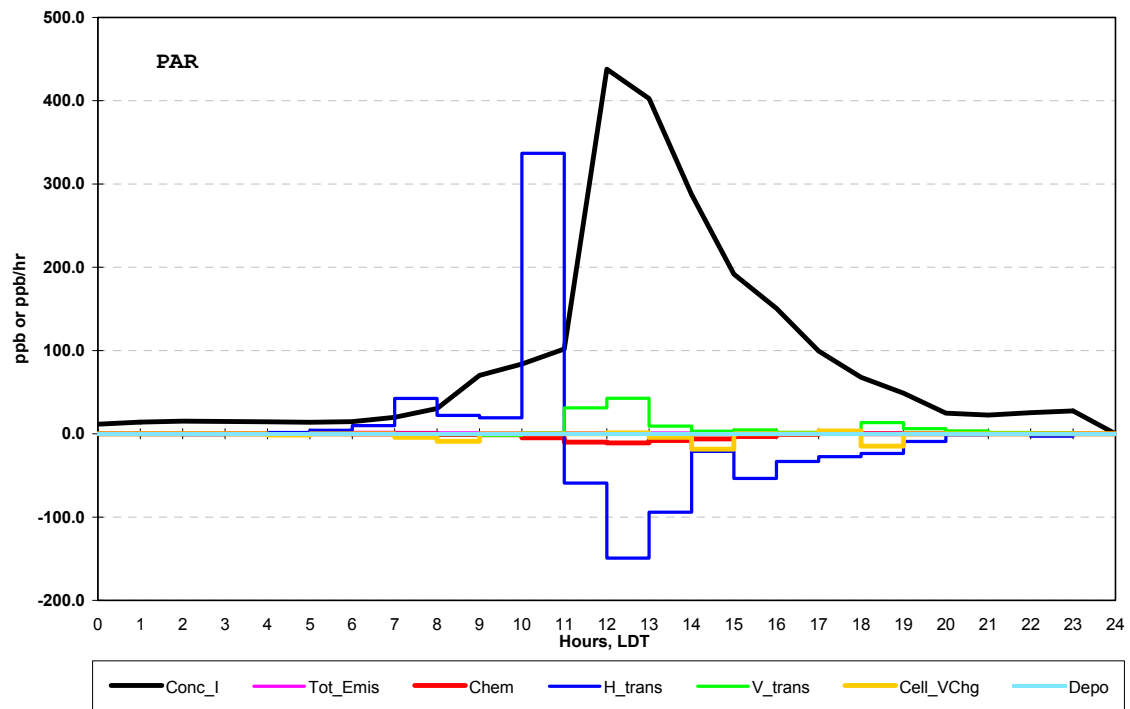
camx403.20000830.base5b.regul

camx403.20000830.base5b.regular.1km.ipr



camx403.20000830.base5b.regul

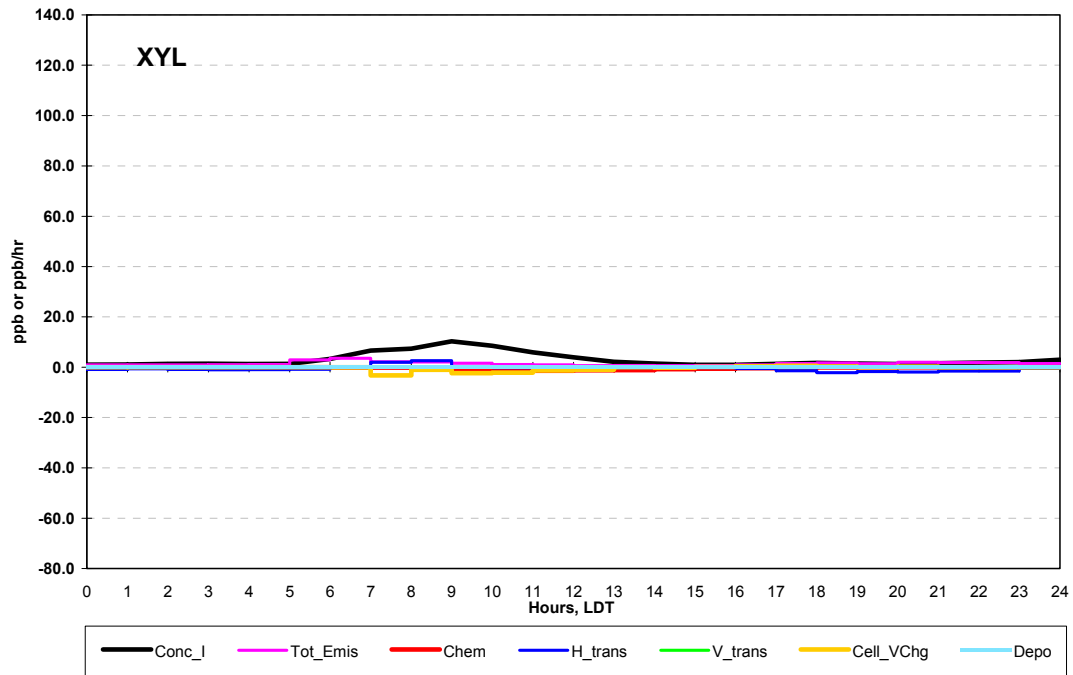
camx403.20000830.base5b.regular.deerpark.1012hr.44004lbs.PAR.1km.ipr



Source Control Volume

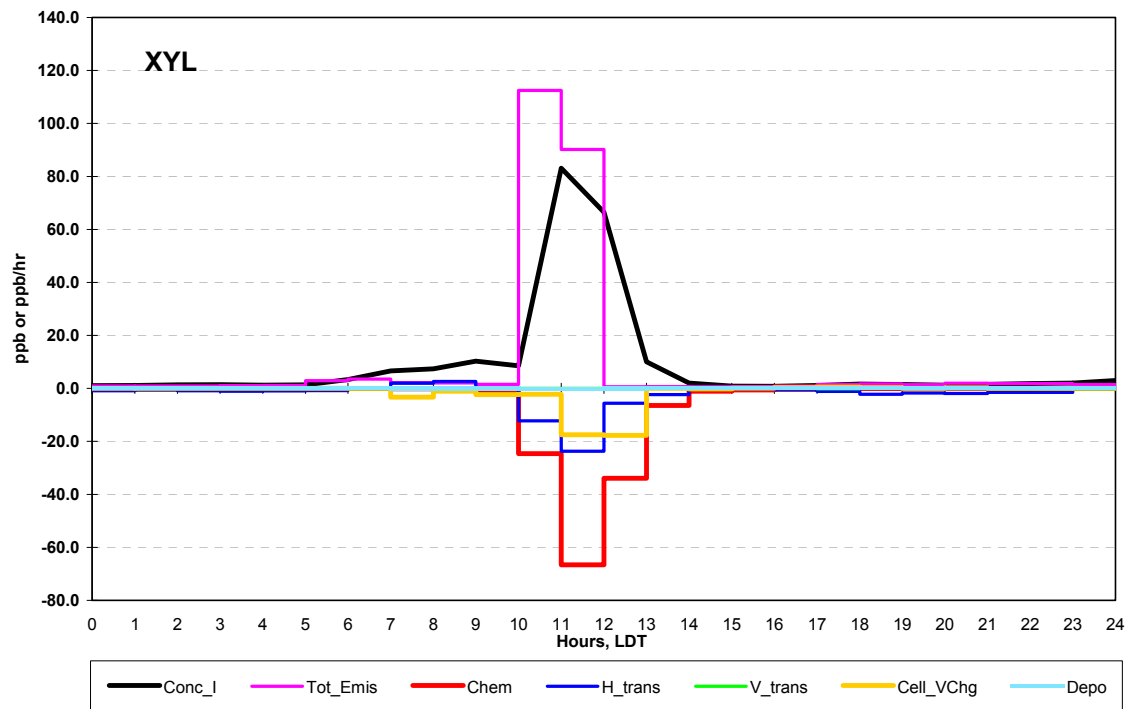
camx403.20000830.base5b.regul

camx403.20000830.base5b.regular.1km.ipr



camx403.20000830.base5b.regul

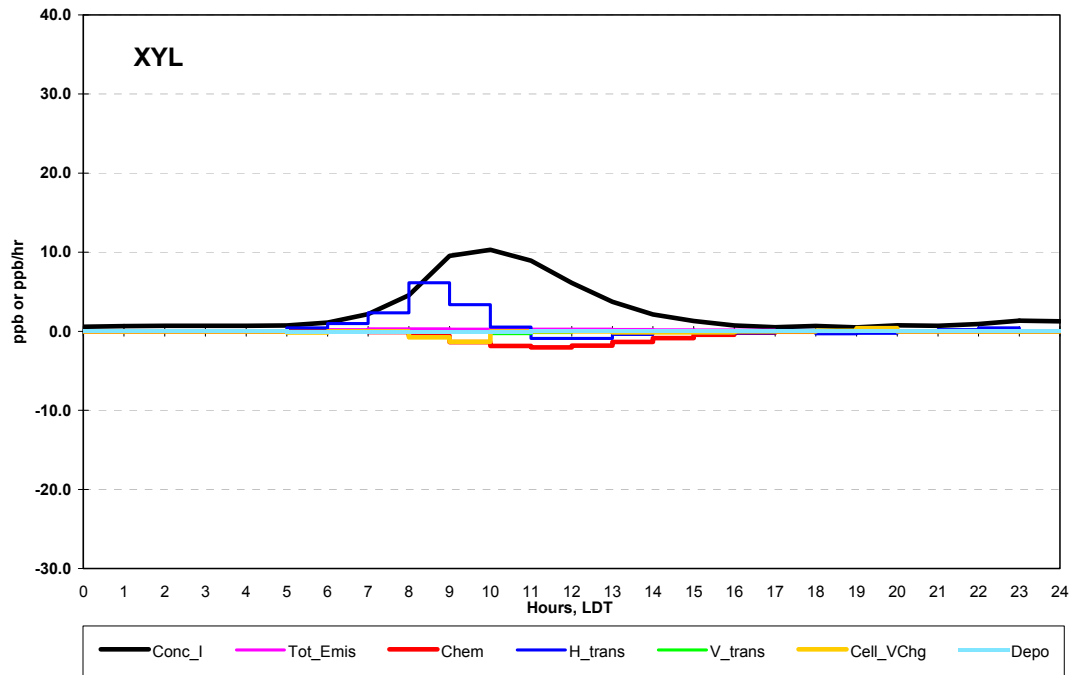
camx403.20000830.base5b.regular.deerpark.1012hr.9045lbs.XYL.1km.ipr



Peak Control Volume

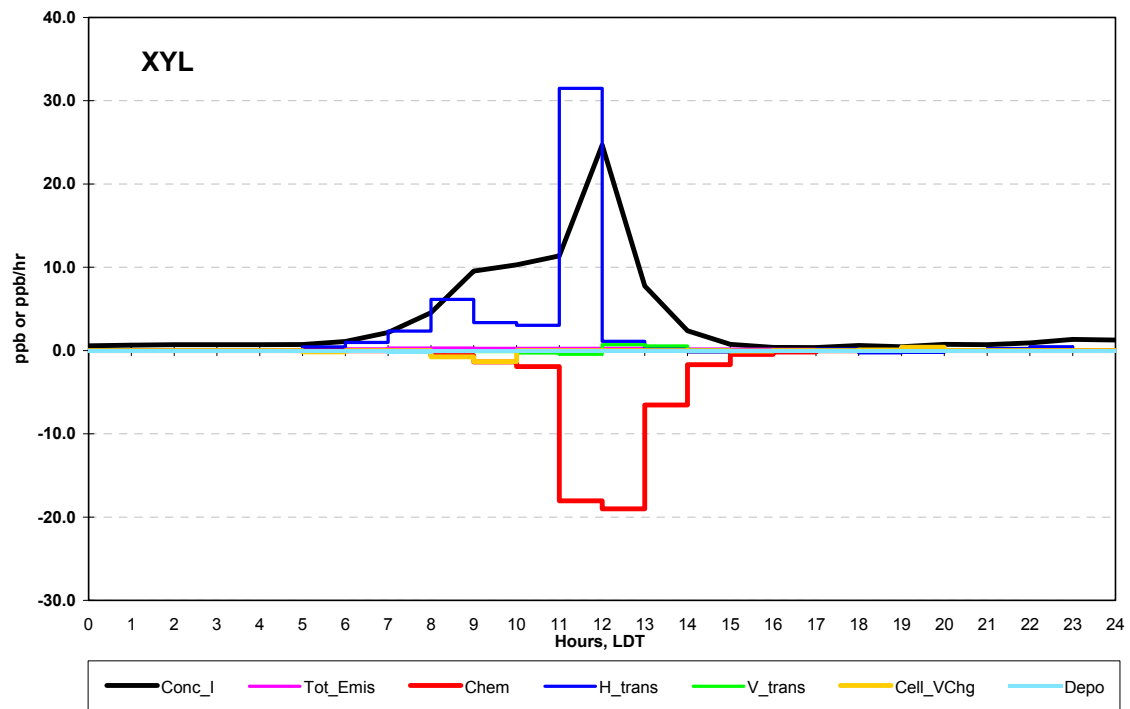
camx403.20000830.base5b.regul

camx403.20000830.base5b.regular.1km.ipr



camx403.20000830.base5b.regul

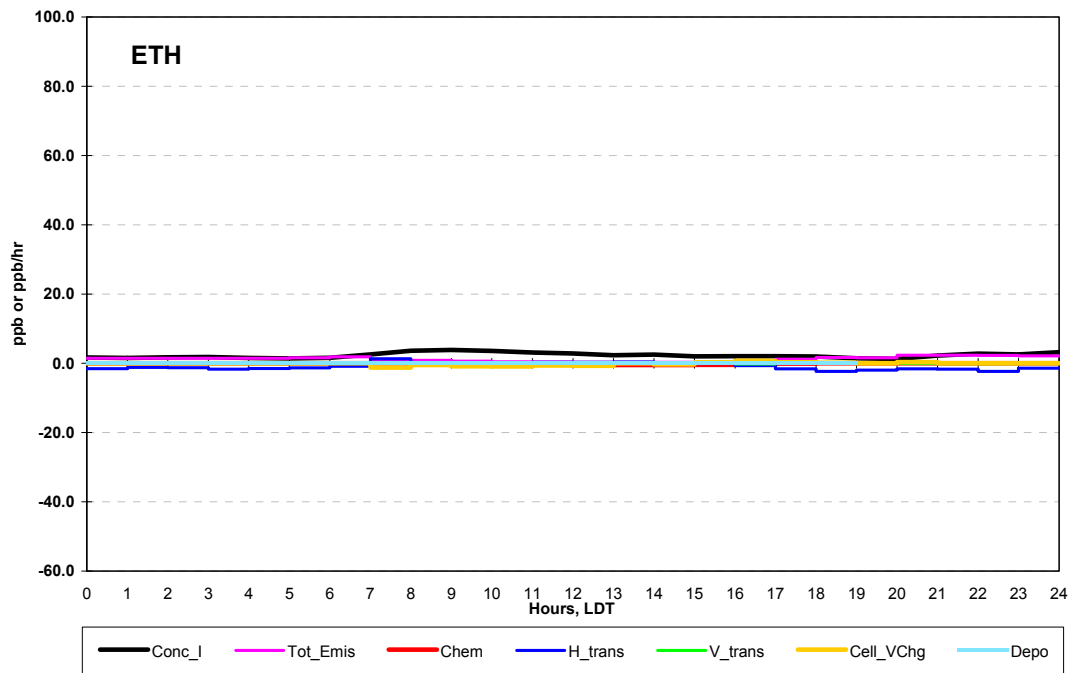
camx403.20000830.base5b.regular.deerpark.1012hr.9045lbs.XYL.1km.ipr



Source Control Volume

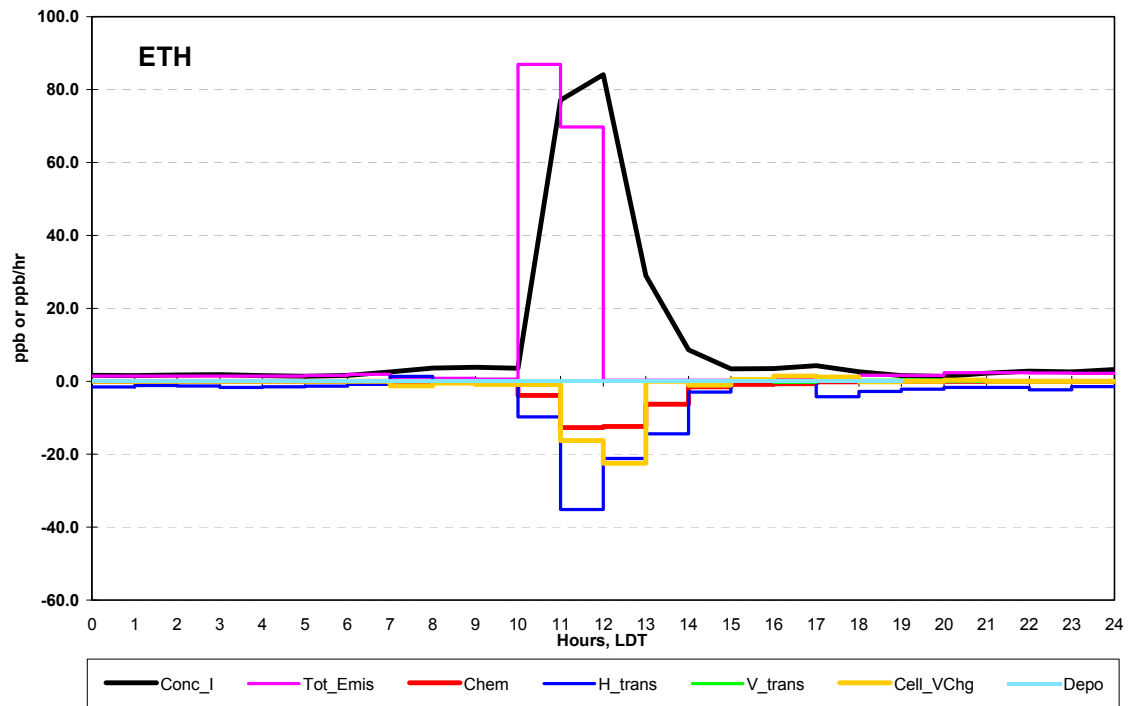
camx403.20000830.base5b.re

camx403.20000830.base5b.regular.1km.ipr

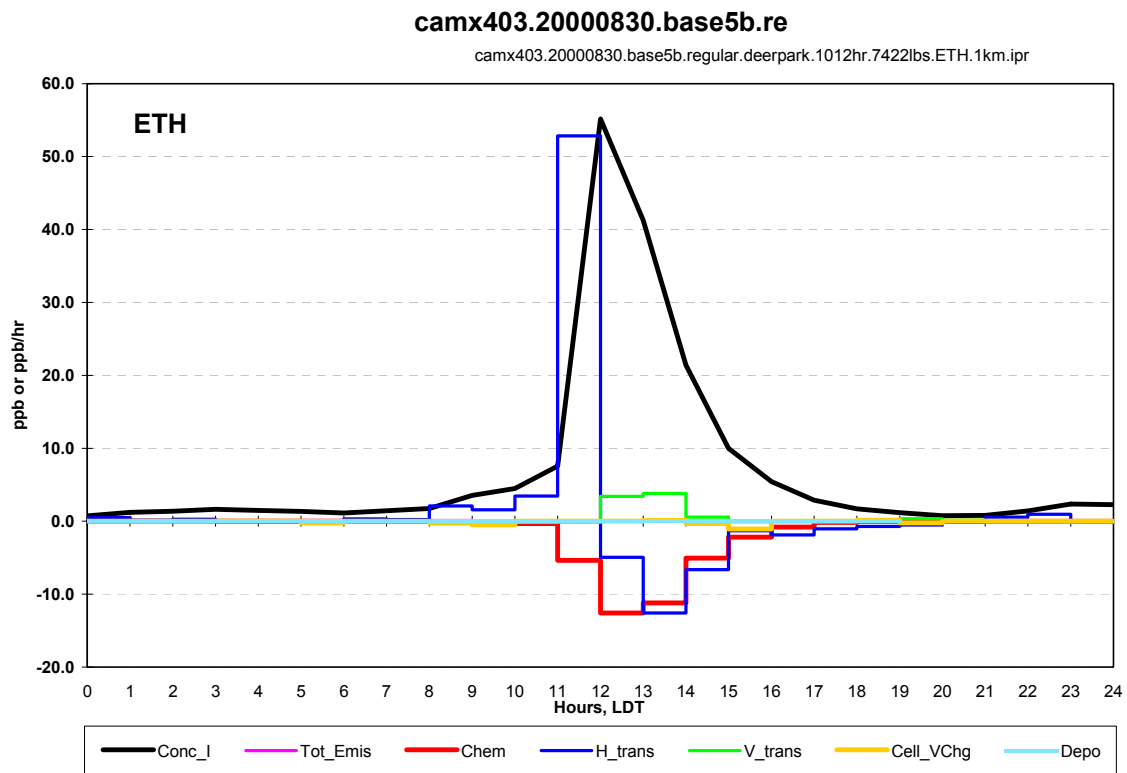
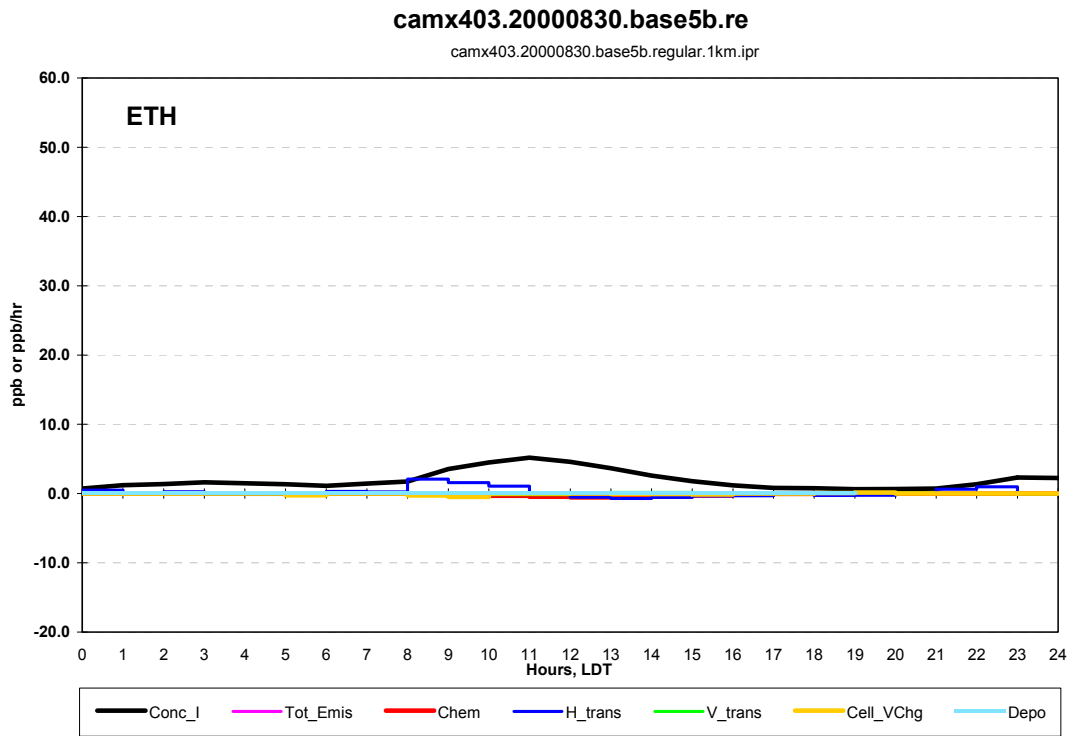


camx403.20000830.base5b.re

camx403.20000830.base5b.regular.deerpark.1012hr.7422lbs.ETH.1km.ipr

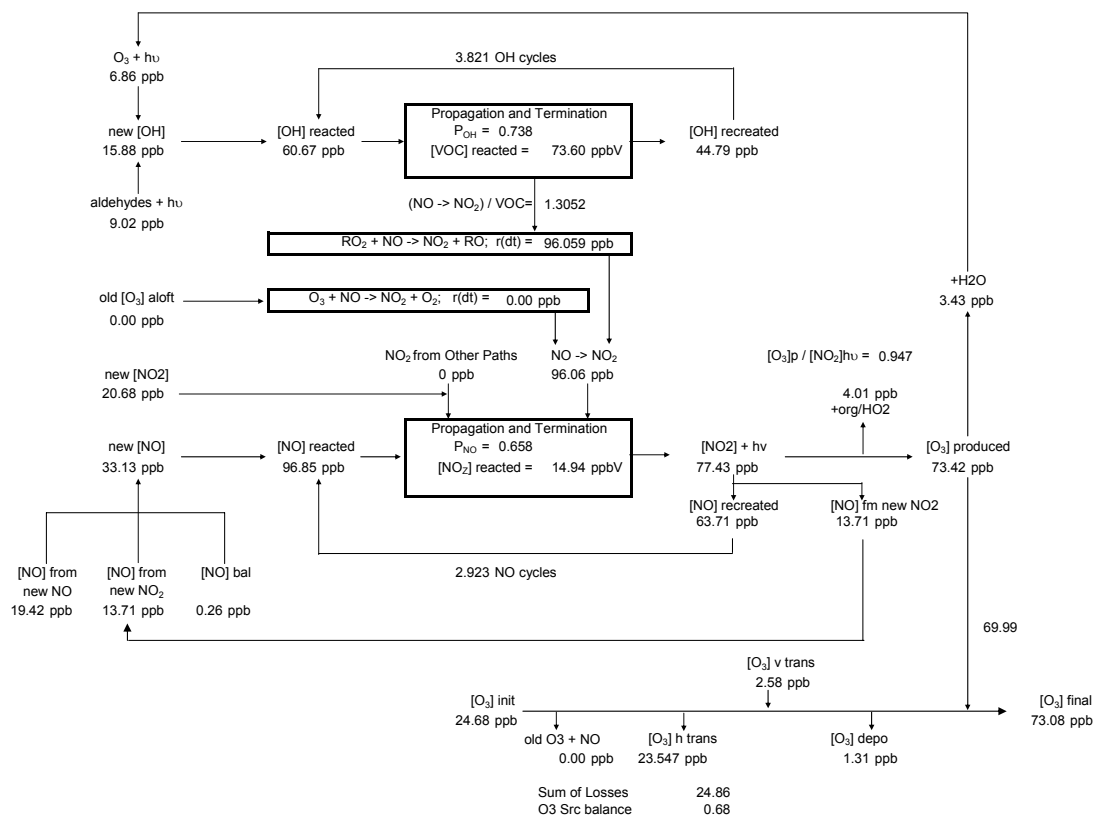


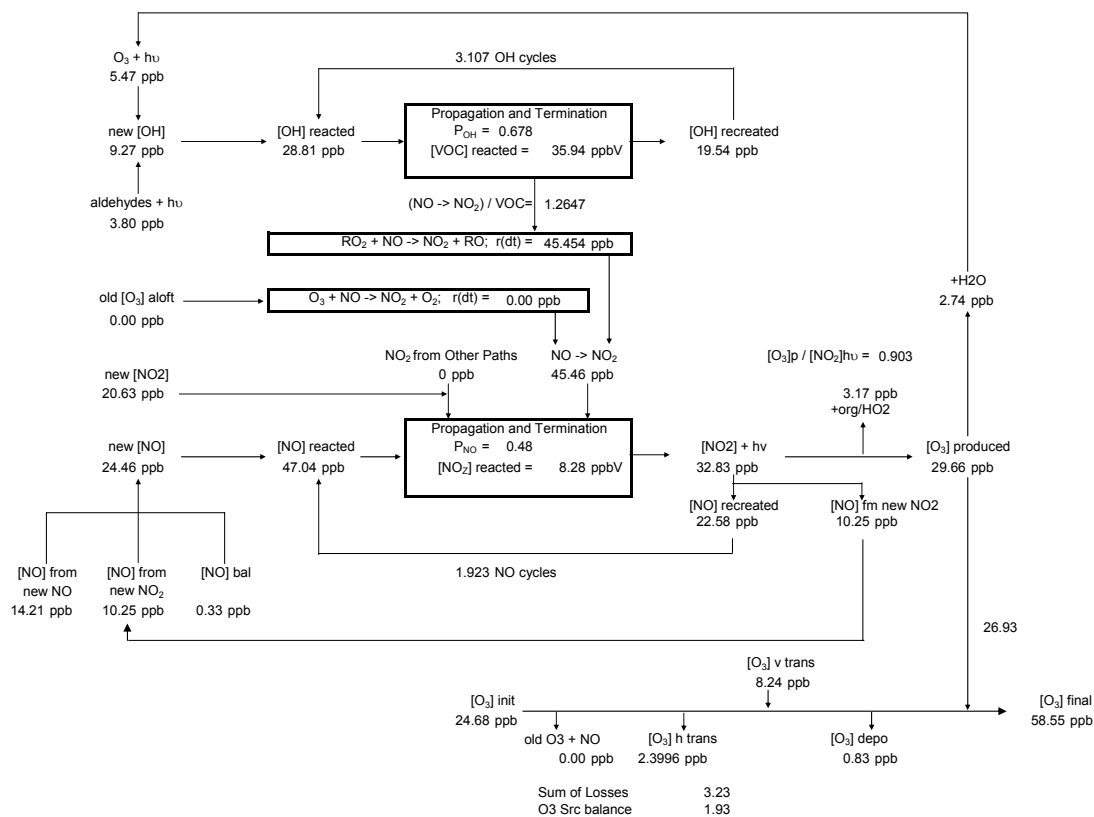
Peak Control Volume



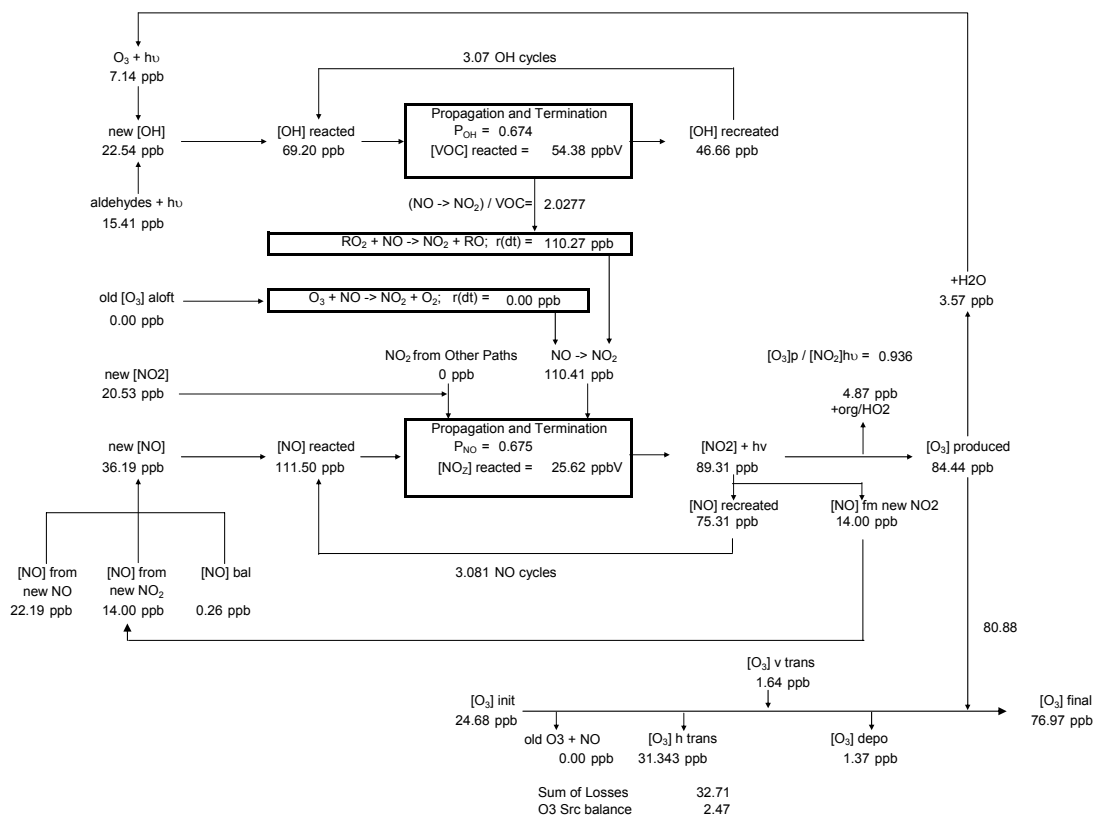
camx403.20000830.base5b.regular.1km.ipr
camx403.20000830.base5b.regular.1km.irr



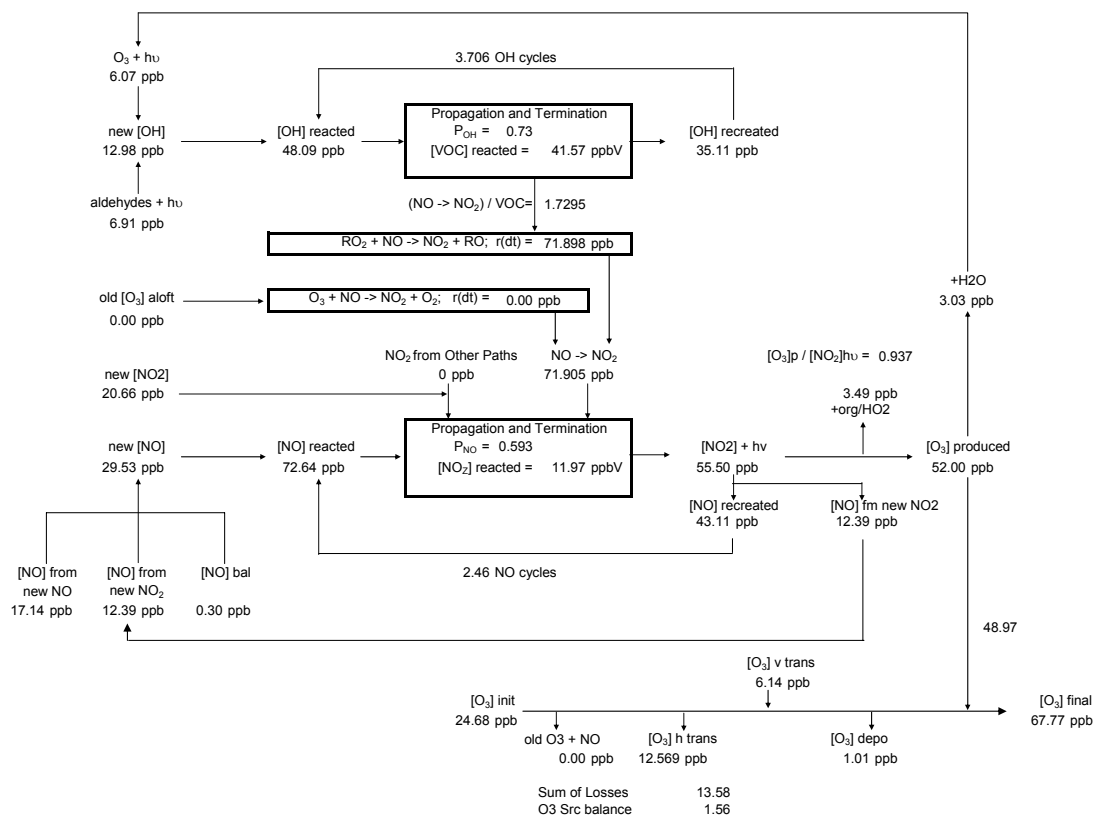




camx403.20000830.base5b.regular.deerpark.1012hr.9045lbs.XYL.1km.ipr
camx403.20000830.base5b.regular.deerpark.1012hr.9045lbs.XYL **Radical Cycle/ NO Cycle/ Ozone**



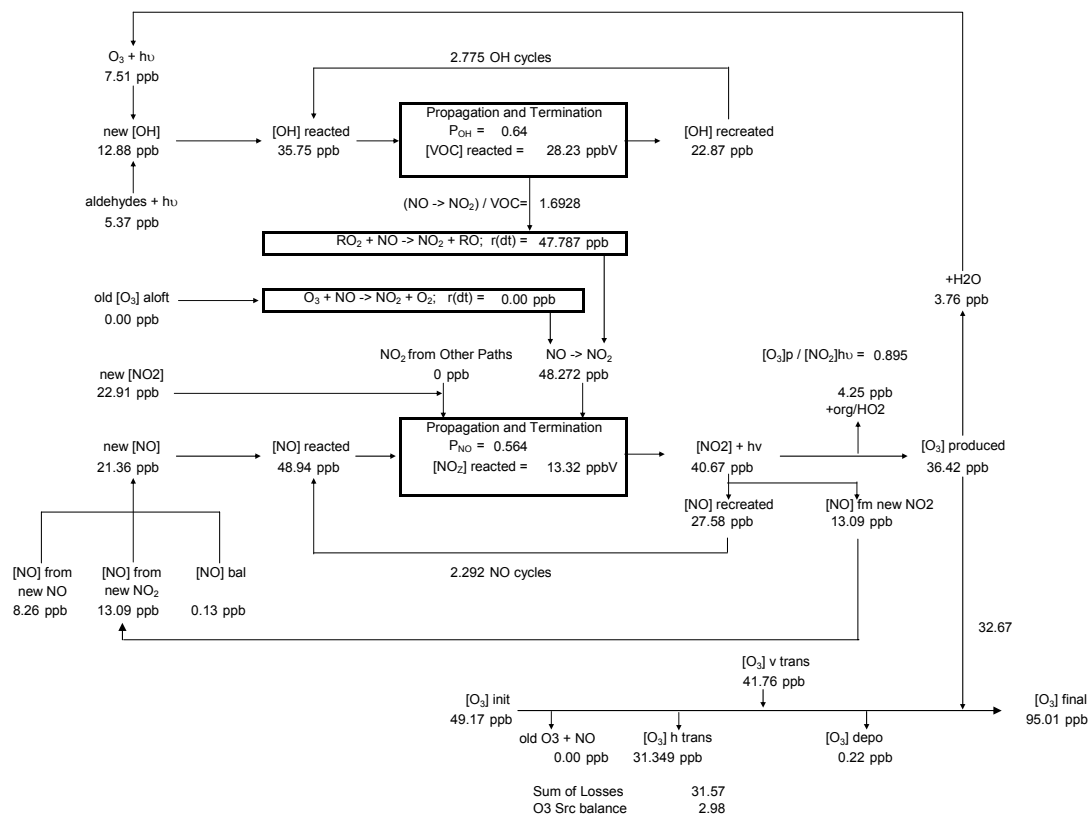
camx403.20000830.base5b.regular.deerpark.1012hr.7422lbs.ETH.1km.ipr
camx403.20000830.base5b.regular.deerpark.1012hr.7422lbs.ETH- **Radical Cycle/ NO Cycle/ Ozone**

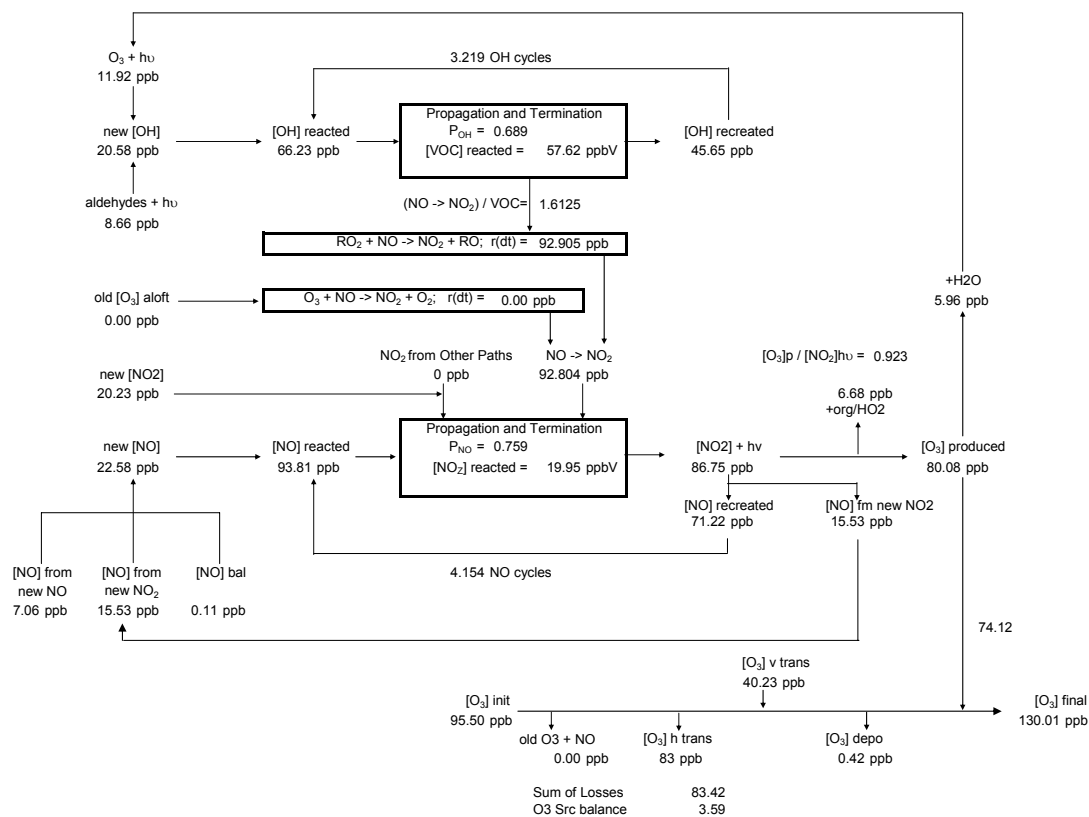


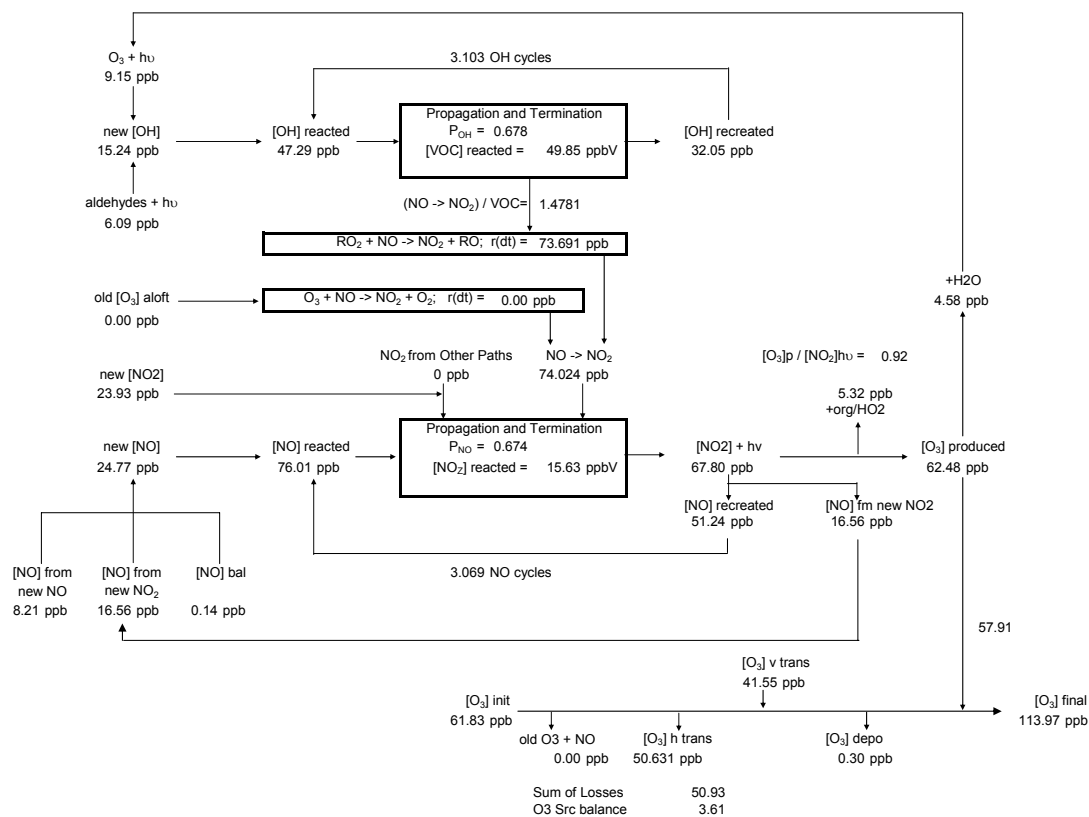
Peak Control Volume

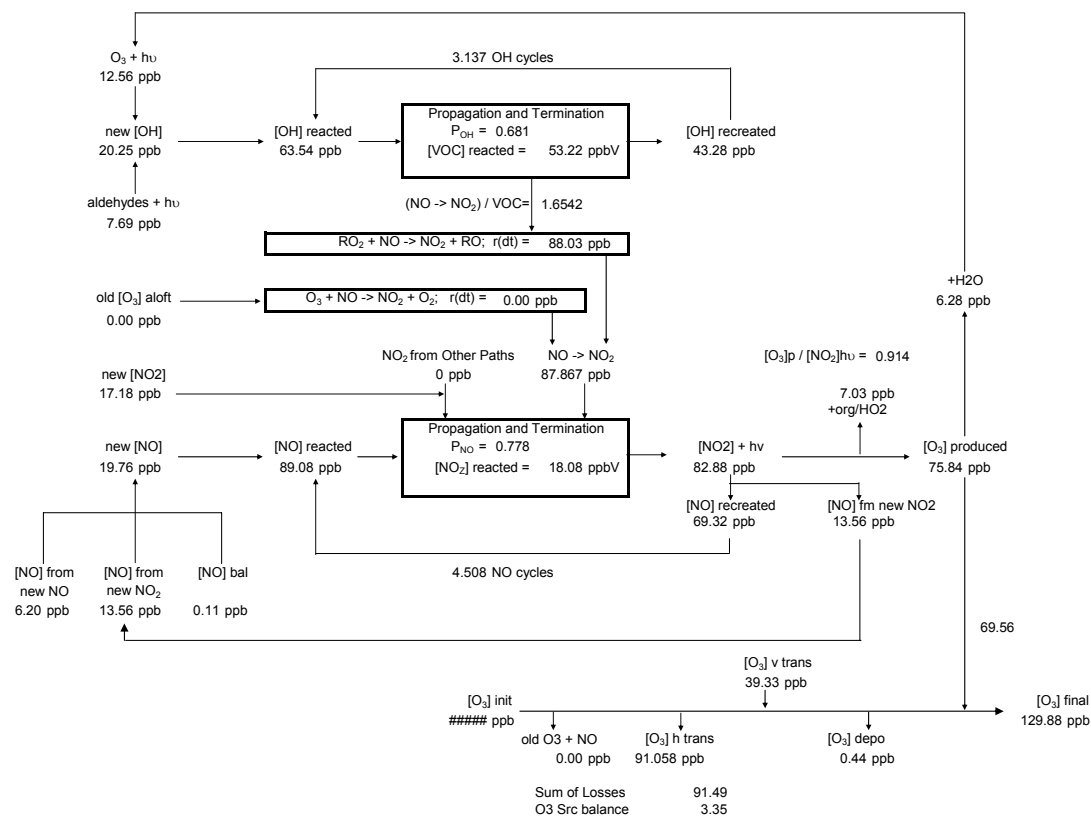
camx403.20000830.base5b.regular.1km.ipr
camx403.20000830.base5b.regular.1km.irr

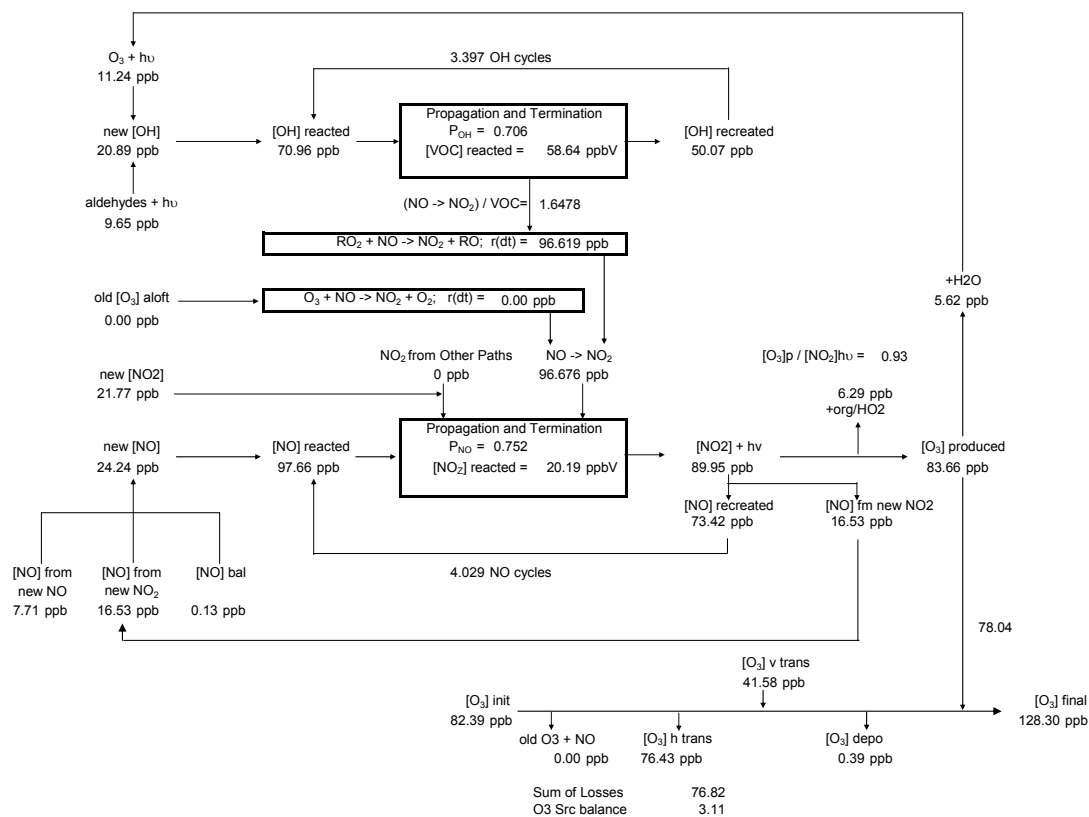
Radical Cycle/ NO Cycle/ Ozone











Bibliography

- Adelman Z. 1999. "A re-evaluation of the carbon bond IV photochemical mechanism." University of North Carolina at Chapel Hill, Department of Environmental Sciences and Engineering, School of Public Health.: 208 <http://airsite.unc.edu/>.
- Air ReSource Control Volumes Board (ARB). 2001. "Protocol for Photochemical Air Quality Modeling for the San Joaquin Valley Severe-Area Ozone attainment Demonstration Plan." Sacramento, CA., California Air ReSource Control Volumes Board <http://www.arb.ca.gov/homepage.htm>
- Allen D.T., Durrenberger C. 2001. "Accelerated Science Evaluation of Ozone Formation in the Houston-Galveston Area: Photochemical Air Quality Modeling." ftp://ftp.tnrcc.state.tx.us/pub/OEPAA/TAD/Modeling/HGAQSE/Reports_2002Feb/UT/AQModeling_20020204.pdf
- American Lung Association (ALA). 2004. "State of the Air Report: 2004." http://lungaction.org/reports/sota04_full.html
- Andreae M. O., Crutzen P. J. 1997. "Atmospheric aerosols: Biogeochemical Source Control Volumes and role in atmospheric chemistry." *Science*, 1052-1058
- Bates D.V. 1995. "The effects of air pollution on children." *Environmental Health Perspective*, 103 (Suppl. 6): 49-53.
- Brookhaven National Laboratory. 2000. Available at: ftp://aerosol.das.bnl.gov/pub/Houston00/HYDROCARBONS_V1.txt
- California Air ReSource Control Volumes Board (CARB) and the Office of Environmental Health Hazard Assessment (2002). "Staff Report: Public Hearing to Consider Amendments to the Ambient Air Quality Standards for Particulate Matter and Sulfates" <ftp://ftp.arb.ca.gov/carbis/research/aaqs/std-rs/pm-final/ch1-6.pdf>
- Carter W. P. 2004. "SAPRC-99 Mechanism Files and Associated Programs and Examples." <http://pah.cert.ucr.edu/~carter/SAPRC99.htm> last accessed 2005-02-23.
- Carter W. P. 1996. "Condensed atmospheric photooxidation mechanisms for isoprene." *Atmospheric Environment* 30 (24), 4275-4290
- Carter W. P. 1994. "Development of ozone reactivity scales for volatile organic compounds." *Journal of the Air and Waste Management Association* 44, 881-899

- Dennis A., Fraser M., Anderson S., and Allen D. T. 2002. "Air Pollutant Emissions Associated with Forest, Grassland and Agricultural Burning in Texas." *Atmospheric Environment* 36, 3779 – 3792.
- ENVIRON. 2004. CAMx Users Guide, v4.00. 2004. www.camx.com
- ENVIRON. 2000. User's Guide Comprehensive Air Quality Model with Extensions (CAMx) version 3.10, ENVIRON International Corporation. Novato, California.
- Galveston-Houston Association for Smog Prevention (GHASP). 2005. "Ozone Smog." <http://www.ghasp.org/issues/smog.html>
- Gauderman W.J., Gilliland G.F., Vora H., Avol E., Stram D., McConnell R., Thomas D., Lurmann F., Margolis H.G., Rappaport E.B., Berhane K., Peters J.M. 2002. "Association between air pollution and lung function growth in Southern California children." *American Journal of Respiratory and Critical Care Medicine*, 166 (1):76-84.
- Gery M. W., Whitten G. Z., Killus J. P., Dodge M. C. 1989. "A Photochemical Kinetics Mechanism for Urban and Regional Scale Computer Modeling." *Journal of Geophysical Research* 94, 925-956
- Gibson G. L. 1999. "Science Algorithms of the EPA Models-3 Community Multiscale Air Quality (CMAQ) Modeling System. Chapter 16 Process Analysis." D. W. Byun, Ching, J.K.S. (Eds.). U. S. Environmental Protection Agency, <http://www.epa.gov/asmdnerl/CMAQ/ch16.pdf>
- Griffin R. J., Cocker III D. R., Seinfeld J. H. 1999. "Estimate of global atmospheric organic aerosol from oxidation of biogenic hydrocarbons." *Geophysical Research Letters*, 26(17), 2721-2724
- Guenther A., Geron C., Pierce T., Lamb B., Harley P., Fall R. 2000. "Natural emissions of non-methane volatile organic compounds, carbon monoxide, and oxides of nitrogen from North America." *Atmospheric Environment* 34, 2205–2230.
- Hindmarsh A. C. 1980. "Isode and Isodi, two new initial value ordinary differential equation solvers." *ACM-Signum newsletter*, vol. 15, no. 4, pp. 10-11.
- Horak F. Jr., Studnicka M., Gartner C., Spengler J.D., Tauber E., Urbanek R., Veiter A., Frischer T. 2002. "Particulate matter and lung function growth in children: A 3-year Follow-up Study in Austrian Schoolchildren." [European Respiratory Journal](http://www.eurrespijournal.org), 19 (5):838-45.
- Jang J. C., Jeffries H. E., Byun D., Pleim J. E. 1995a. "Sensitivity of Ozone to Model Grid Resolution: Part I. Application of High Resolution Regional Acid Deposition Model." *Atmospheric Environment* 29(21): 3085-3100.

- Jang J. C., Jeffries H. E., Tonnesen S. 1995b. "Sensitivity of Ozone to Model Grid Resolution: Part II. Detailed Process Analysis for Ozone Chemistry." *Atmospheric Environment* 29(21): 3101-3114.
- Jeffries H. E., Tonnesen S. 1994. "A Comparison of Two Photochemical Reaction Mechanisms Using a Mass Balance Process Analysis." *Atmospheric Environment* 28(18): 2991-3003.
- Jeffries H. E. 1995. "Photochemical Air Pollution. Chapter 9 in Composition, Chemistry, and Climate of the Atmosphere." Ed. H.B. Singh, Van Nostand-Reinhold, New York, ISBN 0-442-01264-0
- Junquera V., Kimura Y., Vizuete W., Allen D. T., 2005. "Wildfires in Eastern Texas in August and September 2000: Emissions, Aircraft Measurements and Impact on Chemical and Physical Processes" submitted to *Atmospheric Environment*
- Junquera V. 2004. "Inventory of emissions of gaseous compounds and particulate matter from wildfires in east Texas in August and September 2000 and comparison with aircraft measurements." M.S. Thesis, University of Texas at Austin.
- Kimura Y., Vizuete W., Jeffries H. E., Allen D. T. 2005. "Implementation of Process Analysis in a 3-Dimensional Air Quality Model III: Development of sub-domain modeling tools to assess the impact of stochastic emission events on ozone formation in Houston Texas" submitted to *Atmospheric Environment*
- Kleinman L., Daum P., Imre D., Lee Y., Nunnermacker L., Springston S., Weinstein-Lloyd J., Rudolph J. 2002. "Ozone production rate and hydrocarbon reactivity in 5 urban areas: A cause of high ozone concentration in Houston." *Geophysical Research Letters* 30(12): 1639.
- Künzli N., Lurmann F., Segal M., Ngo L., Balmes J., Tager I.B. 1997. "Association Between Lifetime Ambient Ozone Exposure and Pulmonary Function in College Freshmen--Results of a Pilot Study." *Environmental Research*, 72 (1): 8-23.
- Liousse C., Penner J. E., Chuang C., Walton J.J., Eddleman H., Cachier H. 1996. "A global three-dimensional model study of carbonaceous aerosols." *Journal Geophysical Research*, 101(D16), 19411- 19432
- Liu Y. 2004. "Variability of wildland fire emissions across the contiguous United States." *Atmospheric Environment* 38, 3489 – 3499.
- Murphy C., Allen D. T. 2005. "Hydrocarbon Emissions from Industrial Release Events in the Houston Galveston Area and their Impact on Ozone Formation." *Atmospheric Environment In Press*
- National Oceanic and Atmospheric Administration (NOAA). 2004. <ftp://ftp.al.noaa.gov>

- National Oceanic and Atmospheric Administration (NOAA). 2003. "Texas Air Quality Study 2000 Airborne Lidar Aerosol Data." National Oceanic and Atmospheric Administration, Environmental Technology Laboratory, Optical Remote Sensing Division. Web page last modified August 2003. http://www.etl.noaa.gov/et2/data/data_pages/texaqs/air_aerosol.html
- National Center for Atmospheric Research (NCAR). 2004. MM5 Community Model, Pennsylvania State University / National Center for Atmospheric Research. <http://www.mmm.ucar.edu/>
- National Center for Atmospheric Research (NCAR). 2002. Project #2000-828 AESOP/TEXAQS-2000, Texas Air Quality Study, NSF/NCAR L-188 Electra (N308D). National Center for Atmospheric Research, Atmospheric Technology Division, Research Aviation Facility. Web site last updated August 2002. <http://raf.atd.ucar.edu/Projects/AESOP>
- Russell A., Dennis R. 2000. "NARSTO critical review of photochemical models and modeling." *Atmospheric Environment* 34(12-14): 2283-2324.
- Systems Applications International (SAI). 1999. "User's Guide to the Variable Grid Urban Airshed Model (UAM-V)." <http://www.uamv.com/overview.htm>
- Sandberg D. V., Hardy C. C., Ottmar R. D., Snell J. A. K., Acheson A., Peterson J. L., Seamon P., Lahm P., Wade D. 1999. "National strategy plan: Modeling and data systems for wildland fire and air quality." U.S. Department of Agriculture, Forest Service, Pacific Northwest Research Station, 60 p.
- Song J., Vizuite W., Chang S., McDonald-Buller E., Kimura Y., Yarwood G., Allen D. T. 2005. "Comparisons of Modeled and Observed Isoprene Concentrations in Southeast Texas." Submitted to *Journal of the Air & Waste Management Association*
- Sueper D. 2003. Personal communication, March 13, 2003
- Tesche T. W., McNally D. E., Wilkinson J. G., Jeffries H. E., Kimura Y., Emery C., Yarwood G., Souten D. R. 2004. "Evaluation of the 16-20 September 2000 Ozone Episode for use in 1-HR SIP Development in the California Central Valley." *Alpine Geophysics*
- Texas Air Quality Study (TEXAQS). 2000. available at: <http://www.utexas.edu/research/ceer/texaqs/index.html>
- Texas Commission on Environmental Quality (TCEQ) 2004. "The State Implementation Plan for the Control of Ozone Pollution: Attainment Demonstration for the

- Houston/Galveston Ozone Non-attainment Area.” P.O. Box 13087, Austin, Texas 78711-3087, www.tceq.state.tx.us
- Texas Commission on Environmental Quality (TCEQ). 2003. Houston/Galveston Air Quality Science Evaluation. Air Quality Modeling Files. CAMx Modeling Files. Files last updated December 2003. www.tceq.state.tx.us
- Tonnesen S., Jeffries H. E. 1994. "Inhibition of Odd Oxygen Production in Carbon Bond IV and Generic Reaction Set Mechanisms." *Atmospheric Environment* 28(7): 1339-1349.
- U.S. Environmental Protection Agency (EPA). 1999. “Smog--Who Does It Hurt? What You Need to Know About Ozone and Your Health”, EPA Publication No. EPA-452/K-99-001, Research Triangle Park, NC.
- U.S. Environmental Protection Agency (EPA) 1991. “Guidelines for Regulatory Application of the Urban Airshed Model.” EPA Publication No. EPA-450/4-91-1013. Office of Air Quality Planning and Standards, Research Triangle Park, NC.
- Vizuite W., Junquera V., Allen D. T. 2004. “Sesquiterpene emissions and secondary organic aerosol formation potentials for southeast Texas.” *Aerosol Science & Technology*, 38 (S1):167-181
- Vizuite W., Junquera V., McDonald-Buller E., McGaughey G., Yarwood G., Allen D.T. 2002. “Effects of Temperature and Land Use on Predictions of Biogenic Emissions in Eastern Texas.” *Atmospheric Environment* 36, 3321-3337.
- Wang Z., Jeffries H. E. 1998. “SARMAP Air Quality Model (SAQM) Integrated Process Rate Analysis Method User's Guide.” California Air Resource Control Volumes Board. <http://www.arb.ca.gov/ei/sarmap.htm>
- Wang Z. 1997. “Comparison of Three Vertical Diffusion Schemes in The SARMAP Air Quality Model with Integrated Process Rate Analysis Method and Continuous Process Composition and Source Control Volume Receptor Methodology.” PhD Dissertation, University of North Carolina at Chapel Hill. ftp://airsite.unc.edu/PDFS/ESE_UNC/Students/PhDThesis/Wang/
- Wang Z., Langstaff J. E., Jeffries H. E. 1995. “The Application of the Integrated Process Rate Analysis Method for Investigation of Urban Airshed Model (UAM) Sensitivity to Speciation in VOC Emissions Data.” Air & Waste Management Association conference, San Antonio, TX.
- Wiedinmyer C., Guenther A., Estes M., Strange I., Yarwood G., Allen D. T. 2001a. “A land use database and examples of biogenic isoprene emission estimates for the state of Texas, USA.” *Atmospheric Environment* 35, 6465-6477.

- Wiedinmyer C., Friedfeld S., Guenther A., Fraser M., Allen D.T. 2001b. "Measurement and Analysis of Atmospheric Concentrations of Isoprene and its Reaction Products in Central Texas," *Atmospheric Environment*, 35, 1001-1013 (2001b).
- Wilkinson J. G. 1994. "Technical Formulation Document: SARMAP/LMOS Emissions Modeling System (EMS-95)." *Alpine Geophysics*
- Yarwood, G. 2004. Personal Correspondence with ENVIRON Holdings, Inc.
- Yarwood G., Wilson G., Shepard S., Guenther A. 1999a. "User's Guide to the Global Biosphere Emissions and Interactions System – Version 3.1." 101 Rowland Way, Suite 220, Novato, California, available at: <http://www.globeis.com>
- Yarwood G., Wilson G., Emery C., Guenther A. 1999b. "Development of the GloBEIS – A State of the Science Biogenics Emissions Modeling System." Final Report to the Texas Natural ReSource Control Volume Conservation Commission, 12100 Park 35 Circle, Austin, Texas 78753.

Vita

William Gustavo Vizuite was born in Utica, New York, on October 4, 1976. He is the son of Guillermo Gustavo Vizuite and Clelia Vizuite. He received a B.S. in Chemical Engineering in 1998 from the University of Missouri at Rolla. From 1998 – 2000, Will worked at the ExxonMobil Petrochemical Facility in Baton Rouge, Louisiana as a process engineer. In August 2000, he started graduate school at the University of Texas at Austin. While in graduate school, he worked as an Assistant Instructor, Teaching Assistant, Graduate Research Assistant, and College Radio DJ and host of the KVRX 91.7 FM's Monday night free jazz show "Close Enough For Jazz." From 2000 through 2002 Will was awarded the National Consortium for Graduate Degrees for Minorities in Engineering and Science, Inc. (GEM) M.S. Engineering Fellowship. He also was awarded the Thrust - Uniden Endowed Graduate Fellowship in Engineering in 2002 through 2005. He received a M.S. in Chemical Engineering from the University of Texas at Austin in 2003. He has authored papers on photochemical grid modeling, biogenic emission estimation models, and has published in professional journals and presented at several conferences. He is a member of the American Institute of Chemical Engineers, and the American Association for Aerosol Research.

Permanent address: 11642 W. Citrus Grove
Avondale, AZ 85323

This dissertation was typed by the author.